Solid-contact Potassium Ion-selective Electrodes with Plasticizer-free Silicone-based Membranes for Extended Potassium Ion Monitoring in Physiological Samples

A DISSERTATION

SUBMITTED TO THE FACULTY OF

UNIVERSITY OF MINNESOTA

BY

Brian Spindler

IN PARTIAL FULFILLMENT OF THE REQUIREMENTS

FOR THE DEGREE OF

DOCTOR OF PHILOSOPHY

Advisor: Andreas Stein

October 2024

Acknowledgments

First, I would like to thank my parents for supporting me and encouraging me to pursue my interests. I learned a lot growing up on the farm and developed a good work ethic in the process. I would not have gotten this far without your support. Thank you.

I would like to thank my advisor Professor Andreas Stein for his excellent guidance on my research. He is always excited about the work everyone in his lab is doing, and that kept me motivated to keep going, even when I wasn't having much success. You've also given me a lot of good feedback on how to present and write about my research, which helped me land job. I enjoyed working in your lab and really enjoyed the good discussions about various aspects of my research and the overall field itself.

I always referred to Professor Philippe Bühlmann as an unofficial co-advisor because I spent a significant amount of time working in his research lab. I also attended many Bühlmann group meetings. I learned a lot about many fundamental aspects of ion sensors in our discussions and during group meetings. Professors Andreas Stein and Philippe Bühlmann complement each other quite well and I found it easy to work with both of them. I think the advancements made in this dissertation were only possible in collaboration with both of you. Thank you both.

I would like to thank the Stein and Bühlmann group members for their help and support throughout my time at the University of Minnesota. Dr. Jinbo Hu and Dr. Xin Chen taught me a lot about the field of ion-selective electrodes and helped me get started in the first year of my thesis work. I would also like to thank Dr. Evan Anderson for many helpful

discussions regarding the data I collected and for teaching me several very useful lab techniques.

I spent a lot of time collaborating with Dr. Minog Kim for the work described in Chapter 3. Thank you for doing the hard work of scaling up the synthesis for small CIM carbon particles.

Katerina Graf spent three years working with me as an undergraduate research assistant, and she assisted with many of the experiments described in Chapter 2 and some in Chapter 3. You learned things so quickly! I learned a lot about teaching and mentoring while working with you.

Finally, I would like to thank Dr. Shawn Kelley and Dr. James Carney from Medtronic for sponsoring my research.

Abstract

In recent years, wearable potentiometric sensors have been used to monitor the real-time concentration of ions such as K^+, pH, Na^+ in sweat or interstitial fluid. However, a majority of ISEs reported to-date comprise a plasticized poly(vinyl chloride) (PVC) membrane, a mobile ionophore, and mobile ionic sites. Leaching of these species from the ISE into the sample can be toxic to the surrounding tissue and limits the lifetime of ISEs, especially for ISEs with thin sensing membranes, like those in wearable or implantable devices. Solid-contact ion-selective electrodes (SC-ISEs) in direct contact with physiological samples for long-term measurements must be biocompatible and resistant to biofouling.

Silicone ISEs are a promising alternative to plasticized PVC because of their excellent biocompatibility, but little work has been done to study the relationship between silicone composition and ISE performance. In this thesis, we studied the influence of silicone composition on ISE performance in simple KCl solutions and blood plasma. SC-ISEs prepared with different silicone ion-selective membranes (ISMs) and colloid-imprinted mesoporous (CIM) carbon solid contacts have no differences in response slope, selectivity, or drift in simple aqueous salt solutions. However, substantial differences in emf drift were observed in porcine blood plasma in long-term experiments, even between silicones with very similar structure.

Wearable and implantable SC-ISEs need to be sufficiently small to be comfortable for the patient. In the case of CIM carbon as the solid contact material, the particle size is very large, and as a result, the ISE must be quite thick. We show that the particle size of CIM

carbon can be reduced to <15 μm and that SC-ISEs with a total CIM carbon + ion-selective membrane thickness below 100 μm can be prepared. We also discuss the theoretical lower limit of the geometric size of the electrode on how often the SC-ISEs need to be recalibrated to keep error below a defined limit.

To improve biocompatibility and extend SC-ISE lifetime, we prevented ionophore leaching from the ion-selective membrane by covalently attaching it to the silicone membrane. To achieve this, we synthesized a modified version of the K^+-ionophore BME-44 (a bis-crown ether) containing triethoxysilyl groups that react with condensation curing silicones during the curing process. Up to 96% of ionophore can be covalently bound to the silicone membrane polymer and ISEs prepared with this ionophore have excellent selectivity to K^+ vs. Na^+, making them suitable for use in physiological samples.

Finally, I discuss some of the remaining challenges with silicone-based ISEs. I discuss the complexity associated with condensation curing silicones, which I suspect contributes to significant batch-to-batch variability in the behavior of the resulting ISEs, and I propose several methods to make ISEs with more reproducible silicones.

Table of Contents

List of Tables

Chapter 1

Chapter 3

Chapter 4

List of Figures

Chapter 1

Chapter 4

Appendix

List of Abbreviations

3DOM	three-dimensionally ordered macroporous
Å	angstrom
A	geometric area
A	absorbance
a_{K+}	activity of potassium
ATR-FTIR	attenuated total reflectance-Fourier transform infrared spectroscopy
BET	Brunauer-Emmett-Teller
C	capacitance
CIM	colloid-imprinted mesoporous
CD_3CN	deuterated acetonitrile
$(CD_3)_2CO$	deuterated acetone
$CDCl_3$	deuterated chloroform
$CHCl_3$	chloroform
cm	centimeters
C_{OFS}	concentration of salt in the outer filling solution of a reference electrode
C_s	specific capacitance
d	days
d	density
°C	degrees Celsius
DOS	dioctyl sebacate
DSC	differential scanning calorimetry
E	electrical potential
EMF	electromotive force
ε	molar absorptivity
EtOH	ethanol
F	Farad
FTIR	Fourier transform infrared spectroscopy

g	gram
h	hour
h	thickness
HFPB	tetrakis[3,5-bis(1,1,1,3,3,3,-hexafluoro-2-methoxy-2-propyl)phenyl]borate
i	current
IFS	inner filling solution
ISE	ion-selective electrode
ISFET	ion-selective field effect transistor
ISM	ion-selective membrane
K_{ij}	Nicolskii-Eisenman selectivity coefficient
K_{K^+,Na^+}	Nicolskii-Eisenmann selectivity coefficient for selectivity to K^+ vs. Na^+
L	path length
m	meters
m	mass of solid contact material
M	molarity
MeOH	methanol
MHz	megahertz
min	minute
mL	milliliter
mol_{BME}	total moles BME-44
m_t	total mass of parent membrane
m_s	mass of sample membrane
mm	millimeter
mV	millivolt
MWCNTs	multi-walled carbon nanotubes
µm	micrometer
µV	microvolt
nm	nanometer

NMR	nuclear magnetic resonance
NMP	*N*-methyl-2-pyrrolidone
o-NPOE	*o*-nitrophenyl octyl ether
Ω	ohm
P	packing factor
P/P_o	cell pressure relative to pressure of the reference cell
pCO_2	partial pressure of carbon dioxide
PDMS	poly(dimethylsiloxane)
PDMS-OH	hydroxy-terminated poly(dimethylsiloxane)
PEDOT	poly-(3,4-ethylenedoxythiophene)
PEG	poly(ethylene glycol)
p-HEMA	poly(2-hydroxyethylmethacrylate)
pO_2	partial pressure of oxygen
PPG	poly(propylene glycol)
PSAM	poly(dimethylsiloxane)-*co*-poly(propylbenzylamidomethylsiloxane)-*co*-poly(methacryloxypropylmethylsiloxane)
PSCN	poly(dimethylsiloxane)-*co*-poly(cyanopropylmethylsiloxane)-*co*-poly(methacryloxypropylmethylsiloxane)
PSES	poly(dimethylsiloxane)-*co*-poly(*p*-acetylphenoxypropyl-methylsiloxane)-*co*-poly(methacryloxypropylmethylsiloxane)
PSKT	poly(dimethylsiloxane)-*co*-poly(*p*-acetoxypropylmethylsiloxane)-co-poly(methacryloxypropylmethylsiloxane)
PSS	poly(styrenesulfonate)
PU	polyurethane
PVC	poly(vinyl chloride)
PVDF	poly(vinylidene fluoride)
QSDFT	quenched solid density functional theory
R	resistance
R_{in}	input resistance of the voltmeter
R_{mem}	resistance of the ion-selective membrane

SC-ISE	solid-contact ion-selective electrode
SDS	safety data sheet
SEM	scanning electron microscopy
SPE	stretchable potentiometric electrode
t	time
T	temperature
THF	tetrahydrofuran
TBA	tetrabutylammonium
TDDA	tetradodecylammonium
TDMA	tridodecylmethylammonium
TFA	trifluoroacetic acid
TFADB	trifluoroacetyl-*p*-decylbenzene
TPB	tetraphenylborate
TFPB	tetrakis[3,5-bis(trifluoromethyl)phenyl]borate
TpClPB	tetrakis(4-chlorophenyl)borate
UV	ultraviolet
UV-vis	ultraviolet-visible
V	volume
V_C	voltage across capacitor
V_{carbon}	volume of carbon
V_{cell}	voltage across the electrochemical cell
V_{ip}	interparticle volume
V_m	electrical potential measured with a voltmeter
V_{pore}	volume of pores
$V_{p,s}$	specific pore volume
VTIPOS	vinyltriisopropenoxysilane
VTMOS	vinyltrimethoxysilane

Chapter 1

Introduction to Solid-contact Ion-Selective Electrodes and Silicone-based Ion-selective Electrodes

1.1. Clinical analysis of blood analytes to diagnose diseases and monitor treatments

The concentration of ions (e.g., Na^+, K^+, H^+, Cl^-) in physiological samples like blood serum or urine are routinely used, in combination with other information, to diagnose diseases and monitor treatments.[1] Concentration imbalances of these of ions in blood serum can have serious consequences for patients. For example, the K^+ concentration in blood serum in patients is important to monitor because K^+ is critical for transmission of electrical signals in skeletal and cardiac tissues.[2, 3] When the K^+ concentration is too far outside the normal range (3.5–5.5 mM in adults), the risk of arrythmias or heart failure increases.[4, 5] Increased serum K^+ concentration can be caused by several diseases including renal failure and insulin deficiency[1]. Conversely, decreased serum K^+ concentrations can be the result of excess insulin and excess diuresis. In addition a number of drugs can produce changes in the serum K^+ concentration.

Often, diseases that cause changes in the serum concentration of one ion are related to changes in others. For example, in diabetic patients, a lack of insulin can cause changes in K^+ concentration. It can also cause a condition known as diabetic ketoacidosis, which is a decrease in pH (more acidic) due to excessive fat oxidation in the liver.[6] In serious cases, this can lead to coma.

Na^+ is important for regulating osmotic pressure, which influences intra- and extra-cellular volume.[7] Hypernatremia (Na^+ concentration above the normal range) is caused either by excessive water loss or excessive sodium gain. Water loss can be due to many factors, including renal and gastrointestinal diseases, though the most common is lack of access to water. Conversely, hyponatremia (Na^+ concentration below 136 mM) is often

caused by retention of water. This can result in cerebral edema (swelling of the brain), which can be fatal. Causes of hyponatremia are wide ranging and include heart, liver, and lung diseases.[8] It was also shown that the mean Na^+ concentration in hospitalized patients is 5–6 mM lower than in healthy outpatients.[9] Underlying diseases are the most common causes, but it was also shown that patients admitted with normal sodium levels can develop hypernatremia during their time at a hospital. It was suggested that the most common cause was intravenous administration of hypotonic fluids to patients during treatment or operations,[10] though the serum Na^+ concentrations usually return to normal levels within a few days.

Currently, patients must travel to a hospital to have blood drawn at the required times, which then can be analyzed in the laboratory, using dedicated instruments. There are also some point-of-care devices on the market that allow patients to measure the concentrations of certain species in blood plasma, including Na^+, K^+ $Cl^–$, and glucose. However, these devices also require a blood draw, which involves action by the patient. Moreover, the obtained values only provide analyte concentrations at a particular point in time, whereas trends in concentration with time can sometimes be more informative. To improve disease detection and management, wearable and implantable sensors have been developed to measure species concentrations in sweat[11-18] or interstitial fluid.[11, 19-21] For ionic species, ion-selective electrodes (ISEs) are used to perform these measurements. Because these sensors are placed in contact with biological tissue, the sensor components must be biocompatible. Unfortunately, most wearable or implantable sensors reported to date comprise plasticized PVC membranes, which are not biocompatible due to leaching of

membrane components into the surrounding tissue. The goal of the work in this thesis is to produce biocompatible silicone-based ion-selective electrodes that do not contain any plasticizer. This introduction will first explain the construction and operation of ISEs and then describe work that has been done in the literature with silicone-based ISEs.

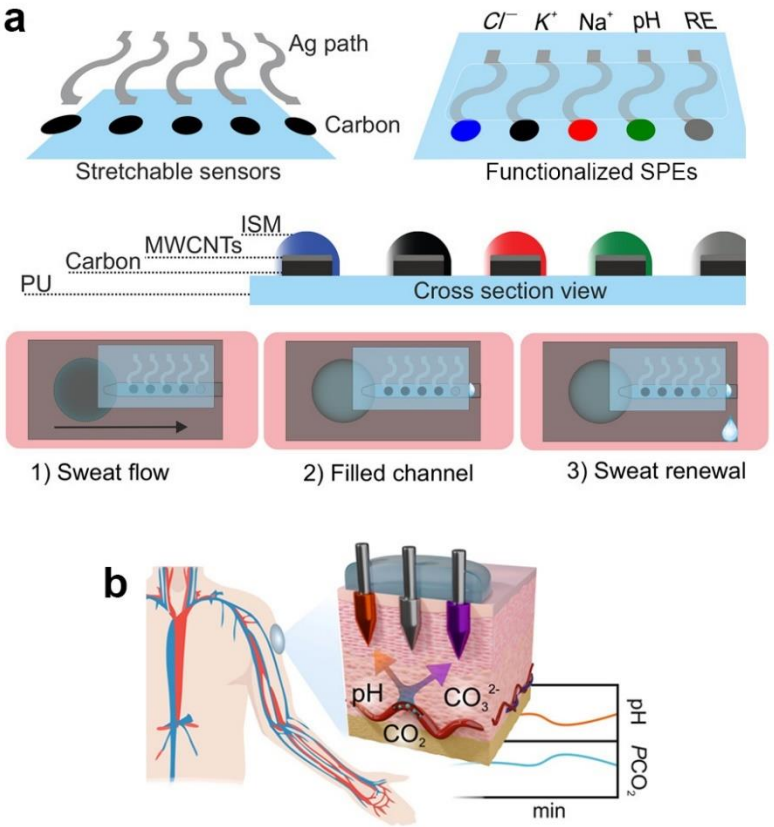

Figure 1.1. Wearable sensor for measuring ion concentrations in sweat or interstitial fluid. (a) Wearable patch sensor with the ISEs arranged in a microfluidic channel for measuring the ion concentrations in sweat. Abbreviations: PU: polyurethane; MWCNTs: multi-walled carbon nanotubes; ISM: ion-selective membrane; SPE: stretchable potentiometric electrode. Reprinted with permission.[12] Copyright 2019. American Chemical Society. (b)

Microneedle sensor that penetrates the skin to measure the ion concentration in interstitial fluid. Reprinted with permission.[13] Copyright 2024, Creative Commons license CC-BY 4.0.

1.2. Operating mechanism of ISEs

Potentiometric sensors are operated by measuring the electrical potential difference between an ion-selective electrode and a reference electrode (Figure 1.2) under zero current conditions.[22] The potential of the ISE is dependent on the primary ion activity (not concentration) in the sample, whereas the reference electrode potential is independent of the sample composition. Ion activity in solution is related to concentration, but it is corrected for effects of ionic strength. At higher concentrations (usually above 1 mM), anions and cations in solution can associate with each other to some extent, lowering the concentration of fully dissociated ions.[23] The dependence of the ISE potential on the activity of the primary ion in the sample is described by the Nernst equation (Eq. 1.1), where E is the measured electrical potential difference between the ISE and the reference electrode, E^0 is the standard potential of the cell, R is the thermodynamic constant, T is the temperature (in Kelvin), z is the charge of the primary ion, F is Faraday's constant, $a_{i,s}$ is the activity of the primary ion (i) in the sample, and $a_{i,m}$ is the activity of the primary in the ion-selective membrane (which is constant when the sensor is functional). In a sample at 25 °C, for an ion with a charge of +1 (e.g., K^+) the potential of the ISE *increases* by 59 mV for every 10-fold increase in ion activity in the sample. Likewise, for an ion with a charge of –1, the potential *decreases* by 59 mV for every 10-fold increase in activity.

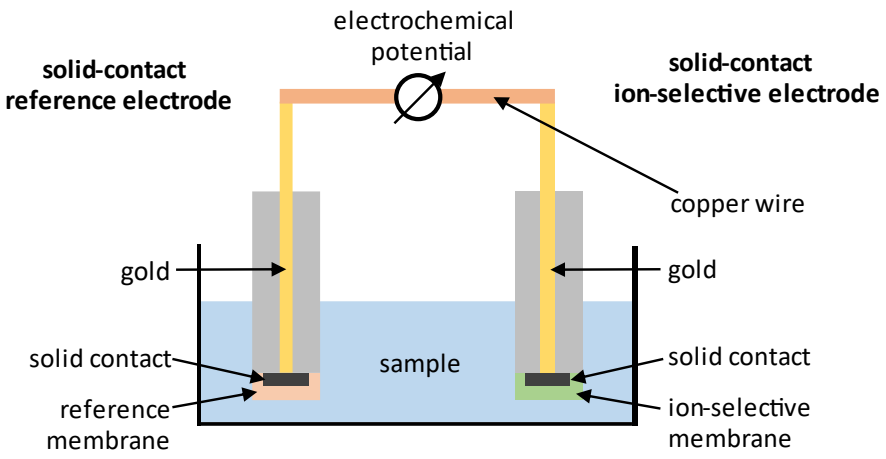

Figure 1.2. Operation of an SC-ISE and SC-RE for measuring ion activity in sample solutions.

$$E = E^0 + \frac{RT}{zF} \ln \left[\frac{a_{i,s}}{a_{i,m}} \right] \qquad (1.1)$$

For an ISE to operate, it must contain a membrane or surface that facilitates a response to the primary ion in the sample and a component or several components that facilitate ion-to-electron transduction. For the former criteria, most ISEs comprise a polymeric membrane[24] with ionophore and ionic sites dissolved within (Figure 1.3). The polymeric membrane must have a glass transition temperature well below room temperature (e.g., *o*-NPOE plasticized PVC: –56 °C)[25] to ensure that the ionophore and ionic sites are mobile within the membrane. The ionophore is a compound that preferentially and reversibly binds to the primary ion in the sample, imparting selectivity to the sensor.[26-28] The ionic site is a hydrophobic ion that raises the primary ion activity in the ion-selective membrane, thereby preventing co-extraction of the primary ion and its counterion from the sample into the bulk of the membrane over the working range of the sensor.[29] As a result, $a_{i,m}$ does not

change in the bulk of the membrane when $a_{i,s}$ changes. When the activity of the primary ion in the sample ($a_{i,s}$) changes, the electrical potential at the sample/membrane interface changes because the primary ion is complexed by the ionophore and extracted into the membrane, but its counterion is not extracted because the free energy of transfer for a hydrophilic counterion is much greater than that for the complexed primary ion. This results in charge separation across the sample/membrane interface, with a length scale on the order of a few nanometers. The extent of charge separation increases with increasing primary ion activity in the sample, and the resulting potential is described by the Nernst equation (Eq. 1.1).

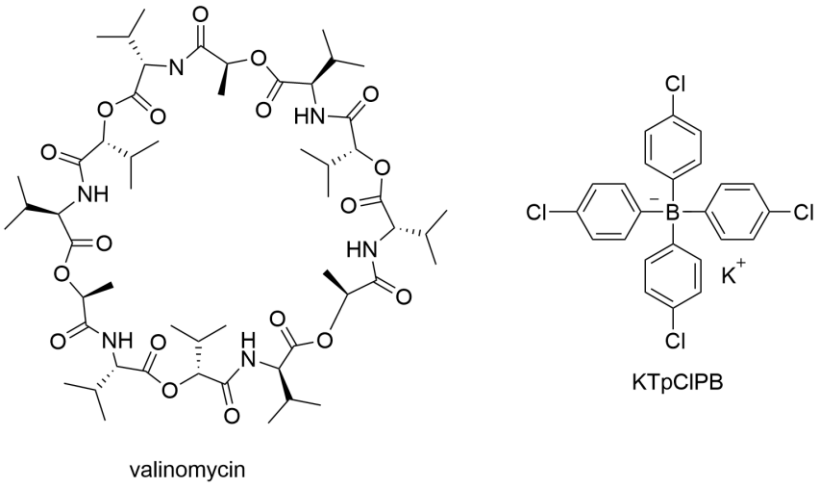

Figure 1.3. Chemical structure of the K^+ ionophore valinomycin and the ionic site potassium tetrakis[4-chlorophenyl]borate.

To facilitate ion-to-electron transduction, the ISE can be configured in several ways. The simplest method is to place an ion-selective membrane (ISM) into an electrode body that has an inner filling solution containing the chloride salt of the primary ion (Figure

1.4a) and a Ag/AgCl wire in contact with the inner filling solution.[30] The same charge separation mechanism responsible for the potential at the sample/membrane interface is responsible for the potential at the inner filling solution/sample interface. Ion-to-electron transduction occurs at the Ag/AgCl wire/sample interface by the redox reaction in Eq. 1.2.

$$AgCl_{(s)} + e^{-} \rightleftharpoons Ag^{0}_{(s)} + Cl^{-}_{(aq)} \qquad (1.2)$$

Because the concentration of the primary ion and chloride in the inner filling solution is constant (ion flux through the membrane is slow), the potential at the inner filling solution/membrane interface (ΔE_2 in Figure 1.4a) and the Ag/AgCl wire/inner filling solution interface (ΔE_3 in Figure 1.4a) does not change on short time scales, and all phase boundary potentials remain constant except for the potential at the membrane/sample interface. The potential across the cell is the sum of the phase boundary potentials at each interface (ΔE_1 in Figure 1.4a).[31] Therefore, to accurately measure changes in potential at the ISM/sample interface, it is critical that all other phase boundary potentials do not change significantly during use. Ideally, the difference in electrical potential is measured under zero current conditions, but in practice, a very small current passes through the cell during measurement. Therefore, it is important that the ion-to-electron transduction system is able to allow for passage of small currents through the cell without a large change in potential at the membrane/transducer interface(s).

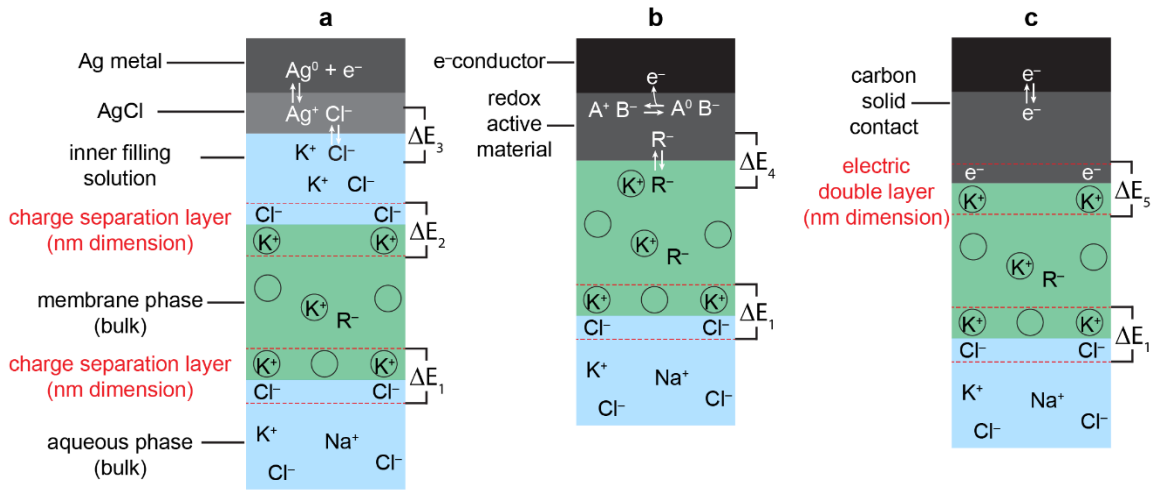

Figure 1.4. Configuration of K^+ ISEs with (a) an inner filling solution and a Ag/AgCl wire, (b) a redox active material, and (c) a high surface area carbon material to facilitate ion-to-electron transduction. Circles represent ionophore, R^- is the anionic site, A^+ is a redox active species (e.g., cation in a conducting polymer), and B^- is the counterion in the conducting polymer (it can be R^- from the ISM or a different anion).

Unfortunately, the inner filling solution makes sensors difficult to miniaturize, and the ISEs require storage in a sealed, humid environment to prevent evaporation of water. Additionally, the long-term stability can be limited by diffusion of sample species and water between the membrane and into the inner filling solution. To address these problems, ISEs with solid contacts were developed that facilitate ion-to-electron transduction at the ISM/solid contact interface through faradaic processes (Figure 1.4b) or double layer capacitance (Figure 1.4c).

SC-ISEs relying on a faradaic process include two classes of materials: conducting polymers[32] and intercalation materials.[33, 34] Conducting polymers (Figure 1.5) are polymers containing redox active functional groups. One example is poly(aniline), which can be

oxidized to form an emeraldine salt. However, this polymer is sensitive to pH, and SC-ISEs prepared with this solid contact are often sensitive to light, O_2, and CO_2.[35, 36] Other conducting polymers including poly-(3,4-ethylenedioxythiophene) poly(styrenesulfonate) (PEDOT:PSS) and poly(pyrrole) have also been used. To eliminate some interferences, solid contacts with more hydrophobic PEDOT analogs have been used to make the conducting polymer more hydrophobic,[37, 38] allowing one to eliminate the electrode response to CO_2 and produce ISEs with drifts as low as 1.5 μV/h for a pH-selective electrode.[38]

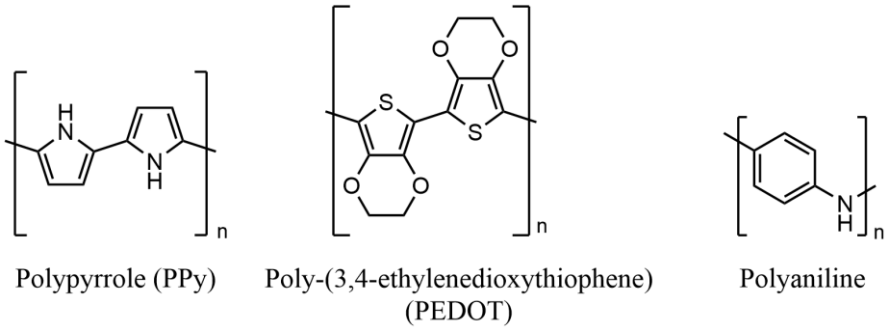

Figure 1.5. Structure of common conductive polymers used in SC-ISEs.

Intercalation materials have also been used as ion-to-electron transducers. Examples include $Li_{0.5}FePO_4$, $Na_{0.33}MnO_2$, and K_xMnO_2.[33, 34] $LiFePO_4$ is often used as the active material in the cathode of lithium-ion batteries.[39] When $LiFePO_4$ is charged, iron is oxidized: $Fe^{2+} \rightleftharpoons Fe^{3+} + e^-$. To balance the charge, a lithium ion moves from the cathode to the anode, resulting in the formation of $FePO_4$. Some materials like $LiFePO_4$ have a relatively constant potential (although the discharge curve is not completely flat) over a wide state of charge. Combining this with their high charge storage capacities, these

cathode materials are attractive materials for use in SC-ISEs because small currents passing through the ion-selective membrane will result in a very small change in potential at the ISM/membrane interface.

SC-ISEs may also be prepared with high surface area conductors where no faradaic processes occur. Instead, ion-to-electron transduction is facilitated through double-layer capacitance at the ISM/solid contact interface (Figure 1.4c).[40] The earliest examples of this were Pt wires coated with an ion-selective membrane.[41, 42] Here, the capacitance at the membrane/conductor interface is confined to the geometric surface area of the Pt wire, which is very low. As a result, the interfacial capacitance is low and small currents passing through the cell during measurement cause the potential of this capacitor to change significantly,[43, 44] thereby causing the electrode potential to drift and requiring that the SC-ISE be recalibrated frequently.

To address this problem, three-dimensionally ordered macroporous (3DOM) carbon was introduced as a solid contact in 2007,[45] which dramatically increased the surface area between the solid contact and the ISM. As a result, these SC-ISEs had low long-term drift (11.7 μV/h). Since then, numerous other types of SC-ISEs have been reported.[46] One of the most notable is colloid-imprinted mesoporous (CIM) carbon,[47] which has mesopores with diameter of 20–40 nm, allowing for the ion-selective membrane components to penetrate into the pores and access the surface of most surface area within the carbon particles. As a result, K^+ SC-ISEs with CIM carbon as a solid contact have been able to achieve long-term drifts as low as 1.3 ± 0.3 μV/h.

For the work described in the rest of this thesis, CIM carbon was used as the solid contact because of its outstanding performance in plasticized PVC-based SC-ISEs. CIM carbon has very little oxygen on its surface and most of the surface area is contained within mesopores with diameters in the range of 20–40 nm. CIM carbon is also relatively easy to synthesize with good batch-to-batch pore diameter reproducibility, making it an attractive solid contact material for research work.

One other important ion sensor configuration is an ion-selective field-effect transistor (ISFET). ISFET devices are built on top of a silicon chip (usually p-doped) (Figure 1.6).[48, 49] The top of the silicon wafer is insulated with an oxide like silica, alumina, or tantalum oxide. In addition, a gate oxide is deposited as a thin layer on top of the Si semiconductor to electrically insulate the Si from the ISM. The ISM acts as the gate for ISFETs. The gate oxide can be coated with the ISM directly, but usually these devices are unstable because the gate oxide surface is sensitive to changes in local pH. As a result, they are sensitive to CO_2.[50] To address this problem, the gate oxide can be coated first with a pH buffered hydrogel (shown in Figure 1.6) and then with the ISM.[51]

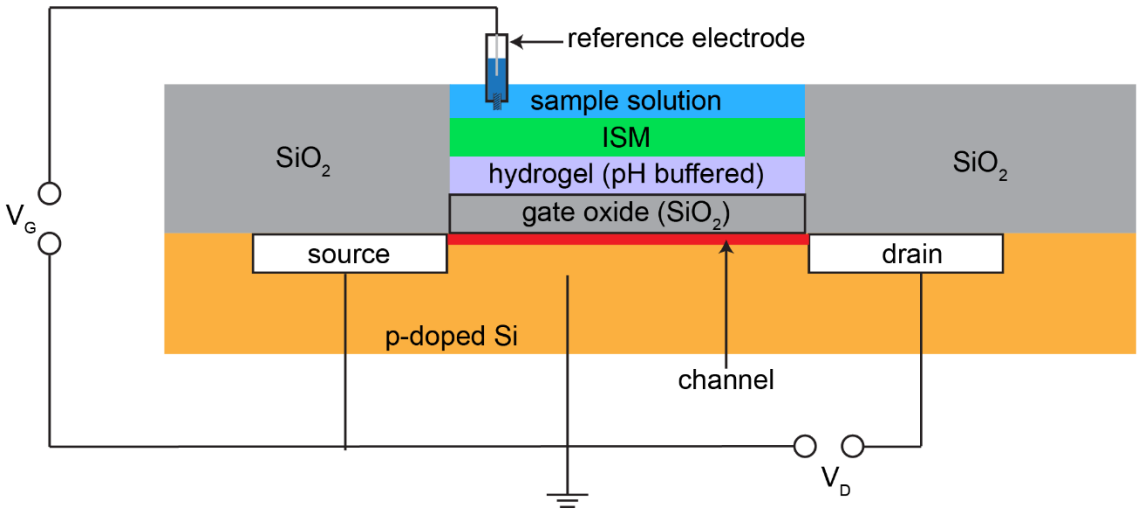

Figure 1.6. Cross-section of an ion-selective field-effect transistor.

ISFETs are operated by applying a potential between the source and drain (usually made of n-doped Si), which causes a current to flow through the p-doped Si near the gate oxide. This region is usually referred to as a channel. The potential at the ISM/sample interface influences the concentration of mobile charge carriers in the channel. The conductivity of the channel increases with increasing charge carrier concentration, which increases the current flowing through the channel. By measuring that current, one can determine the gate potential or changes in the gate potential (V_G) applied by the ISM. These devices can be operated in different modes, but they are all ultimately measuring changes in the potential at the ISM/sample interface. For more details, see reference [48].

1.3. Plasticized PVC membranes

Plasticized PVC ion-selective membranes (Figure 1.7) are most widely used in ISEs because they offer good solubility and mobility of ionophores and ionic sites, and

plasticizers can be used that do not contain coordination sites, which could compete with the ionophore.[52] Additionally, no crosslinking reactions are required to make freestanding membranes with sufficient mechanical robustness. This allows for easy fabrication of ISEs by simply dissolving the membrane components in a solvent (typically tetrahydrofuran) and then drop-casting the membrane onto the desired electrode. As a result, it is possible to make ISEs with excellent reproducibility in structure and electrochemical performance from electrode-to-electrode.[53, 54]

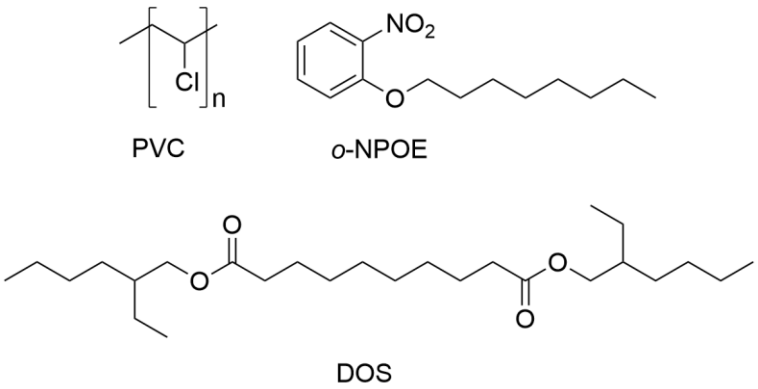

Figure 1.7. Structure of PVC and the two most common plasticizers used to make ISEs.

However, PVC membranes require a lot of plasticizer to function.[55] PVC has a glass transition temperature of 85 °C,[56] well above the typical temperatures at which these ISEs are used (20–40 °C). As a result, none of the polymer chains in pure PVC are mobile, and any species that are contained within the PVC are not expected to be mobile either. Such a membrane would have nearly infinite resistance and would not function. Therefore, a plasticizer is added to solvate the PVC chains and allow for chain sliding at temperatures well below the desired operating temperature. A typical PVC membrane used in ion-selective membranes contains two parts *o*-nitrophenyloctyl (*o*-NPOE) ether (plasticizer) to one part PVC and has a glass transition temperature of –56 °C.[25] For membranes with

dioctyl sebacate (DOS) as plasticizer, the glass transition temperature is –70 °C.[25] These membranes are sometimes called "solvent polymeric membranes" because they are primarily comprised of plasticizer.

Plasticized PVC membranes also have their drawbacks, especially in the context of wearable or implantable, thin SC-ISEs. The main drawback is that plasticizer can leach from the membrane into the sample and can be toxic to the surrounding tissue.[57] Leaching of plasticizer can also limit the lifetime of SC-ISEs, especially when thin ISMs are used.[58] ISEs in contact with samples like blood plasma tend to have significantly shorter lifetimes than those in contact with simple aqueous salt solutions because partitioning of plasticizer into blood plasma is more favorable than into simple aqueous salt solutions.[59] To address these problems, silicone was evaluated as a replacement for plasticized PVC because no plasticizer is required to lower the glass transition temperature[60] and silicones have good biocompatibility.[61]

1.4. Silicone structure and crosslinking chemistry

Silicones have a unique structure, with an —$Si(CH_3)_2$–O–$Si(CH_3)_2$— backbone where each silicon atom contains two methyl groups (Figure 1.8). Interestingly, the Si–O bond distance is short (1.64 Å) and the Si–O–Si bond angle is about 143°, which is much larger than the 109° expected for an sp^3 hybridized atom.[62] This has led some authors to suggest that the Si—O bond contains some $(p\rightarrow d)_\pi$ character.[63] For application of silicone membranes in ISEs, the most important observation is that the activation energy for rotation about the Si–O bond is very low (apparently too low to be measured).[64] Since this

rotation requires very little energy and the silicone chains are linear, they are also flexible, resulting in a low glass transition temperature of –121 °C.

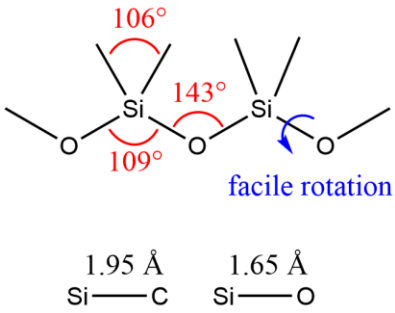

Figure 1.8. Structure of the silicone backbone with bond lengths and angles from reference [62].

Silicones with linear chains are liquid at room temperature, even with molecular weights above 100,000 g/mol. To produce silicone films that hold their shape, the silicone chains must be immobilized by crosslinking them. Due to their linear structure and ease of rotation about the Si—O bond, the glass transition temperature of crosslinked silicone is unchanged. The silicone chains are still flexible enough to have some motion (though very limited) in a crosslinked state.

Several crosslinking methods exist. The most common methods are radical-initiated crosslinking between two methyl groups on nearby silicone chains, hydrosilylation, which involves a Pt-catalyzed reaction between silicones with vinyl groups and silicones with hydrosilane groups, and condensation curing of silicones (Figure 1.9).[65]

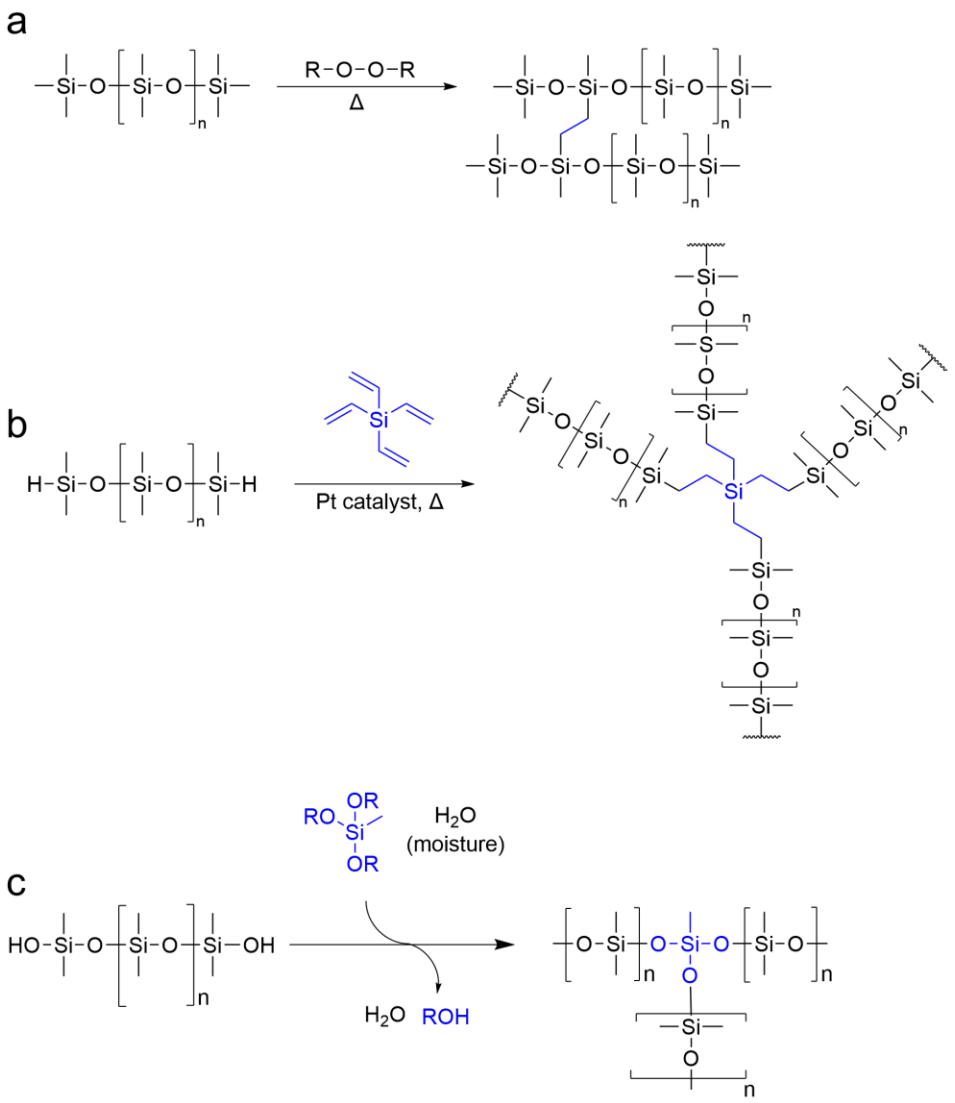

Figure 1.9. Crosslinking chemistry for the most common types of commercial silicones by (a) free radical, (b) hydrosilylation, and (c) condensation curing chemistries.

Radical initiated crosslinking is performed by introducing organic peroxides into the silicone.[65] Upon heating, the peroxides form free radicals, resulting in abstraction of hydrogens from methyl groups on silicon atoms which react to form chemical bonds between the methyl groups on nearby silicone chains. However, this method requires a

stoichiometric amount of peroxide to be added to the silicone matrix because it is converted to alcohol during the reaction. To decrease the amount of peroxides required, small amounts of vinylmethylsiloxane were introduced into the silicones, which can react with one another without consuming the peroxide.[66]

In hydrosilylation-cured silicones (Figure 1.9b), silicone chains with small amounts of vinylmethyl siloxane and methylhydrosiloxane functional groups are mixed with a catalyst (typically Pt).[67, 68] Upon heating, the vinyl and hydrosilane groups react, forming an Si–CH_2–CH_2–Si bridge between different silicone chains, and resulting in formation of a crosslinked silicone network. Crosslinkers like tetravinylsilane can be used, but in many cases, the crosslinker is a silicone co-polymer with either a small fraction of vinylmethylsiloxane or methylhydrosiloxane incorporated into the silicone chain. Hydrosilylation cured silicones are often sold as two-part silicones to prevent crosslinking during storage.

In condensation curing of silicones (Figure 1.9c), linear silicone chains with terminal Si–OH or Si–O–alkyl groups are used.[69, 70] They are mixed with a crosslinker, which is often a low molecular weight silicone with three to four hydrolysable functional groups, most commonly acetoxy or methoxy.[71] Upon exposure to moisture in the air, some of these groups hydrolyze, and reactions between Si–OH on silicone chains and Si–OR groups on the crosslinker result in formation of a crosslinked silicone network. The crosslinking reactions are usually catalyzed by a titanium or tin salt.[72]

Most condensation-curing silicones are one-part silicones, meaning they have all components mixed together by the manufacturer, which is convenient for the eventual user

of the silicone. However, this means that the unused silicone needs to be protected from water. Often, excess crosslinker is added to the one-part condensation-cured silicones, which react with terminal Si–OH groups on the silicone chains. The excess crosslinker in the silicone precursor can react with small amounts of water to release methanol or acetic acid (Figure 1.10).[73] As long as the amount of water is small, the excess crosslinker can act as a water scavenger. This extends the lifetime of the silicone precursor, even when the container is briefly exposed to moisture in the air. In commercial applications like caulks, this allows multiple uses of the same container of caulk.

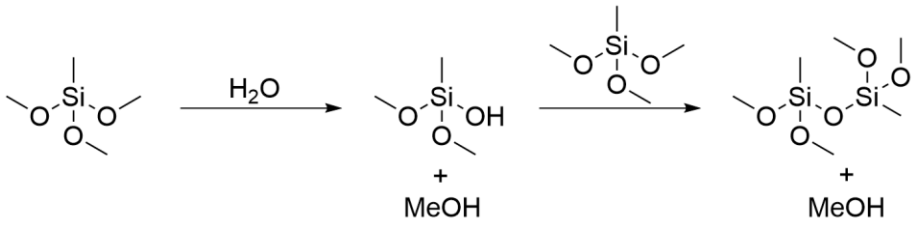

Figure 1.10. Excess crosslinker (methyltrimethoxysilane) added to condensation-curing silicones reacts with water, releasing methanol and forming dimers of crosslinkers. Because the concentration of crosslinker is much higher than the concentration of terminal $SiMe(OR)_2$ groups on the ends of silicone chains, the silicone chains rarely react with each other.

Condensation-curing silicones also have good adhesion to a wide variety of surfaces, especially glass and metal surfaces that have an oxide layer. This is because silicone can form covalent bonds to the surface during curing. For example, on glass surfaces, strong Si–O–Si or Al–O–Si bonds are formed.[74] Formation of covalent bonds to metal oxides on the surfaces of many metals can also improve adhesion.

The identity of the leaving group influences the rate of the crosslinking reaction. Acetate, methoxy, and ethoxy groups are the most common. Acetate is an excellent leaving group. Acetic acid can also catalyze crosslinking as it is released and before it evaporates, making it the leaving group of choice for fast curing silicones. However, acetic acid is corrosive and as a result, these silicones are not suitable for use in application in electronics or on some metal surfaces. For those applications, neutral systems with alkoxy or enoxy leaving groups silicones are used.

Silicones are flexible, elastic materials, but they have poor mechanical and tear strength, and they will tear easily.[65] To improve these properties, hard, inert inorganic fillers are added to most silicone mixtures to reinforce them. Silicone chains interact with the filler particles either by covalent bonding, hydrogen bonding, or weaker physical interactions.[75] The most common fillers are derivatives of fumed silica. Fumed silica can have a high concentration of surface Si–OH groups, which can interact with the silicones by hydrogen bonding or covalently attach to hydroxy-terminated silicones. As a result, these silica surfaces are very hydrophilic and can attract significant amounts of water. To address this problem, hydrophobic fillers can be used. The most common example is silica that is surface-treated with compounds such as hexamethyldisilizane[76] to produce particles with trimethylsilyl functional groups. The hydrophobic surface weakens interactions between silicone chains and the filler, and attracts less water. These properties make silica fillers treated with hexamethyldisilizane the most common choice for reinforcement of condensation-cured silicones, because those silicones are stored for long periods of time

before use. Other types of fillers can also be used (carbon, titania, fibers, other metal oxides), although fillers are not necessarily required for use in ISMs.

1.5. Silicone-based ion-selective membranes

Silicones have been used as an alternative to plasticized PVC membranes, partly because they do not require a plasticizer to obtain a glass transition temperature well below room temperature. However, many reports of silicone-based ion-selective electrodes still involved the use of added plasticizer in order to improve ionophore solubility in the silicone matrix.[60] The discussion that follows here will focus on silicone-based ISEs without added plasticizer. ISMs with condensation-cured silicones are by far the most investigated class of silicones in ISEs. Most of these silicones are commercially available one-component silicones. Although commercial suppliers do not provide the exact composition, some parts of the curing chemistries are known (Figures 1.11 and 1.12). Other silicones have also been used, but their structure and exact curing chemistry is unknown. Notably, condensation-cured silicones with different crosslinkers containing, three, four, and six reactive groups per molecule have been used in ISEs, though to date there are no reports of investigations on the influence of different crosslinkers on the behavior of ISEs. Some examples of silicones that have been used include Dow 3140, which is an alcohol evolving condensation-curing poly(dimethylsiloxane), and Shin-Etsu KE47T, which is an alcohol-evolving condensation curing silicone. Shin-Etsu KE44T has also been used and is a condensation-cured poly(dimethylsiloxane), but is an oxime-evolving silicone.[77] Other silicones include Wacker TRV-ME 625[78] and Silastic E (from Dow Corning)[79] which are hydrosilylation-cured silicones.

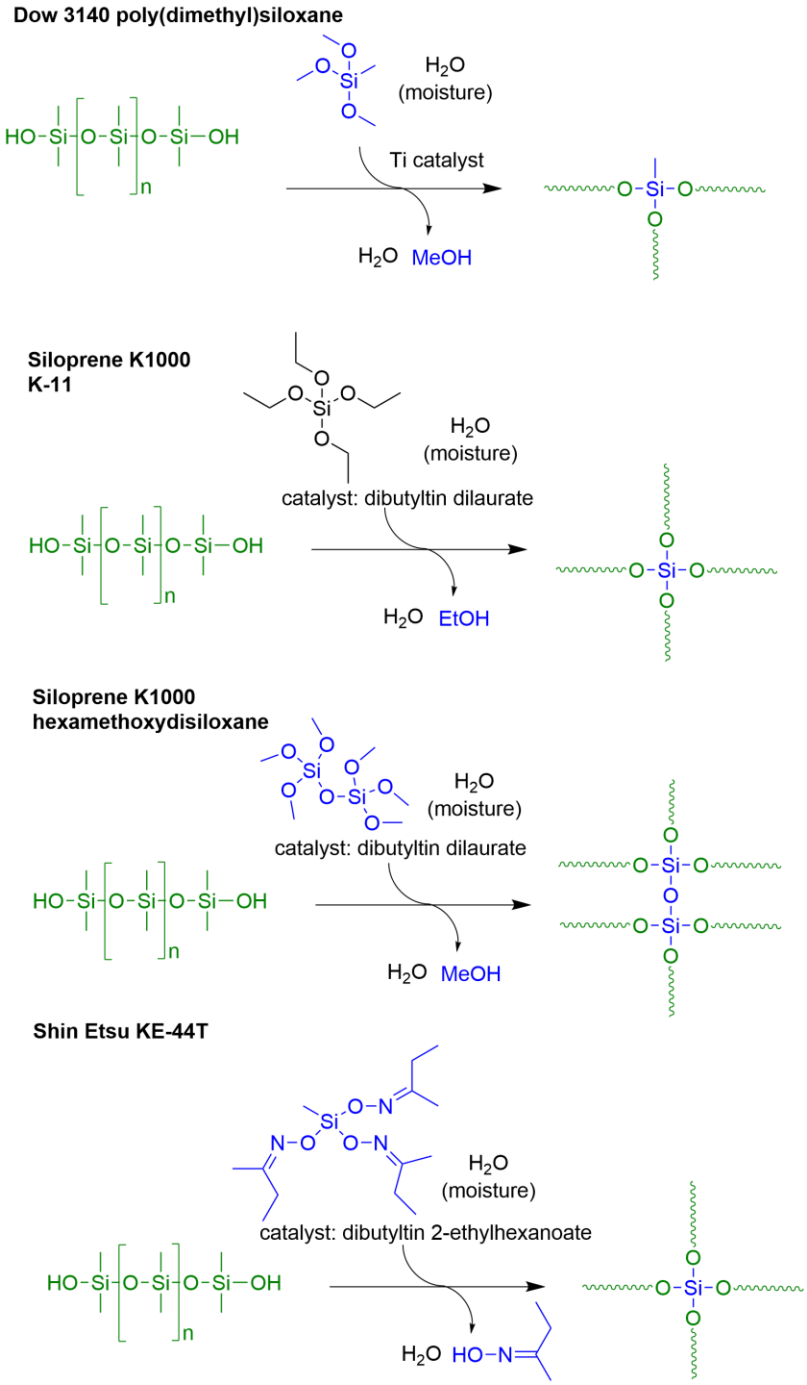

Figure 1.11. Known structures and curing chemistries for poly(dimethylsiloxanes) used for ISEs in the literature. The wavy green lines coming off each oxygen on the right-hand side of the reaction represent linear silicone chains. The curing chemistries were inferred

from the compositions listed in the following sources: Dow 3140: safety datasheet;[80] Siloprene K1000 with K-11: composition listed in reference;[81] Siloprene K1000 with hexamethoxydisiloxane as crosslinker: composition listed in reference;[82] Shin-Etsu KE-44T: inferred from composition in SDS.[83]

Siloxanes containing one trifluoropropylmethyl and one methyl substituent on the silicon atoms have also been investigated (Figure 1.12). They are commonly referred to as fluorosilicones. Fluorosilicones are more polar than poly(dimethylsiloxanes), which makes them attractive materials for use in ISEs because the ionophore and ionic sites tend to be more soluble in these polymers. The most used fluorosilicone in the literature is Dow 730 (Figure 1.11), which is a condensation-curing fluorosilicone. Other fluorosilicones like Shin-Etsu (FE-73) have also been used, which cures by hydrosilylation when heated to 125 °C, though the exact details of the reagents are not known.

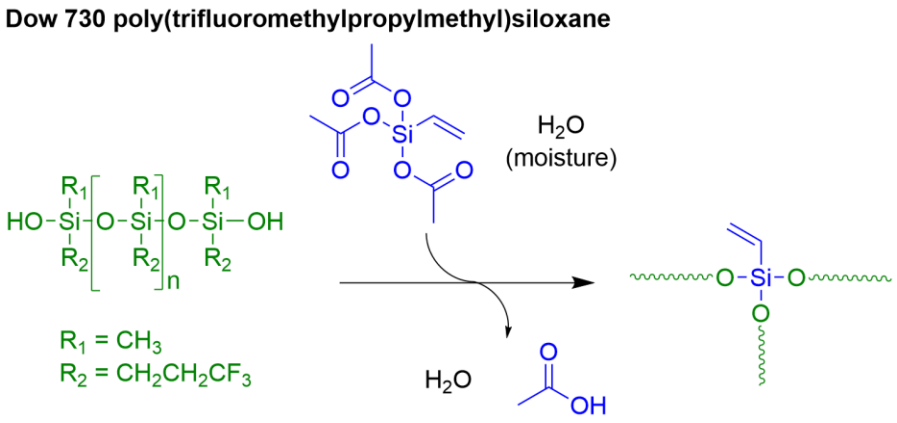

Figure 1.12. Known structure and curing chemistry of fluorosilicone used in the literature (Dow 730). The wavy green lines coming off each oxygen on the right-hand side of the reaction represent linear silicone chains. The curing chemistry is inferred from the composition in the SDS.[84]

The other important type of silicone is a custom-made terpolymer containing 2.8–25% cyanopropylmethylsiloxane (Figure 1.13).[85-91] The cyano groups on the silicone have a large dipole moment, allowing one to significantly increase the polarity of the silicone membrane and increase the solubility of ionophore and ionic sites in the membrane. The methacryloxy groups allow for photo-initiated crosslinking under UV light. No filler was added to these silicones. The custom poly(siloxane) terpolymers are abbreviated with a four-letter code for the functional group followed by the molar percentage of the functionalized siloxane in the polysiloxane. For example, a terpolymer containing 10 mol% cyanopropylmethylsiloxane units is abbreviated as PSCN(10). This abbreviation scheme will be used throughout the rest of this thesis.

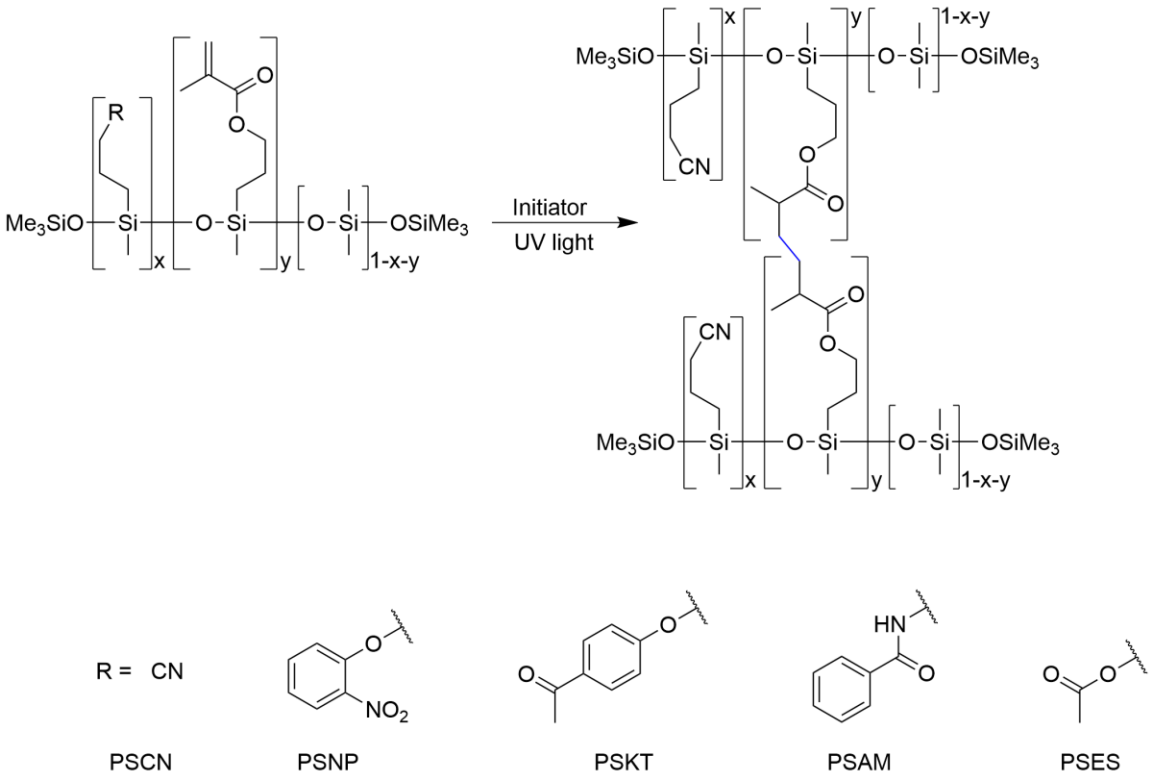

Figure 1.13. Custom-made terpolymers comprising poly(dimethylsiloxane) with some fraction of functionalized silicone (2.8–25%) and a small amount of methacryloxypropylmethylsiloxane for photo-initated crosslinking.

1.6. Na^+ selective membranes with plasticizer-free silicone-based ISMs

Na^+ ISEs are among the most reported ISEs using silicone ISMs in the literature, and published response slopes and selectivities are summarized in Table 1.1. The ionic sites are shown in Figure 1.14 and the ionophores are shown in Figures 1.15 and 1.16. ISEs with Na^+ ionophore I, II, and III in silicone and fluorosilicone membranes have been reported. Each of these ionophores contain acetamide functional groups. ISEs with Na^+ ionophore

I[92] and II[93, 94] have poor selectivity to K^+ vs. Na^+ in either fluorosilicone or poly(dimethylsiloxane) membranes. Interestingly, ISEs with Na^+ ionophore III, which differs from Na^+ ionophore II in that the phenyl and benzyl substituents on the amides are replaced with cyclohexyl groups, had much better selectivity to Na^+ vs. K^+ [92] (log $K_{Na,K}$ = –1.8, log $K_{Na,Ca}$: –3.0) when the membrane was cast directly on a Ag electrode, but a membrane with the same ionophore and fluorosilicone membrane in a conventional setup with inner filling solution had much worse reported selectivity (log $K_{Na,K}$: –0.76, log $K_{Na,Ca}$: –0.65).[94] It should be noted that the anionic site used for each ISE was different. In the former case, sodium tetraphenylborate (NaTPB) was employed, and in the latter case, the more bulky and hydrobphobic sodium tetrakis[3,5-bis(trifluoromethyl)phenyl]borate (Na TFPB) was used. The reasons for the selectivity difference between the two reports are unknown, but it seems unlikely that the difference in identity of ionophore alone would be the cause. If anything, the more bulky TFPB would be expected to be a better anionic site due to its larger size and better stability.

Table 1.1. Na^+-selective silicone-based ISEs reported in the literature without addition of plasticizer. Entries are grouped by ionophore and then by silicone.

silicone	transducer	ionophore	ionic site[b]	response slope (mV/decade)	log K_{ij}	Ref
Dow 730	Ag metal	Na^+ ionophore I	KTpClPB	48	NA	92
Dow 730	SiO_2 on ISFET	Na^+ ionophore II	NaTFPB	55	K^+: –0.8 Ca^{2+}: –1.2	93
Dow 3140	Ag/AgCl with IFS[a]	Na^+ Ionophore II	NaTFPB	53	K^+: –0.59 Ca^{2+}: –1.22	94
Dow 730	Ag/AgCl with IFS	Na^+ Ionophore II	NaTFPB	41	K^+: +0.10 Ca^{2+}: +1.85	94
Dow 730	SiO_2 on ISFET	Na^+ ionophore II	KTpClPB	56	K^+: –0.7 Ca^{2+}: –1.0	93
Dow 3140	Ag/AgCl with IFS	Na^+ Ionophore III	NaTFPB	36	K^+: 0.00 Ca^{2+}: –0.58	94
Dow 730	Ag metal	Na^+ ionophore III	NaTPB	55	K^+: –1.8 Mg^{2+}: –3.4 Li^+: –1.3 Ca^{2+}: –3.0	92
Dow 730	Ag/AgCl with IFS	Na^+ Ionophore III	NaTFPB	49	K^+: –0.76 Ca^{2+}: +0.65	94
Siloprene K-1000 with crosslinker K-11	SiO_2 on a silicon nanowire FET	Na^+ ionophore IV	KTpClPB	72	N.R.	95
Siloprene K-1000 with crosslinker K-11	Na^+ alginate gel coated SiO_2 on a silicon nanowire FET	Na^+ ionophore IV	KTpClPB	58	N.R.	95
Siloprene K-1000 with crosslinker K-11	Ag/AgCl with IFS	Na^+ ionophore IV	KTpClPB	48	N.R.	95
Dow 3140	Ag/AgCl with IFS	Na^+ Ionophore VI	NaTFPB	57	K^+: –1.49 Ca^{2+}: –3.06	94

Dow 730	Ag/AgCl with IFS	Na^+ Ionophore VI	NaTFPB	56	K^+: –1.62 Ca^{2+}: –3.13	94
Dow 730	SiO_2 on ISFET	Na^+ ionophore VI	NaTFPB	56	K^+: –2.3 Ca^{2+}: –3.9	93
Dow 730	SiO_2 on ISFET	Na^+ ionophore VI	KTpClPB	55	K^+: –2.1 Ca^{2+}: –3.6	93
Shin-Etsu Fluorosilicone gel (FE-73) (hydrosilylation)	Ta_2O_5 on α-InGaZnO	Na^+ ionophore VI	NaTFPB	55	K^+: <–1.7	96
Dow 3140	Ag/AgCl with IFS[a]	Na^+ ionophore X	NaTFPB	59	K^+: –2.5 Ca^{2+}: –3.4	97
Dow 3140	Ag/AgCl with IFS[a]	Na^+ ionophore X	NaTFPB	57	K^+: –2.73 Ca^{2+}: –4.15	94
Dow 3140	Ag/AgCl with IFS[a]	Na^+ ionophore X	KTFPB	60	K^+: –2.6 Ca^{2+}: –4.2	98
Shin-Etsu KE44T	ISFET SiO_2	Na^+ ionophore X	none	sub-Nernstian	N.R.	77
Shin-Etsu KE47T	ISFET SiO_2	Na^+ ionophore X	none	Nernstian	K^+: –2.4 Ca^{2+}: –3.9 H^+: –3.0 NH_4^+: –4.1[c]	99
Dow 730	Ag/AgCl with IFS[a]	Na^+ ionophore X	NaTFPB	57	K^+: –2.82 Ca^{2+}: –4.10	94
Dow 730	Poly(3-octylthiophene)-coated SiO_2 on silicon wafer	Na^+ ionophore X	KTFPB	55–57	K^+: –3.6 Ca^{2+}: –4.0	100
Dow 730	SiO_2 on ISFET	Na^+ ionophore X	NaHFPB	57	K^+: –3	101
Shin-Etsu Fluorosilicone gel (FE-73) (hydrosilylation)	Ta_2O_5 on α-InGaZnO	Na^+ ionophore X	NaTFPB	57	K^+: <–2.3	96
PSCN(2.8)[c]	p-HEMA[d] coated on SiO_2 gate of ISFET	Na^+ ionophore X	KTPB	60	K^+: –2.6 Ca^{2+}: –3.5	87

PSCN(2.8) [c]	p-HEMA[d] coated on SiO_2 gate of ISFET	Na^+ ionophore X	covalently attached KTPB 2	not reported	K^+: –2.5 Ca^{2+}: <–3.4	[87]
PSCN(10) [c]	p-HEMA[d] coated on SiO_2 gate of ISFET	Na^+ ionophore X	KTPB	not reported	K^+: –3.0 Ca^{2+}: –3.4	[87]
PSCN(10) [c]	p-HEMA[d] coated on SiO_2 gate of ISFET	Na^+ ionophore X	covalently attached KTPB 2	not reported	K^+: –2.7 Ca^{2+}: –3.4	[87]
PSCN(10) [c]	p-HEMA[d] coated on SiO_2 gate of ISFET	Na^+ ionophore X	KTFPB	Nernstian	K^+: –2.9 Ca^{2+}: –3.6 Mg^{2+}: –4.1	[88]
PSCN(10) [c]	p-HEMA[d] coated on SiO_2 gate of ISFET	Na^+ ionophore X	covalently attached KTPB 3	Nernstian	K^+: –2.7 Ca^{2+}: –3.5 Mg^{2+}: –3.9	[88]
PSCN(10) [c]	p-HEMA[d] coated on SiO_2 gate of ISFET	Na^+ ionophore X	KTFPB	not reported	K^+: –2.5 Ca^{2+}: –3.8 Mg^{2+}: –3.5	[91]
PSCN(10) [c]	p-HEMA[d] coated on SiO_2 gate of ISFET	Na^+ ionophore X	covalently attached KTPB 3	not reported	K^+: –2.6 Ca^{2+}: –3.6 Mg^{2+}: –3.8	[91]
Shin-Etsu KE47T	ISFET SiO_2	mobile oligosiloxane-modified calix[4]arene 1	none	Nernstian	K^+: –2.4[c] Ca^{2+}: –4.0 H^+: –3.1[c] NH_4^+: –4.2[c]	[99]
Shin-Etsu KE47T	ISFET SiO_2	mobile oligosiloxane-modified calix[4]arene 2	none	Nernstian	K^+: –2.0[c] Ca^{2+}: –3.8 H^+: –1.0[c] NH_4^+: –2.8[c]	[99]
Shin-Etsu KE47T	ISFET SiO_2	mobile oligosiloxane-modified calix[4]arene 3	none	Nernstian	K^+: –2.5	[102]

Shin-Etsu KE47T	Ag/AgCl with NaCl IFS[a]	mobile oligosiloxane-modified calix[4]arene 3	none	Nernstian	K^+: –2.5	[103]
Shin-Etsu KE47T	Ag/AgCl with IFS[a]	mobile oligosiloxane modified calix[4]arene 4	none	59	K^+: –1.9[c] Ca^{2+}: –3.7[c]	[104]
PDMS Shin-Etsu KE44T	ISFET SiO_2	unsymmetrical calix[4]arene 1	none	Nernstian	K^+: –2.5	[77]
PDMS Shin-Etsu KE44T	ISFET SiO_2	unsymmetrical calix[4]arene 3	none	Nernstian	not reported	[77]
PDMS Shin-Etsu KE44T	ISFET SiO_2	unsymmetrical calix[4]arene 4	None	Sub-Nernstian	not reported	[77]
PSCN(10) [c]	p-HEMA[d] coated on SiO_2 gate of ISFET	unsymmetrical calix[4]arene 5	covalently attached KTPB 2	not reported	K^+: –2.5 Ca^{2+}: –3.1	[87]
PSCN(10) [c]	p-HEMA[d] coated on SiO_2 gate of ISFET	unsymmetrical calix[4]arene 5	covalently attached KTPB 2	not reported	K^+: –2.4 Ca^{2+}: –3.0	[87]
Shin-Etsu KE47T	Ag/AgCl with IFS	covalently attached calix[4]arene 1	covalently attached NaTPB 1	59	K^+: –2.4	[105]
Shin-Etsu KE47T	Ag/AgCl with IFS	covalently attached calix[4]arene 1	NaTFPB	59	K^+: –2.2	[105]
PSCN(2.8) [c]	p-HEMA[d] coated on SiO_2 gate of ISFET	covalently attached calix[4]arene 2	KTPB	not reported	K^+: –2.6 Ca^{2+}: –3.2	[87]
PSCN(2.8) [c]	p-HEMA[d] coated on SiO_2 gate of ISFET	covalently attached calix[4]arene 2	covalently attached KTPB 2	54–57	K^+: –2.0 Ca^{2+}: NA	[87]

PSCN(10) [c]	p-HEMA[d] coated on SiO_2 gate of ISFET	covalently attached calix[4]arene 2	KTPB	not reported	K^+: –2.5 Ca^{2+}: –3.4	87
PSCN(10) [c]	p-HEMA[d] coated on SiO_2 gate of ISFET	covalently attached calix[4]arene 2	covalently attached KTPB 2	not reported	K^+: –2.3 Ca^{2+}: –3.1	87
PSCN(10) [c]	p-HEMA[d] coated on SiO_2 gate of ISFET	covalently attached calix[4]arene 2	KTFPB	not reported	K^+: –2.6 Ca^{2+}: –3.7 Mg^{2+}: –3.6	91
PSCN(10) [c]	p-HEMA[d] coated on SiO_2 gate of ISFET	covalently attached calix[4]arene 2	covalently attached KTPB 3	not reported	K^+: –2.4 Ca^{2+}: –3.6 Mg^{2+}: –3.8	91
Shin-Etsu KE47T	Ag/AgCl with IFS[a]	covalently attached 16-crown-5	NaTFPB	59	K^+: –1.2	105

[a] Abbreviation for inner filling solution

[b] See Figure 1.14 for the structure of the anionic sites. Note that the cations are also listed for the mobile ionophores. For example potassium tetraphenylborate (TPB) is abbreviated KTPB.

[c] Refers to a terpolymer containing dimethylsiloxane, cyanopropylmethylsiloxane, and methacryloxypropylmethylsiloxane. The structure is shown in Figure 1.13. It is abbreviated as PSCN(*x*) where *x* refers to the molar fraction of cyanopropylmethylsiloxane units.

[d] Abbreviation for pH buffered poly(2-hydroxyethylmethacrylate) hydrogel

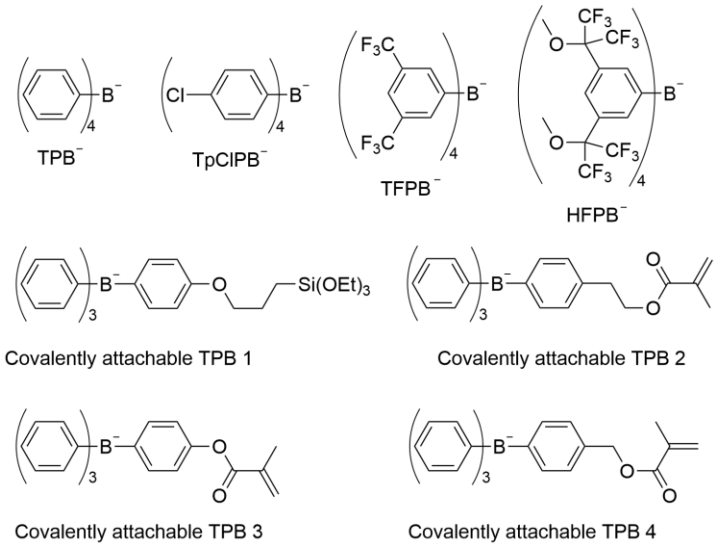

Figure 1.14. Anionic sites used for ISEs reported in the literature.

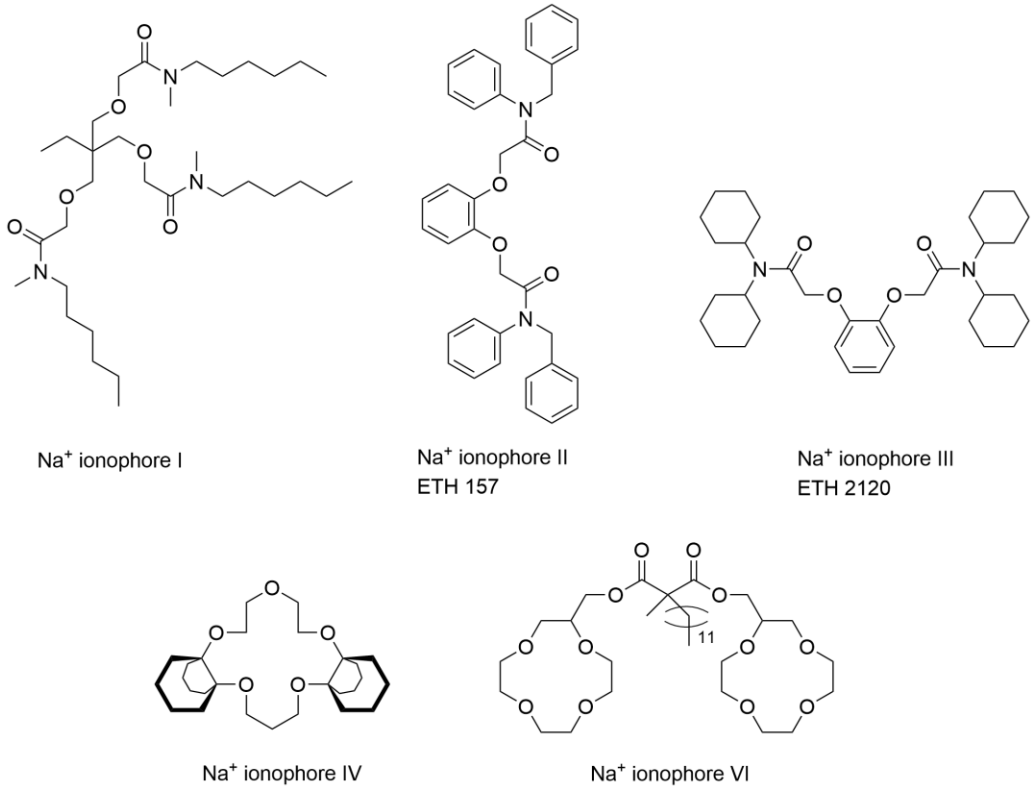

Figure 1.15. Na^+ ionophores used in the literature.

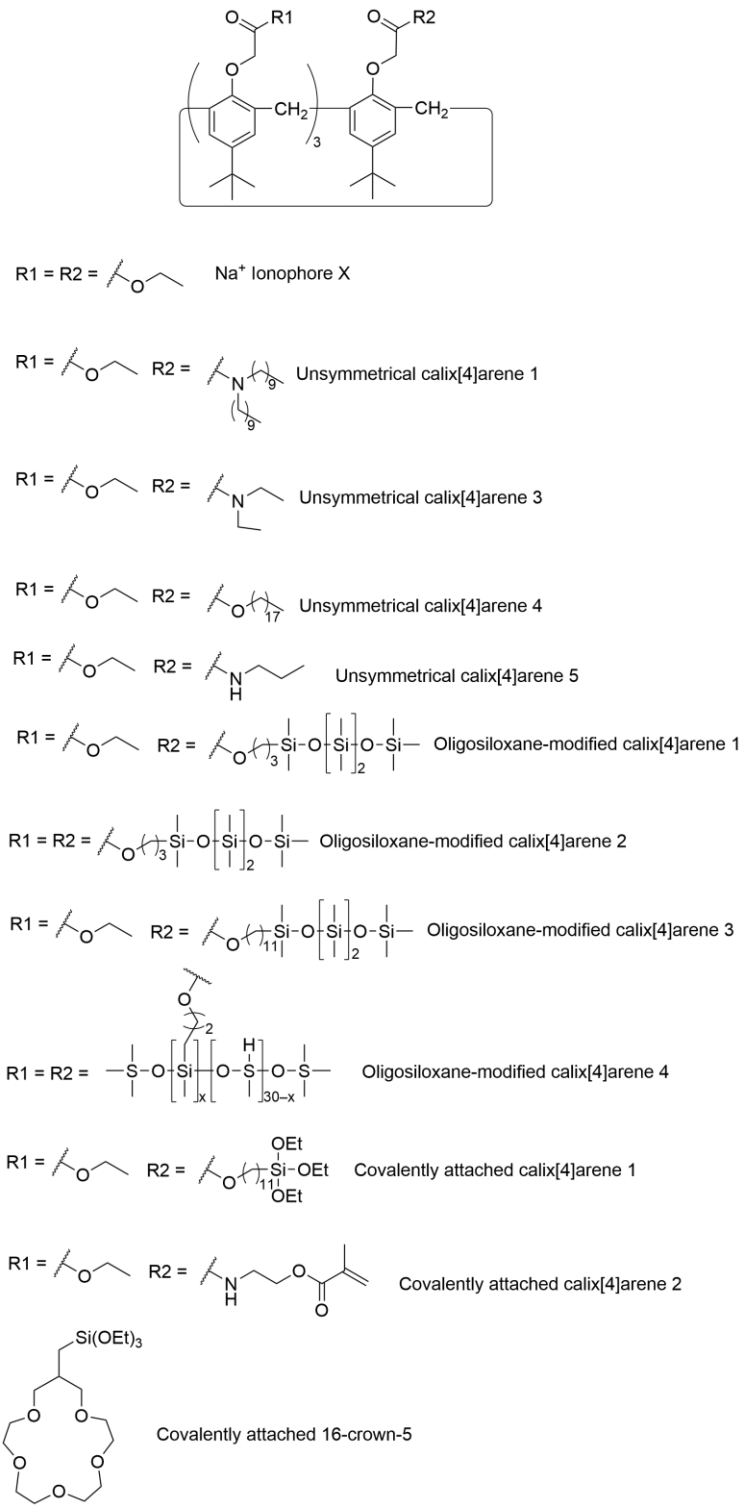

Figure 1.16. Derivatives of calix[4]arene (Na^+ ionophore X) that were either covalently attached to crosslinked silicone networks or to mobile silicone oligomers. [77, 87, 91, 99, 102-105]

The crown ether sodium ionophore IV was used in Siloprene poly(dimethylsiloxane) membranes both in conventional setups and in ISFETs. ISFETs with the membrane coated directly onto the SiO_2 gate had a super-Nernstian response to Na^+,[95] which may be caused by drifting due to pH changes in the water layer formed between the gate oxide and the ISM.[50, 106] When a pH buffered sodium alginate gel was placed between the gate oxide and the ISM, a Nernstian response of 58 mV/decade was obtained. Surprisingly, an ISE with the same membrane composition used in a conventional electrode setup with inner filling solution had a much lower response slope of 48 mV/decade. Unfortunately, no selectivity data for these ISEs was reported. It is not clear how the configuration of the membrane influences ISE performance.

Na^+ ionophore X (Figure 1.16) is a calix[4]arene derivative, and it is the most commonly reported ionophore for silicone-based ISEs. [77, 87, 88, 91, 94, 96-101] As long as anionic sites are added to the silicone membrane, the sensors have Nernstian or near-Nernstian response slopes and good selectivity to Na^+ vs. K^+ (Table 1.1). Although there are some variations in response slopes and selectivity, the composition of the silicone does not have an obvious influence on these properties. Unfortunately, not all ISMs with silicone membranes had ionic sites added. In the case of a PDMS ISM with Shin-Etsu KE47T, alcohol releasing silicone and Na^+ ionophore X added to the membrane without anionic sites, Nernstian responses[99] and good selectivity were observed. In another case using the same PDMS polymer, but with a different crosslinker (Shin-Etsu KE44T, oxime-releasing silicone) sub-Nernstian responses were observed, and selectivity was not measured.[77]

Kimura and co-workers synthesized derivatives of sodium ionophore X to make "unsymmetrical calix[4]arenes" where one of the ethyl esters was replaced with an octadecyl ester or tertiary amides (Figure 1.16).[77] ISFETs prepared with PDMS membranes (Shin-Etsu KE44T) and unsymmetrical calix[4]arene 1 and 3 (both with tertiary amides) had Nernstian responses to Na^+, but the ISM containing ionophore with the longer alkyl chains on the amide had a wider response window. ISFETs prepared with calix[4]arene 5 (octadecyl ester) had poor response slopes. Unfortunately, no anionic sites were added to these membranes, so it is difficult to determine whether the differences in response slope and linear range are caused by the ionophore itself or if there are different impurities in each ionophore contributing to the sensor response. Given other reports of functional ISEs prepared with Na^+ ionophore X and ionic sites, the latter option seems plausible.

Na^+ ionophore X was also modified with silicone oligomers with varying chain lengths (Figure 1.16).[99, 102-104] In one case, one of the ether esters on oligosiloxane-modified calix[4]arene 1 was substituted with an ester containing a linear silicone chain with four silicon atoms, in the other case, all four esters on oligosiloxane-modified calix[4]arene 2 were modified with the same silicone chain. Both had Nernstian responses to Na^+ and good selectivity to K^+ vs. Na^+. ISEs prepared with oligosiloxane-modified calix[4]arene 3, which was similar to oligosiloxane-modified calix[4] arene 1, but with 11 CH_2 spacers between the oxygen on the ester and the silicone chain also had Nernstian responses to Na^+ and good selectivity.[99] Additionally, the resistance of ISEs with these membranes was significantly lower than for the other ionophores. SEM images of the ISM surfaces showed that Na^+ ionophore X largely precipitates from the silicone membrane whereas

oligosiloxane-modified calix[4] arene 3 had fewer crystals on the electrode surface. ISFETs with oligosiloxane-modified calix[4] arene 3 were also used to measure the sodium concentration in undiluted blood serum and urine with good accuracy.[102, 103] Later, oligosiloxane-modified calix[4]arene 4 was developed in which all four esters were modified with a poly(methylhydrosiloxane).[104] Each silicone chain contained 30 Si–O repeat units (Figure 1.16). These ISEs were also used to measure the Na^+ concentration in undiluted blood serum with good accuracy.

The ionophores in the above ISEs were all mobile, even though some were functionalized with silicone chains. Therefore, these ionophores could leach from the membrane, which could limit the lifetime of the ISEs. To address this problem, ISEs were prepared with an analog of Na^+ ionophore X for which the ionophore could covalently attach to the crosslinked silicone network of condensation-curing silicones during the crosslinking step (Figure 1.16).[105] Covalently attachable calix[4]arene was synthesized where one of the ethyl esters was replaced with an undecyl ester containing a terminal triethoxysilyl functional group. ISEs prepared with this ionophore in ShinEtsu KE47T membranes had Nernstian responses to Na^+ without ionic sites and with NaTFPB (mobile ionic sites) or covalently attachable NaTPB 1, which contained a triethoxysilyl group on one of the phenyl rings. However, membranes with anionic sites (mobile or covalently attached) had much better lower detection limits ($< 10^{-6}$ M) and faster response times (<10 s) than membranes without ionic sites (~1 mM lower detection limit and ~60 s response time).

Membranes with cyanopropylmethylsiloxanes (Figure 1.13) were also used to prepare Na^+-selective ISFETs with calix[4]arene derivatives as ionophore.[87, 88, 91] The SiO_2 gates on the ISFETs were all coated with a pH buffered poly(2-hydroxyethylmethacrylate) hydrogel (abbreviated as p-HEMA in Table 1.1) to prevent the ISFETs from responding to CO_2 concentration. Since the cyanopropylmethylsiloxane is a terpolymer containing a small amount of methacryloxy functional groups for crosslinking, the ISM would covalently attach the p-HEMA hydrogel. ISFETs with Na^+ ionophore X and membranes containing 2.8 wt% or 10 wt% cyanopropylmethylsiloxane as copolymer had Nernstian responses to Na^+ and comparable selectivity to Na^+ vs. K^+. ISFETs were also prepared with covalently attachable KTPB 2[87] and KTPB 3[91] as ionic sites, which both have methacryloxy functional groups. Covalent attachment of the ionic site did not seem to affect selectivity significantly. Later, another type of ionic site was reported, KTPB 4 (Figure 1.14), which is similar in structure, the only difference being the number of CH_2 spacers between the phenyl group and the methacryloxy group.[89]

The covalently attachable calix[4] arene 2 in which one ethyl ester was replaced with an amide containing a methacryloxy functional group (Figure 1.16) was synthesized to allow covalent attachment of the ionophore to the copolymer during crosslinking.[87, 91] The authors claimed that covalent attachment of the ionophore to the copolymer resulted in slight worsening of selectivity to Na^+ vs. K^+ for membranes with both 2.8% and 10% cyanopropylmethylsiloxane. To understand the origin of the slight selectivity decrease, unsymmetrical calix[4]arene 5 was synthesized in which one of the ethyl esters was replaced with a propanamide group.[87] The authors claimed that the worsened selectivity

was caused by substitution of the ester with the propanamide group (log $K_{Na,Ca}$: –2.5, log $K_{Na,Ca}$: –3.1) and not by covalent attachment. That said, it is not obvious that the observed differences in selectivity for ISFETs with covalently attachable calix[4]arene 2 and Na^+ ionophore X are statistically significant since log $K_{Na,K}$ ranges from –2.5 to –3.0 and log $K_{Na,Ca}$ from –3.4 to –3.8 for ISFETs prepared with mobile Na^+ ionophore X with 2.8% and 10% cyanopopylmethylsiloxane copolymers. Where covalent attachment of membrane components stood out was during long-term exposure to aqueous sample solutions. Membranes with both covalently attachable calix[4]arene 4 and covalently attachable KTPB 2 maintained their responses to Na^+ and good selectivity after 90 days exposure to aqueous solution, whereas membranes in which at least one of the components was mobile lost their response or selectivity.[87]

1.7. K^+-selective membranes with plasticizer-free silicone ISMs

Most ISEs or ISFETs with plasticizer-free silicone membranes contain valinomycin as the ionophore (Table 1.2 and Figure 1.17). [50, 78, 79, 82, 89, 92, 93, 95, 97, 100, 107-112] For the most part, ISEs with valinomycin have excellent selectivity to K^+ vs. Na^+, regardless of the silicone used for the ion-selective membrane matrix. One challenge with interpreting selectivity data is that the value for selectivity can be biased by primary ions in the membrane contaminating the sample.[113, 114] Therefore, one must ensure that the sensor responds to the interfering ion during the selectivity measurement experiment. In plasticized PVC membranes, the unbiased selectivity coefficient was determined to be log $K_{K,Na} = -4.5$, which is significantly better than most reports of selectivity shown in Table 1.2,[113] but in agreement with a few reports for ISEs with PDMS[107] and fluorosilicone[93, 107] membranes.

Table 1.2. K^+-selective silicone-based ISEs reported in the literature without addition of plasticizer. See Table 1.1 for abbreviation definitions.

silicone	transducer	ionophore	ionic site	response slope (mV/decade)	log K_{ij}	notes	Ref
Dow 3140	Ag/AgCl with IFS	valinomycin	none	55	Na^+: –3.7 Ca^{2+}: –3.7		97
Dow 3140	Ag/AgCl with IFS	valinomycin	KTpClPB	56	Na^+: –3.6 Ca^{2+}: –3.7		97
Dow 3140	Ag/AgCl with IFS	valinomycin	KTFPB	57	Na^+: –3.8 Ca^{2+}: –3.9		97
Dow 3140	Ag/AgCl with IFS (0.1 M KCl)	valinomycin	KTpClPB	55	Na^+: –4.6		107
Dow 3140	Membrane coated onto Ag/AgCl	valinomycin	KTFPB	57	Na^+: –4.2 Li^+: –4.4 NH_4^+: –2.0 Ca^{2+}: –4.8 Mg^{2+}: –4.9		108
Dow 3140	Ag/AgCl with IFS	valinomycin	KTpClPB	56	Na^+: –3.6 Ca^{2+}: –3.7		97
Dow 3140	Ag/AgCl with IFS	valinomycin	KTFPB	57	Na^+: –3.8 Ca^{2+}:–3.9		97
Dow 3140	SiO_2 on ISFET	valinomycin	none	56	Na^+: <–3.7		78
Dow 3140	SiO_2 on ISFET	valinomycin	KTpClPB	56	Na^+: <–3.7		78
Silopren K1000 with crosslinker KA-1	SiO_2 on ISFET	valinomycin	none	56	Na^+: <–3.7		78
Silopren K1000 with crosslinker KA-1	SiO_2 on ISFET	valinomycin	KTpClPB	55	Na^+: <–3.7		78
Siloprene K1000 with KA-1 crosslinker	Ag/AgCl with inner filling solution	valinomycin	none	58	not reported	drop cast from solution in CH_2Cl_2	109

Siloprene K1000 with KA-1 crosslinker	Ag/AgCl with inner filling solution	valinomycin	none	57	not reported	mixed valinomycin with silicone (no solvent)	[109]
Silopren K1000	Ag/AgCl/Membrane	valinomycin	none	56	not reported	The membrane is in contact with Ag/AgCl and the potential is dependent on osmotic strength of the sample. Used in whole blood.	[110]
Siloprene K-1000 with crosslinker K-11	SiO_2 on a silicon nanowire FET	valinomycin	KTpClPB	57	not reported		[95]
Siloprene K-1000 with crosslinker K-11	Ag/AgCl with IFS	valinomycin	KTpClPB	55	not reported		[95]
Silopren K1000 with hexamethoxydislane as crosslinker	Ag/AgCl with KCl IFS	valinomycin	none	59	Na^+: <–4[a]	<10 μV/h drift	[82]
Wacker RTV-ME 625 (hydrosilylation)	SiO_2 on ISFET	valinomycin	not mentioned	no response	NA	irreproducible electrodes	[78]
Silastic E (Dow Corning)	Ag/AgCl with KCl IFS	valinomycin	none	Nernstian	Na^+: –3.5	used to measure K^+ concentration in rat brain	[79]
Silastic E (Dow Corning)	Ag/AgCl with inner filling solution	valinomycin	none	not reported	Na^+: –3.5		[79]
Dow silicone medical grade adhesive	ISFET SiO_2	valinomycin	none	Nernstian	not reported		[50]

Dow 730	Ag metal	valinomycin	KTpClPB	57	Na^+: –3.8 Li^+: –4.3 Ca^{2+}: –4.8		[92]
Dow 730	Ag/AgCl with IFS (0.1 M KCl)	valinomycin	KTpClPB	55	Na^+: –4.7		[107]
Dow 730	SiO_2 on ISFET	valinomycin	KTFPB	58	Na^+: –4.5		[93]
Dow 730	SiO_2 on ISFET	valinomycin	KTpClPB	56	Na^+: –4.2		[93]
Dow 730	Poly(3-octylthiophene)-coated SiO_2 on silicon wafer	valinomycin	NaTFPB	57–58	Na^+: –3.9 Ca^{2+}: –4.5	removed filler ETH 500 as electrolyte	[100]
PSCN(10)	SiO_2 on ISFET	valinomycin	KTFPB	55	Na^+: <–3.5 Ca^{2+}: <–3.5 Mg^{2+}: <–3.5		[111]
PSCN(2.8)	p-HEMA coated on SiO_2 gate of ISFET	valinomycin	KTFPB	Nernstian	Na^+: <–3.0		[89]
Hydroxy-terminated poly(cyanopropylmethyl)-co-dimethyl)siloxane (10–12% cyanopropylmethyl) with $SiCl_4$ as crosslinker.	Ag/AgCl with IFS	valinomycin	KTpClPB	56.5	Na^+: –4.16		[112]
Dow 730	SiO_2 on ISFET	BME-44	KTFPB	57	Na^+: –3.5		[93]
Dow 730	SiO_2 on ISFET	BME-44	KTpClPB	57	Na^+: –3.1		[93]
Silopren K1000 with crosslinker KA-1	SiO_2 on ISFET	hemispherand 1	none	56	Na^+: <–3.1		[78]
Silopren K1000 with crosslinker KA-1	SiO_2 on ISFET	hemispherand 1	none	56	Na^+: <–3.1		[78]
PSCN(2.8)	p-HEMA coated on SiO_2 gate of ISFET	hemispherand 1	KTFPB	Nernstian	Na^+: <–3.0		[89]
PSCN(2.8)	p-HEMA coated on SiO_2 gate of ISFET	hemispherand 2	KTFPB	Nernstian	Na^+: <–3.0		[89]
Silopren K1000 with crosslinker KA-1	SiO_2 on ISFET	hemispherand 3	none	55	Na^+: <–3.3		[78]

Silopren K1000 with crosslinker KA-1	SiO_2 on ISFET	hemispherand 4	none	55	Na^+: <–3.3		[78]
PSCN(10)	p-HEMA coated on SiO_2 gate of ISFET	covalently attached hemispherand 1	covalently attached KTPB 4	56	Na: –3.2		[89]
PSCN(2.8)	p-HEMA coated on SiO_2 gate of ISFET	covalently attached hemispherand 1	covalently attached KTPB 4	not reported	not reported	electrodes had poor slopes due to low solubility of components.	[89]
PSCN(2.8)	p-HEMA coated on SiO_2 gate of ISFET	covalently attached hemispherand 1	KTFPB	56	Na^+: <–3.0		[89]
PSCN(2.8)	p-HEMA coated on SiO_2 gate of ISFET	dimethoxy calix[4]arene crown ether 1	KTFPB	Nernstian	Na^+: <–3.0		[89]
PSCN(10)	p-HEMA coated on SiO_2 gate of ISFET	calix[4]arene crown ether 2	KTFPB	not reported	Na^+: –4.2 Ca^{2+}: –4.0 Mg^{2+}: –3.8		[91]
PSCN(10)	p-HEMA coated on SiO_2 gate of ISFET	covalently attached calix[4]arene crown ether 2	KTFPB	not reported	Na^+: –4.2 Ca^{2+}: –3.8 Mg^{2+}: –3.6		[91]
PSCN(10)	p-HEMA coated on SiO_2 gate of ISFET	calix[4]arene crown ether 2	covalently attached KTPB 3	not reported	Na^+: –4.3 Ca^{2+}: –4.0 Mg^{2+}: –3.8		[91]
PSCN(10)	p-HEMA coated on SiO_2 gate of ISFET	covalently attached calix[4]arene crown ether 2	covalently attached KTPB 3	not reported	Na^+: –4.4 Ca^{2+}: –3.9 Mg^{2+}: –4.0		[91]

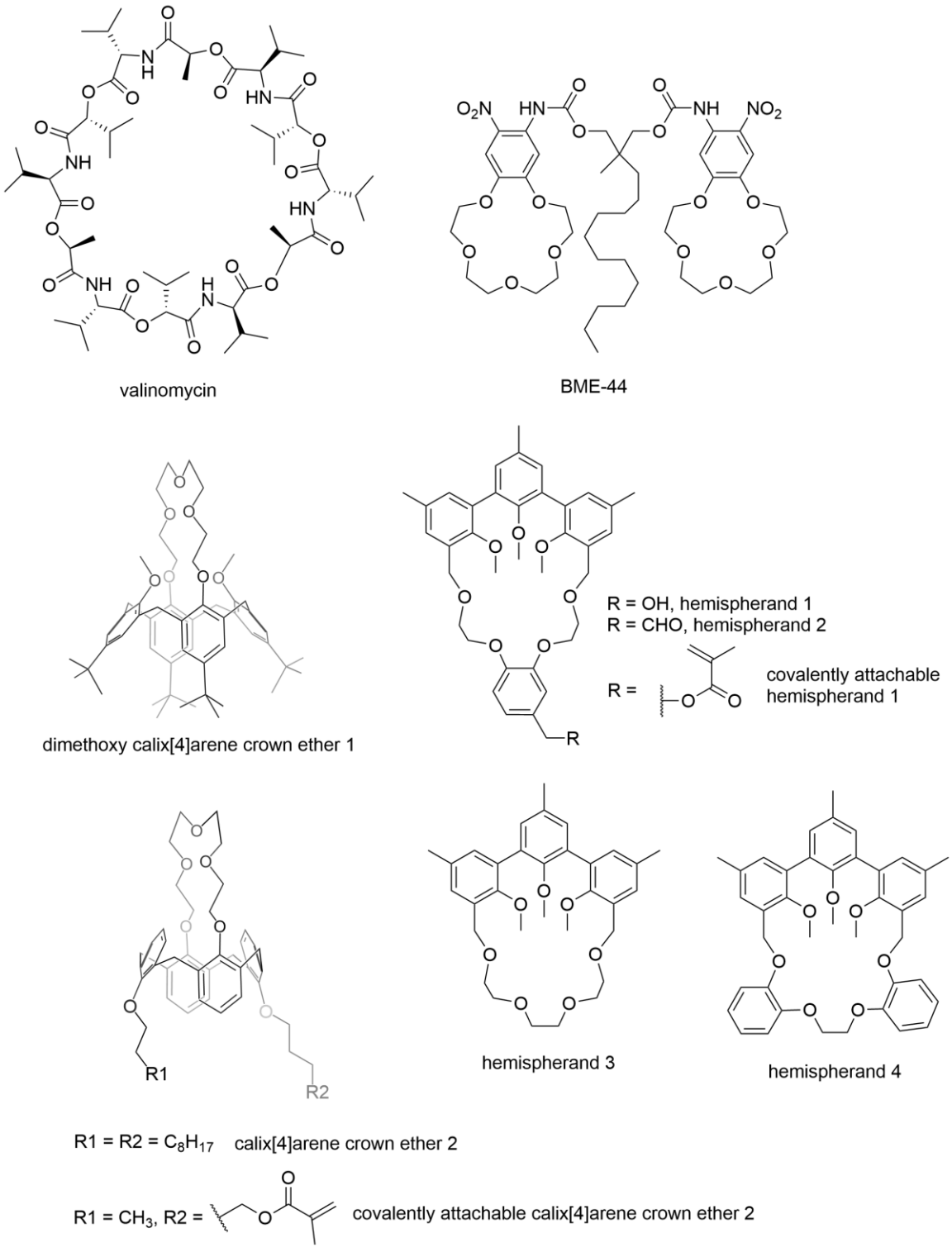

Figure 1.17. K^+ ionophores used in plasticizer-free K^+ ISEs or ISFETs.

Van der Wal and coworkers attempted to make ISFETs with hydrosilylation crosslinking PDMS membranes (Wacker RTV-ME 625) and found that 4 wt% valinomycin inhibits the curing reaction.[78] Membranes could be crosslinked when <1 wt% valinomycin was present, suggesting that valinomycin interacts with the Pt catalyst. Unfortunately, crosslinked membranes prepared with 1 wt% valinomycin did not respond to K^+.

ISFETs with fluorosilicone membranes (Dow 730) and BME-44 (Figure 1.17) as the ionophore with KTFPB or KTpClPB as the anionic sites have also been reported.[93] These ISFETs have Nernstian responses to K^+ and acceptable selectivity to K^+ vs. Na^+. Selectivity is better for ISFETs prepared with KTFPB as ionic sites (log $K_{K,Na}$: –3.5) as compared with KTpClPB (log $K_{K,Na}$: –3.1), though it is not clear whether the difference is statistically significant.

Several hemispherand ligands (Figure 1.17) were evaluated in PDMS membranes (Silopren K1000 with crosslinker KA-1) and in membranes prepared with 2.8% and 10% cyanopropyl-modified terpolymers containing a small amount of methacryloxy functional groups for photo-initiated crosslinking (Figure 1.13). ISEs in both matrixes with mobile hemispherand ligands have acceptable selectivity to K^+ vs. Na^+ (log $K_{K,Na}$ <3.0).[78, 89] Unfortunately, a rigorous measurement of selectivity for these membranes was not performed, so we do not know if the selectivity is actually better than reported. Covalently attachable hemispherand 1, with a methacryloxy functional group for covalent attachment to the cyanopropylmethylsiloxane terpolymer was also used in ISEs. No change in selectivity or response slope was observed when either KTFPB or the covalently attachable ionic site, KTPB 4 (Figure 1.14) was used.[89] Membranes with covalently attachable

ionophore 1 and were also prepared. The ionophore and ionic sites in membranes with 2.8% cyanopropylmethyl siloxane precipitated before crosslinking due to poor solubility in the polymer, and the resulting ISFETs had poor response slopes. The solubility of the covalently attachable hemispherand 1 and covalently attachable TPB 4 was better in membranes with 10% cyanopropylmethyl siloxane units.

ISFETs with calix[4]arene crown ethers have also been prepared with membranes containing cyanopropyl-modified siloxane membranes. ISFETs with dimethoxy calix[4]arene crown ether 1 in 2.8% cyanopropylmethylsiloxane had Nernstian responses to K^+ and good selectivity to K^+ vs. Na^+.[89] ISFETs with calix[4]arene crown ether 2 (without the dimethoxy groups on the phenyl rings) had excellent selectivity to K^+ vs. Na^+ with log $K_{K,Na} = -4.2$ for membranes containing covalently attached KTFPB in the 10% cyanopropylmethyl siloxane terpolymer matrix.[91] ISFETs with covalently attached calix[4]arene crown ether 2 and either mobile ionic sites (KTFPB) or covalently attached KTPB 3 (Figure 1.14) had similar responses and selectivity. ISFETs with covalently attached crown ether 2 had excellent selectivity to K^+ vs. Na^+, rivaling the selectivity of valinomycin.

1.8. Ca^{2+} selective electrodes with plasticizer-free silicone ISMs

Ca^{2+}-selective ISEs have been studied with several different ionophores and anionic sites (Table 1.3 and Figure 1.18). ISEs with ETH-1001 have Nernstian response to Ca^{2+} and good selectivity to Ca^{2+} vs. Na^{+}. However, unlike for Na^{+} and K^{+} ISEs, the anionic sites have a noticeable influence on the response slopes. ISEs with KTpClPB as the anionic site have sub-Nernstian responses to K^{+} in PDMS membranes[97, 107] (Dow 3140) and near-Nernstian responses in fluorosilicone[107] (Dow 730) membranes. When the more hydrophobic anionic sites KTFPB are used, Nernstian responses are observed in PDMS membranes.[97, 115-117] Notably, some solid-contact ISEs are reported for Ca^{2+} selective electrodes using poly(aniline nanoparticles),[115] a poly(aniline)/few layer graphene composite,[117] and poly(3-octylthiophene).[116] The only quantitative long-term drift value reported for the SC-ISEs is with the few layer graphene/poly(aniline) solid contact (200 µV/h).

Table 1.3. Ca^{2+}-selective silicone-based ISEs reported in the literature without addition of plasticizer. See Table 1.1 for silicone and transducer abbreviations.

silicone	transducer	ionophore	ionic site	response slope (mV/decade)	log K_{ij}	notes	Ref
Dow 3140	Ag/AgCl with IFS	ETH 1001	KTpClPB	22	Na^+: –3.4 K^+: –3.4	resistance: 1 GΩ	97
Dow 3140	Ag/AgCl with IFS	ETH 1001	KTFPB	28	Na^+: –3.6 K^+: –3.4	resistance: 500 MΩ	97
Dow 3140	Ag/AgCl with IFS (0.1 M $CaCl_2$)	ETH 1001	KTpClPB	13	K^+: +0.6 Na^+: –1.7		107
Dow 3140	poly(aniline) nanoparticles	ETH 1001	KTFPB	31	Na^+: –3.0 K^+: –3.0 H^+: –3.1		115
Dow 3140	poly(3-octylthiophene)	ETH 1001	KTFPB	27	Na^+: –2.9 K^+: –2.9 H^+: –3.0	"driftless" SC-ISE	116
Dow 3140	few layer graphene/poly(aniline) composite	ETH 1001	KTFPB	28.7	not reported	0.2 mV/h drift	117
Silicone tube (Silastic Brand, Dow Corning)	Ag/AgCl with inner filling solution	ETH 1001	none	no response	not reported		118
Dow 730	Ag/AgCl with IFS (0.1 M $CaCl_2$)	ETH 1001	KTpClPB	25	K^+: –3.8 Na^+: –3.9		107
Silicone tube (Silastic Brand, Dow Corning) Ionophore impregnated in tube by soaking in ionophore solution in xylene	Ag/AgCl with inner filling solution	ETH 129	none	26	Na^+: –3.5	worse selectivity than –3.8 obtained for membrane with *o*-NPOE	118

Silicone tube (Silastic Brand, Dow Corning) Ionophore impregnated in tube by soaking in ionophore solution in THF	Ag/AgCl with inner filling solution	ETH 129	none	26	Na^+: –2.7		118
Dow 730	Ag metal	ETH 129	KTpClPB	31	Na^+: –4.9 K^+: –5.0 Mg^{2+}: –5.0 Li^+: –4.8		92
Dow 730	Poly(3-octylthiophene)-coated SiO_2 on silicon wafer	ETH 5234	KTFPB	26	Na^+: –3.7 K^+: –3.7	removed filler	100
PSCN(10) UV and condensation-cured[a]	SiO_2 on ISFET	ETH 5234	KTFPB	Nernstian	Na^+: <–3.5 K^+: <–3.5 Mg^{2+}: <–4		111

[a] Unique polymer that contained 10 mol% cyanopropylmethylsiloxane units, 90% poly(dimethylsiloxane) units. The polymer was endcapped with diethoxymethacryloxypropyl silane units. The polymer was capable of radical-initiated crosslinking and condensation curing.

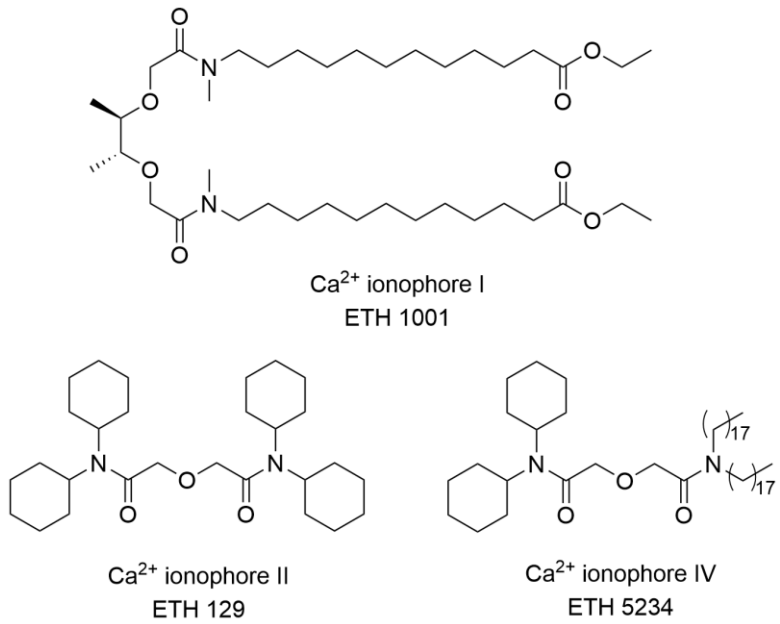

Figure 1.18. Ca^{2+} ionophores used in plasticizer-free silicone membranes.

ISEs with ETH 129 (Figure 1.18) in PDMS membranes constructed from pieces of silicone tubing (Silastic Brand from Dow Chemical) have also been reported.[118] In this system, the ionophore was impregnated into the silicone tubing by dissolving the ionophore in a solvent (xylene or THF) and soaking the silicone tubing in the ionophore solution. These ISEs had near-Nernstian responses to Ca^{2+} with acceptable selectivity to Ca^{2+} vs. Na^{+}. Unfortunately, no anionic sites were added to these membranes. Interestingly, ISEs with ETH 129 impregnated into the silicone tube using xylene (Table 1.3) have an almost one order of magnitude better selectivity to Ca^{2+} vs. Na^{+} (log $K_{Ca,Na}$: –3.5) than those prepared using THF (log $K_{Ca,Na}$: –2.7). The cause for this is not clear, although the original authors suggested that the xylene may have better compatibility with the ionophore and silicone. By far, the best selectivity with ETH 129 is for ISEs prepared with fluorosilicone Dow 730 as the polymer matrix. ISEs had slightly super-Nernstian responses to Ca^{2+} and the selectivity to Ca^{2+} vs. Na^{+} (log $K_{Ca,Na}$: –4.9)[92] was over an order of magnitude better than selectivities observed for ISEs with poly(dimethylslioxane).

ISEs have also been prepared with ETH 5234, which has a structure similar to ETH 129, one of the dicyclohexylamides being replaced with a dioctadecylamide.[100] Interestingly, the selectivity to Ca^{2+} vs. Na^{+} in Dow 730 fluorosilicone membranes is worse than for ETH 129. ISEs with ETH 5234 in 10% cyanopropylmethyl siloxane had similar selectivity to those in Dow 730 fluorosilicone membranes.

1.9. Mg^{2+}-selective electrodes with plasticizer-free silicone ISMs

There is only one report with Mg^{2+}-ISFETs without using a fluorosilicone membrane (Dow 730). ISFETs were ISEs prepared with both KTpClPB and KTFPB as anionic sites, though only ISFETs with the more hydrophobic KTFPB had good selectivity (Table 1.4). ISFETs with Mg^{2+} ionophore III (Figure 1.19) had poor selectivity,[93] but ISFETs with Mg^{2+} ionophore IV (which contains three malonamide groups instead of two) had much better selectivity to Mg^{2+} vs. Na^{+} and Mg^{2+} vs. Ca^{2+}. Selectivities for Mg^{2+} ionophore IV were similar to those reported for Mg^{2+} ionophore IV in plasticized PVC membranes (*o*-NPOE).[119]

Table 1.4. Mg^{2+}-selective silicone-based ISEs reported in the literature without addition of plasticizer.

silicone	transducer	ionophore	ionic site	response slope (mV/decade)	log K_{ij}	notes	Ref
Dow 730	SiO_2 on ISFET	Mg^{2+} ionophore III	KTFPB	29	Na^+: –1.8 K^+: –1.3 Ca^{2+}: +0.2		93
Dow 730	SiO_2 on ISFET	Mg^{2+} ionophore III	KTpClPB	26	not reported		93
Dow 730	SiO_2 on ISFET	Mg^{2+} ionophore IV	KTFPB	27	Na^+: –4.0 K^+: –2.3 Ca^{2+}: –1.2		93
Dow 730	SiO_2 on ISFET	Mg^{2+} ionophore IV	KTpClPB	26	not reported		93

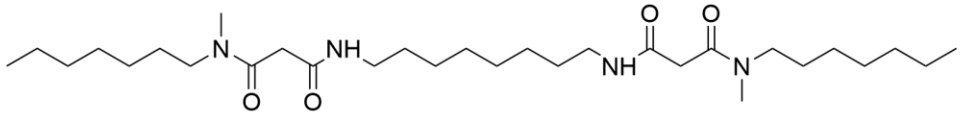

Magnesium ionophore III
ETH 4030

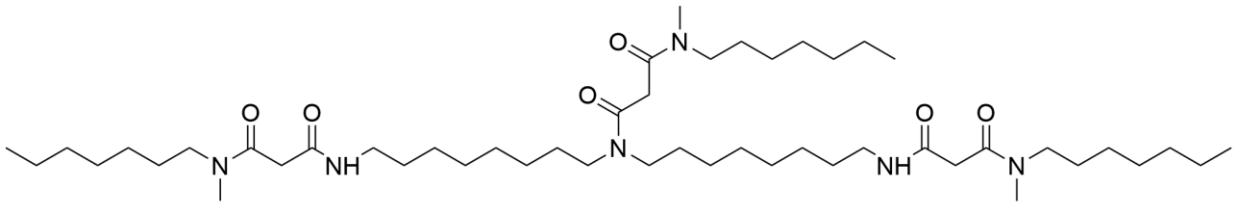

Magnesium ioophore IV
ETH 7025

Figure 1.19. Ionophores for Mg^{2+}-selective electrodes in plasticizer-free silicone membranes.

1.10. H^+-selective electrodes with plasticizer-free silicone ISMs

There are two reports of pH-selective membranes in poly(dimethylsiloxane) membranes. ISEs with tridodecylamine (TDDA , Figure 1.20) as ionophore and KTFPB as anionic sites in Dow 3140 membranes had Nernstian responses to pH (Table 1.5).[97] Unfortunately, selectivity was not reported. ISEs were prepared with the less basic ETH 2418 ionophore and KTpClPB. Selectivity was not quantified for this ionophore in the silicone matrix, but the ISE was used to measure the pH in gastric juice.[81] Plasticizer-free silicone-based ISEs outperformed their plasticized PVC counterparts in gastric juice due to less interference to the drug Dormicum, which is a sedative that was administered to the patients during the experiments.

Table 1.5. H^+-selective silicone-based ISEs reported in the literature without addition of plasticizer.

silicone	transducer	ionophore	ionic site	response slope (mV/decade)	log K_{ij}	notes	Ref
Dow 3140	Ag/AgCl with IFS	TDDA	KTFPB	60	not reported		[97]
Siloprene K1000 with 16 wt% K11 crosslinker	Ag/AgCl with IFS	ETH2418	KTpClPB	59	not reported	used in catheter to measure pH in gastric juice	[81]

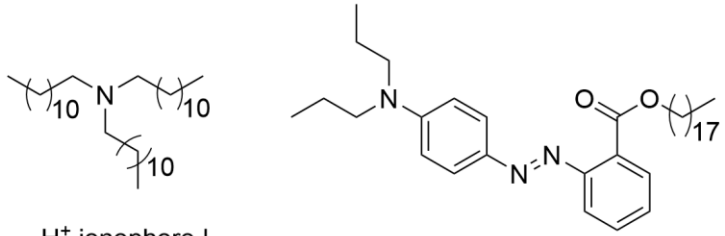

H^+ ionophore I
TDDA

ETH 2418

Figure 1.20. H^+ ionophores used in plasticizer-free silicone-based ISEs and or ISFETs.

1.11. NH_4^+-selective electrodes with plasticizer-free silicone ISMs

NH_4^+-selective electrodes have been made with fluorosilicone membranes (Dow 730).[120] There is also a second report with an unusual silicone obtained by mixing a condensation-curing silicone and a PDMS/cyanopropylmethylsiloxane copolymer containing 10–12 mol% cyanopropylmethylsiloxane units. The two polymers were mixed in a ratio of 78% condensation-curing silicone and 21% of the PDMS/cyanopropylmethylsiloxane copolymer.[112] The ISEs contained nonactin as the ionophore (Figure 1.21).[112, 120] In both cases, sub-Nernstian response slopes were observed (Table 1.6). It is difficult to judge the selectivity because proper calibration curves with and without interfering ions were not reported. That said, the reported NH_4^+ vs. Na^+ selectivity for membranes prepared with fluorosilicone Dow 730 (log $K_{NH_4, Na}$: –2.3) is the same as that observed in *o*-NPOE plasticized PVC membranes.[121] ISEs with the cyanopropylmethylsiloxane polymer had even better selectivity to K^+ vs. Na^+ (log $K_{NH_4,Na}$: –2.64).[112]

Table 1.6. NH_4^+-selective silicone-based ISEs reported in the literature without addition of plasticizer.

silicone	primary ion	transducer	ionophore	ionic site	response slope (mV/decade)	log K_{ij}	notes	Ref
Dow 730	NH_4^+	Au	nonactin	KTpClPB	46	Na^+: <–2.3	containment sensor	[120]
Condensation-cured PDMS (78%) mixed with 21% of a 10–12 mol% cyanopropylmethylsiloxane -PDMS copoylmer	NH_4^+	Ag/AgCl with IFS	nonactin	KTpClPB	50.0	Na^+: –2.64		[112]

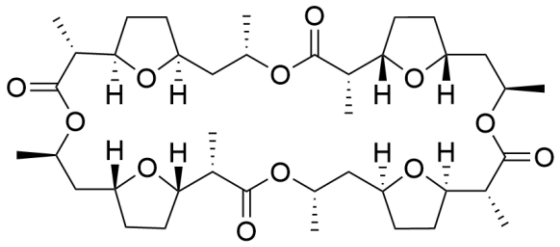

NH_4^+ ionophore I
nonactin

Figure 1.21. NH_4^+ ionophore used in plasticizer-free silicone-based ISEs.

1.12. Cs^+-selective electrodes with plasticizer-free silicone ISMs

There is only one report of Cs^+ ISFETs without plasticizer added to the silicone membrane. The ISFETs were prepared with 10% cyanopropylmethyl-modified PDMS (Figure 1.13) membranes using calix[4]arene 3 or the covalently attachable calix[4]arene 3 ionophore (Figure 1.22).[91] All ISFETs reported had Nernstian responses to Cs^+, and the selectivity to Cs^+ over interfering ions K^+ and NH_4^+ was comparable to that observed for a similar derivative of calix[4]arene crown ether 3 in a liquid *o*-NPOE membrane ($\log K_{Cs,K}$: –2.2; $\log K_{Cs,NH4}$: –2.0). The Cs^+ vs. Na^+ selectivity of the calix[4]arene crown ether 3 with mobile KTFPB anionic sites in the cyanopropylmethylsiloxane PDMS copolymer was $\log K_{Cs,Na}$: –3.4, which is slightly better than that observed in *o*-NPOE plasticized PVC membranes ($\log K_{Cs,Na}$: –3.0).[122] Calix[4] arene crown ether 3 was also covalently attached the cyanoproplymethylsiloxane membrane and no major changes in selectivity were observed. Additionally, no changes in response slope or selectivity were observed when both the ionophore and ionic sites were covalently attached.

Table 1.7. Cs^+-selective silicone-based ISEs reported in the literature without addition of plasticizer. See Table 1.1 for abbreviation definitions for the silicone and transducer.

silicone	transducer	ionophore	ionic site	response slope (mV/decade)	log K_{ij}	Ref
PSCN(10)	p-HEMA coated on SiO_2 gate of ISFET	calix[4]arene crown ether 3	KTFPB	57	Na^+: –3.4 K^+: –2.2 Ca^{2+}: –4.0 NH_4^+: –2.2	91
PSCN(10)	p-HEMA coated on SiO_2 gate of ISFET	calix[4]arene crown ether 3 covalently attached	KTFPB	58	Na^+: –3.2 K^+: –2.2 Ca^{2+}: –4.0 NH_4^+: –2.1	91
PSCN(10)	p-HEMA coated on SiO_2 gate of ISFET	calix[4]arene crown ether 3	covalently attached KTPB 4	57	Na^+: –3.2 K^+: –2.3 Ca^{2+}: –3.8 NH_4^+: –2.2	91
PSCN(10)	p-HEMA coated on SiO_2 gate of ISFET	calix[4]arene crown ether 3 covalently attached	covalently attached KTPB 4	57	Na^+: –3.2 K^+: –2.3 Ca^{2+}: –4.0 NH_4^+: –2.0	91

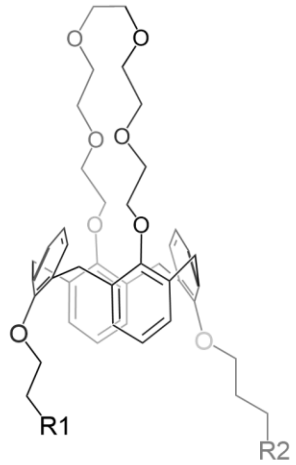

R1 = R2 = C_8H_{17} calix[4]arene crown ether 3

R1 = CH_3, R2 = 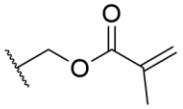 covalently attachable calix[4]arene crown ether 3

Figure 1.22. Cs^+ ionophores used in plasticizer-free ion-selective membranes.

1.13. Pb^{2+}-selective electrodes with plasticizer-free silicone ISMs

To date, three separate papers have described plasticizer-free silicone-based Pb^{2+} ISFETs. [91, 93, 123] A Pb^{2+} ISFET with a fluorosilicone membrane (Dow 730), Pb^{2+} ionophore II (Figure 1.23) and KTpClPB as anionic sites had Nernstian responses to Pb^{2+}. The authors stated that selectivity was poor, but no values were reported.[93]

ISFETs were also prepared with calix[4]arene 7 as ionophore and KTFPB as ionic sites, using a silicone copolymer with propylbenzylamidomethylsiloxane units (Figure 1.13), abbreviated PSAM(10). These membranes had near-Nernstian slopes, but they were not selective to Pb^{2+} vs. Ca^{2+}, presumably due to strong interactions between the amide functional group on PSAM(10) and Ca^{2+}. ISFETs with the same ionopohore and anionic sites, but with a silicone copolymer containing *p*-acetylphenoxypropylmethyl siloxane membranes (Figure 1.13), abbreviated PSKT(10), had much better selectivity to Pb^{2+} vs. Ca^{2+} ($\log K_{Pb,Ca}$: –4.3).[123] Interestingly, the authors noted that ISFETs with PSCN(10) did not give good responses to Pb^{2+}. ISFETs with calix[4]arene 6 as ionophore and covalently attached KTFPB 4 in PSKT(10) membranes had Nernstian responses to Pb^{2+} and similar selectivity to Pb^{2+} vs. Ca^{2+} ($\log K_{Pb,Ca}$: –4.1)[91] as those prepared with calix[4]arene 7. Covalent attachment of calix[4]arene 6 to PSKT(10) did not affect selectivity (Table 1.8).

Table 1.8. Pb^{2+}-selective silicone-based ISEs reported in the literature without addition of plasticizer.

silicone	transducer	ionophore	ionic site	response slope (mV/decade)	log K_{ij}	Ref
Dow 730	SiO_2 on ISFET	Pb^{2+} ionophore II	KTpClPB	30	not reported	93
PSKT(10)[a]	p-HEMA coated on SiO_2 gate of ISFET	calix[4]arene 6	covalently attached KTPB 4	30	K^+: –3.0 Ca^{2+}: –4.1 Cu^{2+}: –2.8 Cd^{2+}: –3.8	91
PSKT(10)[a]	p-HEMA coated on SiO_2 gate of ISFET	covalently attached calix[4]arene 6	covalently attached KTPB 4	30	K^+: –3.0 Ca^{2+}: –4.2 Cu^{2+}: –3.0 Cd^{2+}: –3.8	91
PSAM(10)[b]	p-HEMA coated on SiO_2 gate of ISFET	calix[4]arene 7	KTFPB	25	K^+: –3.7 Cu^{2+}: –3.3 Cd^{2+}: –2.8 Ca^{2+}: not selective	123
PSKT(10)[a]	p-HEMA coated on SiO_2 gate of ISFET	calix[4]arene 7	KTFPB	28	K^+: –3.3 Cu^{2+}: –3.0 Cd^{2+}: –3.8 Ca^{2+}: –4.3	123

[a] Refers to a terpolymer containing dimethylsiloxane, *p*-acetylphenoxypropylmethyl siloxane, and methacryloxypropylmethylsiloxane. The structure is shown in Figure 1.13. It is abbreviated as PSKT(x) where x refers to the molar fraction of *p*-acetylphenoxypropylmethyl units.

[b] Refers to a terpolymer containing dimethylsiloxane, propylbenzylamidosiloxane, and methacryloxypropylmethylsiloxane. The structure is shown in Figure 1.13. It is abbreviated as PSAM(x) where x refers to the molar fraction of propylbenzylamidomethylsiloxane units.

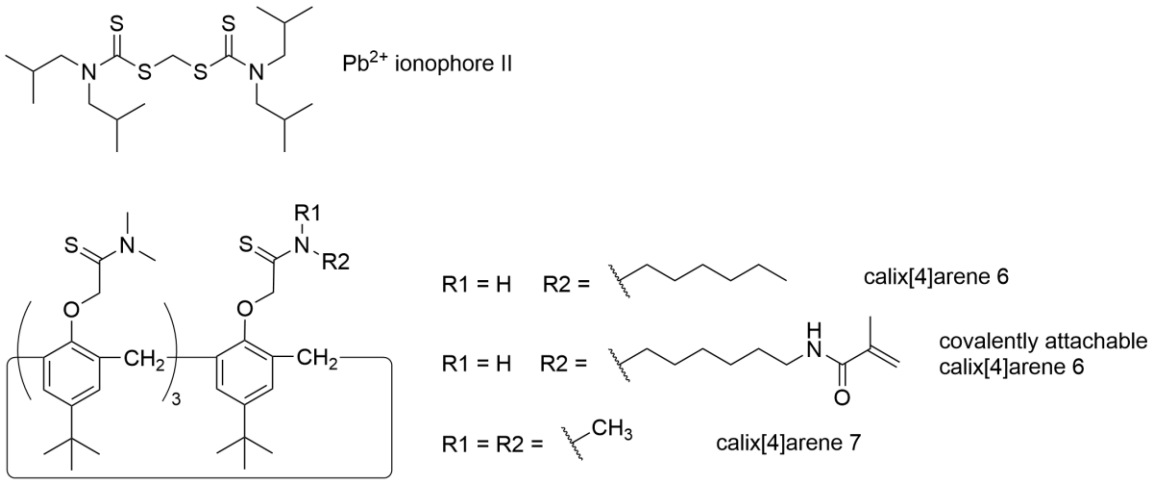

Figure 1.23. Ionophores used in Pb^{2+} ISEs with silicone matrixes without plasticizer.

1.14. Ag^+-selective electrodes with plasticizer-free silicone ISMs

Ag^+ ISFETs were prepared with fluorosilicone membranes (Dow 730, filler removed by centrifugation) with Ag^+ ionophore III, which is the same as Pb^{2+} ionophore II (Figure 1.23).[93] The ISFETs had Nernstian responses to Ag^+, but no selectivity data was provided (Table 1.9). The authors only mentioned that selectivity was poor. Ag^+ ISFETs with several different polysiloxane membranes with and without ionophore were evaluated.[123] An ion exchange membrane with PSCN(10) as the membrane matrix had Nernstian responses to Ag^+ and acceptable selectivity over other interfering ions like Ca^{2+} and K^+ (Table 1.9). Addition of calix[4]arene 8 (Figure 1.24) did not improve selectivity. No substantial improvements to selectivity were found for membranes containing calix[4]arene 8 with PSKT(10) or PSES(10) membranes. Interestingly, ISFETs with PSAM(10) responded to anions above ~1 mM, which may indicate Donnan failure and suggest that the amide groups interact with the Ag^+ ions.

Table 1.9. Ag^+-selective silicone-based ISEs reported in the literature without addition of plasticizer.

silicone	transducer	ionophore	ionic site	response slope (mV/decade)	log K_{ij}	Ref
Dow 730	SiO_2 on ISFET	Ag^+ ionophore III (this is the same as Pb^{2+} ionophore II)	KTpClPB	58	not reported	93
PSCN(10)[a]	p-HEMA coated on SiO_2 gate of ISFET	none	KTFPB	Nernstian	Ca^{2+}: –4.1 Cu^{2+}: –4.5 K^+: –4.6 H^+: –2.0 Hg^{2+}: –2.1 Cd^{2+}: –4.3	123
PSCN(10)[a]	p-HEMA coated on SiO_2 gate of ISFET	calix[4]arene 8	KTFPB	Nernstian	Ca^{2+}: –4.3 Cu^{2+}: –4.4 K^+: –4.7 H^+: –2.5 Hg^{2+}: –2.4 Cd^{2+}: –4.0	123
PSKT(10)[b]	p-HEMA coated on SiO_2 gate of ISFET	calix[4]arene 8	KTFPB	Nernstian	Ca^{2+}: –4.3 Cu^{2+}: –4.4 K^+: –4.7 H^+: –2.5 Hg^{2+}: –2.4 Cd^{2+}: –4.0	123
PSES(10)[c]	p-HEMA coated on SiO_2 gate of ISFET	calix[4]arene 8	KTFPB	Nernstian	Ca^{2+}: –3.9 Cu^{2+}: –4.4 K^+: –5.3 H^+: –2.3 Hg^{2+}: –2.1 Cd^{2+}: –3.9	123

[a] Refers to a terpolymer containing dimethylsiloxane, cyanopropylmethylsiloxane, and methacryloxypropylmethylsiloxane. The structure is shown in Figure 1.13. It is abbreviated as PSCN(*x*) where *x* refers to the molar fraction of cyanopropylmethylsiloxane units.

[b] Refers to a terpolymer containing dimethylsiloxane, *p*-acetylphenoxypropylmethylsiloxane, and methacryloxypropylmethylsiloxane.

[c] Refers to a terpolymer containing dimethylsiloxane, acetoxypropylmethylsiloxane, and methacryloxypropylmethylsiloxane.

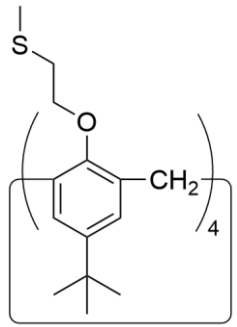

calix[4]arene 8

Figure 1.24. Ag^{+} ionophore used in plasticizer-free silicone membranes.

1.15. Cd^{2+}-selective electrodes with plasticizer-free silicone ISMs

Cd^{2+}-ISFETs have also been reported with Cd^{2+} ionophore I (Figure 1.25) and KTpClPB as anionic sites in a fluorosilicone matrix (Dow 730). They had near-Nernstian response slopes of 25 mV/decade.[93] Unfortunately, selectivity was not reported, although the authors mentioned selectivity was poor. ISFETs with calix[4]arene 9 (Figure 1.25) in PSCN(10) and PSES(10) membranes and KTFPB as anionic sits were evaluated (Table 1.10).[123] ISFETs with PSES(10) membranes had much better selectivity to Cd^{2+} vs. Ca^{2+} ($\log K_{Cd,Ca}$: –4.1) than those prepared with PSCN(10) ($\log_{Cd,Ca}$: –2.2). Selectivity for ISFETs with PSES(10) membranes were also superior to membranes comprising dioctyl phthalate-plasticized PVC ($\log K_{Cd,Ca}$: –3.8).[123] The authors also noted that the membranes were not selective to Cd^{2+} vs. Cu^{2+}, but no selectivity value was reported.

Table 1.10. Cd^{2+}-selective silicone-based ISEs reported in the literature without addition of plasticizer.

silicone	transducer	ionophore	ionic site	response slope (mV/decade)	log K_{ij}	Ref
Dow 730	SiO_2 on ISFET	Cd^{2+} ionophore I	KTpClPB	25	not reported	93
PSCN(10)[a]	p-HEMA coated on SiO_2 gate of ISFET	calix[4]arene 9	KTFPB	Nernstian	Ca^{2+}: –2.2 K^+: –1.9 Pb^{2+}: –1.4 Cu^{2+}: not selective	123
PSES(10)[b]	p-HEMA coated on SiO_2 gate of ISFET	calix[4]arene 9	KTFPB	Nernstian	Ca^{2+}: –4.1 K^+: –2.6 Pb^{2+}: –2.0 Cu^{2+}: not selective	123

[a] Refers to a terpolymer containing dimethylsiloxane, cyanopropylmethylsiloxane, and methacryloxypropylmethylsiloxane. The structure is shown in Figure 1.13.

[b] Refers to a terpolymer containing dimethylsiloxane, acetoxypropylmethylsiloxane, and methacryloxypropylmethylsiloxane.

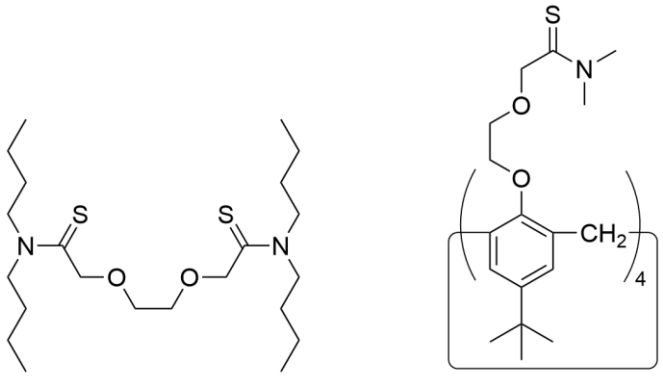

Cd^{2+} ionophore I
ETH 1062

calix[4]arene 9

Figure 1.25. Cd^{2+} ionophore used in silicone-based ISEs without plasticizer.

1.16. CO_3^{2-}-selective electrodes with plasticizer-free silicone ISMs

There is only one report in the literature of a successful preparation of a somewhat functioning carbonate ISE without addition of plasticizer.[107] A carbonate ISE doped with TFADB (Figure 1.26) in a fluorosilicone (Dow 730) membrane with TDMACl (Figure 1.27) had sub-Nernstian responses to carbonate and was selective to CO_3^{2-} over Cl^-. A similar ISE with a less polar PDMS membrane (Dow 3140) did not respond. Others have reported the use of PDMS (Dow 3140) for a CO_3^{2-} selective electrode with TFADB as ionophore, but[124] 14.2% or 21.9 wt% plasticizer (bis(2-ethylhexyl) adipate was required.

Table 1.11. CO_3^{2-}-selective silicone-based ISEs reported in the literature without addition of plasticizer.

silicone	transducer	ionophore	ionic site	response slope (mV/decade)	log K_{ij}	Ref
Dow 730	Ag/AgCl with IFS (0.1 M)	TFADB	TDMACl	–22	Cl^-: –4.0 $salicylate^-$: +2.4	[107]
Dow 3140	Ag/AgCl with IFS (0.1 M)	TFADB	TDMACl	none	not reported	[107]

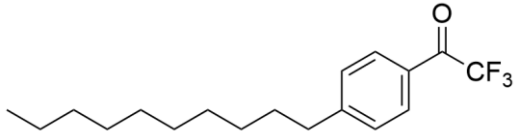

TFADB

Figure 1.26. CO_3^{2-} ionophore used in silicone-based ISEs without plasticizer.

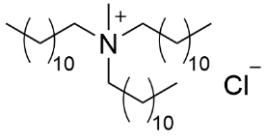

TDMACl

Figure 1.27. Cationic site used in plasticizer-free silicone-based CO_3^{2-} ISEs and NO_3^- ion exchange membranes.

1.17. NO_3^- anion exchange electrodes

Ion-exchange membranes do not contain an ionophore. Instead, only an ionic site is required to get a response to ions. In this case, selectivity follows the Hoffmeister series: ion exchange membranes are more selective to hydrophobic ions than hydrophilic ones. I have included them here since there were no plasticizers added and some of the work illustrates important points about the choice of functional groups that might be suitable for use in polymeric matrices of ISEs.

Knoll et al. demonstrated anion-exchange electrodes with Dow 730 fluorosilicone as the ionophore and tridodecylmethylammonium nitrate as the cationic site species (Figure 1.27).[120] These electrodes had Nernstian responses to NO_3^- (–57 mV/decade), with lower detection limits below 10 µM and selectivity log $K_{NO3,Cl}$ = –1.3 (Table 1.12). Addition of plasticizer (*o*-NPOE, 29.3 wt%) had little effect on the potentiometric behavior. Högg et al. reported a similar NO_3^- ion exchange membrane with centrifuged Dow 730 as the membrane matrix and tetradodecylammonium bromide as the cationic site (Figure 1.28).[93] These membranes also had Nernstian responses to K^+, though the selectivity to NO_3^- vs. Cl^- was significantly better (log $K_{NO3,Cl}$: <–2.7) than those reported by Knoll.[120]

NO_3^--selective ISFETs prepared with a cationic site, trimethoxysilylpropyl-trimethylammonium chloride (TMA) (Figure 1.28), covalently attached to a hydroxy-terminated poly(cyanopropylmethyl)siloxane/poly(dimethylsiloxane) copolymer during crosslinking had Nernstian responses to NO_3^-, but slightly worse selectivity (log $K_{NO3,Cl}$: <–2.0)[111] than that observed for the fluorosilicone membrane with mobile ionic sites (Table 1.12). The authors noted that the selectivity of the ISFET was dependent on the

crosslinking conditions, but they did not elaborate further. They did mention that attempts to incorporate covalently attachable TMA cationic site into poly(cyanopropylmethyl)silioxane/poly(dimethylsiloxane)/poly(methacryloxypropyl-methyl)siloxane copolymer (UV-cured) did not yield functional electrodes.

Reinhoudt and coworkers synthesized several silicone co-polymers of poly(dimethylsiloxane) with methracryloxy side groups and a third side group of either[90] cyanopropylmethylsiloxane (PSCN), phenylmethoxy ketone (PSKT), methyl ester (PSES), or phenylamide (PSAM) (Figure 1.13). Anion exchange membranes on pHEMA-coated ISFETs prepared with these polymers containing tetrabutylammonium as the cationic site had Nernstian responses to NO_3^-. All membranes had Nernstian or near-Nernstian responses to NO_3^-. Membranes with cyano, ketone, and ester functional groups incorporated into the silicone had good selectivity to NO_3^- vs. Cl^-, however the selectivity worsened when amide side groups were added. The authors attributed the worsened selectivity to hydrogen bonding between the amide and chloride. ISFETs with the tetrabutylammonium cationic site had limited lifetimes, presumably due to leaching from the membrane. Half of the ISFETs with 11-methacryloyloxyundecyldiethylmethyl-ammonium iodide ionic sites (Figure 1.28) covalently attached to the polymer still functioned after 190 days of exposure to running tap water.

Table 1.12. NO_3^--ion exchange electrodes reported in the literature without addition of plasticizer.

silicone	primary ion	transducer	ionophore	ionic site	response slope (mV/decade)	log K_{ij}	notes	Ref
Dow 730	NO_3^-	SiO_2 on ISFET	none	TDDABr	–58	SO_4^{2-}: –4.4 Cl^-: –2.7	ion exchange membrane	93
10–12% cyanopropylmethyl-siloxane-PDMS (condensation cured)	NO_3^-	SiO_2 on ISFET	none	covalently attached TMA	–58	SO_4^{2-}: –2.8 Cl^-: –2.0 Br^-: –0.8		111
PSCN(25)[a]	NO_3^-	p-HEMA coated on SiO_2 gate of ISFET	none	covalently attached DEMA	–57	SO_4^{2-}: –3.1 Cl^-: –2.2 Br^-: –1.0		90
PSAM(25)[b]	NO_3^-	p-HEMA coated on SiO_2 gate of ISFET	none	covalently attached DEMA	–58	SO_4^{2-}: –3.1 Cl^-: –1.5 Br^-: –0.7		90
PSCN(25)[a]	NO_3^-	p-HEMA coated on SiO_2 gate of ISFET	none	TBA^+ Br^-	–56	SO_4^{2-}: –3.2 Cl^-: –2.3 Br^-: –1.0		90
PSCN(10)[a]	NO_3^-	p-HEMA coated on SiO_2 gate of ISFET	none	TBA^+ Br^-	–57	SO_4^{2-}: –3.0 Cl^-: –2.2 Br^-: –1.0		90
PSCN(25)[a]	NO_3^-	p-HEMA coated on SiO_2 gate of ISFET	none	TBA^+ Br^-	–56	SO_4^{2-}: –3.2 Cl^-: –2.6 Br^-: –1.0		90
PSKT(10)[c]	NO_3^-	p-HEMA coated on SiO_2 gate of ISFET	none	TBA^+ Br^-	–60	SO_4^{2-}: –2.6 Cl^-: –2.2 Br^-: –0.9		90
PSES(10)[d]	NO_3^-	p-HEMA coated on SiO_2 gate of ISFET	none	TBA^+ Br^-	–56	SO_4^{2-}: –2.9 Cl^-: –2.3 Br^-: –1.2		90

PSAM(10)[b]	NO_3^-	p-HEMA coated on SiO_2 gate of ISFET	none	$TBA^+ Br^-$	–54	SO_4^{2-}:– 2.9 Cl^-: –1.6 Br^-: –0.5		[90]
PSAM(25)[b]	NO_3^-	p-HEMA coated on SiO_2 gate of ISFET	none	$TBA^+ Br^-$	–57	SO_4^{2-}:–3.1 Cl^-: –1.6 Br^-: –0.6		[90]
Dow 730	NO_3^-	Au	none	TDDMA NO_3^-	–57	Cl^-: –1.3 SO_4^{2-}: –1.9		[120]

[a] Refers to a terpolymer containing dimethylsiloxane, cyanopropylmethylsiloxane, and methacryloxypropylmethylsiloxane. The structure is shown in Figure 1.13. It is abbreviated as PSCN(*x*) where *x* refers to the molar fraction of cyanopropylmethylsiloxane units.

[b] Refers to a terpolymer containing dimethylsiloxane, propylbenzylamidosiloxane, and methacryloxypropylmethylsiloxane.

[c] Refers to a terpolymer containing dimethylsiloxane, *p*-acetylphenoxypropylmethylsiloxane, and methacryloxypropylmethylsiloxane.

[d] Refers to a terpolymer containing dimethylsiloxane, acetoxypropylmethylsiloxane, and methacryloxypropylmethylsiloxane.

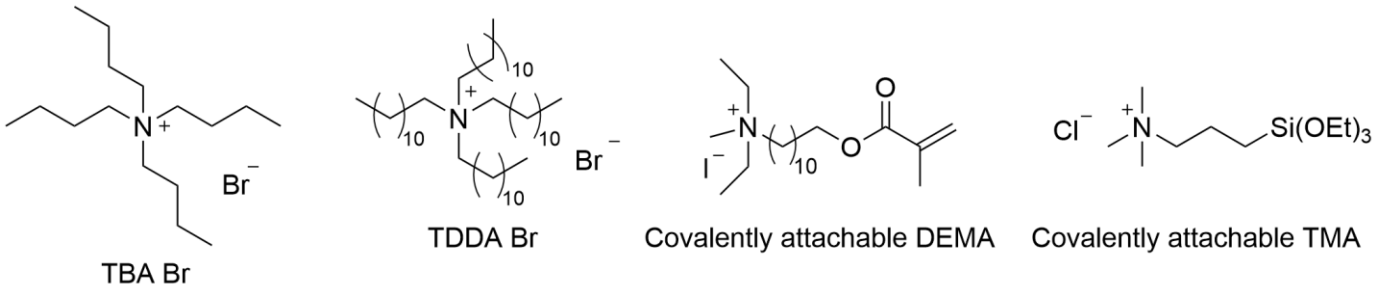

Figure 1.28. Cationic Sites used in plasticizer-free silicone-based NO_3^- ion exchange membranes.

1.18. Silicone-based SC-ISEs in physiological samples

One interesting example of a silicone-based ISE was that of a tube used as an ion-selective electrode to measure the K^+ concentration of the solution flowing through the tube (Figure 1.29).[125] The device comprised a silicone tube impregnated with valinomycin in chloroform. The tube was then placed into a secondary fixture that contained an inner filling solution and a Ag/AgCl wire. The wall of the inner silicone tube is the ion-selective membrane. These electrodes were used to measure the K^+ concentration in blood serum and whole blood. The electrodes maintained their response even after 300 min exposure to serum or whole blood. No quantitative information on response slopes, detection limits, or selectivity was given. The authors noted that they had used these tube-based ISEs in experiments to develop artificial pancreas for diabetic patients. Notably, a similar approach was used for Ca^{2+} ISEs with ETH 129 or ETH 1001 as ionophore.[118] In this case, however, plasticizer (o-NPOE) and an anionic site (KTpClPB) was required to obtain ISEs with Nernstian responses. Attempts were made to produce membranes without plasticizer and anionic sites. Unfortunately, no attempts were reported for ISEs without plasticizer, but with anionic added sites. At the time these experiments were performed, the role of anionic sites on sensitivity and selectivity was not yet understood.

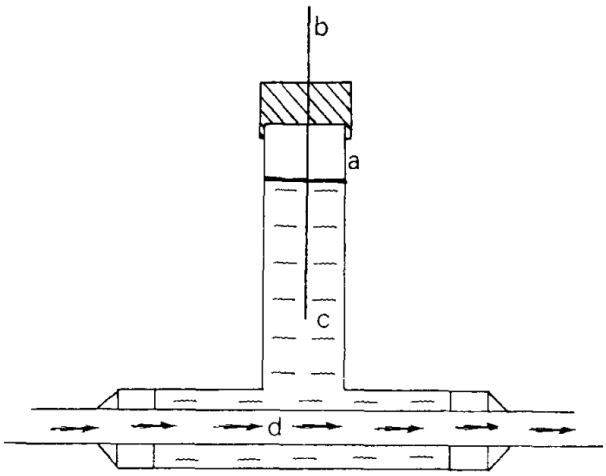

Figure 1.29. Schematic of a silicone tube that acts as a K^+ ion-selective electrode for the in-line measurement of K^+ concentration in blood serum or whole blood. Figure obtained from reference [125]. (a) Fixture for forming a seal around the silicone tube containing blood serum; (b) Ag/AgCl wire; (c) inner filling solution; (d) silicone tube with blood serum or whole blood flowing through. Reprinted with permission.[125] Copyright 1990, Elsevier.

A combination K^+ and pCO_2 sensor was developed with Ag/AgCl wires and inner filling solutions as transducers.[126] Valionmycin was doped into a silicone tube (with dioctyl sebacate as plasticizer) by soaking the tube in a THF-based solution containing valinomycin. No anionic site was added to the silicone. Plasticizer was required to lower the resistance of the K^+ ISM to reduce the noise during data collection. The device also contained a Severinghaus-type pCO_2 sensor which utilized a plasticized PVC membrane doped with tridodecylamine as ionophore to measure changes in H^+ concentration in the solution contained within the silicone catheter caused by diffusion of CO_2 through the

catheter wall. The K^+ ISE had Nernstian responses to K^+ and excellent selectivity to K^+ vs. Na^+. The device was used to measure the real-time K^+ and pCO_2 concentrations in whole blood of a canine over a period of about 4 h. The results from the sensors agreed well with the results from a commercial blood gas analyzer.

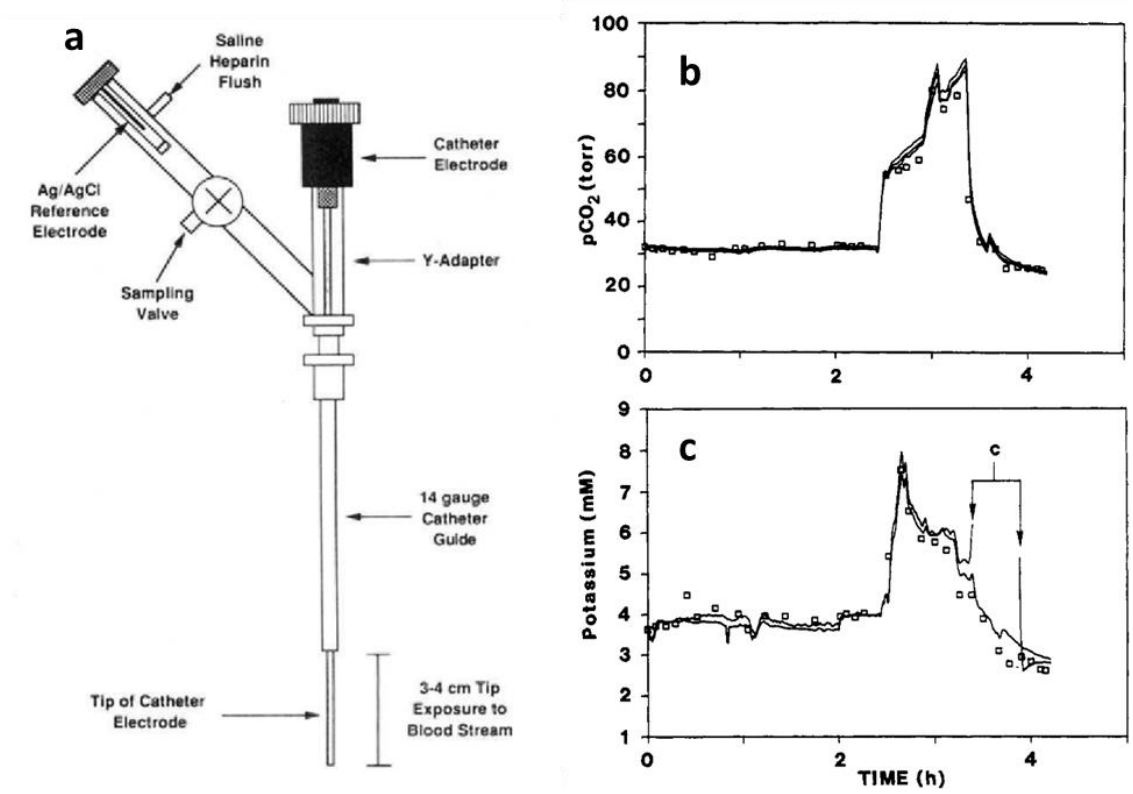

Figure 1.30. (a) Schematic of the catheter electrode implant assembly used for in-vivo studies. Results from the (b) pCO_2 and (c) K^+ sensors during in-vivo measurements (canine) with continuous heparin infusion. Data in the open squares represent values with commercial blood gas analyzers. Both figures are reprinted with permission.[126] Copyright 1989, American Chemical Society.

This device was later modified to develop a dual lumen catheter-type electrode with a silicone rubber tubing doped with tridodecylamine as a pH ionophore to make a pH ISE.[127] In one lumen, a Ag/AgCl wire with a pH buffered inner filling solution was used to measure the sample pH. In the second lumen, a Ag/AgCl wire in unbuffered solution was used. CO_2 from the sample can diffuse through the catheter wall and change the pH inside the unbuffered lumen. Measurement of the emf difference between the two lumens can be used to measure the pCO_2. The second lumen also contained a cobalt wire for potentiometric determination of pO_2. These electrodes were used to monitor the pO_2, pCO_2, and pH of whole blood with different values for concentration of each species over a period of 4 h at 37 °C. The values obtained with the dual lumen sensor agreed well with those measured using a commercially available blood gas analyzer. The authors noted that the pH and pCO_2 electrodes drifted significantly upon first exposure to blood plasma. To mitigate drift, the electrodes were conditioned in blood for 4 h before use. Unfortunately, to make functional pH ISEs from the catheter wall, plasticizer (*o*-NPOE) also needed to be impregnated. This time, KTFPB was also added. Interestingly, in both cases, the catheter was cleaned or purified before the impregnating steps by soaking in ethanol then toluene, or by Soxhlet extraction in toluene. Presumably this was done to remove any impurities introduced by coatings or processing aids during fabrication of the catheter, although no analysis of the extracts was performed.

1.19. Dissertation overview

The goal of this research is to develop a biocompatible K^+ sensor that can be used in wearable or implantable sensors. Currently, almost all wearable or implantable sensors comprise plasticized PVC membranes, which are not biocompatible. In the preceding sections, a number of examples ISEs or ISFETs with plasticizer-free silicone membranes were presented. Most of these reports focused on Na^+, K^+, and Ca^{2+} ISEs in conventional electrode setups with inner filling solutions, which are too large to use in a wearable or implantable setup or on ISFETs without solid contacts. Only a few reports of solid-contact ISEs exist with silicone membranes and only one report contains a quantitative measurement of long-term drift. Moreover, very little work has been done with plasticizer-free silicone ISEs in real physiologic samples like sweat or blood plasma. Accurate measurements are far more challenging to obtain for these samples than for simple aqueous salt solutions due to the presence of proteins and other organic species, especially in blood plasma.

To address these shortcomings, Chapter 2 focuses on the development of solid-contact K^+ ISEs with plasticizer-free silicone membranes using valinomycin as the ionophore and CIM carbon as the solid contact. To understand the influence of different components in the silicone membranes on the response, selectivity, and long-term drift, SC-ISEs prepared with different silicones were evaluated, including one silicone prepared in-house for which we know the exact composition. We show that SC-ISEs prepared with our own silicone, a commercially available silicone (Dow 3140), and a commercially available fluorosilicone (Dow 730) have Nernstian responses to K^+, excellent selectivity to K^+ vs. Na^+, and low

drift in aqueous KCl solution. We also show that the long-term drift of SC-ISEs with plasticizer-free silicone membranes increases significantly in blood plasma and that drift is influenced by silicone composition. After 42 h exposure to blood plasma, ISEs with each type of silicone tested respond to K^+. Selectivity worsens slightly, but is still good enough for use blood plasma.

Wearable and implantable sensors will need to be small to comfortably fit in the desired sample. In Chapter 3, we discuss some of the theoretical limitations on the minimum electrode size required to achieve sensors with the desired long-term stability. We also improve on the SC-ISEs shown in Chapter 2 by creating SC-ISEs with a lower total thickness. One limitation on sensor thickness is the size of the solid-contact particles (CIM carbon) as they were bigger than our target sensor thickness. We studied different methods to reduce the particle size of CIM carbon. We found that probe sonication followed by size separation by sedimentation was the most effective method. These smaller CIM carbon particles were used to make functional K^+ SC-ISEs with a total membrane+solid contact thickness < 100 μm.

In Chapter 4, we address the problem of ionophore leaching from the membrane, which can be toxic to the surrounding tissue and limit the lifetime of the ISE. We synthesized a derivative of the K^+ ionophore BME-44 that contains a triethoxysilyl group which covalently attaches to the crosslinked silicone network during curing of condensation-cured silicones. We show that pre-reacting the silicone with the ionophore before crosslinking allows for much better attachment of ionophore to the silicone. We also demonstrate that mobile and covalently attachable BME-44 can adsorb onto high surface

area solid contacts like CIM carbon, which is an important effect to consider when developing solid-contact silicone-based ISEs. On gold electrodes without the high surface area CIM carbon, we show that the silicone ISEs with a covalently attachable derivative of BME-44 as ionophore have Nernstian responses to K^+ and excellent selectivity to K^+ vs. Na^+. We also show that covalent attachment of the ionophore to silicone results in less phase separation of the ionophore from the silicone as compared to ISEs prepared with mobile BME-44. As a result ISEs with the covalently attachable BME-44 derivative have lower resistances and better selectivity than those prepared with mobile BME-44.

In Chapter 5, we conclude that plasticizer-free silicone matrixes are promising candidates for use in wearable and implantable SC-ISEs. In this thesis research, we demonstrated that K^+ SC-ISEs maintain their responses to K^+ after 42 h exposure to blood plasma and retain sufficient selectivity to accurately measure the K^+ concentration in blood plasma. We also demonstrated that the K^+ ionophore BME-44 can be covalently attached to the crosslinked silicone network to produce functional K^+ ISEs. We note, however, that there is still much to learn about the influence of silicone curing chemistry and structure on ISE performance. We propose several factors related to the curing chemistry and silicone network structure that may be impact ISE performance. We also propose several methods to study those factors.

Chapter 2. Influence of the Composition of Plasticizer-free Silicone-based Ion-selective Membranes on Signal Stability in Aqueous and Blood Plasma Samples

This chapter was reproduced from "Influence of the Composition of Plasticizer-free Silicone-based Ion-selective Membranes on Signal Stability in Aqueous and Blood Plasma Samples" by Spindler, B.D.; Graf, K.I.; Dong, X.I.N.; Kim, M.; Chen, X.V.; Bühlmann, P.; Stein, A. in *Anal. Chem.* **2023,** 95, 12419-12426. Copyright 2023, American Chemical Society.

Katerina Graf contributed to the silicone composition optimization and potentiometry experiments in this chapter. Minog Kim provided the CIM carbon used to make the solid-contact ion-selective electrodes described in this chapter.

Portions of this work were supported by Medtronic PLC. Parts of this work were carried out in the University of Minnesota Characterization Facility, which receives partial support from the NSF through the MRSEC (award number DMR-2011401) and the NNCI (award number ECCS2025124) programs.

2.1. Introduction

Ion-selective electrodes (ISEs) are widely used in clinical settings for analysis of ion activity in body fluids and in industrial settings for process monitoring.[22, 121, 128-131] Recently, there has also been an increased interest in real-time measurement of ion activity in sweat and interstitial fluid as a noninvasive method to diagnose disease.[11, 12, 18, 20, 132-135] To facilitate this, solid-contact ISEs (SC-ISEs) with solid-contact reference electrodes have been integrated into wearable devices, including patches that can be adhered to skin.[11, 12] For both wearable and implantable ISEs, the ion-selective membrane must be biocompatible. Unfortunately, the majority of ion-selective membranes reported to date comprised plasticized poly(vinyl chloride) (PVC) matrixes, which have poor biocompatibility owing to the large amount of plasticizer required to lower the glass transition temperature of PVC.[55, 57, 58] Furthermore, leaching of plasticizer can limit the lifetime of the sensor.

Several polymers have been studied as alternatives to PVC, including silicones,[60] acrylate- and methacrylate-based polymers,[136, 137] and polyurethanes.[110] Among these, silicones have a long history of use in implants owing to their excellent biocompatibility[138] and are a promising alternative to plasticized PVC membranes for wearable and implantable devices. In addition, silicones have low glass transition temperatures, eliminating the need for a plasticizer. These advantageous properties prompted efforts in the 1980s and 1990s to produce small, biocompatible ion-selective field effect transistors (ISFETs)[50, 77, 78, 89, 99, 102, 106] with silicone membranes that could be used to measure real-time ion activities directly in physiological samples like blood. However, these ISFETs

never made it past the research stage, presumably due to large drifts caused by formation of a water layer at the gate oxide and ion-selective membrane interface.[50] Additionally, silicone has a low polarity, and as a result, many ionophores have poor solubility in silicones. Therefore, plasticizer is added in some cases (10–30 wt%) into silicone membranes to improve the solubility of the ionophore, which brings some of the same drawbacks mentioned for plasticized PVC membranes.[94, 115, 120, 139-141]

Much of the work using silicone-based ISEs in the literature involves the use of commercially available one-component or two-component silicones, though there are a few reports of silicones prepared specifically for application in ISEs.[85-87, 89] Commercially available silicones often have fillers and other additives to improve mechanical properties, which may impact ISE performance.[93, 101] Even though silicone-based ISEs have been known for 50 years, the effects of polymer structure, polymerization catalysts, fillers, and curing conditions on long-term stability in biological samples have not been studied with much detail. The only long-term drifts reported to date are, for measurements in aqueous solution, for a conventional silicone-based ISE with valinomycin as ionophore (0.8 μV/h)[82], a Ca^{2+} SC-ISE with ETH1001 as ionophore (200 μV/h),[116] a coated Ag wire K^+ ISE with a fluorosilicone membrane containing 10.5 wt% dioctyl sebacate (DOS) as plasticizer and a Ag^+ salt redox modifier (10 μV/h),[142] and a K^+ ISE with a silicone membrane coated directly onto a Ag/AgCl electrode (<200 μV/h).[110]

Although there has been a lot of work to characterize the properties of SC-ISEs in aqueous solution (with the exception of long-term drift), little attention has been paid to the effects of continuous long-term exposure of SC-ISEs to real samples like sweat or blood

plasma.[143] To investigate the effects of different silicones on the sensor properties, we prepared plasticizer-free K^+ SC-ISEs with colloid-imprinted mesoporous (CIM) carbon as the solid contact[47] using a commercially available silicone and fluorosilicone as well as a silicone prepared in house. CIM carbon was chosen as the solid contact material because previous work with plasticized PVC-based ISEs prepared with CIM carbon solid contacts has shown very low long-term potential drift (1.3 μV/h) and insensitivity to interference from light and CO_2. We show here that small changes in silicone composition do not affect the response slope and are all compatible with an excellent selectivity even after blood plasma exposure. However, they give rise to some differences in emf drift when measurements are performed in porcine plasma.

2.2. Experimental section

2.2.1. Materials

Reagents were purchased from the following sources: tetrahydrofuran (anhydrous, inhibitor-free), toluene (anhydrous, 99.9%), dichloromethane (anhydrous), Ludox AS-40 colloidal silica, potassium hydroxide, Teflon (60 wt % aqueous dispersion), trifluoroacetic acid (99%), valinomycin, potassium tetrakis(*p*-chlorophenyl)borate (KTpClPB), and hydroxy-terminated poly(dimethylsiloxane) (average molecular weight ~110,000) from Sigma Aldrich (St. Louis, Mo); vinyltrimethoxysilane (tech-95, VTMOS) and vinyltriisopropenoxysilane (tech-95) from Gelest (Morrisville, PA); Dow Corning 3140 silicone (**Silicone 2**) from Pilots HQ LLC (Waterford, MI); Dow Corning 730 FS solvent resistant sealant (**Fluorosilicone 1**) from Aircraft Spruce (Corona, CA); mesophase pitch

from Mitsubishi Gas Chemicals (Tokyo, Japan); Chemglass Life Sciences Pyrex tubing (10 ± 0.4 mm outer diameter, 2.0 ± 0.2 mm wall thickness) was purchased from Fisher Scientific (Waltham, MA). All reagents were used without further purification. Deionized water was purified to a resistivity of 18.2 MΩ with a Milli-Q PLUS reagent-grade water purification system (Millipore, Bedford, MA). Graphite rods (fine extruded, 0.25-inch diameter) were purchased from Graphite Store (Northbrook, IL). The silicone resulting from condensation curing of a precursor solution containing hydroxy-terminated poly(dimethylsiloxane) (PDMS-OH), VTMOS, and trifluoroacetic acid is referred to as **Silicone 1**. Porcine blood was obtained from Medtronic PLC (Fridley, MN). Citrate phosphate dextrose adenine solution (63 mL) was added as anticoagulant to 450 mL of porcine blood. To obtain plasma, the red blood cells were removed by centrifugation (2000 g) at room temperature for 20 min.

2.2.2. CIM carbon synthesis

The CIM carbon was prepared following our previously reported procedure.[47] Mesophase pitch (2.0 g) was ground into a powder and dispersed in 40 mL of an ethanol/water mixture (60/40, v/v) at 50 °C. While stirring, 40 mL of Ludox AS-40 colloidal silica suspension was added to the flask, and the mixture was stirred at 50 °C for 18 h. The mixture was then transferred to an open beaker and kept at 50 °C until all solvent had evaporated. The resulting pitch–silica composite was ground to a fine powder. The powder was transferred to an alumina combustion boat and heated under N_2 flow (0.5 L/min) at a rate of 5 °C/min to 400 °C, at which it was held for 2 h. The mixture was then

heated under N_2 flow (0.5 L/min) at a rate of 5 °C/min to 900 °C, at which temperature it was held for 4 h. To remove the silica, the carbon–silica composite was soaked in a 6 M KOH solution at 180 °C for 48 h in a Teflon-lined steel autoclave. The resulting CIM carbon was collected by filtration and washed with water until the filtrate reached pH 7. The CIM carbon was dried under vacuum at 120 °C overnight to remove water. The CIM carbon was heated in a reducing atmosphere (5% H_2, 95% N_2 flowing at 0.5 L/min) at a rate of 5 °C/min to 900 °C and held at that temperature for 5 h. After cooling, the resulting CIM carbon was manually ground into a fine powder with an agate mortar and pestle for 5 min.

2.2.3. Graphite/glass electrode fabrication

A 0.25-inch diameter graphite rod (7.5 cm length) was sanded down to fit into a Pyrex tube (10 ± 0.4 mm outer diameter, 2 ± 0.2 mm wall thickness, 5 cm length). The graphite rod was placed in the glass tube with some of the rod sticking out of the tube on both sides. It was fixed to the glass tubing with epoxy on one end of the glass tube. The epoxy was cured in air at room temperature for 18 h. On the side opposite the epoxy, a Teflon suspension (60 wt%) was drop cast onto the graphite rod and glass tube to fill the gaps between the graphite and the glass. The water was evaporated by placing the electrodes in an oven at 110 °C for 18 h. The drop casting and drying steps were repeated two additional times to ensure that the gaps were completely filled with Teflon. After the final drying, the side of the electrode opposite the epoxy was sanded down with 60 grit sandpaper until the graphite was flush with the glass tube. Then, the electrodes were polished with successively

finer sandpaper (150, 320, and 600 grit) until a smooth surface on the glass and graphite was achieved. The electrodes were bath sonicated in water for 10 min to remove any leftover particles from the sandpaper. The electrodes were polished over polishing cloth with aqueous dispersions of alumina (0.3 μm followed by 0.05 μm, Buehler, Lake Bluff, IL). The electrodes were rinsed with water and cleaned by sonication in water, followed by sonication in acetone. They were allowed to dry in air before use.

These glass/graphite electrodes are inexpensive electrodes with a glass body, suitable for forming a strong bond to the ion-selective membrane (see Figure 2.2). No specialized glass is required to form a seal. The surface hydroxyl groups on the glass bodies allow the silicone ion-selective membrane to covalently attach to the electrode during curing. This prevents delamination of the ion-selective membrane from the electrode surface during use. The epoxy holds the graphite rod tightly in place, which prevents twisting or moving of the graphite rod during routine use. The epoxy was only applied on the side of the electrode opposite the ion-selective membrane because most epoxies contain amine catalysts, which could leach into the ion-selective membrane and cause a loss of K^+ selectivity. Some gaps between the graphite rod and the glass were present after the epoxy was cured. These gaps were filled with Teflon so that the ion-selective membrane would not fill the gaps between the glass and graphite during drop casting. The Teflon also provides a hydrophobic barrier between the epoxy and the ion-selective membrane.

2.2.4 CIM carbon disk fabrication

A mass of 0.42 g of 60 wt% Teflon dispersion in H_2O was diluted with 4.58 mL H_2O to 5 wt%. CIM carbon (100 mg) was mixed with 100 µL of the 5 wt% Teflon dispersion with an agate mortar and pestle. The Teflon/CIM carbon/water mixture was mixed manually until the carbon particles stuck together, producing one piece of CIM carbon, which was then pressed into a film (thickness: 137 ± 6 µm) using a roller press. CIM carbon disks were cut out of this film with a hole punch (4.8 mm), and water was removed by heating the disks in a vacuum oven at 120 °C for 18 h.

2.2.5 ISE fabrication

Precursor solutions for **Silicone 1**, **Silicone 2**, and **Fluorosilicone 1** based K^+ ISEs were prepared as follows. For **Silicone 1**-based K^+ ISEs, 200 mg PDMS-OH, 10.8 µL VTMOS, 67 µL trifluoroacetic acid, 2.0 mg valinomycin, and 0.45 mg KTpClPB (50 mol % with respect to valinomycin) were dissolved in 1.0 mL toluene. For **Silicone 2**-based K^+ ISEs, 200 mg **Silicone 2**, 2.0 mg valinomycin, and 0.45 mg KTpClPB were dissolved in 1.0 mL THF. For **Fluorosilicone 1**-based K^+ ISEs, 200 mg **Fluorosilicone 1**, 2.0 mg valinomycin, and 0.45 mg KTpClPB were dissolved in 1.0 mL THF.

To prepare the ISEs, a CIM carbon/Teflon disk was placed on top of a graphite/glass electrode and centered. Then, 20 µL of solvent (THF for the **Silicone 2** and **Fluorosilicone 1** ISEs and toluene for the **Silicone 1**-based ISEs) was deposited onto the CIM carbon layer. This wetted the CIM carbon and allowed the solvent to infiltrate the pores of the CIM carbon, displacing air from its pores and helping to prevent the formation of air pockets in

the ion-selective membrane (ISM) layer while the silicone was curing. When the solvent had evaporated sufficiently to expose the top of the CIM carbon layer (usually 1–2 min after drop casting for THF and 5 min for toluene), the ISM solution was applied first as a 20 µL portion, followed by four 50 µL portions. The **Silicone 2** and **Fluorosilicone 1** ISEs were cured in air at room temperature for 96 h, whereas the **Silicone 1** ISEs were cured in an oven at 55 °C for 96 h. ISEs from **Batch 1** had a total thickness (membrane + carbon layer) of 820 ± 70, 610 ± 70, and 480 ± 30 µm for **Silicone 1**, **Silicone 2**, and **Fluorosilicone 1**, respectively. We found that the age of **Fluorosilicone 1** affects the response slope and selectivity of the sensors and recommend not to use **Fluorosilicone 1** batches beyond the manufacturer's expiration date. No such effect was observed for **Silicone 2**.

Two batches of SC-ISEs (**Batch 1** and **Batch 2**) were used to evaluate the effects of long-term exposure to porcine plasma. See the appendix for the use history of each batch.

2.2.6. Potentiometric measurements

ISE potentials were measured using an EMF 16 voltmeter (10 TΩ input impedance) controlled with EMF-Suite 1.03 software (Lawson Labs, Malvern, PA). Potentials were measured against a double-junction Ag/AgCl reference electrode (DX200, Mettler Toledo, Switzerland) with a 3 M KCl/saturated AgCl inner filling solution and 1.0 M LiOAc bridge electrolyte. Activity coefficients were calculated using a two-parameter Debye-Hückel approximation,[144] and all electrode potentials were corrected for liquid junction potentials using the Henderson equation.[145] Before use, ion-selective electrodes were conditioned in

1 mM KCl at 25 °C for 23 h (**Batch 1**) and 37 °C for 744 h (**Batch 2**). Calibration curves were measured at 25 °C (the temperature was controlled using a jacketed flask connected to a VWR water circulator). The K^+ concentration of the sample was adjusted by successive addition of concentrated KCl solutions to the sample solution. Potentials were measured for 2–4 minutes after each addition. The selectivity coefficients for K^+ vs. Na^+ were measured using the fixed interference method[146] (FIM) at 25 °C with a 1 M NaCl background electrolyte. ISE resistance was measured by the known shunt method.

Long-term drift was measured in a 1 mM KCl solution at 37 °C, without stirring, relative to an Ag/AgCl wire. The temperature was controlled with a temperature control box. Drift was calculated as the slope of a linear regression of potential vs. time from 20–144 h at 37 °C.

Oxygen sensitivity was measured in a 1 mM KCl solution at room temperature with stirring, relative to a Ag/AgCl double junction reference electrode with a 1 M lithium acetate outer filling solution. Potentials were first measured in solution open to air for 92 min. The solution was then saturated with argon, then oxygen, and then argon again by bubbling the pure gases through the sample solution for 32, 40, and 30 min, respectively. Potentials were recorded while bubbling the gases through the solution.

2.2.7. Measurement of membrane resistivity

For measurements of membrane resistivity, 1.0 mL of the ion-selective membrane solutions for **Silicone 1**, **Silicone 2**, and **Fluorosilicone 1** were cast onto a Teflon dish (25 mm diameter). The **Silicone 1** membrane was cured at 55 °C for approximately 96 h and

the **Silicone 2** and **Fluorosilicone 1** membranes were cured at room temperature for 96 h. The same procedure was used to produce membranes not doped with ionophore and anionic sites. Before use, the membranes were conditioned in 1 mM KCl overnight. Disks (6 mm diameter) were cut out of the master membrane using a hole punch and assembled into Phillips bodies with a Ag/AgCl internal reference electrode containing a 1 mM KCl inner filling solution.[30] Membrane resistance was measured using the known shunt method.[147]

2.2.8. ISE performance in animal blood

The K^+ activity in porcine plasma was measured by two methods using the **Silicone 1**, **Silicone 2**, and **Fluorosilicone 1** K^+ SC-ISEs (**Batch 1**) prepared on the graphite/glass electrodes after extensive exposure to aqueous solution and other physiological samples (see the appendix for more information). ISE potentials were measured at 25 °C relative to the potential of an Ag/AgCl double junction reference electrode with a 1.0 M lithium acetate outer-filling solution. A three-point calibration curve from 10^{-3} M KCl to 10^{-2} M KCl was collected for each ISE by measuring the ISE potential in solutions of 10^{-3}, $10^{-2.5}$, and then 10^{-2} M KCl for 5 min each without stirring. The ISE potentials measured after five minutes in each solution were corrected for liquid junction potential and activity coefficients and used to prepare a calibration curve for each ISE. After the calibration, each ISE was placed in the porcine plasma, and the potential was recorded for five minutes. The potential at the end of this period was corrected for the liquid junction potential (see Section 2.2.9) and used to calculate the K^+ activity in the porcine plasma using the preceding calibration curve for each ISE. The above sequence of K^+ calibration and measurement of

K^+ activity in porcine plasma was repeated three additional times. For the subsequent analyses, the measuring time in the porcine plasma was 5, 10, and 20 min for the 2nd, 3rd, and 4th analyses, respectively. The measuring time was 5 min for each calibration preceding a measurement in porcine plasma. After the fourth K^+ measurement in porcine plasma, a final three-point calibration curve was collected. The average and standard deviations of the K^+ concentrations from all four measurements in porcine plasma are listed in Table 2.4.

The method of standard addition was also used to measure the K^+ concentration in porcine plasma at 25 °C. The ISE potentials were allowed to stabilize in the porcine plasma for 12 min before adding aliquots of 3.00 M KCl solution to raise the K^+ concentration. After each standard addition, the sample was stirred for 15 s to ensure complete mixing of the porcine plasma and KCl solution. Then, each potential was recorded for 5 min without stirring. The potentials at the end of each 5-min period were recorded and used to calculate the concentration of K^+ in the porcine plasma.

2.2.9. Estimation of liquid junction potential

The liquid junction potential at the reference electrode/sample interface in porcine plasma and blood at 25 °C was estimated by the method of Bjerrum.[148] Using this method, the liquid junction potential at the interface between the sample solution and the outer filling solution of the reference electrode is assumed to be zero when the outer filling solution contains a salt at infinite concentration. Making infinitely concentrated salt solutions is not practical, but the liquid junction potential can be estimated by measuring the change in potential between the ISE and reference electrode as the salt concentration

in the outer filling solution of the reference electrode is varied. The liquid junction potential at the reference electrode/sample interface changes whereas the ISE potential does not change. The "junction-free" potential can be calculated by performing a linear regression on potential vs. $1/C_{OFS}$ and extrapolating to zero (C_{OFS} is the concentration of salt in the outer filling solution of the reference electrode). The liquid junction potential is then calculated from the linear regression by Equation 2.1 where $E(0)$ is the "junction-free" potential and $E(1/C_{OFS})$ is the measured potential when the salt concentration in the outer filling solution is equal to C_{OFS}.

$$E_{LJ} = E(1/C_{OFS}) - E(0) \qquad (2.1)$$

For the porcine plasma samples, the **Silicone 2**-based ISEs were used for the liquid junction potential determination because for this membrane composition, the standard deviation of the measured K^+ concentration in porcine plasma was the lowest of all the ISEs tested. The liquid junction potential was determined by varying the concentration of lithium acetate in the outer filling solution (0.5, 0.7, and 1.0 M LiOAc). The reference electrode was allowed to equilibrate for 24 h after changing the outer filling solution. Potentials were recorded after 60 min in porcine plasma. The liquid junction potential in porcine plasma was 0.09 ± 0.22 mV (see Figure 2.12).

2.2.10. Differential scanning calorimetry (DSC)

Membranes without ionic sites and ionophore were cured using the same conditions used for curing the regular ISEs. DSC of each membrane was carried out using a TA Instrument Q1000 DSC (New Castle, DE) equipped with a liquid nitrogen cooling system. Samples were equilibrated at 40 °C for 2 min. Then, the samples were cooled to -170 °C at 10 °C/min, followed by heating back to 40 °C at 10 °C/min.

2.2.11. Attenuated total reflectance infrared spectroscopy (ATR-FTIR)

FTIR spectra were collected using a Thermo Scientific Nicolet iS50 FT-IR spectrometer with a diamond crystal for ATR. ATR-FTIR spectra were collected in the range of 400 to 4000 cm^{-1}.

2.3. Results and discussion

2.3.1 Silicone curing

Silicone 1 is a home-made silicone, whereas **Silicone 2** and **Fluorosilicone 1** are commercial one-component silicones. All three cure to an elastomer upon exposure to moisture in the air (Figure 2.1). The precursor of **Silicone 2** contains hydroxy-terminated poly(dimethylsiloxane) (PDMS-OH), methyltrimethoxysilane (crosslinker), a titanium catalyst,[78] and silica filler treated with hexamethyldisilazane. When crosslinker is mixed with PDMS-OH, the Si-OH functional groups react with the crosslinker, releasing methanol and producing crosslinker-terminated PDMS chains.[149] Upon exposure to humid air, some of the methoxy groups of the still unreacted crosslinker and the crosslinker-

terminated PDMS are hydrolyzed, releasing more methanol and producing additional Si-OH functional groups, which then react with Si-OH or Si-OMe groups to form a crosslinked polymer. **Fluorosilicone 1** is an acetic acid-evolving fluorosilicone that cures in a similar manner as **Silicone 2**. It contains hydroxy-terminated poly(trifluoropropylmethyl)siloxane, a silica filler (treated with hexamethydisilazane), and vinyltriacetoxysilane as crosslinker. Upon exposure to moisture, acetate groups are hydrolyzed, releasing acetic acid, which further catalyzes crosslinking.

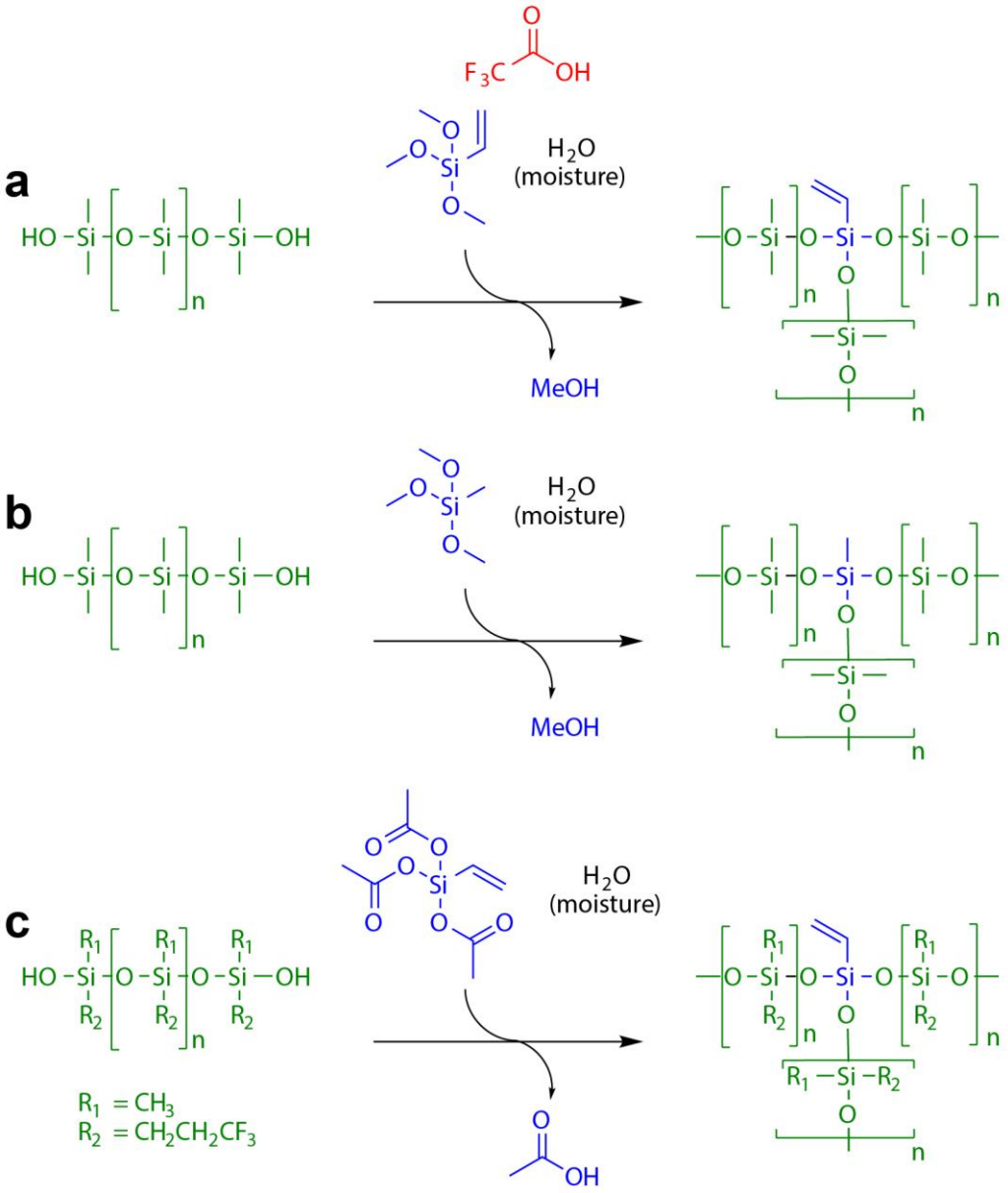

Figure 2.1. Moisture-activated curing of silicones. (a) **Silicone 1**; (b) **Silicone 2**; (c) **Fluorosilicone 1**. The compounds shown in green, blue, and red are polymer chains, crosslinkers, and catalysts, respectively.

Although these commercial silicones are attractive candidates for use in plasticizer-free ion-selective electrodes, the complete composition of their precursor formulations is not public information. This makes it challenging to understand how the ISE response characteristics are affected by the silicone composition and what species remain in the silicone matrix upon curing.[60] To compare ISEs prepared with **Silicone 2** and **Fluorosilicone 1** to a silicone of known composition, we prepared our own PDMS by adapting a reported procedure.[150] This silicone contains no added fillers and contains trifluoroacetic acid as the catalyst, which can be removed by evaporation after curing. To make ISEs with our own silicone, we first optimized the curing conditions to obtain a crosslinked silicone with minimal amounts of catalyst and crosslinker. Hydroxy-terminated poly(dimethylsiloxane) (PDMS-OH, 100 mg), trifluoroacetic acid (TFA, catalyst, 33.6 µL), and crosslinker (amounts shown in Table 2.1) were dissolved in 0.5 mL of tetrahydrofuran (THF) or toluene. A volume of 10 µL of the resulting silicone precursor solution was drop-cast onto a Teflon sheet and cured in air for 24 h. To find the optimum reagent ratios, the amounts of trifluoroacetic acid and crosslinker were varied. The effects of using different crosslinkers, vinyltriisopropenoxysilane (VTIPOS, acetone-evolving) and vinyltrimethoxysilane (VTMOS, methanol-evolving), were also studied.

In the report by Mincheva,[150] hydroxy-terminated silicone reacted rapidly with the crosslinker VTIPOS in the presence of an organic acid or base catalyst to form a crosslinked polymer. We were able to produce crosslinked silicone membranes with this curing chemistry (Table 2.1), but the resulting silicones were yellow and silicones with high crosslinker concentration were cloudy. The cloudiness is likely caused by

condensation of the crosslinker to form vinyl-functionalized silica particles,[151-153] and the yellow/brown color may be due to acid-catalyzed self-condensation of acetone, producing conjugated molecules that absorb light in the visible region.[154] To avoid contamination of the silicone membrane with these side products, we used VTMOS as crosslinker instead. However, silicones prepared with VTMOS as crosslinker and THF as the solvent did not produce elastomers. Instead, the silicones remained liquid, indicating that the crosslinking reaction was inefficient.

Table 2.1. Optimization of silicone precursor solution composition and curing temperature.[a] The entry highlighted in grey indicates the silicone precursor solution composition and curing conditions used for **Silicone 1**.

VTIPOS (mg)	VTMOS (mg)	solvent	curing temperature (°C)	state of resulting material	appearance of resulting material
5	–	THF	22	elastomer	clear, yellow
50	–	THF	22	elastomer	cloudy, yellow
–	5	THF	22	liquid	clear, colorless
–	50	THF	22	liquid	clear, colorless
–	5	THF	55	liquid	clear, colorless
–	50	THF	55	liquid	clear, colorless
–	5	toluene	22	tacky	clear, colorless
–	25	toluene	22	tacky	cloudy, colorless
–	5	toluene	55	elastomer	clear, colorless
–	25	toluene	55	elastomer	cloudy, colorless

[a] Amounts of 100 mg PDMS-OH, 50 mg TFA, and 0.5 mL of solvent were used for all entries in this table. The optimized conditions are highlighted in grey.

To increase the activity of the catalyst and the rate of crosslinking with VTMOS, toluene was used as the solvent instead of THF. When cured at room temperature, the resulting silicones were tacky, that is, not fully cured and sticky when the surface was touched with a spatula. The silicone prepared in the same way but with VTMOS as crosslinker in a 5:100 w/w ratio to the PDMS-OH was clear and colorless, whereas the silicone prepared with a composition of VTMOS and PDMS-OH in a 100:50 ratio (w/w)

was cloudy. The same trends were observed for the silicones prepared at 55 °C, but the produced silicones were not tacky. Instead, a robust silicone film that could be peeled from the Teflon sheet was produced. The silicone produced from the precursor solution in toluene with a composition of PDMS-OH, VTMOS, and TFA of 100:5:50 (w:w:w) was elastic, clear, and colorless. This PDMS precursor composition, cured at 55 ˚C, was used for the preparation of K^+ SC-ISEs; it is denoted as **Silicone 1**.

2.3.2. Response characteristics of K^+ SC-ISEs prepared with silicones and CIM carbon.

Solid-contact K^+ ISEs were prepared with **Silicone 1**, **Silicone 2,** or **Fluorosilicone 1** as the ion-selective membrane matrix, valinomycin as ionophore, KTpClPB to provide ionic sites, CIM carbon as the solid contact, and graphite rods encased in glass bodies as the contacting electron conductor (Figure 2.2c–2.2e). After initial conditioning in 1 mM KCl at 25 °C for 22 h, all three types of SC-ISEs exhibited Nernstian responses to K^+, excellent selectivity to K^+ versus Na^+, and micromolar detection limits (Figure 2.3 and Table 2.2). No changes in response characteristics (measured at 25 °C) were observed after storage in 1 mM KCl solution at 37 °C for 18 days (see Table 2.2 and Figure 2.5). All three types of SC-ISEs were also insensitive to oxygen (Figure 2.6), consistent with PVC-based ISEs prepared with CIM carbon as the solid contact.[47] Interestingly, there is no significant difference in selectivities for these ISEs and ISEs with membranes prepared with PVC (plasticized with DOS), silicone, or fluorosilicone membranes as reported in the literature.[47,113,107]

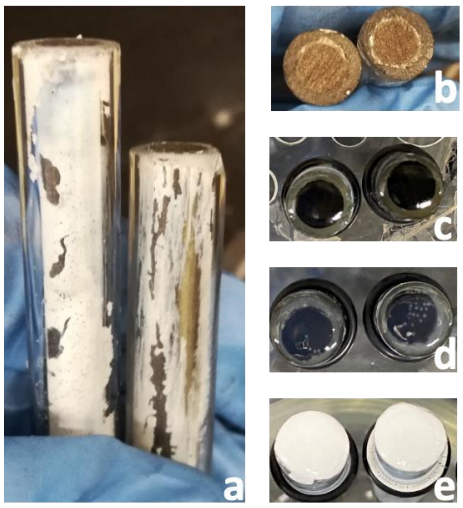

Figure 2.2. Images of K^+ ISEs prepared on graphite/glass electrodes. (a) Side view of graphite/glass electrodes; (b) top view of graphite/glass electrodes; (c) top view of SC-ISEs prepared using **Silicone 1**; (d) top view of SC-ISEs prepared with **Silicone 2**; (e) top view of SC-ISEs prepared with **Fluorosilicone 1**.

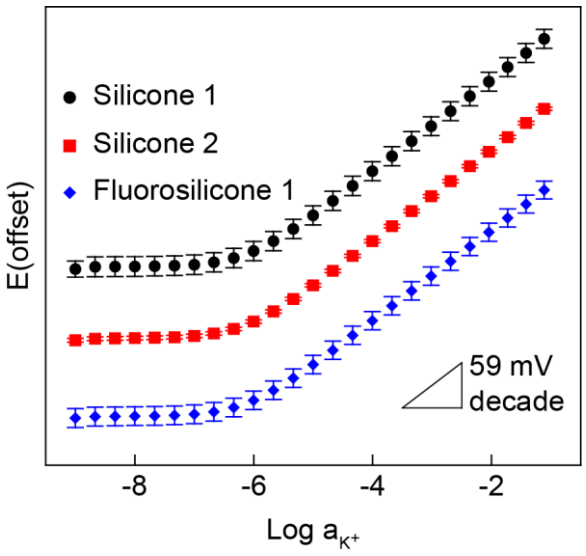

Figure 2.3. Potentiometric response curves of solid-contact K^+ ISEs (**Batch 1**) prepared with **Silicone 1**, **Silicone 2**, or **Fluorosilicone 1** as polymeric matrix after conditioning in 1 mM KCl at 25 °C for 23 h. Symbols represent average potentials for four identically prepared ISEs, and error bars represent standard deviations. See Figure 2.4 for responses of individual ISEs.

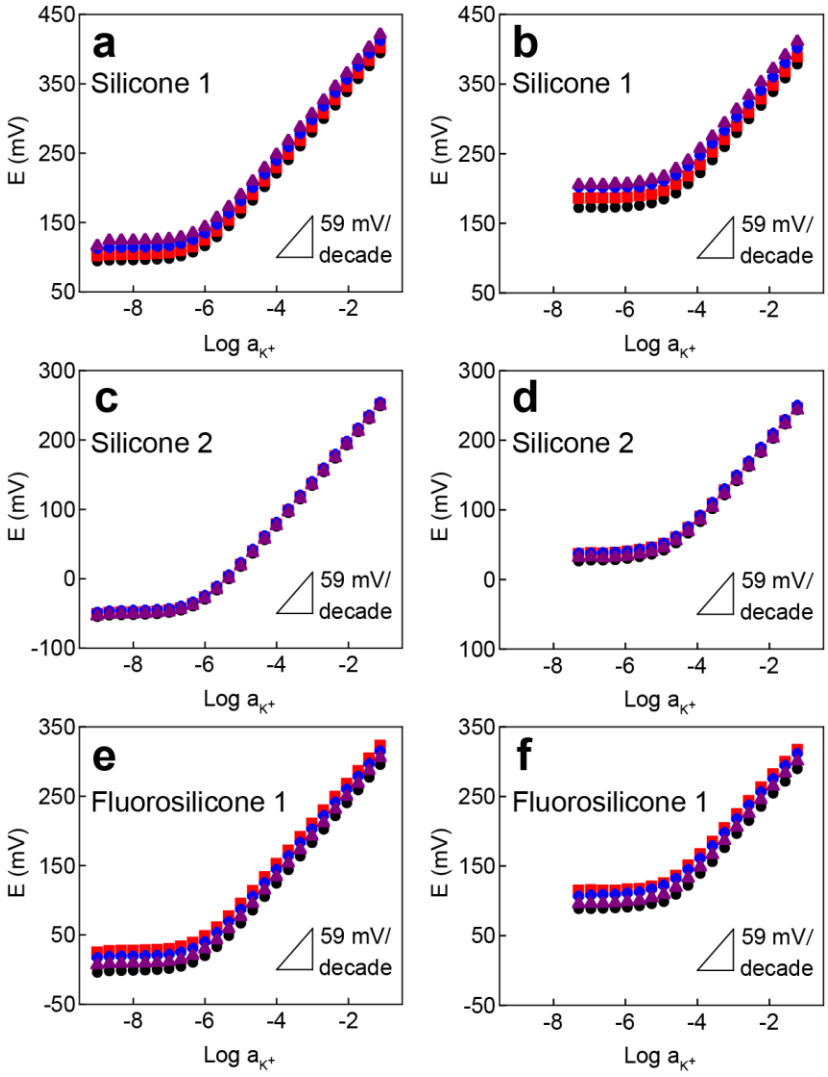

Figure 2.4. Measured potentials, *E*, of K^+ SC-ISEs (**Batch 1**) as a function of the logarithm of K^+ activity in aqueous solution after the initial conditioning of the ISEs in 1 mM KCl at 25 °C. Left column: measured potentials of K^+ ISEs in pure KCl solution for SC-ISEs prepared with (a) **Silicone 1**, (c) **Silicone 2**, (e) **Fluorosilicone 1**. The K^+ activity was adjusted by adding aliquots of KCl solution to the sample. Right column: Measured potentials of K^+ ISEs to K^+ in the presence of a 1 M NaCl (FIM) background for SC-ISEs prepared with (b) **Silicone 1**, (d) **Silicone 2**, (f) **Fluorosilicone 1**. The K^+ activity was adjusted by diluting the sample solution with 1 M NaCl. The four differently colored symbols in each graph represent the measured potentials of four identical K^+ ISEs. Potentials were measured against a free-flowing double-junction reference electrode with a 1 M lithium acetate outer filling solution. The measured potentials were corrected for the liquid junction potential at the free-flowing double junction.

Table 2.2. Response characteristics of **Silicone 1**, **Silicone 2**, and **Fluorosilicone 1**-based SC-ISEs (**Batch 1**) after conditioning in 1 mM KCl solution.

polymer matrix	response slope[a] (mV/decade) after 23 h at 25 °C	response slope[a] (mV/decade) after 433 h at 37 °C	$\log K_{K^+,Na^+}$ after 23 h[b] at 25 °C	$\log K_{K^+,Na^+}$ after 433 h[b] at 37 °C	drift (25 °C)[c,d] (µV/h)	drift (37 °C)[e,f] (µV/h)
Silicone 1	60.0 ± 0.1	59.4 ± 0.1	-4.52 ± 0.08	-4.56 ± 0.04	336 ± 111	9 ± 6
Silicone 2	59.9 ± 0.1	59.5 ± 0.1	-4.60 ± 0.01	-4.58 ± 0.01	216 ± 38	27 ± 18
Fluorosilicone 1	59.1 ± 0.1	59.0 ± 0.1	-4.70 ± 0.02	-4.49 ± 0.05	308 ± 264	3 ± 6

[a] Response slopes were measured at 25 °C even though the temperature during conditioning was 37 °C.

[b] Selectivity was measured by the fixed interference method at 25 °C.

[c] Drift calculated by linear fit of potentials measured during 25 °C stability experiment from 18–23 h.

[d] Potential measured relative to a double junction Ag/AgCl reference electrode with a 1 M lithium acetate salt bridge.

[e] Drift calculated by linear fit of potentials measured during 37 °C stability experiment from 20–143 h.

[f] ISE potentials referenced to a Ag/AgCl wire placed in the sample solution.

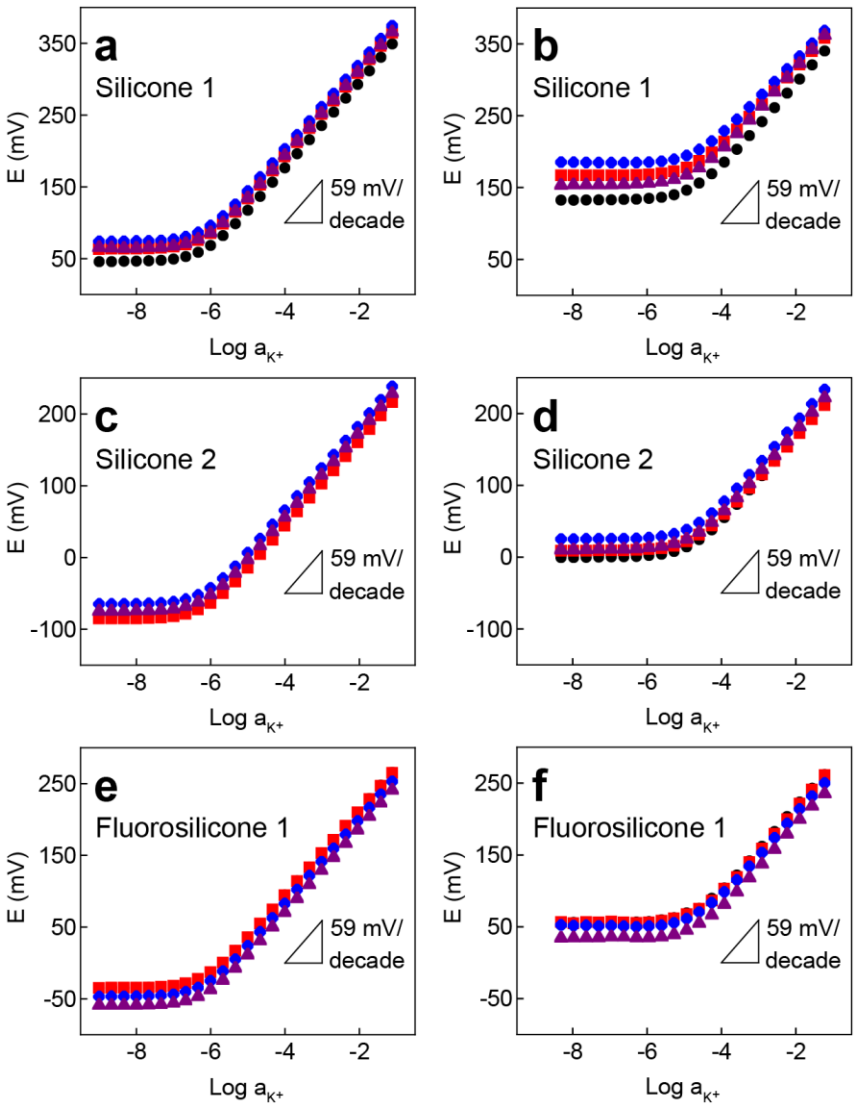

Figure 2.5. Measured potentials, *E*, of K^+ SC-ISEs (**Batch 1**) as a function of the logarithm of K^+ activity in aqueous solution after conditioning the ISEs in 1 mM KCl at 37 °C for 18 days. Left column: measured potentials of K^+ ISEs in pure KCl solution for SC-ISEs prepared with (a) **Silicone 1**, (c) **Silicone 2**, (e) **Fluorosilicone 1**. The K^+ activity was adjusted by adding aliquots of KCl solution to the sample. Right column: Measured potentials of K^+ ISEs to K^+ in the presence of a 1 M NaCl (FIM) background for SC-ISEs prepared with (b) **Silicone 1**, (d) **Silicone 2**, (f) **Fluorosilicone 1**. The K^+ activity was adjusted by diluting the sample solution with 1 M NaCl. The four differently colored symbols in each graph represent the measured potentials of four identical K^+ ISEs. Potentials were measured against a free-flowing double-junction reference electrode with a 1 M lithium acetate outer filling solution. The measured potentials were corrected for the liquid junction potential at the free-flowing double junction.

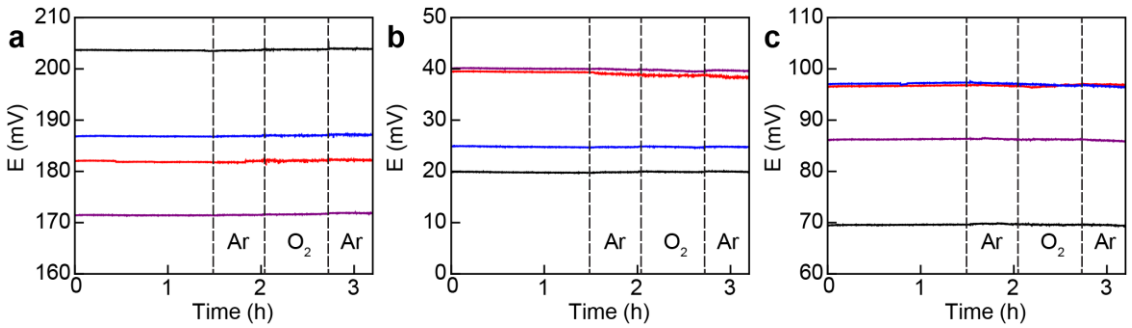

Figure 2.6. Effect of oxygen on the potentials of K^+ SC-ISEs (**batch 2**) prepared with (a) **Silicone 1**, (b) **Silicone 2**, and (c) **Fluorosilicone 1** in 1 mM KCl solution at room temperature. Each line represents the potential of four identically prepared ISEs. The potentials of ISEs prepared in the same batch were measured at the same time, in the same solution, relative to a Ag/AgCl double junction reference electrode with a 1 M lithium acetate outer filling solution. 100% argon or 100% oxygen was bubbled through the sample solution during the time periods between the dotted vertical lines in each graph.

2.3.3. Long-term stability of K^+ SC-ISEs

For wearable and implantable applications, it is important to know how often the sensors need to be recalibrated.[155] To understand these characteristics, the potentials of the K^+ SC-ISEs (**Batch 1**) were measured during initial conditioning at 25 °C for 23 h relative to a double junction Ag/AgCl reference electrode (Figure 2.7). SC-ISEs prepared with **Silicone 2** and **Fluorosilicone 1** exhibited a large increase in potential in the first 3 h, followed by a smaller drift toward higher and lower potentials, respectively, whereas SC-ISEs prepared with **Silicone 1** showed only a small drift toward higher potential throughout the entire measurement. Noting that the added ionic site salt comprised the primary ion, the large initial changes in potential are likely caused by water uptake into the ISE membranes[116] and leaching of hydrophilic ionic and uncharged impurities from the membranes into the aqueous solution.

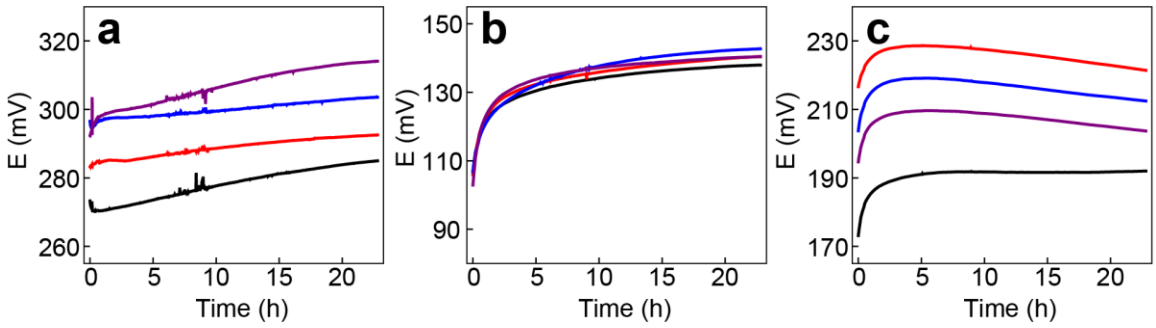

Figure 2.7. Potential of K^+ SC-ISEs (**Batch 1**) during the first exposure to 1 mM KCl solution at 25 °C relative to a double junction Ag/AgCl reference electrode with a 1.0 M lithium acetate outer filling solution (a) **Silicone 1**, (b) **Silicone 2**, (c) **Fluorosilicone 1**.

Further conditioning of the SC-ISEs in 1 mM KCl at the physiological temperature (37 °C) revealed that SC-ISEs prepared with all types of silicones tested can reach very low potential drift values (Figure 2.8). The **Silicone 1** and **Fluorosilicone 1** membranes exhibited average drifts of 9 ± 6 and 3 ± 6 µV/h, respectively, values that are comparable to those of PVC-based SC-ISEs prepared with CIM carbon[47] and 3DOM carbon.[45] The drift for **Silicone** 2 SC-ISEs (27 ± 18 µV/h) did not differ significantly (95% confidence limit) from those for **Silicone 1** and **Fluorosilicone 1**. The same is true for the ISEs prepared in **Batch 2** (see Figure 2.9 and Table 2.3).

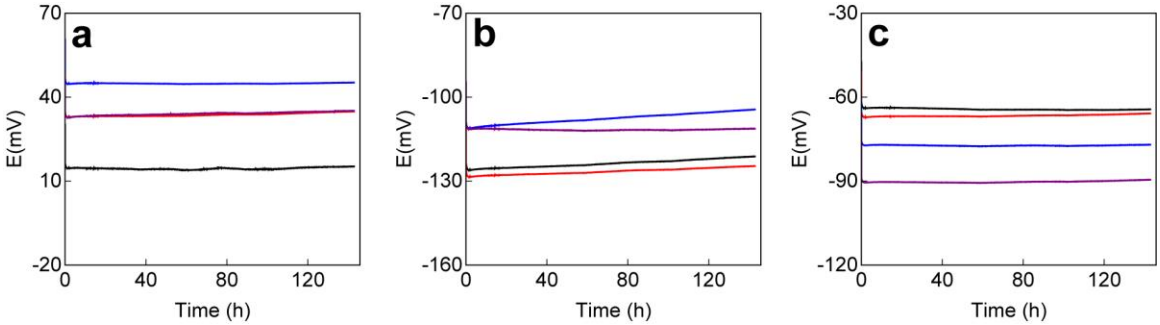

Figure 2.8. Response of K^+ SC-ISEs (**Batch 1**) with conditioning in 1 mM KCl solution at 37 °C relative to a Ag/AgCl wire (a) **Silicone 1**, (b) **Silicone 2**, (c) **Fluorosilicone 1**. Shown in each graph are potentials for four identically prepared ISEs. See the appendix for the prior history of these electrodes.

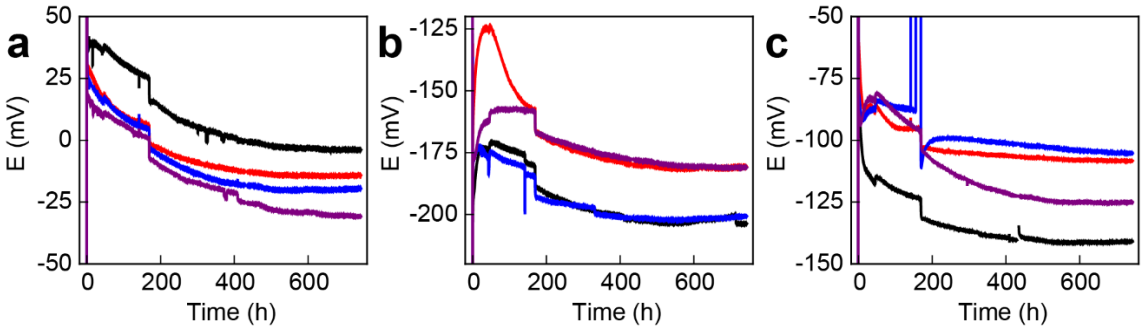

Figure 2.9. Potential of (a) **Silicone 1**, (b) **Silicone 2**, and (c) **Fluorosilicone 1** based SC-ISEs (**Batch 2**) during first exposure to 1 mM KCl solution at 37 °C. Potentials were measured relative to a Ag/AgCl wire. The large decrease in potential for all electrodes at 167 h is caused by refilling of water into the beaker (some water evaporated over time). The beaker was resealed with Parafilm and water evaporation was not measurable during the remainder of the conditioning experiment. The large spike in the blue curve in (c) may have been caused by a bubble covering all the ion-selective membrane, resulting in an open circuit. When water was added to the beaker, the electrodes were shaken to remove bubbles from the membrane surfaces. See Figure 2.10 for the response of the SC-ISEs to K^+ in pure KCl solution and in the presence of a 1 M NaCl background (FIM) after the 31-day exposure to 1 mM KCl solution at 37 °C shown in this figure.

Table 2.3. Response characteristics of **Silicone 1**, **Silicone 2**, and **Fluorosilicone 1**-based SC-ISEs. Each row has two lines of data within it: the first and second lines contain data for **Batch 1** and **Batch 2**, respectively.

property **Batch 1** **Batch 2**	**Silicone 1**	**Silicone 2**	**Fluorosilicone 1**
response slope after conditioning in 1 mM KCl at 37 °C (mV/decade)[a,b]	59.4 ± 0.1 60.5 ± 0.8	59.5 ± 0.1 60.3 ± 0.7	59.0 ± 0.1 59.6 ± 0.5[c]
response slope after long-term exposure to porcine plasma (mV/decade)[a,d]	58.4 ± 0.2[e] 62.7 ± 0.4[b]	58.7 ± 0.1[e] 62.1 ± 0.4[b]	56.9 ± 0.4[e] 62.1 ± 0.4[b]
detection limit after conditioning in 1 mM KCl at 37 °C (μM)[a]	0.7 ± 0.1 8.5 ± 0.6	0.6 ± 0.1 9.2 ± 0.8	0.6 ± 0.1 9.0 ± 0.2
detection limit after long-term exposure to porcine plasma at 37 °C (μM)[a,d]	65 ± 1 1.6 ± 0.2	66 ± 1 1.9 ± 0.1	67 ± 3 2.4 ± 0.2
$\log K_{K^+,Na^+}$ after conditioning in 1 mM KCl at 37 °C[a]	-4.56 ± 0.04 <-4.71[f]	-4.58 ± 0.01 <-4.70[f]	-4.49 ± 0.05 <-4.73[f]
$\log K_{K^+,Na^+}$ after long-term exposure to porcine plasma at 37 °C[a,g]	-4.58 ± 0.04 -4.04 ± 0.07	-4.59 ± 0.04 -4.00 ± 0.02	-4.53 ± 0.02 -3.90 ± 0.02
drift during conditioning in 1 mM KCl at 37 °C (μV/h)[h]	9 ± 6 2 ± 8	27 ± 18 7 ± 5	3 ± 6 3 ± 5
drift during exposure to porcine plasma at 37 °C (μV/h)[i,j]	-612 ± 58 -495 ± 50	-115 ± 42 -55 ± 51	-211 ± 30 -297 ± 69

[a] Response slopes, detection limits, and selectivity coefficients were measured at 25 °C even when drift was measured at 37 °C.

[b] Calculated by linear fit of the calibration data from 10^{-3} to 10^{-1} M K^+.

[c] Calculated by linear fit of the calibration data from 10^{-4} to 10^{-3} M K^+.

[d] Determined from calibration curve measured immediately after long-term exposure to porcine plasma at 37 °C.

[e] Calculated by linear fit of the calibration data from 10^{-3} to 10^{-1} M K^+.

[f] The detection limit could not be determined with the FIM because the emf of these ISEs when exposed to 1 M NaCl solution did not substantially from the emf in pure water (i.e., the lower detection limit in the attempted FIM experiment was still determined by K^+).

[g] FIM selectivity measurements were conducted immediately after the calibration curve outlined in the footnote[d] (**Batch 2**) and after storing in 1 mM KCl for 17 days (**Batch 1**).

[h] The potential for the ISEs were referenced to the Ag/AgCl wire placed in the sample solution.

[i] Potential measured relative to a double junction Ag/AgCl reference electrode with a 1 M lithium acetate salt bridge.

[j] Drifts were measured relative to a double junction reference electrode at 37 °C. Drifts were calculated from the linear fit of the potentials from 30–39 h (**Batch 1**) and 30–41 h (**Batch 2**).

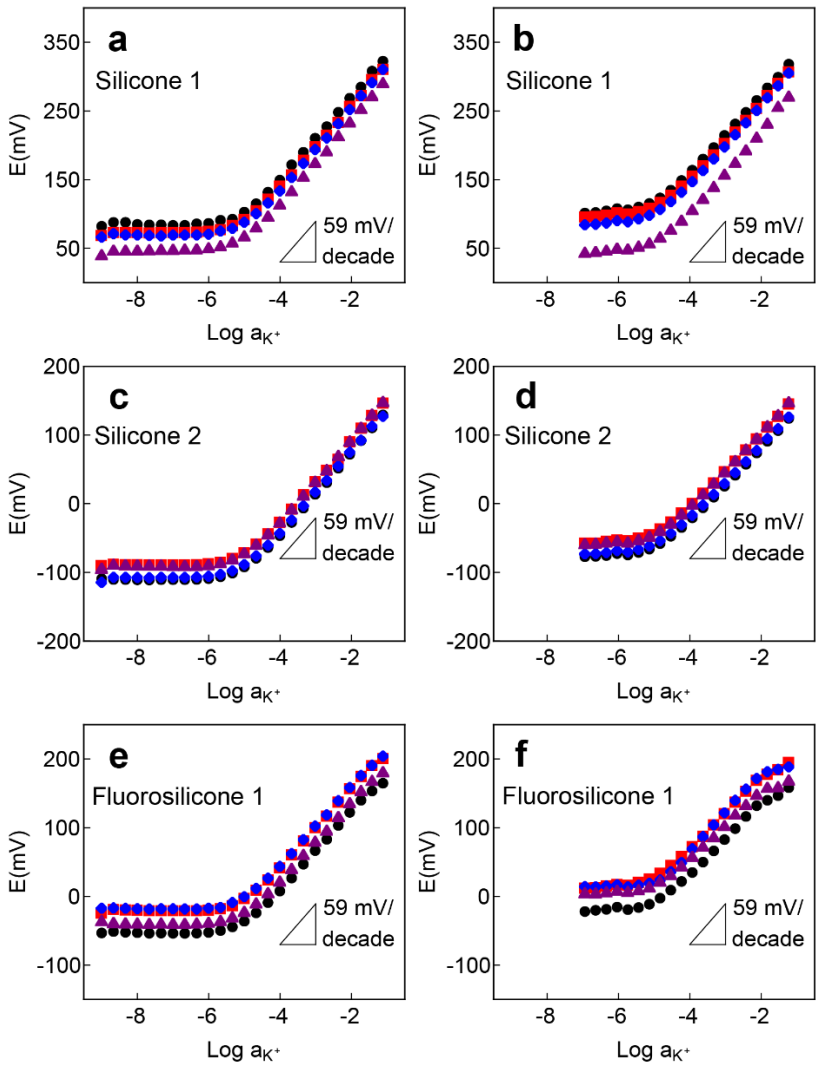

Figure 2.10. Measured potentials, *E*, K^+ SC-ISEs (**Batch 2**) as a function of the logarithm of K^+ activity in aqueous solution after initial conditioning of the ISEs in 1 mM KCl at 37 °C for 31 days. Left column: measured potentials of K^+ ISEs in pure KCl solution for SC-ISEs prepared with (a) **Silicone 1**, (c) **Silicone 2**, (e) **Fluorosilicone 1**. The K^+ activity was adjusted by adding aliquots of KCl solution to the sample. Right column: Measured potentials of K^+ ISEs to K^+ in the presence of a 1M NaCl (FIM) background for SC-ISEs prepared with (b) **Silicone 1**, (d) **Silicone 2**, (f) **Fluorosilicone 1**. The K^+ activity was adjusted by diluting the sample solution with 1 M NaCl. The four differently colored symbols in each graph represent the measured potentials of four identical K^+ ISEs. Potentials were measured against a free-flowing double-junction reference electrode with a 1 M lithium acetate outer filling solution. The measured potentials were corrected for the liquid junction potential at the free-flowing double junction.

2.3.4. Performance of K^+ ISEs upon exposure to porcine blood plasma

To test the sensor behavior in clinically relevant samples, we chose porcine plasma as a model system because it contains all the relevant chemical species (interfering ions, proteins, lipids, and organic compounds) one would expect to encounter in wearable or implantable applications. Additionally, blood plasma does not contain red blood cells, which simplifies the system and eliminates complications caused by leaching of K^+ from the blood cells into the plasma, but it does mean that any effects red blood cells may have on the ISEs are neglected. K^+ activities and concentrations were measured in porcine plasma and compared to the values determined by ion chromatography (Table 2.4). A 3-point calibration curve was used to calculate the K^+ activity from the measured ISE potential (**Batch 1**) in porcine plasma (Figure 2.11), with all data corrected in the usual manner for the liquid junction potential and activity coefficients. The potentials measured in porcine plasma were corrected for the liquid junction potential using Bjerrum's method (see experimental section 2.2.9 and Figure 2.12).

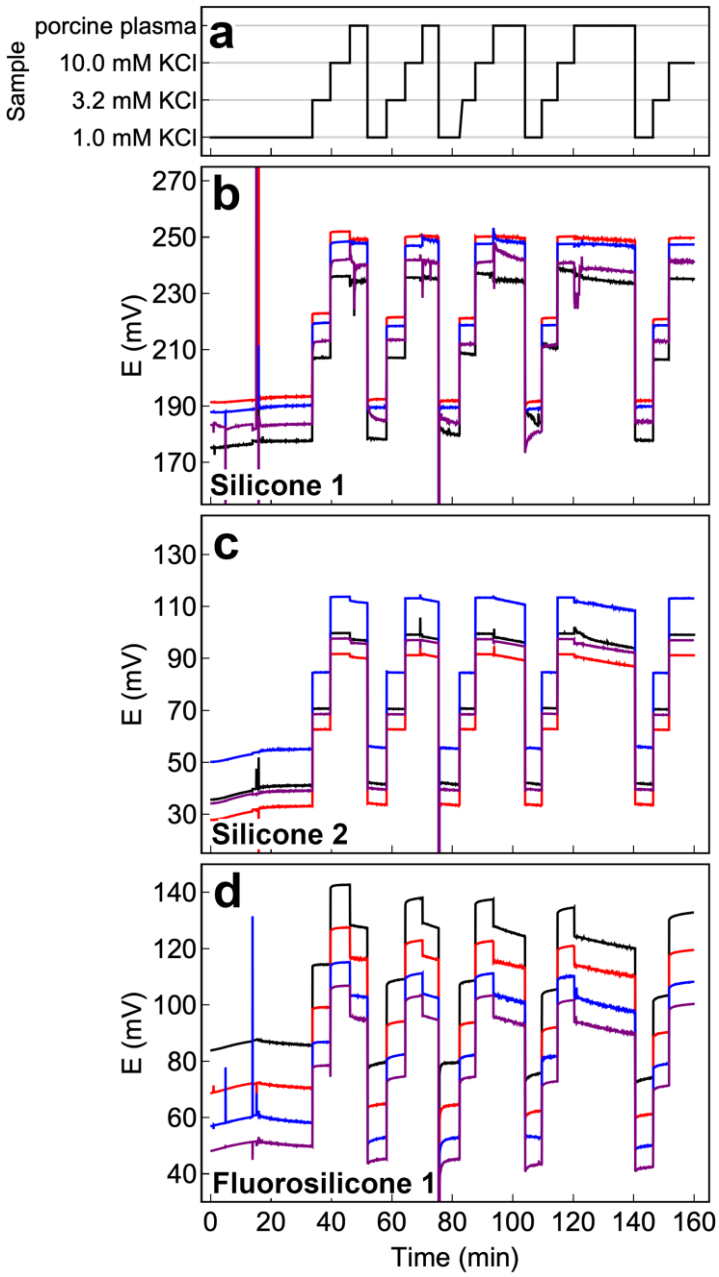

Figure 2.11. Response of K^+ SC-ISEs (**Batch 1**) to 10^{-3}, $10^{-2.5}$, 10^{-2} M KCl, and porcine plasma at 25 °C vs. a double-junction Ag/AgCl reference electrode with a 1.0 M lithium acetate bridge. The ISEs were rinsed with H_2O before transferring them to each new sample solution. (a) Sample composition vs. time, response of (b) **Silicone 1**, (c) **Silicone 2**, and (d) **Fluorosilicone 1**-based ISEs to the calibration solutions and porcine plasma. Each line in one graph represents the potential of four identically prepared ISEs. The concentration of KCl (not activity) in the calibration solutions is listed on the *y*-axis in (a).

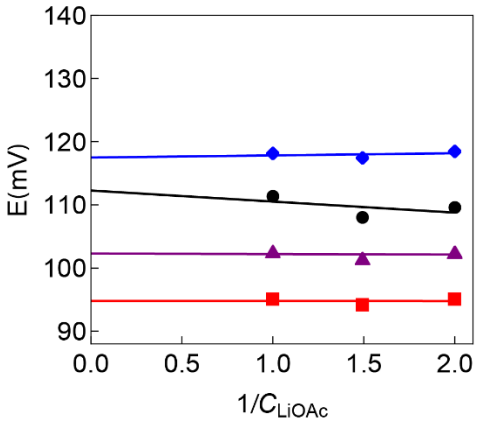

Figure 2.12. Estimation of liquid junction potential using the method of Bjerrum in porcine plasma. The potential difference between the **Silicone 2**-based ISEs (**Batch 1**) and the double junction reference electrode was measured as the concentration of lithium acetate in the outer filling solution was varied. The four different symbols in each graph represent the measured potentials for four identical ISEs relative to the same double junction reference electrode.

The activity of K^+ in porcine plasma measured with the SC-ISEs is lower than the concentration determined by ion chromatography (Table 2.4), which is expected since the ionic strength of blood is approximately 150 mM. To compare the two values, the activity coefficient for K^+ in blood plasma was estimated using the extended Debye–Hückel equation. Approximating the plasma as a solution with 150 mM ionic strength, the activity coefficient for K^+ in blood plasma is 0.73.[156] Using the K^+ concentration in the porcine plasma from ion chromatography, the expected activity of K^+ in the porcine plasma is 7.4 ± 0.1 mM, which is in agreement with the results from the **Silicone 2**-based SC-ISEs (7.6 ± 0.4 mM). The measured K^+ activity from the **Silicone 1** and **Fluorosilicone 1**-based SC-ISEs was 8.1 ± 0.5 and 5.5 ± 0.5 mM, respectively. Notably, upon exposure to porcine plasma, the **Fluorosilicone 1**-based ISEs exhibited a quick step change toward lower

potential, followed by a large drift toward lower potential (Figure 2.11d). **Silicone 1** and **Silicone 2**-based ISEs did not have the same large step change upon exposure to porcine plasma. Using a student's t-test assuming unpaired data with unequal variances, the difference between ion chromatography values and those obtained using **Silicone 1** or **Fluorosilicone 1**-based SC-ISEs is statistically significant even at the 99% confidence limit.

Table 2.4. Measured K^+ activity and concentration in porcine blood plasma using SC-ISEs from **Batch 1**. Values are reported as average ± standard deviation.

silicone or measurement technique	**K^+ activity in porcine plasma (mM)**	**K^+ concentration in porcine plasma (mM)** [a]
Silicone 1	8.1 ± 0.5 (n = 16)[b]	10.9 ± 0.3 (n = 4)
Silicone 2	7.6 ± 0.4 (n = 16)[b]	11.1 ± 0.1 (n = 4)
Fluorosilicone 1	5.5 ± 0.5 (n = 16)[b]	11.8 ± 0.4 (n = 4)
ion chromatography (n = 11)	7.4[c] ± 0.1	10.2[d] ± 0.1

[a] The K^+ concentration was measured with the method of standard addition.

[b] The K^+ activity was measured four times with each ISE, resulting in 16 total measurements (see section 2.2.8 for more information).

[c] The K^+ activity calculated from the K^+ concentration measured by ion chromatography using the extended Debye–Hückel equation, considering the blood plasma as a solution with an ionic strength of 150 mM.

[d] This K^+ concentration is well above the expected concentration in porcine plasma (4.4–6.7 mM),[157] likely because some red blood cells burst during collection, storage, or handling of the blood, which is known to raise the K^+ concentration in plasma.

To better understand the ISE performance in blood plasma, measurements were also performed with the method of standard addition, making it possible to determine the K^+ concentration (rather than the activity). With 95% certainty, the K^+ concentrations measured using SC-ISEs prepared with **Silicone 1** and **Silicone 2** were higher than the value measured by ion chromatography. The slightly higher than expected concentrations can be explained by the drifts toward lower potential observed in this experiment (Figure 2.13g and Figure 2.13h). For SC-ISEs prepared with **Fluorosilicone 1,** the measured K^+ concentration was significantly higher than the values obtained using ISEs prepared with **Silicone 1** and **Silicone 2** (the differences are statistically significant at the 95% confidence limit). Notably, even though the K^+ concentration and activity as determined with the **Fluorosilicone 1** ISEs differs from the value measured by ion chromatography, the sensors still have Nernstian responses to changes in K^+ concentration in blood plasma (Figure 2.13f). Evidently, the process that causes the potential of the **Fluorosilicone 1** SC-ISEs to decrease in blood plasma does not affect selectivity of the sensor during short-term exposures. So long as the sensor responds to K^+ and the EMF offset in blood plasma is constant during the method of standard addition experiment, the EMF offset will not affect the value of the measured K^+ concentration.

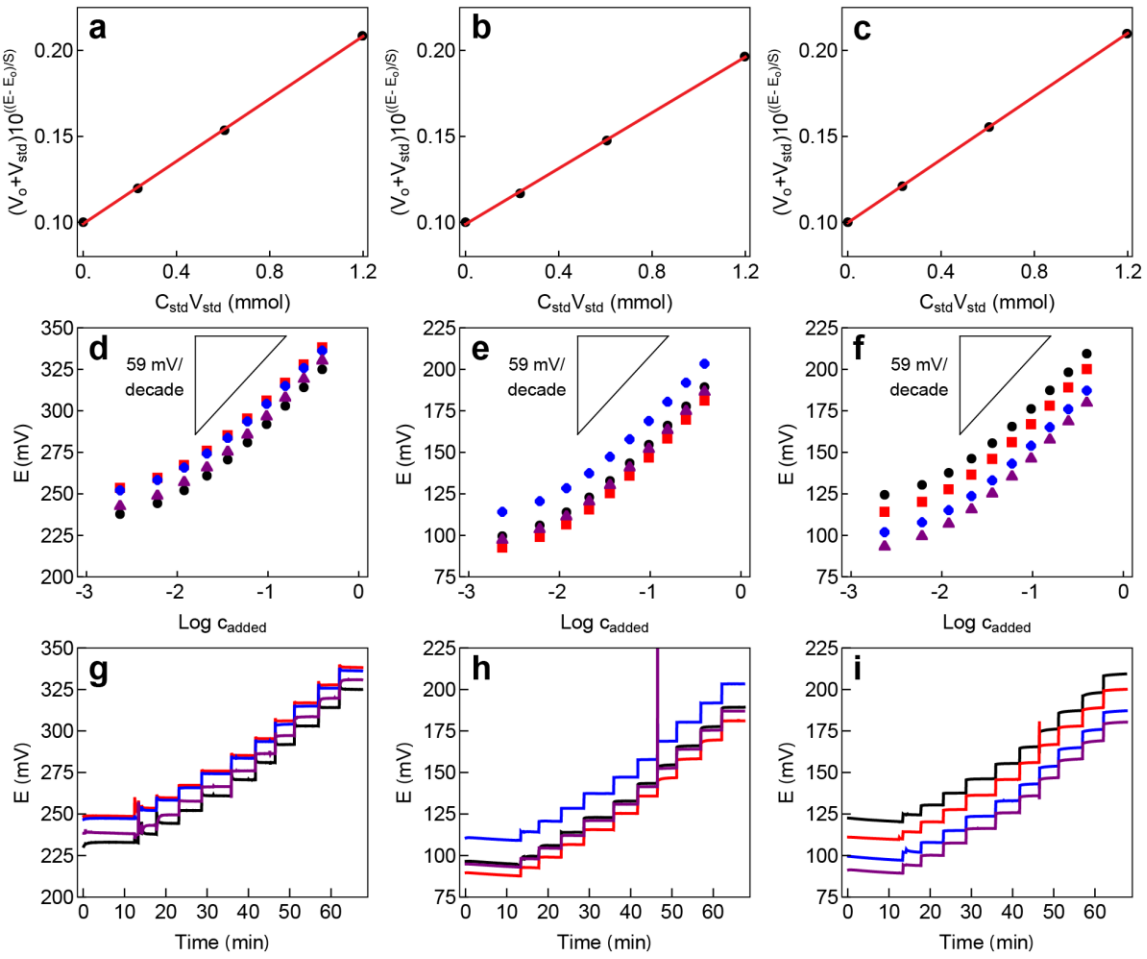

Figure 2.13. Determination of K^+ concentrations in porcine plasma by the method of standard addition at 25 °C. Top row: standard addition plots for one SC-ISE (**Batch 1**) prepared with each type of silicone or fluorosilicone studied in porcine plasma (a) **Silicone 1**, (b) **Silicone 2,** (c) **Fluorosilicone 1**. Middle row: potential vs. logarithm of added concentration of K^+ (d) **Silicone 1**, (e) **Silicone 2**, (f) **Fluorosilicone 1**. Bottom row: The corresponding measured potentials vs. time for ISEs prepared with (g) **Silicone 1**, (h) **Silicone 2**, (i) **Fluorosilicone 1**. Potentials were measured against a free-flowing double-junction reference electrode with a 1 M lithium acetate outer filling solution.

2.3.5. Performance of ISEs during long-term exposure to porcine plasma at 37 °C

The stability of the ISEs (**Batch 2**) in porcine plasma was measured at 37 °C over a period of 41 h (see Figure 2.14 and Table 2.5). The **Silicone 1**-based ISEs (Figure 2.14d) had a large, continuous drift toward lower potential during the 41 h exposure to porcine plasma, whereas ISEs prepared with **Silicone 2** (Figure 2.14e) had a much smaller drift (-55 ± 51 μV/h) after an initial decrease in potential within the first hour. The difference in drift between SC-ISEs prepared with different silicone membranes was consistent between two different batches of ISEs (see Figure 2.14 and Table 2.3).

As the **Silicone 1** SC-ISE, the **Fluorosilicone 1** SC-ISEs too had a large drift toward lower potential, but the drift decreased with increasing exposure time to porcine plasma. The magnitude of the drift (30–41 h) for **Fluorosilicone 1** SC-ISEs is 297 μV/h, which is larger than the reported drift of 85 ± 15 μV/h in whole blood using a sensor prepared with a plasticized **Fluorosilicone 1** (10.5% DOS) membrane coated onto a Ag electrode.[142] However, in that report, a stop-flow setup was used, and the ISEs were only exposed to blood for approximately 10 minutes at a time before being washed with KCl solutions.

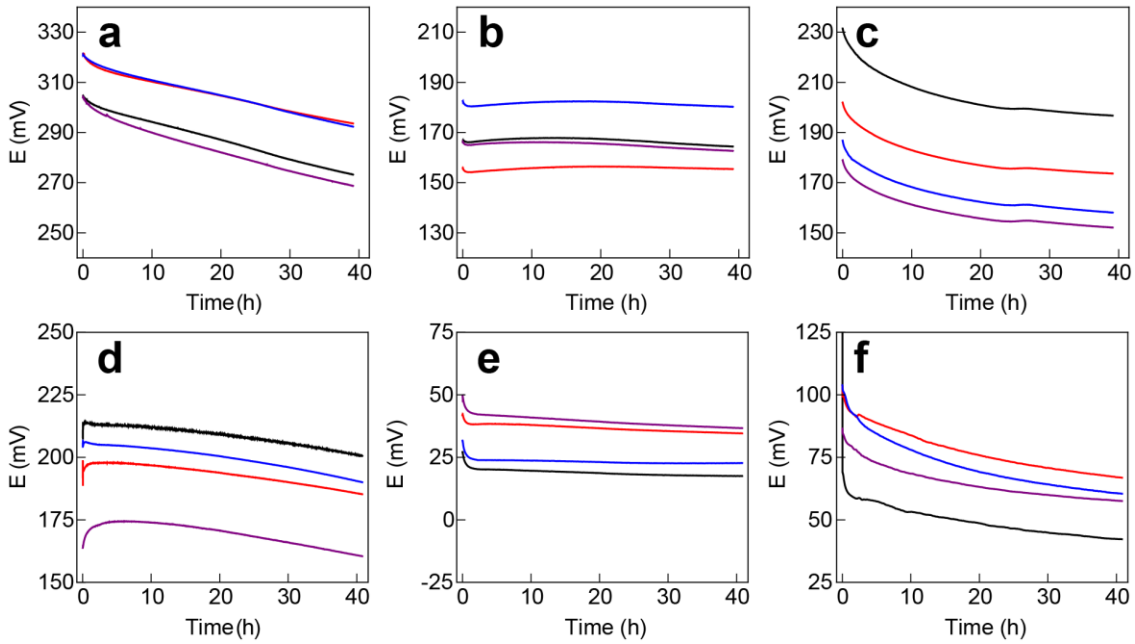

Figure 2.14. Long-term potential stability of solid-contact K^+ ISEs in porcine plasma at 37 °C. Top row: ISEs from **Batch 1** prepared with (a) **Silicone 1**, (b) **Silicone 2**, (c) **Fluorosilicone 1**. Bottom row: ISEs from **Batch 2** prepared with (d) **Silicone 1**, (e) **Silicone 2**, (f) **Fluorosilicone 1**. Each line represents the potential of four identically prepared ISEs. The potentials of ISEs prepared in the same batch were measured at the same time, in the same solution, relative to a Ag/AgCl double junction reference electrode with a 1 M lithium acetate outer filling solution.

Table 2.5. Stability and response characteristics of SC-ISEs (**Batch 2**) during and after exposure to porcine plasma at 37 °C for 41 h.

silicone	drift[a] (µV/h)	response slope[b] (mV/decade)	detection limit[c] (µM)	selectivity[d] ($\log K_{K^+,Na^+}$)
Silicone 1	-495 ± 50	62.7 ± 0.4	1.6 ± 0.2	-4.04 ± 0.07
Silicone 2	-55 ± 51	62.1 ± 0.4	1.9 ± 0.1	-4.00 ± 0.02
Fluorosilicone 2	-297 ± 69	62.1 ± 0.4	2.4 ± 0.2	-3.90 ± 0.02

[a] Drifts were measured relative to a double junction reference electrode at 37 °C for 41 h and calculated as a linear fit of potentials from 30–41 h.

[b] Response slopes were calculated from a calibration curve at 25 °C in the range of 10^{-4} to 10^{-1} M KCl, collected immediately after the 41 h exposure to porcine plasma at 37 °C.

[c] Detection limits were obtained from a calibration curve collected immediately after exposure to porcine plasma for 41 h.

[d] FIM selectivity measurements were conducted immediately after the calibration curve outlined in [b].

After exposure to porcine plasma for 41 h at 37 °C, the response and selectivity of the K^+ ISEs was measured again at 25 °C (Table 2.5). ISEs prepared with all silicones and the fluorosilicone maintained a Nernstian response to K^+ (Figure 2.15). Although the selectivity worsened slightly, it was still high enough for use in physiological samples. This effect might be caused by extraction of neutral hydrophobic species, such as lipids, from the blood plasma.[158] Uptake of such species into the membrane could also be responsible for the observed sensor drift in blood plasma, raising the question whether conditioning of new sensors in plasma could reduce subsequent drift and improve the accuracy of measurements. Interestingly, the selectivity of SC-ISEs that had been stored in 1 mM KCl solution for 17 days after a 39 h exposure to blood plasma (**Batch 1**) was the same as before long-term exposure to porcine plasma (Table 2.3, Figure 2.16), suggesting that the effect of porcine plasma exposure on the selectivity is reversible.

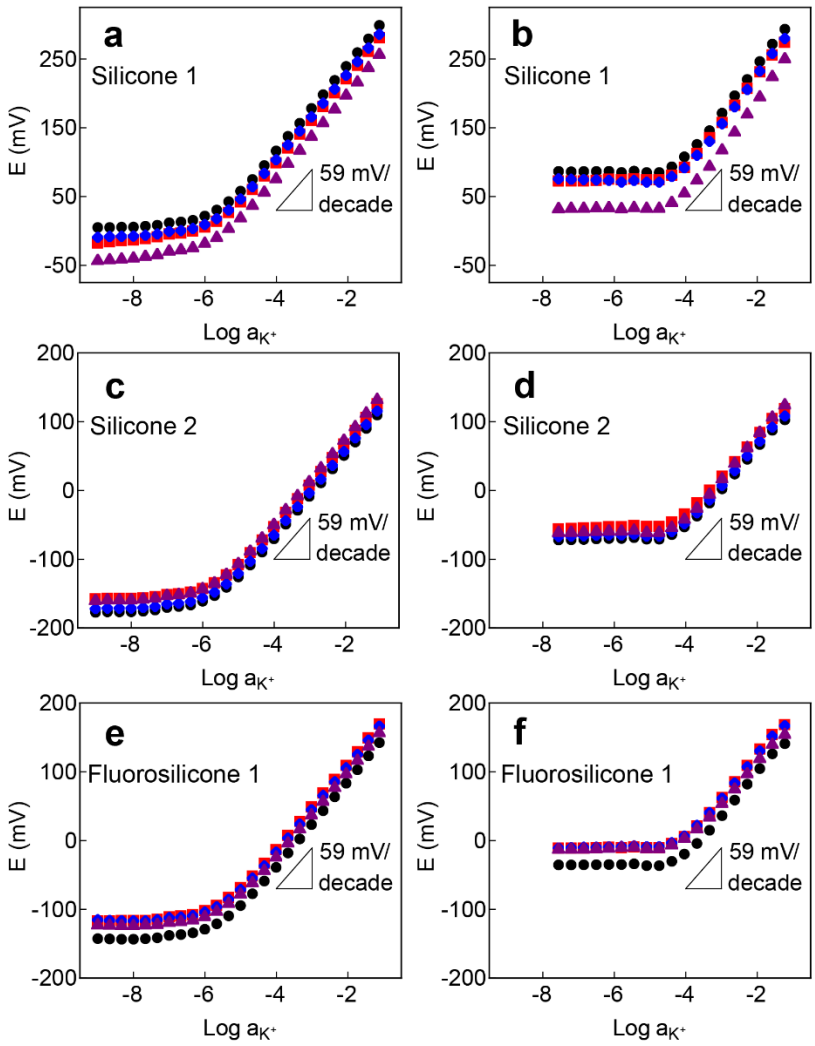

Figure 2.15. Measured potentials, *E*, of K^+ SC-ISEs (**Batch 2**) as a function of the logarithm of K^+ activity in aqueous solution after initial conditioning of the ISEs in 1 mM KCl at 37 °C for 31 days and exposure to porcine plasma at 37 °C for 41 h. Left column: measured potentials of K^+ ISEs in pure KCl solution for SC-ISEs prepared with (a) **Silicone 1**, (c) **Silicone 2**, (e) **Fluorosilicone 1**. The K^+ activity was adjusted by adding aliquots of KCl solution to the sample. Right column: Measured potentials of K^+ ISEs to K^+ in the presence of a 1 M NaCl (FIM) background for SC-ISEs prepared with (b) **Silicone 1**, (d) **Silicone 2**, (f) **Fluorosilicone 1**. The K^+ activity was adjusted by diluting the sample solution with 1 M NaCl. The four differently colored symbols in each graph represent the measured potentials of four identical K^+ ISEs. Potentials were measured against a free-flowing double-junction reference electrode with a 1 M lithium acetate outer filling solution. The measured potentials were corrected for the liquid junction potential at the free-flowing double junction.

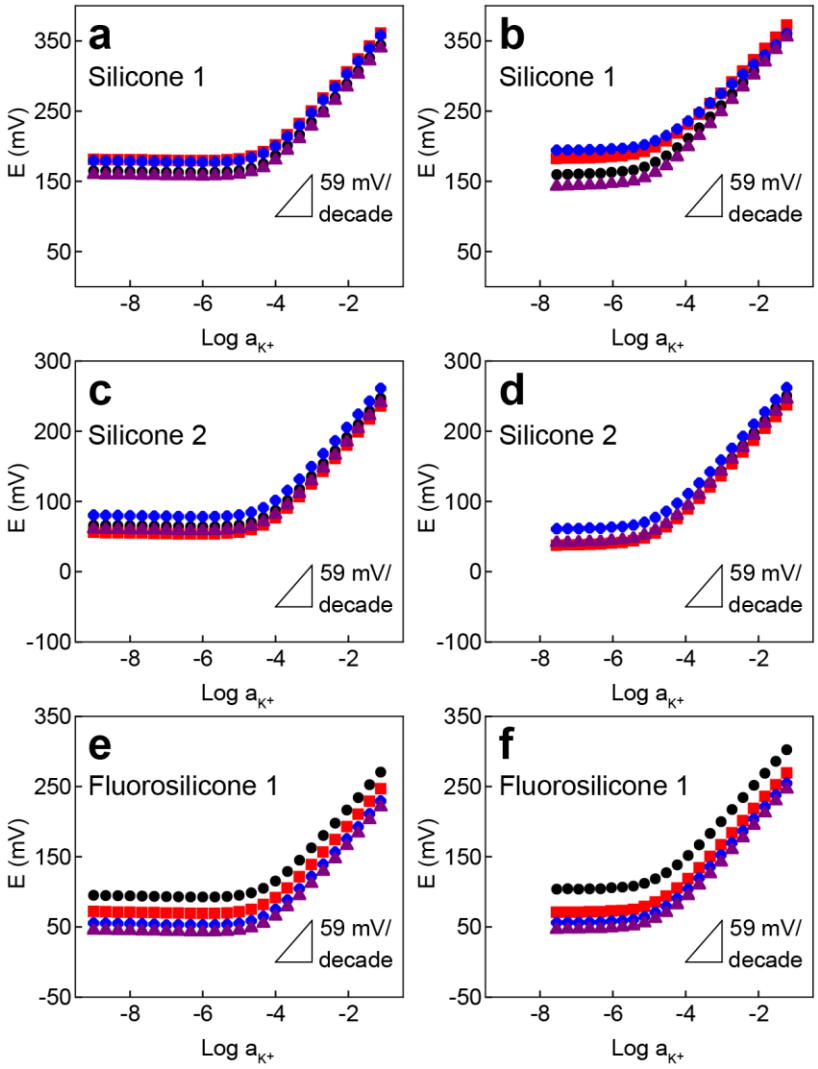

Figure 2.16. Measured potentials, *E*, of K^+ SC-ISEs (**Batch 1**) as a function of the logarithm of K^+ activity in aqueous solution after exposure to porcine plasma at 37 °C for 39 h followed by storage in 1 mM KCl for 17 days. Left column: measured potentials of K^+ ISEs in pure KCl solution for SC-ISEs prepared with (a) **Silicone 1**, (c) **Silicone 2**, (e) **Fluorosilicone 1**. The K^+ activity was adjusted by adding aliquots of KCl solution to the sample. Right column: Measured potentials of K^+ ISEs to K^+ in the presence of a 1 M NaCl (FIM) background for SC-ISEs prepared with (b) **Silicone 1**, (d) **Silicone 2**, (f) **Fluorosilicone 1**. The K^+ activity was adjusted by diluting the sample solution with 1 M NaCl. The four differently colored symbols in each graph represent the measured potential of four identical K^+ ISEs. Potentials were measured against a free-flowing double-junction reference electrode with a 1 M lithium acetate outer filling solution. The measured potentials were corrected for the liquid junction potential at the free-flowing double junction.

To explore whether there are any differences in their membrane structure, **Silicone 1** and **Silicone 2** were analyzed by ATR-FTIR (Figure 2.17) and differential scanning calorimetry (DSC; see Figures 2.18 and 2.19). However, no notable differences between the two silicones were observed. The DSC data for **Silicone 1** and **Silicone 2** are typical for silicones; both had a low glass transition temperature of -118 °C and peaks corresponding to melting at -45 °C and crystallization between -73 and -75 °C. The ATR-FTIR spectra are also consistent with the structure of silicones. **Silicone 2** contains a peak at 470 cm^{-1} that likely corresponds to symmetric Si-O-Si bending modes from the silica filler in **Silicone 2**.[159] This peak is not present in **Silicone 1**, but it can also be found in the FTIR spectrum of **Fluorosilicone 1** (Figure 2.20), which also contains silica filler. It is unclear whether the filler affects the drift of these sensors in blood plasma or whether there are other more important structural features not readily detected by FTIR or evident from DSC. For example, membranes prepared with **Silicone 2** (100 ± 50 GΩ cm and 3 ± 1 GΩ cm for undoped and doped membranes, respectively) have a much lower resistivity than membranes prepared with **Silicone 1** (200 ± 100 and 40 ± 30 GΩ cm for undoped and doped membranes, respectively, measured with the known shunt method, see Table 2.6), which might be caused by a lower crosslink density of **Silicone 2** as compared to **Silicone 1**; ions are expected to have a lower mobility in a more crosslinked polymer.

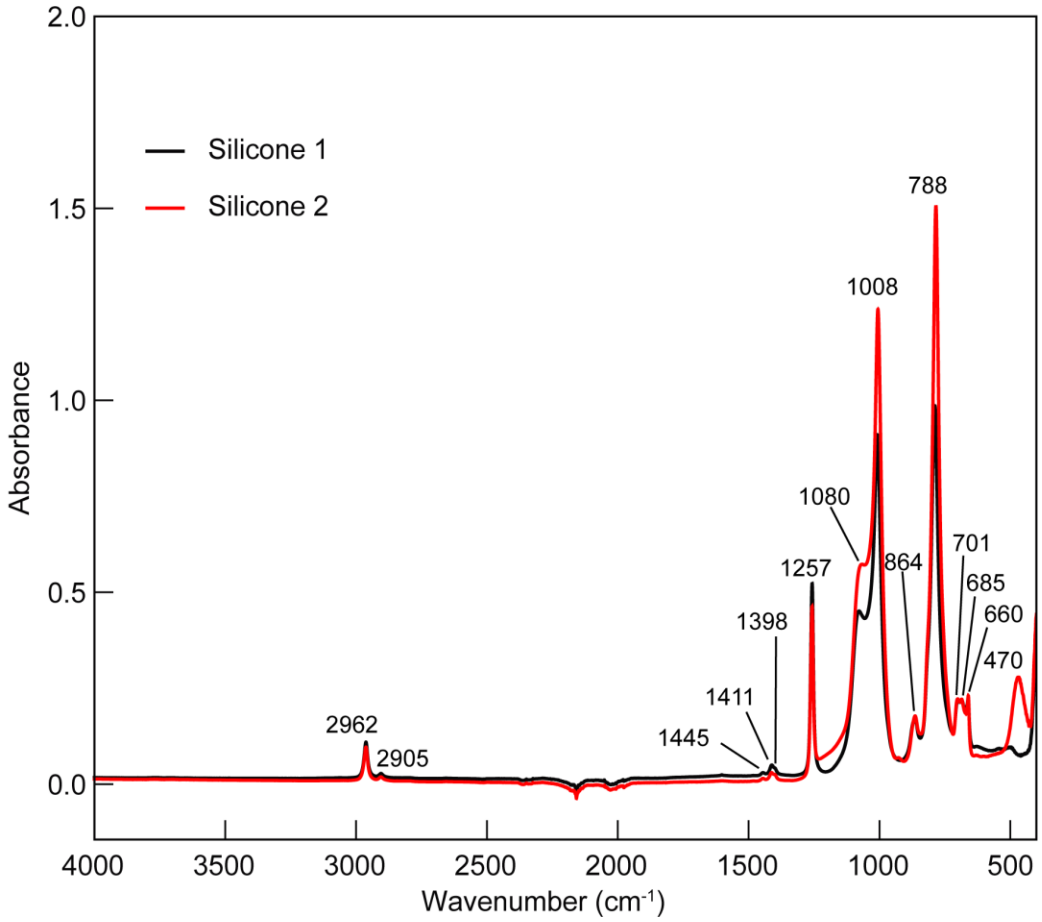

Figure 2.17. ATR-FTIR spectra of neat **Silicone 1** and **Silicone 2**.

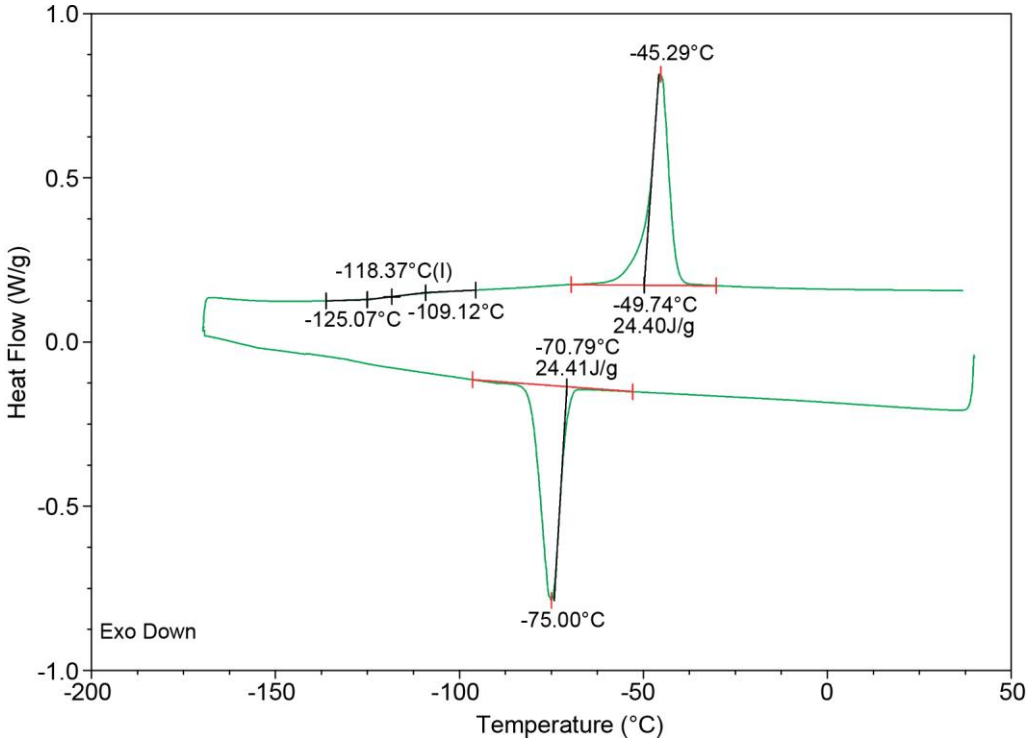

Figure 2.18. DSC of neat **Silicone 1**.

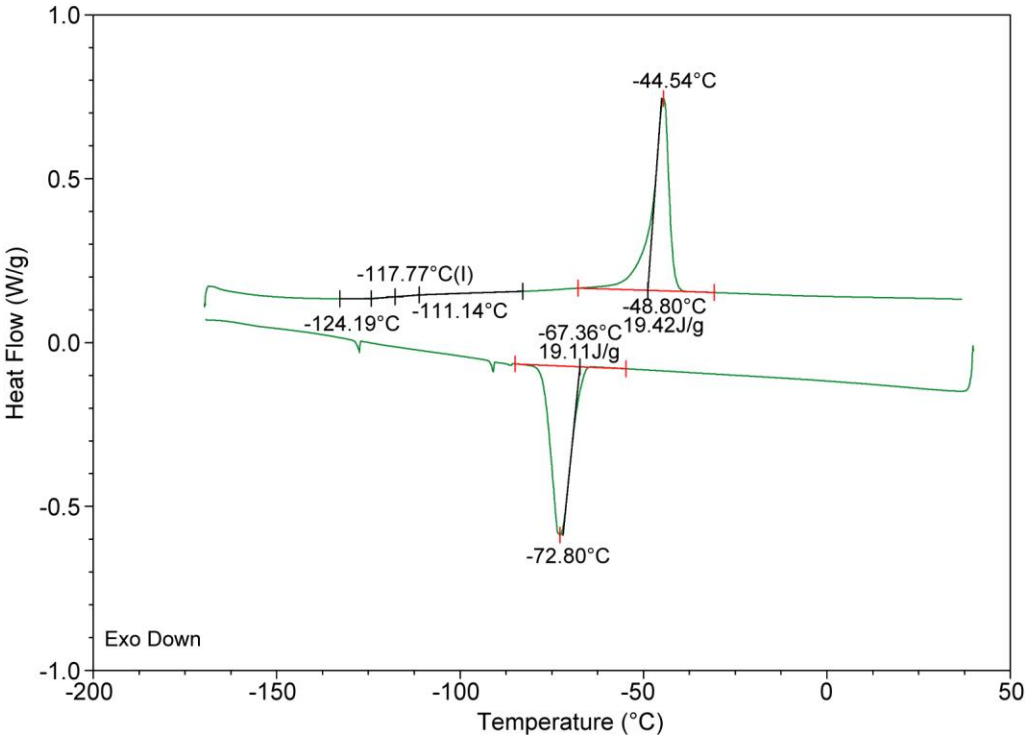

Figure 2.19. DSC of neat **Silicone 2**.

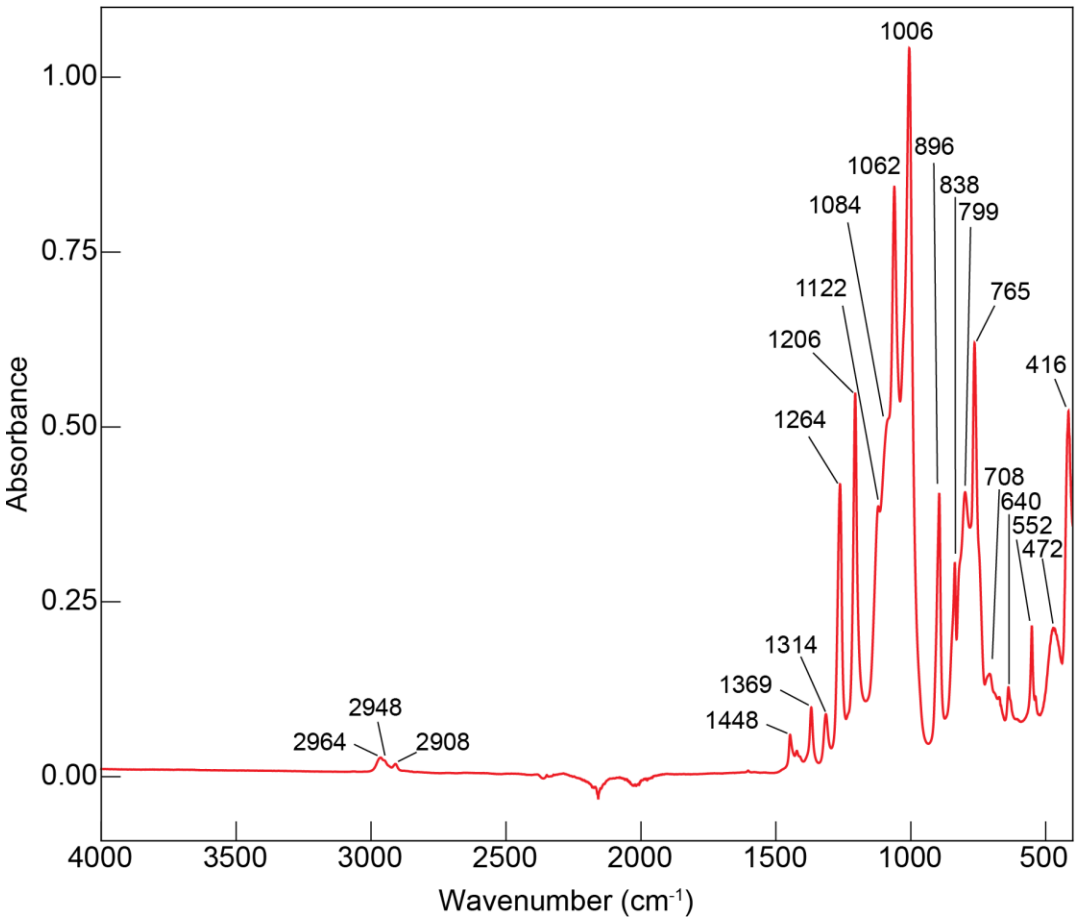

Figure 2.20. ATR-FTIR spectrum of **Fluorosilicone 1**.

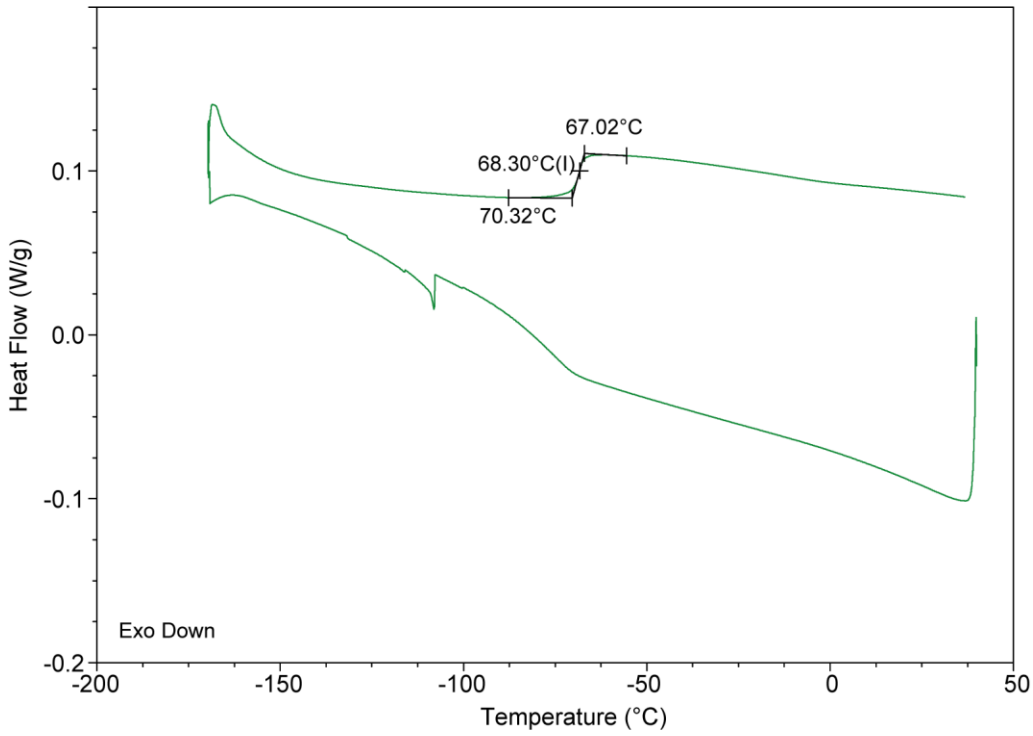

Figure 2.21. DSC of neat **Fluorosilicone 1**.

Table 2.6. Resistance of K^+ SC-ISEs prepared on the graphite/glass electrodes and resistivity of doped (valinomycin, KTpClPB) and undoped silicone membranes assembled into conventional Phillips bodies.[30]

silicone	solid-contact ISE resistance (GΩ)	[a]resistivity of membranes with ionophore and anionic sites (GΩ cm)	[a]resistivity of blank membranes (GΩ cm)
Silicone 1	1.3 ± 0.4	40 ± 30	200 ± 100
Silicone 2	0.13 ± 0.01	3 ± 1	100 ± 50
Fluorosilicone 1	0.056 ± 0.017	0.4 ± 0.2	4 ± 1

[a] Resistivity was measured by the known shunt method for silicone membranes assembled into Phillips bodies with a Ag/AgCl internal reference electrode and a 1 mM KCl inner filling solution.

2.4 Conclusions

With this work, we show that SC-ISEs prepared with plasticizer-free silicone or fluorosilicone membranes and CIM carbon as the solid contact have Nernstian response slopes, excellent selectivity, and as far as we know, the lowest potential drifts reported so far for SC-ISEs with silicone membranes in aqueous salt solutions. Of the reports in the literature on silicone-based ISEs, only a few contain quantitative data for long-term stability (Table 2.7). The drift of K^+ SC-ISEs prepared in this work with **Silicone 2** and CIM carbon as solid contact in aqueous salt solutions (7 ± 5 μV/h) is much lower than the reported value for a Ca^{2+} SC-ISE prepared with a silicone ISM and graphene/polyaniline solid contact (200 μV/h),[117] though differences in conditioning time and sample temperature may contribute to the difference in drift. The authors of that paper also mentioned possible dissolution of polyaniline into the ISM, which may have also contributed to drift, whereas ISEs prepared with CIM carbon do not suffer from such a problem. The drift of SC-ISEs prepared with **Fluorosilicone 1** (3 ± 5 μV/h) and CIM carbon as the solid contact is also lower than that reported for a K^+ ISE prepared with plasticized (DOS) **Fluorosilicone 1** (10 μV/h) on a Ag electrode.[142]

Table 2.7. Drifts reported for silicone or fluorosilicone-based ISEs in the literature.

membrane composition	electrode type	ion	ionophore	drift (μV/h)	reference
Fluorosilicone 1 (10.5% DOS)	ISM on Ag electrode	K^+	valinomycin	10	[142]
Fluorosilicone 1 (10.5 % DOS)	ISM on Ag electrode	Ca^{2+}	ETH 1001	160	[142]
Fluorosilicone 1 (12.4% DOS)	ISM on Ag electrode	Na^+	ETH 2120	40	[142]
Fluorosilicone 1 (12.2% DOS)	ISM on Ag electrode	H^+	TDA	170	[142]
Silicone 1	solid-contact (Graphene/ Polyaniline)	Ca^{2+}	ETH 1001	200	[117]
Silopren K-1000 with Silopren K-11 crosslinker	ISM on a Ag/AgCl electrode	K^+	valinomycin	<200	[110]
92 wt% Silopren K-1000 2.9 wt% crosslinking agent[a] 5.1 wt% valinomycin	conventional	K^+	valinomycin	<0.8	[82]

[a] The crosslinking agent is a mixture of dibutyltindilaurate and hexamethoxysilane (1/2, w/w)

This work also shows that small differences in silicone composition can have a large influence on the long-term stability of SC-ISEs, especially in complex samples. In blood plasma, SC-ISEs prepared with **Silicone 2** exhibited a drift of -55 ± 51 μV/h, much lower than ISEs prepared with **Silicone 1** (-495 ± 50 μV/h) and **Fluorosilicone 1** (-297 ± 69 μV/h). Although the structures of **Silicone 1** and **Silicone 2** are nominally the same, the difference in drift is large. The cause of this difference is not well understood and will be the subject of future study. The recent literature has emphasized the importance of minimizing long-term drifts of SC-ISEs, and typically those drifts are measured in electrolyte solutions. The example here shows that drift in aqueous solution does not

necessarily correlate to drift in real samples, emphasizing the importance of drift measurements in samples for which the sensors are developed.

Chapter 3. Decreasing the CIM Carbon Particle Size by Probe Sonication and Sedimentation to Reduce the Thickness of Solid-Contact Ion-selective Electrodes with CIM Carbon Solid Contacts

A part of this chapter was reproduced from "Design Criteria for Nanostructured Carbon Materials as Solid Contacts for Ion-Selective Sensors" by Chipangura, Y. E.; Spindler, B. D.; Bühlmann, P.; Stein, A. in *Adv. Mater.* **2024,** *36,* 2309778. Copyright 2024, John Wiley and Sons.

In that publication, Y.E. Chipangura contributed to sections that are not included in this chapter. Minog Kim contributed to the carbon particle size separation and electrode fabrication work in this chapter. Katerina I. Graf contributed to the potentiometry experiments in this chapter.

Portions of this work were supported by Medtronic PLC. Parts of this work were carried out in the University of Minnesota Characterization Facility, which receives partial support from the NSF through the MRSEC (award number DMR-2011401) and the NNCI (award number ECCS2025124) programs.

3.1 Introduction

Wearable and implantable ion-selective sensors reported to date are either small patches with integrated solid-contact ion-selective electrodes (SC-ISEs) positioned in a flow channel[12, 15, 18, 160] that adhere to the skin to measure ions in sweat, or the sensing components are coated directly onto a needle,[11, 13, 19] which is then inserted into the tissue of interest. One other notable approach is the use of microneedles made with hydrolauronic acid functionalized-poly(methyacrylate), which is mechanically robust enough to penetrate the skin, but then allows for transport of interstitial fluid to SC-ISEs on a patch outside the skin.[20] For each of these approaches, the SC-ISE will need to have a small overall geometry to fit on the device. The double-layer capacitance at the membrane/solid contact interface[161] (Figure 3.1a) is an important factor to consider when determining the long-term stability of an implantable sensor because small currents are passed through the cell during measurement of the potential.[46] Those currents can charge up the double-layer capacitor, resulting in a change in the potential at the membrane/solid contact interface (ΔE_2), and as a result, a change in the measured electrical potential that is not caused by a change in the sample ion concentration. This results in measurement error and can require more frequent recalibration. When the geometric area of the electrode decreases, the double layer capacitance also decreases, making this problem worse.

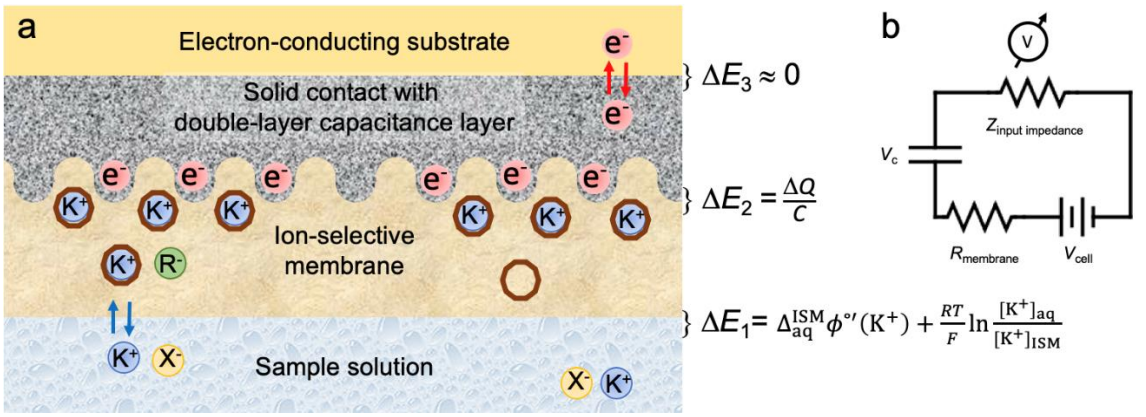

Figure 3.1. (a) Schematic diagram of a solid-contact ion-selective sensor electrode, showing the four phases involved during sensor operation (electron-conducting substrate, electric-double-layer forming solid contact, ion-selective membrane (ISM), and aqueous sample solution), the species present in each phase, and the corresponding interfacial potentials. The brown circles refer to a K^+-selective ionophore, R^- to anionic sites, X^- to counter anions in solution, K^+ to free potassium ions, and K^+ surrounded by a red circle to K^+–ionophore complexes. Q = charge, C = capacitance, $\Delta_{aq}^{ISM}\phi^{o\prime}(K^+)$ = standard ion transfer potential of K^+ from the ISM to the aqueous phase. (b) Simplified equivalent circuit of an ion-selective sensor with a solid contact. The solid contact is represented by the capacitance C, the largest sensor resistance (that of the polymeric membrane) by $R_{membrane}$, the potential difference between the ISE and the reference electrode by the voltage source, V_{cell}, and the input impedance by $R_{input\ impedance}$.

Nanostructured carbon solid contacts have very high surface areas which result in a large increase in double-layer capacitance while keeping the geometric area of the electrode the same. This comes at the expense of a thicker solid contact layer, but if the textural features or pores within the carbon solid contact are small, a sufficiently high double-layer capacitance can be achieved for use in potentiometric sensors without a substantial increase in sensor thickness. One cannot make the pore sizes too small though, because ions in the ion-selective membrane need to be able to reach the surface of the carbon solid contact.[46] Surface area that is inaccessible to ions in the membrane will not

contribute to double layer capacitance. Therefore, the choice of solid contact material has a large impact on the stability of an SC-ISE.

For wearable and implantable applications, the total thickness of the carbon and ISM layers should be as thin as possible to improve device comfort and minimize disturbance to tissue. The ion-selective membrane must completely cover the solid contact layer. If any solid contact material pokes through the ion-selective membrane, it will short-circuit the ion-selective membrane, and the sensor will not function because the potential of the electrode will be dominated by the potential at the solid contact/sample interface. However, increasing the thickness of the ion-selective membrane beyond what is required to completely cover the solid contact is unnecessary. For some electrode configurations, the carbon solid contact layer thickness will determine the minimum thickness achievable for the electrode. However, unlike for the ISM, there is a minimum thickness of carbon required to produce an ISE with sufficiently low long-term drift for the intended application.

To determine the minimum amount of carbon required, one must consider the required accuracy of the sensor and determine how frequently the sensor can feasibly be recalibrated. Both factors are related to the long-term emf drift of the sensor, which is dependent on charging of the double layer capacitor at the membrane/carbon interface due to leakage currents flowing through the voltmeter. The potential drift or change in potential (E) with time (t) equals $\Delta E/\Delta t = i/C$, where i is the current and C is capacitance. The current depends on the input impedance of the voltmeter, the resistance of the ISM, the voltage of the cell, and the capacitance of the solid contact at its interface with the ISM. The latter

parameter is controlled by the surface area of the solid contact, which is a function of carbon morphology when nanostructured solid contact materials are used. A higher capacitance results in smaller signal drift. Thus, outstanding stability in potential has been achieved in recent years with sensors using nanostructured carbon as the solid contact.

To estimate the potential drift caused by charging of the capacitive interface of the ion-selective membrane and the underlying solid contact, the ISE setup can be thought of as a serial combination of a resistor and capacitor, where the solid contact acts as an asymmetric double-layer capacitor, and the resistance is limited by the input impedance of the voltmeter (Figure 3.1b). The potential difference between the ion-selective electrode and reference electrode is the DC voltage measured by a high input impedance voltmeter. When the circuit is closed, a small current will flow, very slowly charging up the capacitor, resulting in signal drift. With the very high input impedance of the voltmeters that are typically used in research (~10^{13} Ω), the current is extremely small for most situations, and exceptionally small signal drifts can be achieved. However, for the design of economical, self-contained, wearable sensors, such a high impedance may not be feasible, and a larger current would result in larger potential drifts. This can be counteracted by using a solid contact with a higher double-layer capacitance. The need for solid contacts with high specific capacitance becomes even more important in the case of highly miniaturized sensors, such as in microneedle array sensors.

For systems of practical relevance, the input impedance of the voltmeter is much larger than the resistance of the ISE membrane, R_{mem}. Assuming that there is no potential across the capacitive interface, V_C, at the start of the measurement ($t = 0$), and that a current limited

by the input resistance, R_{in}, of the voltmeter flows through the cell as soon as the measurement is started (charging up the capacitor until $V_c = V_{cell}$), the potential across the capacitor and the potential measured with the voltmeter, V_m, are given by Equations 3.1 and 3.2, respectively.

$$V_c = V_{cell}\left(1 - e^{\frac{-t}{R_{in}C}}\right) \qquad (3.1)$$

$$V_m = V_{cell} - V_c \qquad (3.2)$$

Figure 3.2 illustrates the predicted time dependence of V_C and V_m for V_{cell} = 500 mV, R_{in} = 10 TΩ, and three representative capacitances.

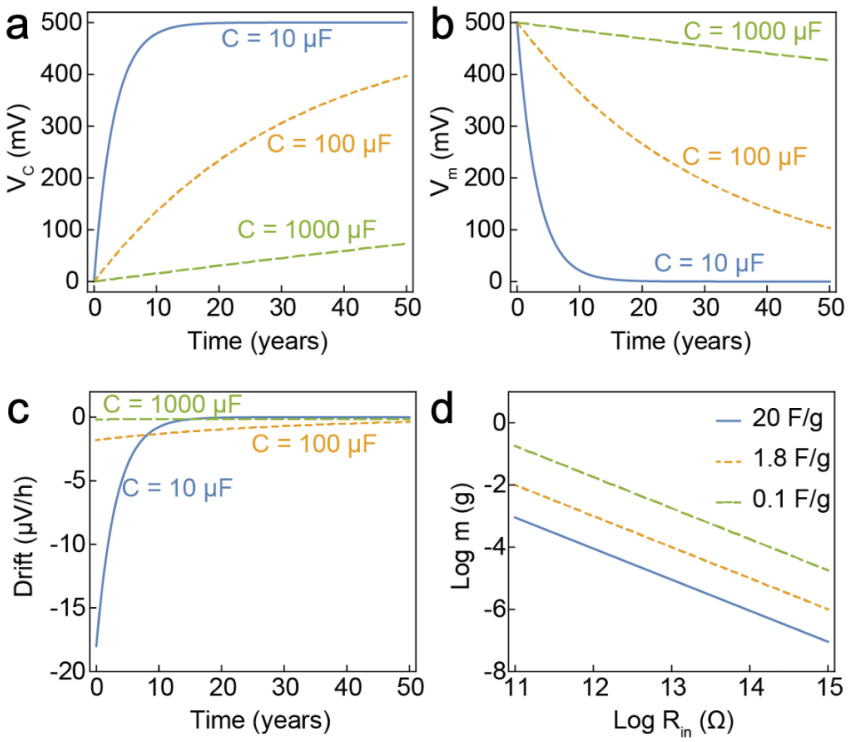

Figure 3.2. Theoretically predicted drift of SC-ISEs when caused exclusively by charging of the electric double layer at the carbon/ISM interface. (a) Potential across the capacitor, V_C. (b) Measured potential, V_m, across the voltmeter after the circuit is closed (assuming V_{cell} = 500 mV, R_{in} + R_m = 10 TΩ). (c) Drift of V_m after the circuit is closed with V_{cell} = 500 mV and R_{in} = 10^{13} Ω. (d) Influence of specific capacitance and input impedance on the minimum mass of solid contact material required to achieve a drift of 1 µV/h for a cell with V_{cell} = 500 mV. C_s values of 20 and 1.8 F/g are values reported for CIM and 3DOM carbon, respectively. The value of 0.1 F/g was included for illustration purposes only.

The expression for drift of V_m is obtained from the derivative of Equation 3.2 with respect to time, giving Equation 3.3.

$$\frac{dV_m}{dt} = -\frac{V_{cell}}{R_{in}C}\, e^{\frac{-t}{R_{in}C}} \qquad (3.3)$$

As illustrated by Figure 3.2c for different values of C, the largest drift occurs immediately after the start of the measurement but eventually decreases with time. The x-

axes of Figures 3.2a–c are shown in years to highlight the expected charging of the capacitive interface. However, drift on the time scale of days or weeks is usually of interest, and longer term drift may also be affected by other factors. Moreover, the thus predicted drift is largest at the start of the experiment. This value can be obtained by evaluating Equation 3.3 at $t = 0$, giving Equation 3.4, which is most relevant for designing sensors for applications in continuous monitoring.

$$\left.\frac{\mathrm{d}V_\mathrm{m}}{\mathrm{d}t}\right|_{t=0} = -\frac{V_\mathrm{cell}}{R_\mathrm{in}C} \qquad (3.4)$$

The minimum frequency of sensor recalibration depends on sensor drift and the acceptable error for a given application. If it is impractical to recalibrate a sensor during operation (such as, for a wearable or implantable sensor), then one can determine the maximum allowable drift to keep the measurement error under the acceptable limit for the duration of use. For a pre-defined maximum allowable drift and assuming that charging of the carbon/membrane interfacial capacitance is the only factor determining potential drift, one can obtain the minimum capacitance required at the membrane/carbon interface for an SC-ISE paired with a voltmeter with a given R_in by inserting the respective values into Equation 3.4. The specific capacitance of the solid contact material is also of high importance; the minimum mass (m) of carbon required to achieve a pre-defined drift decreases with increasing specific capacitance, C_s (Equation 3.5).

$$m = \left|\frac{V_\mathrm{cell}}{R_\mathrm{in}C_\mathrm{s}\left.\frac{\mathrm{d}V_\mathrm{m}}{\mathrm{d}t}\right|_{t=0}}\right| \qquad (3.5)$$

The input impedance, double layer capacitance, and mass of carbon required to target a maximum emf drift are all important factors to consider when designing SC-ISEs for a

specific application. The combination of these factors becomes especially important when designing SC-ISEs with small form factors because the amount of solid contact material that can fit onto a small electrode is limited. Figure 3.2d shows the effect of specific capacitance and input impedance on the minimum mass of carbon required to achieve an initial drift of 1 μV/h for a cell with V_{cell} = 500 mV. For a voltmeter with an input impedance of 10 TΩ, a minimum of 9 μg CIM carbon (C_s = 20 F/g), 100 μg 3DOM carbon (C_s = 1.8 F/g), or 1800 μg of a carbon with C_s = 0.1 F/g is required to achieve a drift of 1 μV/h.

Therefore, the thickness of the carbon layer will be dependent on these factors and on the geometric area of the electrode. From the required mass of the carbon, one can estimate the volume occupied by the carbon, its pores, and the interparticle volume (V_{carbon}, V_{pore}, and V_{ip}) from the density of carbon (d), its specific pore volume ($V_{p,s}$), and the packing factor (P) as shown in Equation 3.6.

$$V_{\mathrm{carbon}} + V_{\mathrm{pore}} + V_{\mathrm{ip}} = m\left(V_{\mathrm{p,s}} + \frac{1}{d}\right)(2 - P) \qquad (3.6)$$

The packing factor is defined as the fraction of volume occupied by the carbon particles and its pores divided by the volume occupied by the carbon, its pores, and the interparticle volume (Equation 3.7).

$$P = \frac{V_{\mathrm{carbon}} + V_{\mathrm{pore}}}{V_{\mathrm{carbon}} + V_{\mathrm{pore}} + V_{\mathrm{ip}}} \qquad (3.7)$$

For a planar electrode, the total volume of the carbon, its pores, and the interparticle volume can also be expressed as the product of the geometric area (A) and the thickness of the carbon layer (h). To obtain the minimum thickness of the carbon layer on a planar surface, these variables can be substituted into Equation 3.6 and rearranged to give Equation 3.8.

$$h = \frac{m}{A}\left(V_{\mathrm{p,s}} + \frac{1}{d}\right)(2 - P) \qquad (3.8)$$

To determine the minimum thickness of the carbon layer required to achieve a drift of 1 µV/h, Equation 3.8 was plotted versus geometric area of the electrode (Figure 3.3) for carbon materials with different specific capacitances, but with all other assumptions kept the same, including pore volume. As the geometric area of the electrode decreases, the carbon layer thickness increases. We also see that as the specific capacitance decreases, the minimum thickness of the carbon layer increases. Therefore, using carbon materials with high specific capacitance is critical for reducing the geometric area of an electrode without increasing its thickness too much.

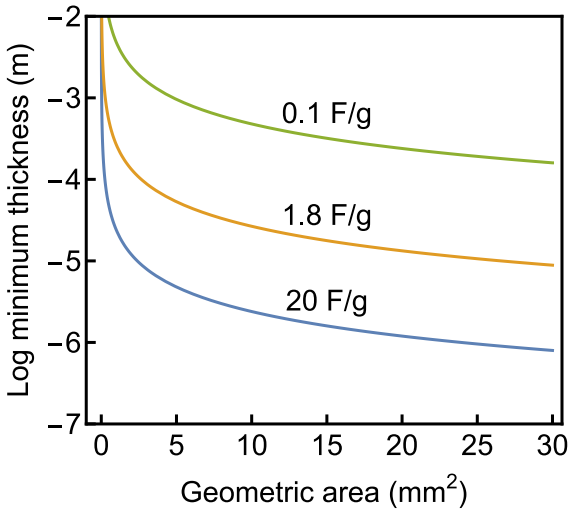

Figure 3.3. Minimum thickness of the carbon-based solid contact layer for carbon materials having capacitances of 20, 1.8, and 0.1 F/g to achieve a drift of 1 µV/h. The carbon was assumed to have a density of 1.5 g/mL with a pore volume of 1.46 cm^3/g and a packing factor of 0.75. The cell was assumed to have a potential of 500 mV, and the voltmeter has an input impedance of 10^{13} Ω. The scale on the y-axis is in log meters.

To illustrate how this translates to real electrodes, we can consider the outer surface of a microneedle used in transcutaneous pH and CO_3^{2-} sensors[13] with a diameter of 160 µm and a coating length of 500 µm. If we approximate the needle as a cylinder, it has a geometric surface area of 0.58 mm. If we use CIM carbon to coat this microneedle and assume a specific capacitance of 20 F/g, a pore volume of 1.46 cm^3, a glassy carbon density of 1.5 g/mL, a packing factor of 0.75, a cell potential of 500 mV, and an input impedance of 10^{13} Ω, then the carbon layer must be at least 41 µm thick to achieve a long-term emf drift ≤1 µV/h. Adding 82 µm to the diameter of a 160 µm needle represents a noticeable increase in diameter. If we increase the input impedance of the voltmeter to 10^{15} Ω, a carbon layer thickness of only 0.41 µm is required, which represents a much smaller increase in the microneedle size. It is important to note that an input impedance of 10^{15} Ω is pushing the limits of electronics currently available and as a result, decreasing electrode sizes further will become even more difficult.

Numerous carbon solid contacts have been used over the years, including three-dimensionally ordered macroporous (3DOM) carbon,[45] single[40, 162] and multi-walled carbon nanotubes,[163] reduced graphene oxide,[164, 165] carbon black,[166] and colloid-imprinted mesoporous (CIM) carbon.[47] Among these materials, CIM carbon stands out as a solid contact material for application in SC-ISEs for several reasons. SC-ISEs prepared with valinomycin as the ionophore in a polyvinyl chloride (PVC) matrix plasticized with 2-nitrophenyl octyl ether (*o*-NPOE) have some of the lowest long-term drifts reported to date (1.3 µV/h)[47] and one of the highest specific capacitances reported for a carbon solid contact. Additionally, K^+ SC-ISEs prepared with plasticizer-free silicone matrixes have

low long-term drift (as low as 3 µV/h).[167] CIM carbon is an effective solid contact because it has a high surface area, and it contains interconnected mesopores with diameters of 24–30 nm, which is large enough to allow for the relevant ions to enter the pores. The oxygen content on the surface of CIM carbon is low, and the resulting ISEs are insensitive to CO_2, O_2, and light.[47] It is also an attractive material because the synthesis is simple and should be compatible with manufacturing methods for large scale production (see Chapter 2 for synthesis details).

One drawback of CIM carbon is that by mass, most as-synthesized CIM carbon prepared by the method described in Section 2.2.2 consists of particles with sizes of 1–50 µm. This makes fabrication of SC-ISEs with a thickness <100 µm challenging because multiple layers of carbon particles are required to cover the underlying conductor (Figure 3.4), resulting in a thick CIM carbon layer (approximately 130–150 µm).

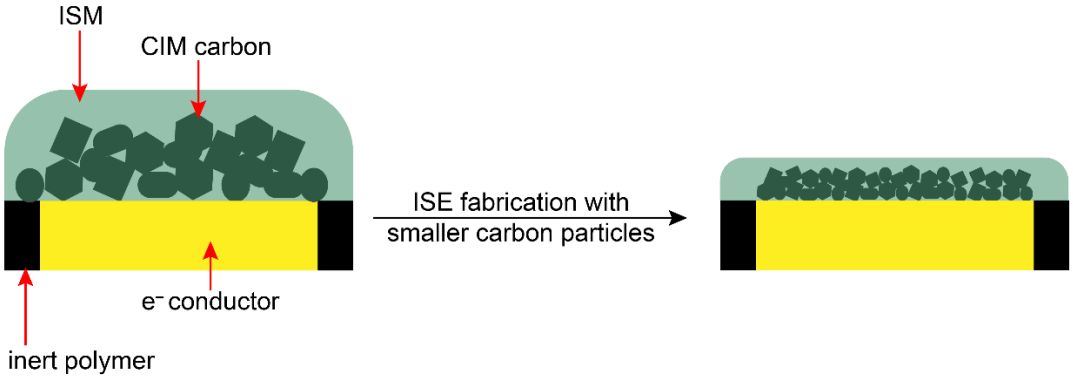

Figure 3.4. Schematic showing that smaller CIM carbon particles allow for fabrication of thinner SC-ISEs.

To address this problem, we investigated different methods to decrease the particle size of CIM carbon. Of the methods tested, we show that probe sonication is the most effective method to produce small CIM carbon particles, though some large particles remain. The

small and large particles can be separated by sedimentation. Importantly, we show that the CIM carbon pores and the hydrophobic surface are maintained after probe sonication and sedimentation. We also show that SC-ISEs prepared with these solid contacts having a total thickness (membrane+carbon layer) of 80 µm can be achieved, and the resulting SC-ISEs have Nernstian responses, the expected selectivity to K^+ vs. Na^+, and can reach low long-term drift.

3.2 Experimental section

3.2.1. Materials

Reagents were purchased from the following sources: potassium bromide (FT-IR grade ≥99%), potassium tetrakis(*p*-chlorophenyl)borate (KTpClPB), valinomycin (Selectophore^{TM}); tetrahydrofuran (≥99.9%, anhydrous, inhibitor-free), *N*-methyl-2-pyrrolidone (NMP) (anhydrous, 99.5%) were purchased from Sigma-Aldrich (St Louis, MO); ethanol (200 proof, anhydrous) from Decon Laboratories, Inc (King of Prussia, PA); dichloromethane (≥99.5%) from Fischer Scientific (Waltham, MA); Dow 3140 silicone from Pilots HQ LLC (Waterford, MI); aluminum foil (180 mm with x 15 µm thick) and poly(vinylidene fluoride) (PVDF) (≥99.5%) from MTI corporation (Richmond, CA). Deionized water was purified to a resistivity of 18.2 MΩ·cm with a Milli-Q PLUS reagent-grade water purification system (Millipore, Bedford, MA). CIM carbon was synthesized using the procedure described in Chapter 2.

3.2.2 CIM carbon particle size reduction

Ball milling, bath sonication, and probe sonication were evaluated for reducing the CIM carbon particle size. For ball milled CIM carbon, CIM carbon was ball milled using an agate ball-and-cup set in an 8000M Mixer/Mill high-energy ball mill (SPEX SamplePrep) for 30 min. For bath sonication, CIM carbon (110 mg) was mixed with 10 mL EtOH:H_2O (1:1 v/v) and bath sonicated for 1 h at room temperature using a Branson 3800 ultrasonic bath. The CIM carbon was collected by filtration and dried in a vacuum oven at 110 °C for 14 h. For probe sonication, CIM carbon (322 mg) was mixed with 10 mL EtOH/H_2O (1:1) v/v. The mixture was probe sonicated at 0 °C (ice bath) for 1 h (5 s pulse, followed by 5 s relaxation) using a 750-watt Cole-Parmer ultrasonic processor at 35% amplitude with a 3/16" diameter microtip. The solvent was evaporated using a rotary evaporator to give dry CIM carbon powder (319 mg). Several batches of CIM carbon were combined for the size separation. The dried, probe-sonicated CIM carbon (4.03 g) was mixed with 1.0 L dichloromethane in a 1 L glass bottle. The mixture was bath sonicated for 30 min, and the carbon was allowed to settle overnight. The top 800 mL (containing the small CIM carbon particles) was siphoned off. The bottom 200 mL was diluted with 800 mL dichloromethane, bath sonicated again for 30 min, and allowed to settle overnight. The top 800 mL was siphoned off and combined with the top 800 mL from the first separation. This process of redispersing, and separating the bottom layer was repeated one additional time. The top 800 mL from the first, second, and third separations were combined and the solvent was evaporated to dryness on a rotary evaporator. The solid was

further dried in a vacuum oven at 110 °C overnight to give small CIM carbon as a black powder (400 mg, 10% yield).

3.2.3. CIM carbon characterization

To get an estimate of particle size distribution, each CIM carbon sample was dispersed in ethanol by bath sonication for 5 min, one drop of solution was then drop cast onto a silicon wafer and allowed to dry in air overnight in a semi-closed container. The dried carbon was then coated with 2 nm iridium using an EM ACE600 sputter coater from Leica Microsystems (Wetzlar, Germany). Scanning electron microscope (SEM) images were acquired for each sample with a JEOL 6500 SEM operated at a 5.0 kV accelerating voltage. The SEM images at 500× magnification were analyzed using ImageJ (National Institutes of Health) to count the particles and determine their two-dimensionally projected surface area. To obtain particle length and volume, the particles were assumed to be cubic, since the particles have irregular shapes and did not look spherical (see Figure 3.5). The length of a particle was obtained from the square root of its area and the volume was obtained by raising its area to the power of 3/2.

Transmission FTIR spectra were collected using a Nicolet Magna 760-IR spectrometer. A mass of 1 mg of CIM carbon was mixed with 100 mg KBr and ground to a fine powder in an agate mortar and pestle. A mass of 30 mg of the fine powder was pressed into a 13 mm diameter pellet using a stainless-steel die set (International Crystal Laboratories, Garfield, NJ) using a hydraulic press until the pressure reached 1.5 GPa. N_2 gas sorption measurements were performed on an iQ2 gas sorption analyzer (Quantachrome, Boynton

Beach, FL). Samples were outgassed at 120 °C under vacuum for 12 h before measurement. The specific surface area was calculated using the Brunauer-Emmett-Teller (BET) method. The pore size distribution and cumulative pore volume were calculated from the adsorption branch of the isotherm using the slit/sphere/cylinder QSDFT model for carbon in the ASiQwin software from Quantachrome.

3.2.4. Fabrication of SC-ISEs

Amounts of 150 mg of small CIM carbon, 600 µL NMP, and 291 µL of a 5 wt% PVDF solution in NMP (15 mg PVDF) were mixed in an agate mortar and pestle until a black, uniform slurry was obtained. The carbon slurry was cast onto Al foil using a doctor blade to form a uniform film of CIM carbon on the foil. Two separate films of CIM carbon were prepared on two separate sheets of Al foil. One carbon film was dried at room temperature in a fume hood for 18 h and the other was dried in a vacuum oven at 120 °C for 18 h. To coat the carbon with ion-selective membrane, 4.0 mg valinomycin, 1.0 mg KTpClPB, and 400 mg Dow 3140 silicone were dissolved in 1.0 mL THF. Some of the ion-selective membrane (ISM)-forming solution was pipetted onto the Al foil to form a thick layer of solution. Using a doctor blade, the CIM carbon layer was covered with the ISM solution. The ISM was allowed to dry in air for 1 h. Then, a second coating of ISM solution was applied. The films were cured in air at room temperature for 96 h. Electrode disks (0.25-inch diameter) were punched out from the films and assembled into electrode bodies with a 0.25-inch inner diameter, with the ion-selective membrane side facing out. A graphite rod was inserted into the electrode body to contact the Al foil. The graphite rod was pressed

against the Al foil by putting the electrode body screw cap on and gently tightening it. An electrical wire was placed between the screw cap and the graphite rod, to allow for easy connection to the voltmeter during operation.

3.2.5. Potentiometric measurements

SC-ISEs were conditioned in 1 mM KCl at 37 °C. Potentials were measured relative to a double junction Ag/AgCl reference electrode with a saturated AgCl/3 M KCl inner filling solution and a 1.0 M lithium acetate bridge solution (DX-200, Mettler Toledo, Columbus, OH). Potentials were measured using an EMF-16 voltmeter (Lawson Labs Inc, Malvern, PA). K^+ calibration curves were measured at 25 °C by successive addition of aliquots of standard KCl solutions to the sample solution. Potentials were corrected for liquid junction potential using the Henderson formalism.[145] Activity coefficients were calculated using a two-parameter Debye-Hückel approximation.[144]

3.3. Results and discussion

3.3.1. CIM carbon particle size reduction

To reduce the total thickness of SC-ISEs, the thickness of the carbon layer needed to be reduced. The as-made CIM carbon (Figure 3.5a) comprises a significant quantity of large particles (>50 μm). CIM carbon is synthesized by mixing silica spheres with mesophase pitch (a synthetic carbon material containing mostly aromatic species). The mesophase pitch is melted to mix with the silica spheres, and then carbonized. After carbonization, carbon/silica composite is one big piece of material that is then ground into a fine powder with a mortar and pestle. The particle sizes of the as-made CIM carbon are

likely defined by how the carbon/pitch composite breaks during the grinding process and likely does not change during silica extraction and H_2 treatment steps.

Any carbon film will contain several layers of particles to ensure that the underlying conductor is completely covered with CIM carbon, which is required to maximize double layer capacitance and prevent water layer formation. Therefore, it is likely not possible to produce a CIM carbon film with a thickness <100 μm with the as-made CIM carbon. To reduce the CIM carbon particle size, ball milling, bath sonication, and probe sonication were evaluated. The particles were counted using ImageJ in multiple SEM images of different areas on the silicon wafer for each sample. Image J provides a list of particles with their area. Each particle was assumed to be a cube, and its length was calculated as the square root of its projected area. Histograms of the CIM carbon particle sizes (Figure 3.6) show that in all cases, the majority of particles have a size less than 5 μm, with only a few particles with sizes above 5 μm. Counting particles by number, however, is misleading as one large particle contains significantly more mass than one small particle. To account for this, volume-weighted histograms were also plotted, where the *y*-value is the sum of the cubed lengths (estimated volume) for particles in each bin. From the volume-weighted histograms, the normalized cumulative particle size was calculated and plotted in each graph in Figure 3.6. From this data, less than 20% of the bath sonicated CIM carbon (by volume) corresponds to particles with dimensions <10 μm in size and 7% with dimensions less than 5 μm in size. Ball milling the CIM carbon is very effective at breaking down the large particles, with 72% of the large particles (by volume) having a size <10 μm and 16% with size <3 μm. Probe sonicating CIM carbon was not as effective in breaking up the large

particles, but it did produce a lot of very small particles, with 33% of particles (by volume) having a size <5 μm and 26% of particles having a size of < 3 μm.

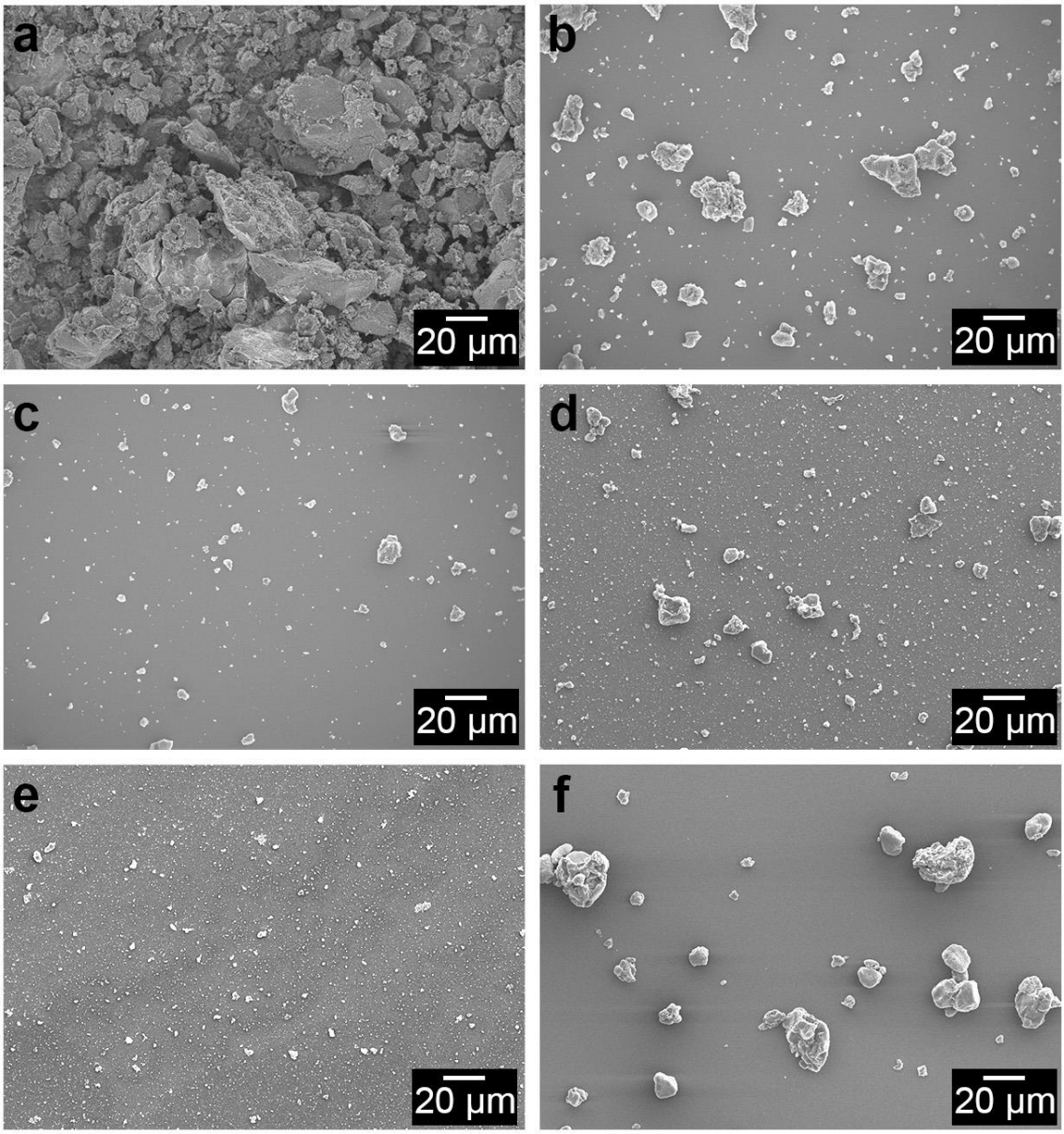

Figure 3.5. SEM images of (a) as-made CIM carbon and CIM carbon particles deposited on a silicon wafer after (b) bath sonication, (c) ball milling, (d) probe sonication, (e) probe sonication and sedimentation (top fraction after first sedimentation step, small particles), and (f) probe sonication and sedimentation (bottom fraction after first sedimentation step, large particles).

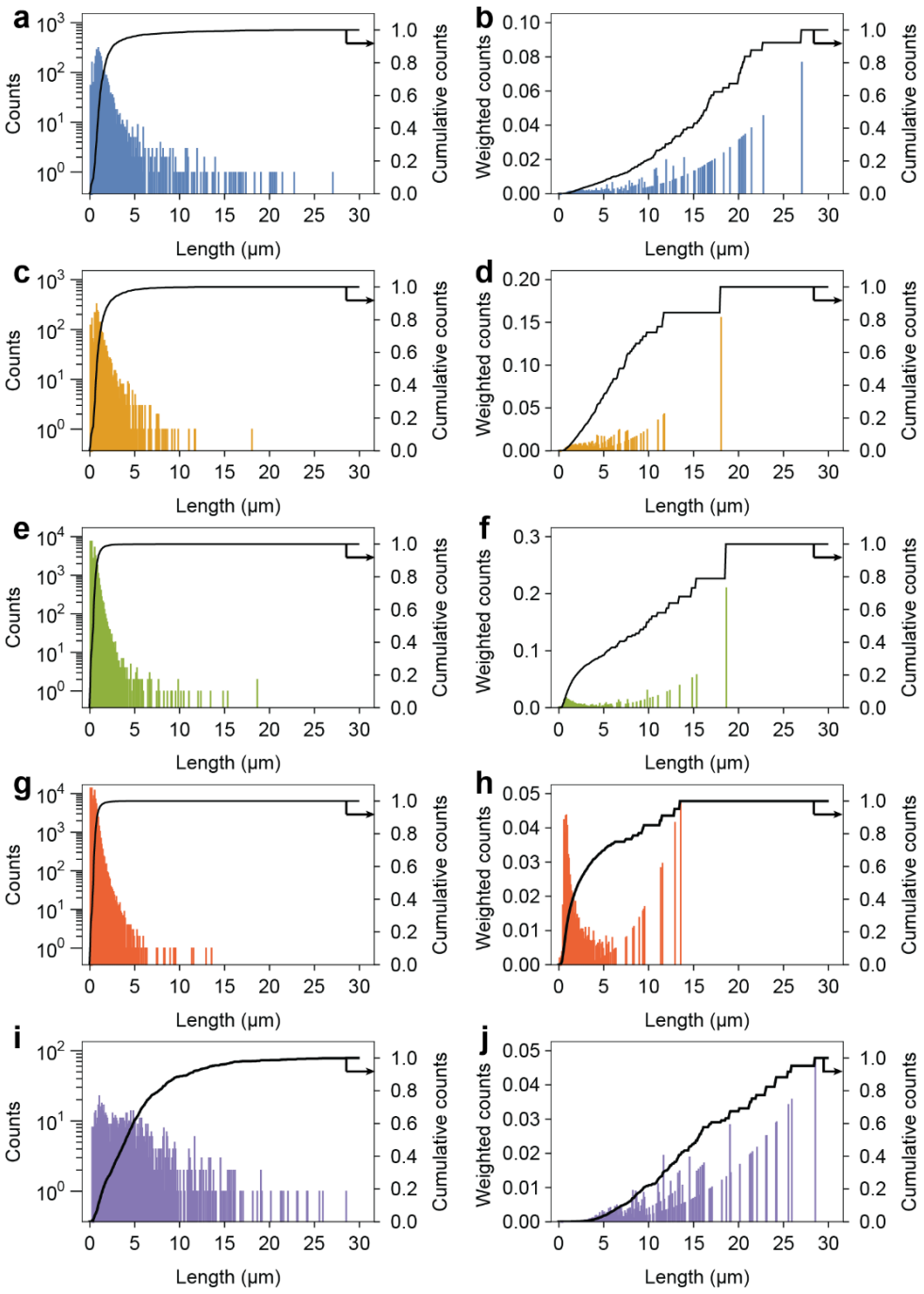

Figure 3.6. Histograms for particle size distributions based on particle counts (left column) and their corresponding volume-weighted histograms (right column) of (a,b) bath sonicated (c,d) ball milled, (e,f) probe sonicated, (g,h) probe sonicated and size separated (top fraction after first sedimentation step, small particles), and (i,j) probe sonicated and size separated (bottom fraction after first sedimentation step, large particles).

Since probe sonication produced the smallest CIM carbon particles, we chose to separate the large particles from the small particles by gravity sedimentation in dichloromethane (Figure 3.7). Dichloromethane was chosen as the solvent because its density (1.3 g/mL) is lower than that of glassy carbon (1.5 g/mL), but it is still close enough to allow for efficient size separation. Other organic solvents were evaluated, but they were ineffective because all CIM carbon would settle to the bottom within a few minutes. After sedimentation from dichloromethane for 24 h, the top 800 mL fraction was separated from the bottom 200 mL. After the first sedimentation step, the top 800 mL contained CIM carbon particles with 70% of particles by volume having a size of less than 5 µm and 57% of all particles having a size <3 µm. All particles had a size less than 14 µm (Figure 3.5e, Figure 3.6g, and Figure 3.6h) whereas the bottom fraction (after the first sedimentation step) contained almost exclusively large carbon particles (Figure 3.5f, Figure 3.6i, and Figure 3.6j). The yield for small CIM carbon particles was low, so the 200 mL containing large particles was re-used in additional probe sonication and sedimentation steps to give a total yield of 10%. Although this yield of the small CIM carbon particles was still low, the amount obtained was sufficient for further analysis and use in SC-ISEs.

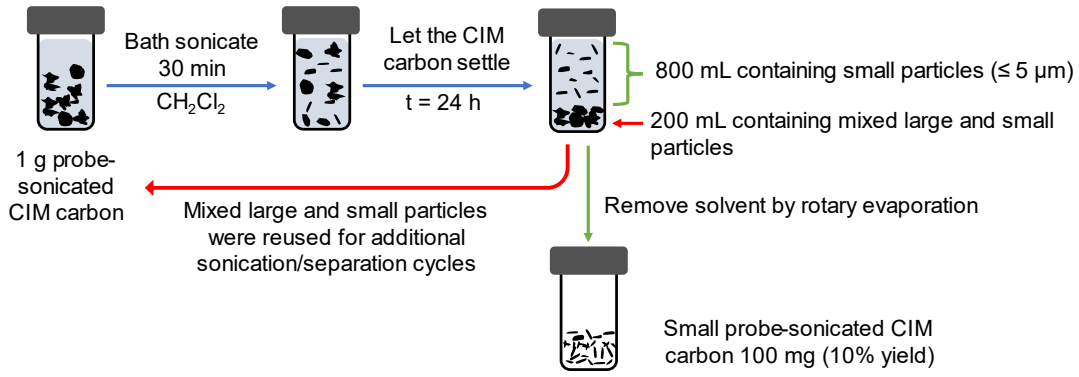

Figure 3.7. Schematic of the sedimentation process for size separating the large and small probe sonicated CIM carbon particles.

3.3.2. Characterization of small CIM carbon

Analysis of the CIM carbon particles by N_2 gas sorption showed that the mesopores were maintained after probe sonication and sedimentation (Figure 3.8). Neat CIM carbon has a type IV isotherm with H2 hysteresis, consistent with a mesoporous carbon material with ink-bottle pores.[168] The DFT pore size distribution obtained from the isotherm shows that CIM carbon has pores with diameters in the range of 25–35 nm, with some additional pores near 40 nm. The pores with diameters in the range of 25–35 nm are formed during the CIM carbon synthesis and are defined by the size of the silica sphere template during the imprinting and carbonization steps. The pores near 40 nm may be caused by defects in the pore wall of adjacent pores or from aggregates in the silica sphere template. The isotherm for the probe sonicated CIM carbon looks very similar to that of neat CIM carbon, indicating no change in pore structure. The small probe sonicated CIM carbon still exhibits a hysteresis from 0.8 to 0.9 P/P_o, indicating that the mesopores are maintained. There is also a large increase in adsorbed nitrogen at high pressure, which indicates that the small CIM carbon contains more textural porosity than neat CIM carbon. This is expected, since

smaller particles have more surface exposed on the outside of the particle. As a result, more pores can form between adjacent particles where capillary condensation of nitrogen can occur at high relative pressure during the gas sorption experiment.

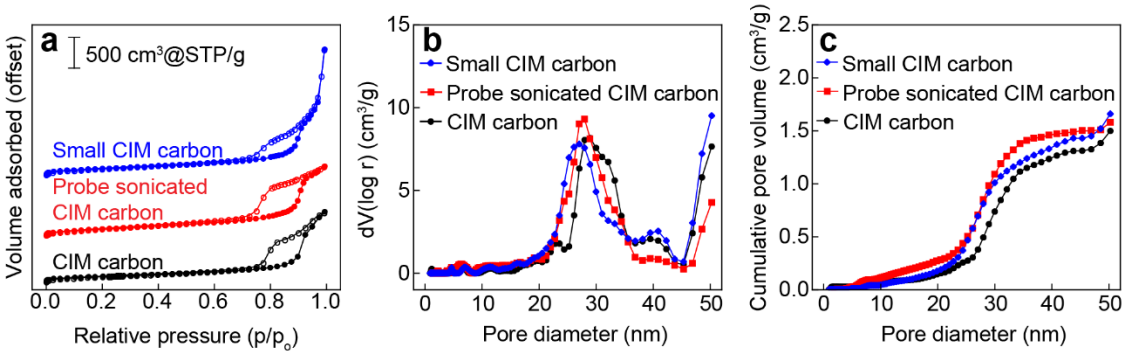

Figure 3.8. N_2 gas sorption analysis of neat, probe sonicated, and small CIM carbon. (a) N_2 gas sorption isotherm, (b) pore size distribution, and (c) cumulative pore volume. The pore size distribution and cumulative pore volume were calculated from the adsorption branch of the isotherm using the slit/cylinder/sphere model for carbon in the ASiQwin software from Quantachrome.

Transmission FT-IR analysis indicates that no measurable introduction of oxygen to the carbon surface occurred during probe sonication and sedimentation (Figure 3.9). The FTIR spectra of CIM carbon after probe sonication only shows very weak absorptions between 900 and 1600 cm^{-1}, which likely correspond to C=C stretches. Almost no C–H stretches are observed just below 3000 cm^{-1}, and there is no peak corresponding to –OH in any samples except for the CIM carbon sample that had been freshly silica extracted using an aqueous KOH solution. Surprisingly, the probe sonicated CIM carbon in Figure 3.9 that had not been hydrogen treated also did not show any evidence of surface –OH groups. It is not clear how probe sonication in an EtOH:H_2O (1:1 v/v) causes reduction of surface –OH groups, though others have also reported that graphene oxide can be reduced in deionized

water at 95 °C[169] and even by bath sonication in water at 50 °C.[170] It is possible that the high local temperatures induced during probe sonication cause –OH elimination reactions to occur on the surface of the CIM carbon. This experiment should be repeated to confirm this result. The lack of –OH peaks observed in the FTIR spectrum for the small CIM carbon (which was H_2 treated before the probe sonication step) shows that it also has a low oxygen content. A low oxygen content is an important characteristic for solid contact materials in SC-ISEs, because a hydrophobic surface prevents water layer formation and eliminates sensitivity of the SC-ISE to reactive gases like CO_2 and O_2. Therefore, the small CIM carbon was deemed acceptable for use as a solid contact material for SC-ISEs.

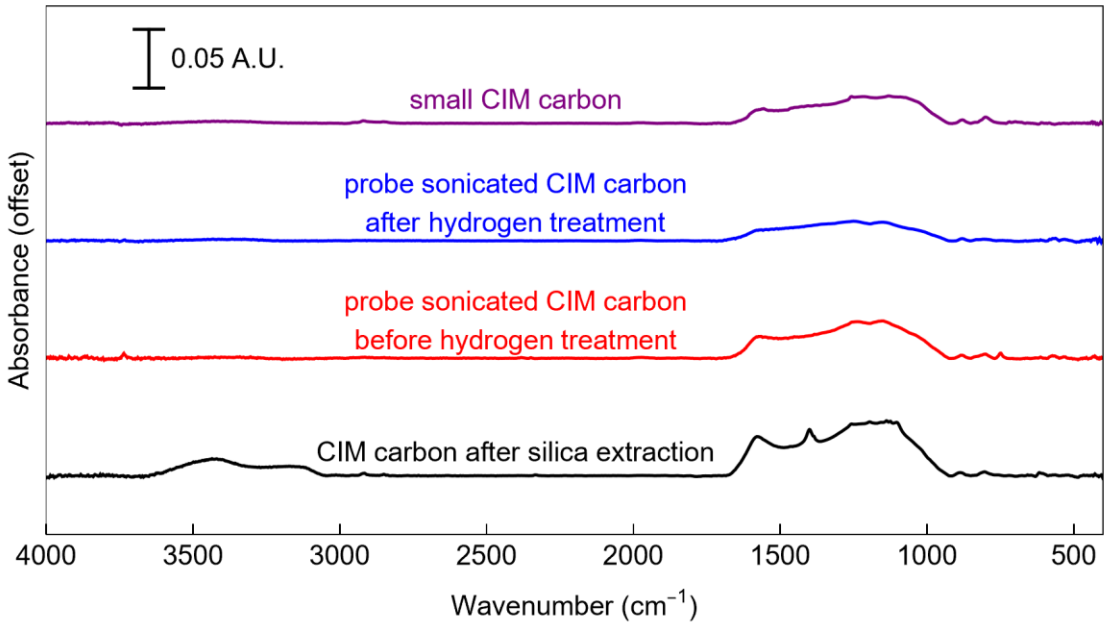

Figure 3.9. Transmission FTIR spectra of CIM carbon after silica extraction (sample was not H_2 treated), probe sonication (sample was not H_2 treated), probe sonication followed by H_2 treatment, and small CIM carbon (which was H_2 treated before the probe sonication and sedimentation steps).

3.3.3. Fabrication of SC-ISEs with small carbon

SC-ISEs were prepared by casting films of CIM carbon with PVDF as binder onto a sheet of aluminum foil, using a doctor blade to coat the carbon and ion-selective membrane layers (Figure 3.10). Use of a doctor blade allows for good control over the thickness of the deposited carbon layer. NMP was used as the solvent for casting the carbon film. Because NMP has a high boiling point (202 °C), we compared films that were dried in air at room temperature in a fume hood overnight and ones dried in a vacuum oven at 120 °C before application of the ion-selective membrane. Attempts to compress the dried carbon layers using a roll press resulted in carbon delaminating from the Al foil. Therefore, the ion-selective membrane was coated directly onto the CIM carbon layer after drying. The ISM was cast on the CIM carbon layer using a doctor blade, with the height of the blade set just high enough to avoid touching the CIM carbon layer. SC-ISEs with one and two coatings of ISM were prepared because the ISM solution contained a significant amount of solvent that evaporates, resulting in a significantly lower thickness of the dried and cured ISM layer than was set using the height adjustment on the doctor blade. The CIM carbon layer had a thickness of 57 ± 4 μm. SC-ISEs with one and two coatings of ISM had total thicknesses of 80 ± 13 and 133 ± 18 μm, respectively. The total ISE thicknesses here are much lower than those prepared on the graphite/glass electrodes shown in Chapter 2 (613 ± 41 μm).

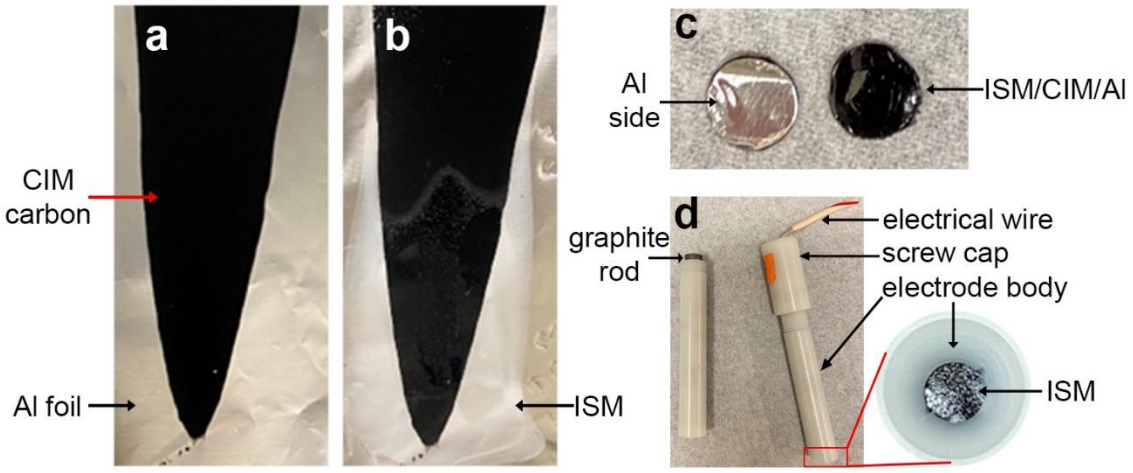

Figure 3.10. Fabrication and assembly of SC-ISEs into electrode bodies for use in potentiometric experiments. (a) CIM carbon cast onto Al foil, (b) CIM carbon coated with a K^+ ion-selective membrane, (c) disks of Al/CIM/ISM punched out of the parent membrane after the ISM was cured, and (d) assembly of the Al/CIM/ISM disks into an electrode body for use in potentiometry.

The SC-ISEs were assembled into electrode bodies with a 0.25-inch inner diameter with the ISM side facing out of the electrode (Figure 3.10d). Electrical contact was made on the Al-facing side using a graphite rod, and a slight pressure was applied to form a seal between the ISM and electrode body. This was done to ensure that no water could make contact with the graphite and short the electrode.

3.3.4. Potentiometric Results

The SC-ISEs were conditioned in 1 mM KCl at 37 °C. Potentials were recorded during the conditioning step (shown in Figure 3.11a). Data for only three out of six SC-ISEs total are shown in Figure 3.11. The other three SC-ISEs did not respond to K^+ and had very low resistance. When disassembling those SC-ISEs, water was found inside the electrode body, suggesting that the electrode setup is prone to formation of leaks around the ion-selective

membrane, resulting in failure of the sensor. However, three of the SC-ISEs did not form leaks, allowing for determination of their electrochemical properties.

Upon exposure to 1 mM KCl solution, changes in potential occur in the first 20 h exposure to 1 mM KCl at 37 °C. After the initial decrease in potential, the SC-ISE drifts slowly decrease. Drifts as low as 3 µV/h can be achieved, although the only electrode to achieve this was the one identified by the blue curves. The SC-ISEs corresponding to the red curves had some abrupt steps during the initial conditioning (cause is unknown), but lines fit between the steps from 50 h to 67 h showed that the drift was <17 µV/h, which is comparable to those measured for SC-ISEs prepared on graphite/glass electrodes after extensive conditioning in 1 mM KCl at 37 °C. The SC-ISE corresponding to the black curves had a much higher drift of 100 µV/h, though the cause for this is also unknown. It may be related to the quality of the seal formed between the electrode body and the silicone membrane.

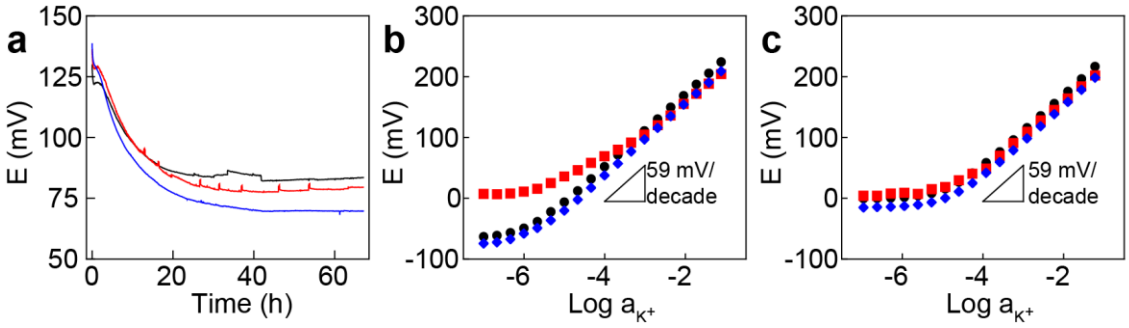

Figure 3.11. Potentiometric data for K^+ SC-ISEs in aqueous solution. (a) Potentials monitored during initial exposure to 1 mM KCl at 37 °C, (b) emf response to K^+ activity, (b) emf response to K^+ activity in the presence of a 1 M NaCl background. All potentials were measured relative to a double junction Ag/AgCl reference electrode with a saturated AgCl/3 M KCl inner filling solution and a 1.0 M lithium acetate bridge.

Table 3.1. Properties of SC-ISEs prepared with small CIM carbon.

electrode	# ISM coatings	thickness of ISM and carbon (μm)	response slope (mV/decade)	$\log K_{K^+,Na^+}$	log R (Ω)
black	1	80 ± 13	59.5	–4.67	7.9
red	2	133 ± 18	53.0	–4.65	7.7
blue	2	133 ± 18	58.9	–4.66	7.4

The SC-ISEs also had Nernstian responses to K^+, excellent lower detection limits, and the expected selectivity to K^+ vs. Na^+ (Table 3.1). Notably, these SC-ISEs with small CIM carbon have a lower ionophore-to-CIM carbon ratio than those in Chapter 2, yet they still have high selectivity to K^+ vs. Na^+. Evidently, the interaction between valinomycin and CIM carbon is not as strong as the corresponding interaction between BME-44 and CIM carbon (see Chapter 4).

3.4. Conclusion

To fabricate ISEs with a low thickness (<100 μm), the size of particles used for the solid contacts needs to be sufficiently small to ensure complete coverage of the underlying conductor with carbon, while also not containing larger carbon particles that can poke through the ion-selective membrane. In this work, we show that the CIM carbon particle size can be reduced by probe sonication and sedimentation, with 70% (by volume) of the resulting carbon having a size of 5 μm or smaller. Crucially, the pores were maintained and no new surface oxygen groups were introduced during the size reduction process. The yield for this process was only 10%, but it might be possible to produce CIM carbon with

the desired small particle size by modification of the CIM carbon synthesis, and this will be the subject of future study.

SC-ISEs with CIM carbon solid-contacts and silicone ion-selective membranes with a total thickness (carbon + membrane) of 80 ± 13 µm can be manufactured on aluminum foil by coating the separate layers with a doctor blade. K^+ SC-ISEs with both 80 ± 13 µm and 133 ± 18 µm thickness have Nernstian responses to K^+ and excellent selectivity to K^+ vs. Na^+. We also showed that long-term drifts as low as 3 µV/h (for an SC-ISE with 133 ± 18 µm thickness) can be reached, making SC-ISEs with this composition promising candidates for use in wearable and implantable sensors. Additionally, these SC-ISEs were fabricated using methods that are commonly used to manufacture lithium-ion batteries. With some optimization, this method could be adapted to allow for mass manufacture of cheap SC-ISEs for applications in areas outside the healthcare field (e.g., process or environmental monitoring).

Chapter 4. Potassium Ion-selective Electrodes with BME-44 Ionophores Covalently Attached to Condensation-cured Silicone Membranes

This chapter is reproduced from "Potassium Ion-selective Electrodes with BME-44 Ionophores Covalently Attached to Condensation-cured Silicone Membranes" by Spindler, B.D.; Chen, X.V.; Graf, K.I.; Bühlmann, P.; Stein, A. in *Langmuir* **2024**, 20, 18112–18121.

Xin Chen and Katerina Graf contributed to the synthesis of the covalently attachable BME-44 derivative described in this chapter.

Portions of this work were supported by Medtronic PLC. We also thank Reza Jahanbekam for assistance acquiring the confocal Raman microscopy data.

4.1 Introduction

Development of wearable and intradermal ion-selective electrodes (ISEs) for real-time monitoring of ion concentrations has become a topic of significant interest in recent years[11-13, 132, 134, 135, 171, 172] due to advancements in all-solid-state ion-selective electrodes that allow for elimination of inner filling solutions and, therefore, easier miniaturization of ISEs.[32, 173-175] A majority of ISEs reported to-date comprise a plasticized poly(vinyl chloride) (PVC) membrane, a mobile ionophore, and mobile ionic sites. Leaching of these species from the ISE into the sample can be toxic to the surrounding tissue,[55, 57, 176, 177] causes emf drift, and limits the lifetime of ISEs,[58, 147, 178, 179] especially for ISEs with thin sensing membranes, like those in wearable or implantable devices. Lifetimes are further limited when ISEs are immersed in more hydrophobic samples like blood plasma or interstitial fluid because the partitioning of plasticizer, ionophore, and ionic sites from the membrane to the sample is greater than in pure aqueous salt solutions.[59, 179] Leaching of membrane components into the sample may be one of the reasons why to date wearable and implantable SC-ISEs have only been used for short term experiments (≤30 min).[11-13, 132, 134, 135, 171, 172]

To address these challenges, plasticized PVC can be replaced as the membrane matrix with silicones,[60, 167] polyacrylates and polymethacrylates,[137] or polyurethanes,[180] which have low glass transition temperatures without addition of plasticizers. One strategy to address the problem of ionophore leaching is to modify existing ionophores with functional groups that can be covalently attached to polymer membranes without affecting the functional groups responsible for binding to the target ion. Examples include derivatives

of valinomycin,[181, 182] BME-44 (linked to PVC),[183] and hemispherrand-21[85, 89] as covalently attachable K^+ ionophores; a bis(12-crown-4) ether,[104] a 16-crown-5 ether,[105] and calix[4]arene[87, 104, 105, 184] as covalently attachable Na^+ ionophores; and a derivative of ETH 129[185] as a covalently attachable Ca^{2+} ionophore. Alternatively, the ionic site can be attached to the polymer backbone.[105, 186-188] However, for ISEs with response times sufficiently fast to be of practical relevance, only one of the two components can be covalently attached to the ISE membrane.[186]

Covalent attachment of the ionophore to the polymer membrane can also improve the response times and selectivity of ISEs with low polarity polymer matrixes in which the ionophore has poor solubility. This has been demonstrated with Na^+ ionophores that were either covalently attached to a condensation-cured silicone during crosslinking[105] or to a silicone oligomer that did not have crosslinking functional groups.[99, 103, 104] In the latter case, the silicone chains with ionophore were mobile species that remained in the ion-selective membrane (ISM) due to the hydrophobicity of the silicone oligomer. In the former case, ionophores were functionalized with a triethoxysilyl group that participates in the crosslinking reaction during condensation curing of silicone.[105] Other ionophores have been modified with methacrylate groups for covalent attachment of hemispherand ligands to silicone/cyanopropylmethylsiloxane/methacrylate copolymers.[89]

Although others have attached ionophores to silicone matrixes,[89, 91, 105] little attention has been paid to the influence of reaction and curing conditions on the degree of ionophore attachment to the silicone membrane. Leaching of membrane components that do not get attached to the crosslinked silicone network can still cause emf drift of the ISE and be toxic

to tissue, even when the majority of the ionophore has been successfully attached to the silicone. To fabricate biocompatible, plasticizer-free K^+ SC-ISEs for use in wearable and implantable sensors, we chose to synthesize a modified version of the K^+-ionophore BME-44 containing triethoxysilyl groups that react with condensation-curing silicones during the curing process. We show that up to 96% of ionophore can be covalently bound to the membrane polymer if the ISE membrane precursor solution is allowed to react for 45 min before drop casting. We also show that ISEs prepared with the covalently attachable BME-44 derivative have Nernstian responses to K^+, better selectivity to K^+ vs. Na^+ than those prepared with mobile BME-44, and approximately 10 times lower resistance.

4.2. Experimental section

4.2.1. Materials

Reagents were purchased from the following sources: (2,2,5-trimethyl-1,3-dioxan-5-yl)methanol (96%), 4'-acetylamino-5'-nitrobenzo-15-crown 5 (99%), 4-vinylbenzyl chloride (90%), chlorobenzene (ACS reagent, ≥99.5%), phosgene solution in toluene (15 wt%), sodium hydride (60 wt% dispersion in mineral oil), Teflon dispersion in water (60 wt%), Karstedt's catalyst (0.05 M in poly(dimethylsiloxane), vinyl terminated), trifluoroacetic acid (ReagentPlus, 99%), tetrahydrofuran (anhydrous, inhibitor-free, ≥99.9%), dimethylformamide (anhydrous, ≥99.8%), pentane (reagent grade, 98%), toluene (99.9%), dichloromethane (anhydrous, ≥99.8%), fuming sulfuric acid (reagent grade, 20% as free SO_3), molecular sieves 3A, hydroxy-terminated poly(dimethylsiloxane) (average molecular weight ~110,000 g mol^{-1}, abbreviated as PDMS-OH in this manuscript), and

mobile BME-44[189] (K^+ ionophore III, Selectophore) from Sigma Aldrich (St Louis, MO); 37% hydrochloric acid from VWR (Radnor, PA); triethylamine (reagent grade, 99%), ethanol (200 proof), diethyl ether (anhydrous, 2% ethanol as stabilizer), ethyl acetate (Certified ACS), hexanes (Certified ACS), and Chemglass Life Sciences Pyrex tubing (10 ± 0.4 mm outer diameter, 2.0 ± 0.2 mm wall thickness) from Fisher Scientific (Waltham, MA); trichlorosilane (98%) from BeanTown Chemical (Hudson, NH); vinyltrimethoxysilane (tech-95, abbreviated as VTMOS) from Gelest (Morrisville, PA); sodium tetrakis[3,5-bis(trifluoromethyl)phenyl]borate dihydrate ($NaTFPB \cdot 2H_2O$) from Dojindo (Kumamoto, Japan). The synthesis of colloid-imprinted mesoporous (CIM) carbon and fabrication of CIM carbon disks with 5 wt% Teflon as binder were performed as reported previously.[47, 167] Graphite rods (fine extruded, 0.25-inch diameter) were purchased from Graphite Store (Northbrook, IL).

4.2.2. Synthesis of 2,2,5-trimethyl-5-(((4-vinylbenzyl)oxy)methyl)-1,3-dioxane (2)

A mass of 1.0 g (6.24 mmol) of (2,2,5-trimethyl-1,3-dioxan-5-yl)methanol (**1**) was added to a 50-mL round bottom flask containing a magnetic stir bar. The flask was sealed with a septum and attached to a Schlenk line. The flask was evacuated and backfilled with nitrogen three times. A volume of 25 mL dimethylformamide was added to the flask. The solution was cooled to 0 °C and then NaH (60 wt% dispersion in mineral oil, 250 mg, 6.24 mmol) was added to the flask. The suspension was stirred at 0 °C for 10 min, then allowed to warm to room temperature and stirred for 5 h. After 1 h, most NaH had dissolved, and the solution had a faint yellow color. Then, 4-chlorovinylbenzene (0.89 mL, 6.24 mmol)

was added to the solution, and the solution was stirred at room temperature for 18 h. The solution was quenched by adding 10 mL H_2O to the reaction mixture. The product was extracted from this solution with pentane (10 mL for the first extraction and 5 mL for the second and third extractions). The combined pentane layers were washed with water (3 × 5 mL) and dried over anhydrous Na_2SO_4. The dried pentane layer was loaded onto a basic alumina column for further purification. Pentane was passed through the column until 4-chlorovinylbenzene was eluted. The product was then eluted with 5% (v/v) dichloromethane/pentane. The solvent was removed by ambient pressure distillation to give **2** as a clear, colorless liquid (273 mg, 16%, unoptimized yield). R_f = 0.5 (basic alumina, 5% ethyl acetate/hexanes). ^{1}H NMR (400 MHz, $(CD_3)_2CO$) δ 7.45 (d, J = 8.2 Hz, 2H), 7.36 (d, J = 8.2 Hz, 2H), 6.78 (dd, J = 17.6, 11.0 Hz, 1H), 5.84 (dd, J = 17.7 Hz, J = 1.0 Hz, 1H), 5.25 (dd, J = 11.0 Hz, J = 0.9 Hz, 1H), 4.54 (s, 2H), 3.68 (d, J = 11.8 Hz, 2H), 3.58 (d, J = 11.8 Hz, 2H), 3.49 (s, 2H), 1.36 (s, 3H), 1.29 (s, 3H), 0.89 (s, 3H). ^{13}C NMR (400 MHz, $(CD_3)_2CO$) δ 139.70, 137.61, 128.38, 126.93, 113.88, 98.23, 73.97, 73.53, 66.91, 35.02, 26.63, 21.67, 18.50. MS (ESI): m/z calcd. for $C_{17}H_{24}O_3Na^+$: 299.1623 (100.0%), 300.1657 (18.4%), 301.1690 (1.6%); found: 299.1627 (100%), 300.1660 (9.4%), 301.1709 (1.0%)

4.2.3. Synthesis of 2-methyl-2-(((4-vinylbenzyl)oxy)methyl)propane-1,3-diol (3)

2,2,5-trimethyl-5-(((4-vinylbenzyl)oxy)methyl)-1,3-dioxane (273 mg, 0.99 mmol) was added to a 50 mL round bottom flask containing a magnetic stir bar. Then, a solution of H_2SO_4 (0.1 g, 1.01 mmol) in 4.9 mL H_2O was added to the flask, resulting in formation of

a biphasic mixture. The flask was equipped with a reflux condenser, and the reaction mixture consisting of two phases was stirred for 58 °C for 4 h. Upon cooling to room temperature, the product precipitated as a white solid, which was collected by filtration, washed with water (5 × 5 mL), and dried on a Buchner funnel for 1 h. Further drying under vacuum at 60 °C for 18 h gave **3** as a white solid (220 mg, 94%). ^{1}H NMR (400 MHz, CD_3CN) δ 7.43 (d, J = 8.1 Hz, 2H), 7.32 (d, J = 8.1 Hz, 2H), 6.75 (dd, J = 17.7, 10.8 Hz, 1H), 5.82 (dd, J = 17.6, 0.8 Hz, 1H), 5.25 (dd, J = 11.0, 0.9 Hz, 1H), 4.47 (s, 2H), 3.43 (d, J = 3.0 Hz, 2H), 3.37 (s, 2H), 2.83 (t, J = 5.4 Hz, 1H), 0.82 (s, 3H). ^{13}C NMR (400 MHz, CD_3CN) δ 139.65, 137.75, 137.46, 128.68, 127.03, 114.34, 74.69, 73.63, 66.90, 41.92, 17.26. MS (ESI): m/z calcd. for $C_{14}H_{20}O_3Na^+$: 259.1310 (100%), 260.1344 (15.1%), 261.1377 (1.1%); found: 259.1290 (100%), 260.1267 (13%).

4.2.4. Synthesis of 4’-amino-5’-nitrobenzo-15-crown-5 (4)

This compound was synthesized from 4’-acetylamino-5’-nitrobenzo-15-crown-5 using a previously reported procedure.[189] Briefly, 0.5 g (1.35 mmol) was mixed with 3 mL 37% HCl in a 10 mL round bottom flask equipped with a reflux condenser and a magnetic stir bar. The mixture was heated to 100 °C for 20 min, then cooled back to ambient temperature. The solution was transferred to a beaker and diluted with 20 mL water. A solution of 5 wt% Na_2CO_3 was added to the reaction mixture until the pH was greater than 7. Dichloromethane (50 mL) was added and mixed with the aqueous solution for 1 min. The mixture was transferred to a separatory funnel, and the dichloromethane layer was removed. The aqueous layer was extracted with dichloromethane (2 × 10 mL). The

combined organic layers were washed with water (2 × 10 mL). The organic layer was dried over anhydrous sodium sulfate and then concentrated to dryness using a rotary evaporator. The solid was dried in a vacuum oven at 30 °C overnight to obtain compound **4** as an orange solid (400 mg, 91% yield). ^{1}H NMR (400 MHz $CDCl_3$) δ 7.55 (s, 1H), 6.14 (br, s, 2H), 6.10 (s, 1H), 4.11 (m, 4H), 3.92 (m, 2H), 3.87 (m, 2H), 3.74 (m, 8H).

4.2.5. Synthesis of vinylbenzyl BME-44 (6)

Caution: this reaction involves the use of phosgene solution in toluene. Phosgene is a very toxic gas with a high vapor pressure. The solution must be handled with proper safety procedures to prevent exposure. A special reaction apparatus was assembled in a draft hood and used to contain and trap excess phosgene. A schematic of this reaction vessel is shown in Figure 4.1. A 50-mL 2-neck round bottom flask was used. The side neck was sealed with a rubber septum. The other neck was connected to a Liebig condenser, which was connected to a 3-way adapter. The top connection on the 3-way adapter was sealed with a rubber septum and the side connection was hooked up to a second condenser. The condenser was connected to a receiving flask through a vacuum adapter. The exhaust from the vacuum adapter was connected to a dual scrubber system to trap phosgene and prevent it from escaping the reaction setup. The first scrubber contained toluene and solid KOH (this prevents water vapor from the second scrubber from reaching the reaction flask), and the second scrubber contained an aqueous KOH solution. The exhaust from the second scrubber was vented out the back of the fume hood. All joints were sealed with vacuum grease, except for the joint connecting the reflux condenser to the reaction glass, which

was sealed with a Teflon sleeve. A hot plate with an oil bath used to heat the reaction mixture was placed on a lab jack. The reaction setup was positioned to allow the hot plate and oil bath to be easily removed by lowering the lab jack.

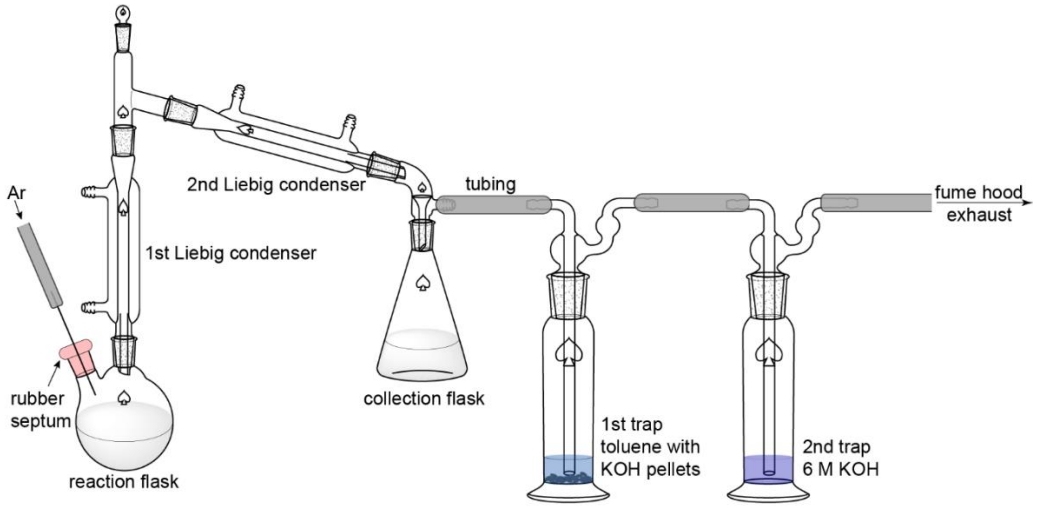

Figure 4.1. Setup for reaction of 4'-amino-5'-nitrobenzo-15-crown-5 with phosgene. The schematic was made using the glassware artwork in the software ChemDraw 21.0 (PerkinElmer, Waltham, MA).

First, 4'-amino-5'-nitrobenzo-15-crown-5 (**4**, 420 mg, 1.28 mmol) was added to the 50-mL round bottom flask through the side neck. Then a septum was used to close the side neck, and the flask was connected to an argon line by way of a needle inserted into the septum. A light stream of Ar was passed through the reaction setup such that bubbles of Ar were passing through the two traps. All joints were adjusted until no leaks could be detected. Then, Ar was passed through the vessel at room temperature for 1 h to displace air and water from the reaction vessel. Chlorobenzene (5 mL, pre-dried over molecular sieves 3A) was added, and the mixture was stirred for 5 min, resulting in the formation of a dark orange suspension. The needle connected to the Ar line was positioned well above

the solution. Then, 15 wt% phosgene solution in toluene (21.1 g solution, 3.2 g phosgene, 31.9 mmol) was added to the reaction vessel via a syringe through the septum. Any phosgene remaining in the reagent bottle was immediately quenched in a 6 M KOH solution. *Do not store unused phosgene solution in an opened phosgene container in the lab, even if the solution came in a container sealed with a septum.* Upon adding the phosgene solution, compound **4** slowly began to dissolve, and the solution became bright yellow. The water flow through the two Liebig condensers was started, and the reaction mixture was slowly heated to 111 °C over 2 h (note: at around 60–70 °C, gas evolution noticeably increases, and the reaction solution may gently bubble for a few minutes). Once at reflux, the reaction mixture was stirred for 4 h. Phosgene and some solvent was then removed by turning the water flow through the first (vertical) Liebig condenser off, raising the bath temperature to 121 °C, and sparging the reaction mixture with argon by adjusting the position of the needle connected to the argon tank such that the tip was in the reaction mixture. The reaction mixture was stirred at these conditions for 2 h, resulting in evaporation of most of the solvent. The reaction mixture was transferred to a 50-mL one-neck round-bottom flask, and the remaining solvent was removed under vacuum with a rotary evaporator to give an orange solid. The solid was dissolved in 10 mL dichloromethane under an argon atmosphere. Compound **3** (145 mg, 0.61 mmol) was dissolved in 1 mL dichloromethane (pre-dried over molecular sieves 3A) and added to the reaction mixture, followed by addition of triethylamine (62 µL, 0.44 mmol). The reaction mixture was stirred at room temperature for 16 h. Upon dilution with 10 mL dichloromethane, the reaction mixture was washed with 1 M HCl (2 × 10 mL) and H_2O (3

× 10 mL). The dichloromethane layer was dried over anhydrous Na_2SO_4 and then concentrated to dryness under vacuum on a rotavap to give a sticky orange solid. Et_2O (5 mL) was added to the flask, and the resulting suspension was stirred for 4 h. The yellow solid was collected by filtration and washed with Et_2O (3 × 2 mL). The solid was recrystallized from ethyl acetate to give **6** as a yellow solid (285 mg, 47%). ^{1}H NMR (400 MHz, CD_3CN) δ 9.96 (s, 2H), 7.98 (s, 2H), 7.47 (s, 2H), 7.33 (d, J = 8.2 Hz, 2H), 7.29 (d, J = 8.2 Hz, 2H), 6.64 (dd, J = 17.7, 11.0 Hz, 1H), 5.72 (dd, J = 17.7, 0.9 Hz, 1H), 5.19 (dd, J = 10.9, 0.8 Hz, 1H), 4.49 (s, 2H), 4.23 (m, 4H), 4.08 (m, 8H), 3.79 (m, 8H), 3.62 (m, 16H), 3.49 (s, 2H), 1.06 (s, 3H). ^{13}C NMR (400 MHz, CD_3CN) δ 156.76, 153.87, 144.33, 139.20, 137.72, 137.31, 133.19, 129.05, 128.67, 126.92, 114.24, 110.14, 103.06, 73.51, 73.02, 71.62, 71.54, 70.70, 70.54, 70.09, 69.66, 69.58, 69.14, 68.90, 40.45, 17.47. MS (ESI): m/z calcd. for $C_{44}H_{56}N_4O_{19}K^+$: 983.3177 (100%), 984.3210 (47.6%), 985.3244 (11.1%), 986.3192 (3.4%); found: 983.3202 (100%), 984.3219 (35.2%), 985.3217 (11.5%), 986.3251 (2.7 %).

4.2.6. Synthesis of triethoxysilyl BME-44 (7)

All solvents were pre-dried over molecular sieves 3A. Vinylbenzyl BME-44 (**6**, 30.1 mg, 31.9 μmol) and a new magnetic stir bar was added to a 1-mL sealed HPLC vial. The mixture was dried at 90 °C under high vacuum to ensure that any traces of water were removed from the vial. The vial was cooled to room temperature and backfilled with nitrogen. In a second vial under an N_2 atmosphere, a stock solution of Karstedt's catalyst was prepared by diluting 24.2 μL of Karstedt's catalyst in vinyl-terminated PDMS (0.05

M) with 1.0 mL anhydrous tetrahydrofuran. In a third vial under N_2, a stock solution of $HSiCl_3$ was prepared by diluting 164 µL $HSiCl_3$ with 836 µL with anhydrous THF. The Karstedt's catalyst solution (52.6 µL, 63.7 nmol) and the $HSiCl_3$ solution (39.3 µL, 63.7 µmol) was added to the vial containing compound **6**. Upon stirring, all solid dissolved, and the vial was sealed with Parafilm and stirred at room temperature under nitrogen for 2 h. Then, an additional aliquot of $HSiCl_3$ solution was added (39.3 µL, 63.7 µmol). The reaction mixture was stirred for an additional 37 h at room temperature. Ethanol (150 µL) was added into the vial, and the solution was stirred for another 10 min at room temperature, followed by removal of the solvent with a high vacuum at room temperature and backfilling of the vial with nitrogen. The thus obtained raw product was recrystallized from a mixture of ethyl acetate/hexane (1/7, v/v, 150 µL). The supernatant was removed from the vial with a syringe, and the solid that was sticking to the flask walls was washed with ethyl acetate/hexane (1/7, v/v, 2 × 150 µL) under a nitrogen atmosphere by adding the solvent mixture to the vial using a syringe, swirling the solution around for 2 min, and then removing the supernatant with a syringe. The solid was then dried under vacuum at 65 °C for 1.5 h to give compound **7** as a yellow solid (27.6 mg, 78%). ^{1}H NMR (400 MHz, CD_3CN) δ 9.97 (s, 2H), 7.96 (s, 2H), 7.55 (s, 2H), 7.20 (d, J = 8.0 Hz, 2H), 7.13 (d, J = 8.0 Hz, 2H), 4.45 (s, 2H), 4.21 (m, 4H), 4.06 (m, 8H), 3.79 (m, 14H), 3.62 (m, 16H), 3.47 (s, 2H), 2.60 (m, 2H), 1.17 (m, 9H), 1.05 (s, 3H), 0.87 (m, 2H). ^{13}C NMR (400 MHz, CD_3CN) δ 156.76, 153.89, 145.00, 144.32, 136.77, 133.22, 129.03, 128.60, 128.57, 110.15, 103.08, 73.80, 73.12, 71.63, 71.53, 70.69, 70.52, 70.10, 69.67, 69.58, 69.13, 68.98, 58.99, 40.48, 29.26, 18.66, 17.51, 13.20. MS (ESI): m/z calcd. for $C_{50}H_{72}N_4O_{22}SiK^+$: 1147.4046 (100%),

1148.4079 (54.1%), 1149.4113 (14.3%), 1150.4048 (1.8%); found: 1147.4054 (100%), 1148.4087 (43.3%), 1149.4017 (23.2%), 1150.3886 (6.3%).

4.2.7. Characterization of synthesized compounds

^{1}H and ^{13}C NMR spectra were obtained with a Bruker Avance III HD AX-400 (400 MHz) spectrometer. High resolution mass spectra were obtained with a Bruker BioTOF II ESI/TOF-MS using either poly(ethylene glycol) (PEG) or poly(propylene glycol) (PPG) as a calibration standard. See the appendix for the spectra of each compound.

4.2.8. ISE fabrication

Gold disk electrodes (2 mm diameter gold embedded in a Kel-F cylindrical body, CH Instruments, Austin, TX) were polished over polishing cloth with dispersions of alumina (0.3 µm and 0.05 µm Buehler, Lake Bluff, IL), rinsed with water, and then bath sonicated in water and ethanol (5 min each). The electrodes were soaked in a 1 mM solution of octanethiol for 18 h at room temperature. The electrodes were rinsed with ethanol and dried in air. A solution of the ISM components was prepared by dissolving 100 mg hydroxy-terminated poly(dimethylsiloxane) in 0.5 mL toluene. This solution was then transferred to a vial containing 1.1 mg compound **7** and 0.24 mg NaTFPB·$2H_2O$ (25 mol% with respect to the ionophore). Then, 5.2 µL vinyltrimethoxysilane and 33.6 µL trifluoroacetic acid were added. The solution was stirred for 45 min, followed by drop-casting of 10 µL of the ISM solution onto each gold electrode. The membranes were cured in an oven at 55 °C for 144 h. These ISEs are referred to in the following with the abbreviation Au/SC_8H_{17}/ISM.

To take advantage of the covalent bonding of silicone ISMs to glass, we also prepared SC-ISEs by insertion of graphite rods into tightly fitting glass tubes, with the flat end of the graphite rod flush with the end of the glass tube. The procedure for fabrication of these graphite/glass SC-ISEs was adapted from our previously reported procedure.[167] Graphite/glass electrodes were prepared by inserting a graphite rod into a glass tube, such that graphite protruded from both ends of the glass tube. On one end, the graphite rod was fastened to the glass by coating the graphite/glass joint with two-part epoxy adhesive. After curing the adhesive overnight, the gaps between the graphite rod and the glass tube were filled with a 60 wt % Teflon dispersion in H_2O by drop casting the Teflon dispersion onto the end of the glass tube without adhesive. The H_2O was then removed by drying the electrodes in an oven at 110 °C overnight. The graphite rod protruding from the end that was not sealed with epoxy adhesive was sanded down such that the graphite was flush with the glass tube. The electrodes were polished with 60, 150, 320, and 600 grit sandpaper, then further polished over a polishing cloth with an alumina dispersion (0.3 µm followed by 0.05 µm). They were then bath sonicated in H_2O, followed by ethanol (5 min each). The electrodes were dried in air before use. To prepare ISEs on the graphite/glass electrodes, a CIM carbon/Teflon disk (95/5, wt/wt), (137 ± 6 µm thick, 4.8 mm diameter) was placed on top of the graphite/glass electrode and centered over the graphite. Then, 50 µL toluene was drop cast onto the CIM carbon layer to wet the CIM carbon to infiltrate the pores. This helped prevent air pockets from forming when the ISM was drop cast. When the solvent had evaporated sufficiently to expose the top of the CIM carbon layer (~5 min), the ISM (stirred for 5 min after adding trifluoroacetic acid and crosslinker) was applied in four 50-

µL portions. ISEs were cured at 55 °C in air for 480 h. These ISEs are referred to in the following as graphite/CIM/ISM electrodes.

After use in aqueous solution, these ISEs were divided into two groups. ISEs of the first and second group were coated again with an ISM solution (50 µL) that had been stirred for 5 and 45 min before drop casting, respectively. The membranes were then cured in an oven at 55 °C for 360 h.

4.2.9. Determination of the fraction of ionophore covalently attached to the polymeric silicone matrix

A known portion of the solution comprising the ISM components that had been stirred for 5 or 45 min after addition of vinyltrimethoxysilane and trifluoroacetic acid was poured onto a Teflon sheet, cured in an oven at 55 °C, and weighed (Table 4.1). Curing was continued at 55 ºC, and pieces of the membrane (~50 mg) were torn from the parent membrane and weighed at the cure times listed in Table 4.1. The torn piece of membrane was then Soxhlet extracted with dichloromethane (60 mL) for 24 h. The dichloromethane in the Soxhlet extractor transferred back to the round bottom flask once every 24 min (~60 extractions total). The dichloromethane in the extract was then evaporated under vacuum using a rotary evaporator. The residue was dissolved in dichloromethane, transferred to a 5.00 mL volumetric flask and diluted to the mark with dichloromethane. The solution was analyzed by UV-vis spectroscopy using a Thermo Scientific Evolution S220 UV-Visible Spectrophotometer equipped with a borosilicate cell with a 1 cm path length. A single point

calibration was performed using a 37.9 µM solution of mobile BME-44 in dichloromethane (ε = 11865 $M^{-1}cm^{-1}$ at 400 nm). The percentage of ionophore extracted was calculated by:

$$\%\text{ionophore} = \frac{A\,V\,m_t}{\varepsilon\,L\,mol_{\text{BME}}\,m_s} \times 100\% \qquad (4.1)$$

where A, ε, V, L, mol_{BME}, m_t, and m_s, are the measured absorbance at 400 nm, molar absorptivity of BME-44 at 400 nm, volume of solution in the volumetric flask (0.005 L), path length of the cell (1 cm), total mol BME-44 in the parent membrane, total mass of the parent membrane, and mass of the sample membrane used for Soxhlet extraction, respectively.

4.2.10 Potentiometric measurements

Potentials were measured with an EMF 16 voltmeter with a 10 TΩ input impedance (Lawson Labs, Malvern, PA). Potentials were measured relative to a Ag/AgCl reference electrode with a 3.0 M KCl/sat. AgCl inner filling solution and a 1.0 M lithium acetate bridge electrolyte. Ion activities were calculated using a two-parameter Debye-Hückel approximation,[144] and potentials were corrected for the liquid junction potential using the Henderson equation.[145] ISEs were conditioned in 1 mM KCl at room temperature overnight before use. K^+ calibration curves were measured by addition of aliquots of KCl solution to the sample solution from 10^{-9} to 10^{-1} M KCl. Selectivity to K^+ vs. Na^+ was measured by the fixed interference method[27]: aliquots of KCl/1.0 M NaCl solutions were successively added to a sample solution containing 1.0 M NaCl, resulting in KCl concentrations between 10^{-9} and 10^{-1} M, with a constant background of 1.0 M NaCl. Resistances were measured by the known shunt method.[147, 190]

4.2.11. Microscopy

Transmission optical microscope images were acquired using a VHX-7000 UM optical microscope (Keyence, Osaka, Japan). Confocal Raman spectra were acquired using a Alpha300R confocal Raman microscope equipped with a 532 nm laser (WiTec, Ulm, Germany).

4.2.12. N_2 gas sorption analysis of graphite

Graphite powder was obtained from graphite rods for N_2 gas sorption analysis. To obtain a powder, the graphite rod was rubbed against a metal file. N_2 gas sorption measurements were performed on an iQ2 gas sorption analyzer (Quantachrome, Boynton Beach, FL). Samples were outgassed at 120 °C under vacuum for 12 h before measurement. The specific surface area was calculated using the Brunauer-Emmett-Teller (BET) method. The pore size distribution and cumulative pore volume were calculated from the adsorption branch of the isotherm using the slit/sphere/cylinder QSDFT model for carbon in the ASiQwin software from Quantachrome.

4.2.13 Use history of SC-ISEs of graphite/CIM/ISM electrodes

After curing, the electrodes were conditioned in a 1 mM KCl solution overnight at room temperature for 16 h. Then, K^+ calibration curves and selectivities (fixed interference method)[27] of the ISEs were measured. Resistances were measured with the known shunt method.[147] The electrodes were conditioned in 1 mM KCl solution for an additional 7 days. Selectivities, response slopes, and resistances were measured again. The electrodes were

then rinsed with water and allowed to dry in air in a fume hood overnight. The electrodes were then coated with a fresh portion (50 μL) of ion-selective membrane (half the ISEs were coated with a precursor solution that had been stirred for 5 min and the other half were coated with a precursor solution that had been stirred for 45 min). The ISE membranes were cured at 55 °C in an oven for 15 days. The ISEs were conditioned in 1 mM KCl at room temperature for 22 h. Then, K^+ calibrations, selectivities, and resistances were measured for the ISEs.

4.3. Results and discussion

4.3.1. Synthesis of a covalently attachable ionophore BME-44 (compound 7)

To covalently attach BME-44 to condensation-cured silicones, we synthesized a derivative of BME-44 with a triethoxysilyl anchoring group (Figure 4.2) by modifying a synthesis previously reported for BME-44.[189] In the original synthesis of BME-44, the crown ether isocyanate, **5**, was formed from the corresponding amine with phosgene as reagent. In this work, several attempts were made to replace the reagent phosgene with the less hazardous 1,1'-carbonyldiimidazole, but this resulted in the formation of numerous by-products that were difficult to remove from the raw product of **5**.[191] The higher reactivity of phosgene appears critical to the formation of **5**. A detailed description for the safe handling of phosgene in the synthesis of **5** is included in Section 4.2.5.

For the attachment of the ionophore to the silicone polymer backbone, we chose to introduce the triethoxysilyl group as the linkage that connects to the two crown ether functional groups of **7**. We first synthesized compound **3**, the linker between the two crown ether rings. The vinylbenzene functional group was chosen over the commercially

available analog of compound **3** with an allyl ether functional group because hydrosilylation of the vinylbenzyl ether in later steps (i.e, formation of **7** from **6**) can be performed without competing isomerization side reactions. We did not find the separation of side products with structures similar to the desired product to be feasible by recrystallization or chromatography, so hydrosilylation of compound **6** must be efficient in order to produce compound **7** with high purity. The final recrystallization from ethyl acetate/hexanes (1/7, v/v) after formation of **7** is only performed to remove the excess silane and, possibly, some of the Pt catalyst. Since the amount of hydrosilylation catalyst added to the reaction was very small (0.002 molar equivalents of Pt with respect to **6**), we do not expect the residual Pt to negatively affect the degree of ionophore attachment to the silicone membrane or the response and selectivity of the corresponding ISEs.

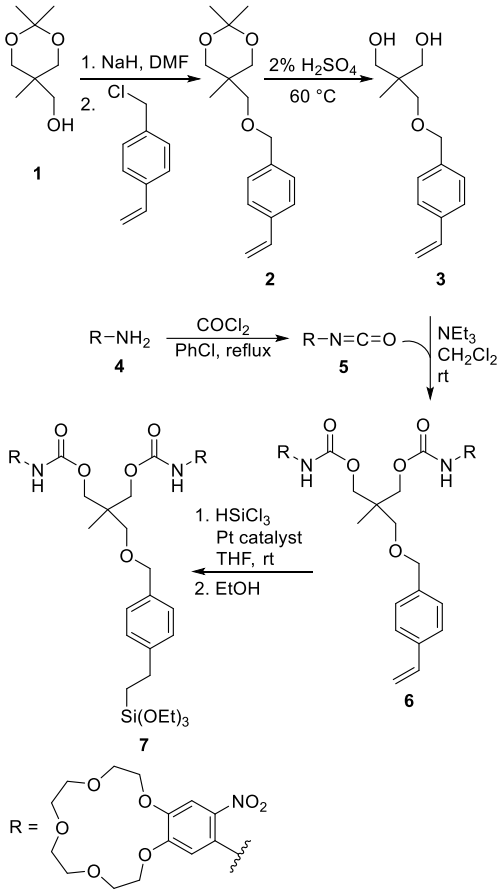

Figure 4.2. Synthesis of covalently attachable BME-44 derivative (**7**).

Hydrosilylation of compound **6** was performed using trichlorosilane instead of triethoxysilane because trichlorosilane is more reactive[192] and because the hydrosilylation reaction could be carried out quantitatively at room temperature. Attempts to perform the hydrosilylation reaction with triethoxysilane directly required high temperatures and resulted in some hydrogenation of the vinyl group on compound **6** (data not shown), giving the ethyl benzyl side product of **6** that could not be separated from the desired compound or covalently attached to the silicone matrix. The trichlorosilyl group was then converted to a triethoxysilyl group. Although the trichlorosilane functionality on the intermediate to

compound **7** is more reactive and would attach to silicone chains more rapidly, the less reactive triethoxysilane functionality was preferred because hydrolysis of the Si–O bond is slower, making the compound easier to handle and store. Si–Cl groups would react rapidly even with traces of water to form oligomers of the ionophore.

4.3.2. Covalent attachment of ionophore to silicone

To determine the optimal curing conditions for maximum attachment of **7** to the silicone membrane, cured ISE membranes were Soxhlet-extracted with dichloromethane for 24 h. We chose dichloromethane as the solvent because mobile BME-44 and the covalently attachable BME-44 derivative have good solubilities in this solvent and we found that mobile BME-44 could be completely removed from the silicone membrane by Soxhlet extraction (see Figure 4.3). The amount of ionophore-related species that were not covalently attached to the silicone polymer network and could, therefore, be extracted from the silicone was quantified by UV-vis spectroscopy using the absorbance at 400 nm, which originates from the NO_2-substituted aromatic rings (Figure 4.4). We assume this absorbance to be independent of whether the ionophore is covalently attached to the crosslinked silicone, covalently attached to silicone chains that are not connected to the crosslinked silicone network, or present in the form of ionophore oligomers.

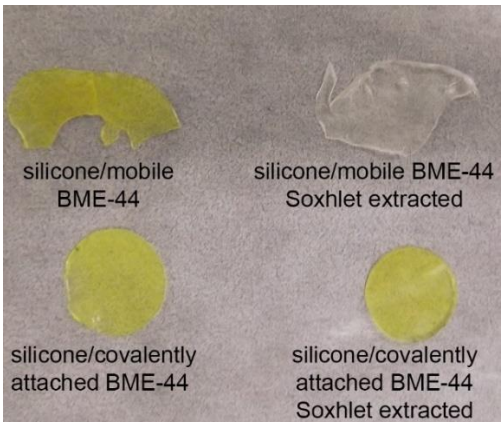

Figure 4.3. Photograph of ISE membranes (precursor solution stirred for 45 min before drop casting) prepared with mobile BME-44 and covalently attached BME-44, before and after Soxhlet extraction with dichloromethane for 24 h. Both the mobile BME-44 and the covalently attached BME-44 have a bright yellow color.

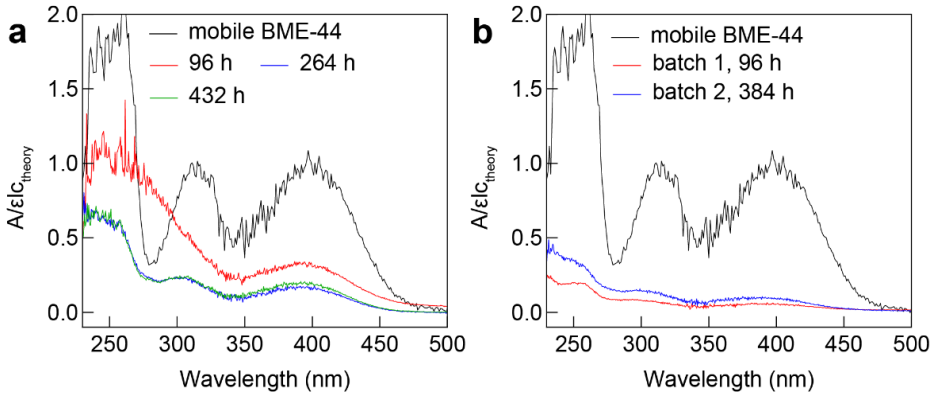

Figure 4.4. UV-vis spectra of the extract collected by Soxhlet extraction from silicone ISE membranes prepared with compound **7**. The ISE precursor solution containing PDMS-OH, VTMOS, trifluoroacetic acid, compound **7**, and NaTFPB·2H_2O in toluene was stirred for (a) 5 min or (b) 45 min before drop casting onto a Teflon sheet. To allow for easier comparison of the spectra, the *y*-axis is normalized to the maximum amount of ionophore that could be extracted from each sample (c_{theory}). For reference, the UV-vis spectrum of mobile BME-44, which was used to determine the molar absorptivity (ε) at 400 nm, is also included in each graph. The times denoted in the legend refer to the amount of time the membrane cured at 55 °C before Soxhlet extraction was performed. Data in (a) are all from the same parent membrane, whereas data in (b) are from two different membranes (batch 1 and batch 2).

We stirred all components of the sensing membrane (polymer, crosslinker, catalyst, ionophore, ionic sites) in a sealed container for either 5 or 45 min before drop casting them onto a solid contact. We chose the stir time of 5 min because that is the typical amount of time needed to dissolve the ionophore and ionic sites. The longer stir time of 45 min was used because it is significantly longer than 5 min and, therefore, permitted formation of some silicone oligomers, while still allowing quick preparation of ISE membranes. Notably, the longer reaction time reduced the fraction of ionophore that was extractable from the membrane (i.e., it resulted in more efficient attachment of ionophore to the silicone polymer backbone), especially at shorter cure times (Table 4.1). The catalyst, crosslinker, and solvent are volatile and begin to evaporate upon drop casting, which limits the time during which the catalyst is present to facilitate ionophore attachment to the growing silicone chains and crosslinking of those chains. Once the catalyst has evaporated to a significant extent, the ionophore attachment and crosslinking reactions become slow. Stirring the precursor solution for a longer time in a sealed container before drop casting increases the time during which the ionophore and crosslinker can react with terminal Si–OH groups on the PDMS-OH in the presence of the catalyst, which may be the reason for the more complete attachment of ionophore to the silicone under those conditions.

Table 4.1. Fraction of ionophore species extracted with dichloromethane from the cured membrane prepared with compound **7**. See Figure 4.4 for the UV-vis spectra of each extract.

Cure time (h)	% ionophore extracted[a] (precursor solution stirred 5 min before drop casting)	% ionophore extracted[b] (precursor solution stirred 45 min before drop casting)
96	32	3.9
264	16	-
384	-	8.3
432	19	-

[a] All data collected using the same parent membrane.

[b] Data points from two separate but identically prepared membranes.

Analysis of the Soxhlet extracts of the sensing membranes by positive ion ESI/TOF mass spectrometry (Figure 4.5) showed that the extract did not contain substantial concentrations of compound **7** or any related partially hydrolyzed species, such as $RSi(OH)_x(OEt)_y$. No peaks (aside from background peaks) were observed in the mass spectrum (*m*/*z*: 200–3000), which suggests that the extracted ionophore species were either attached to small silicone oligomers that were not part of the silicone network of the sensing membrane, or they were present in the form of ionophore oligomers. Additionally, no evidence of decomposition of the ionophore (such as hydrolysis of urethane bonds) was observed, indicating that the ionophore is compatible with the silicone curing conditions.

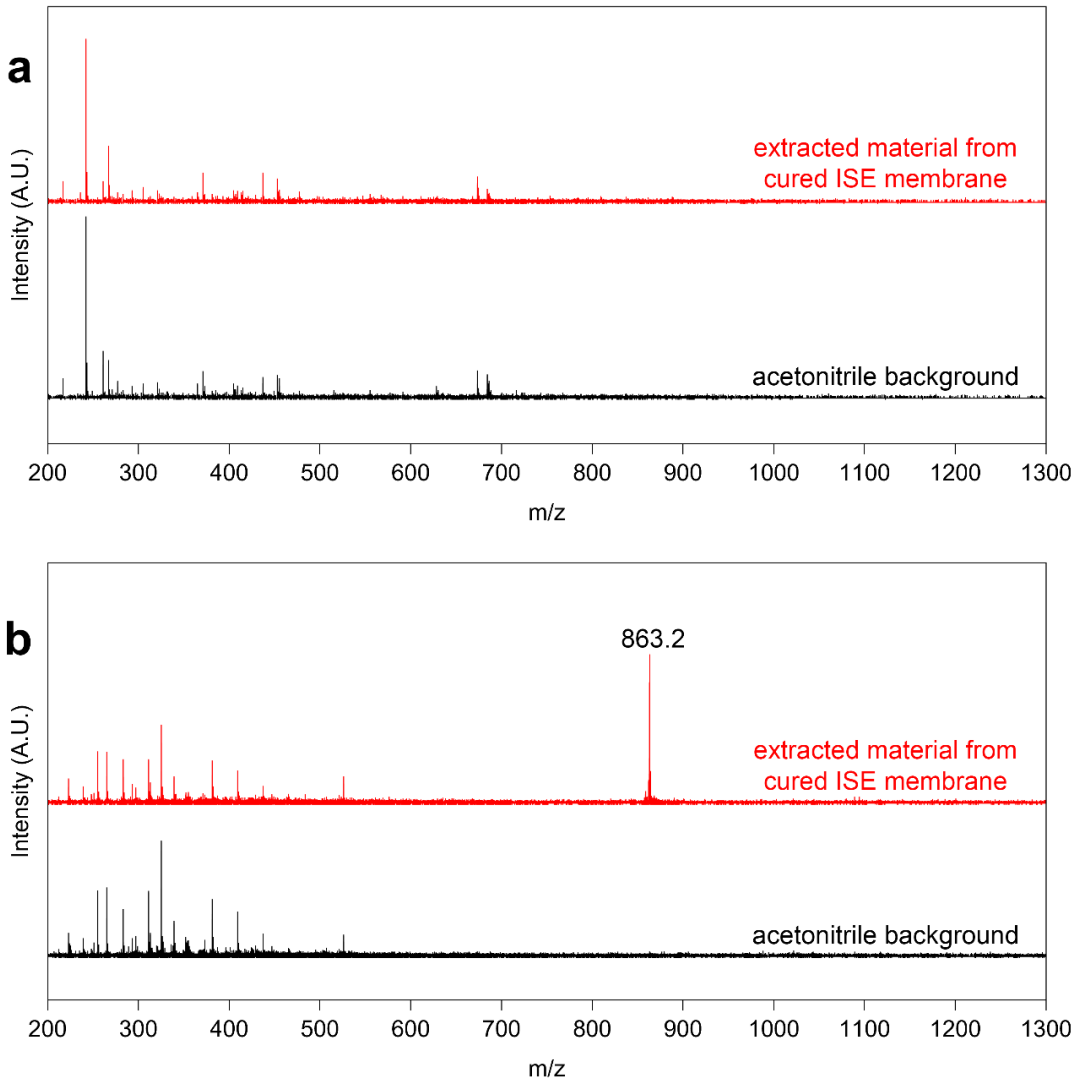

Figure 4.5. Mass spectra of extract collected from an ISE membrane prepared with compound **7** as ionophore and NaTFPB·2H_2O as the anionic site. The mass spectra for (a) positive and (b) negative ionization modes are shown. The membrane precursor solution was stirred for 45 min before casting onto a Teflon sheet and then cured for 96 h in air at 55 °C before Soxhlet extraction was performed (extracted with CH_2Cl_2 for 24 h). The peak at *m/z* = 863.2 in (b) corresponds to the anionic site. No other peaks that were not also present in the background were observed. The lack of peaks corresponding to the ionophore suggests that the ionophore-related species detected by UV-vis spectroscopy are either oligomers or attached to silicone chains that are not attached to the crosslinked silicone network.

Most silicone-based ISEs reported to date were fabricated with commercial one-component silicones cured at room temperature in which the polymer, crosslinker, and catalyst are premixed.[60, 105] In these silicones, all terminal Si–OH groups are expected to have reacted with crosslinker or have been replace with terminal alkoxy or acetoxy functional groups.[193] For these silicones, stirring the ISM precursor solution before drop casting is not expected to affect ionophore attachment to the silicone because there will be no Si–OH groups present until the silicone is exposed to water vapor. One advantage of the silicone used in this work is the ability to adjust the silicone composition and preparation procedure to produce silicone membranes optimized for the intended purpose.

Achieving 96% attachment of ionophore to silicone matrix is very important in the context of wearable and implantable SC-ISEs as it will improve the lifetime of the ISE and decrease emf drift caused by ionophore leaching. For K^+ measurements in clinical settings, the value of K^+ concentration measured with the SC-ISE needs to be accurate within ±0.3 mM of the true value,[194] which corresponds to a potential difference of 1.5 mV for a sample with 5 mM K^+. Once the emf of the ISE has drifted more than 1.5 mV, it will need to be recalibrated to perform measurements with high accuracy. Leaching of only 4% of ionophore from the membrane would result in a maximum potential change of -1.0 mV whereas leaching of 10%, 20%, and 30% would result in a potential change of -2.7, -5.7 and -9.1 mV, respectively. With 96% of BME-44 covalently attached to the silicone membrane, leaching of ionophore alone would not cause an emf drift large enough to require recalibration.

4.3.3. Response and selectivity

We initially attempted to prepare SC-ISEs on graphite/glass electrodes with CIM carbon[47] as a solid contact. However, these ISEs, with either mobile or covalently attached ionophore, exhibited sub-Nernstian responses to K^+ (Figure 4.6) and poor selectivities, which may be caused by ionophore adsorption onto the CIM carbon (375 m^2/g)[195] and graphite surfaces (26 m^2/g; see Table 4.2, Figures 4.7, 4.8, and 4.9), as this has been previously shown too for a freely mobile ionophore.[195] Evidently, ionophore adsorption onto the carbon surface can no longer occur once the ionophore is covalently attached to the silicone network of the sensing membrane. However, when the sensing membrane is cured in situ, i.e., in contact with a high surface area carbon solid contact, ionophore molecules that have not yet reacted with the growing silicone network are still mobile and can, therefore, adsorb onto the carbon surfaces. This depletes the membrane of ionophore groups, resulting in SC-ISEs with poor selectivity (Figure 4.10).

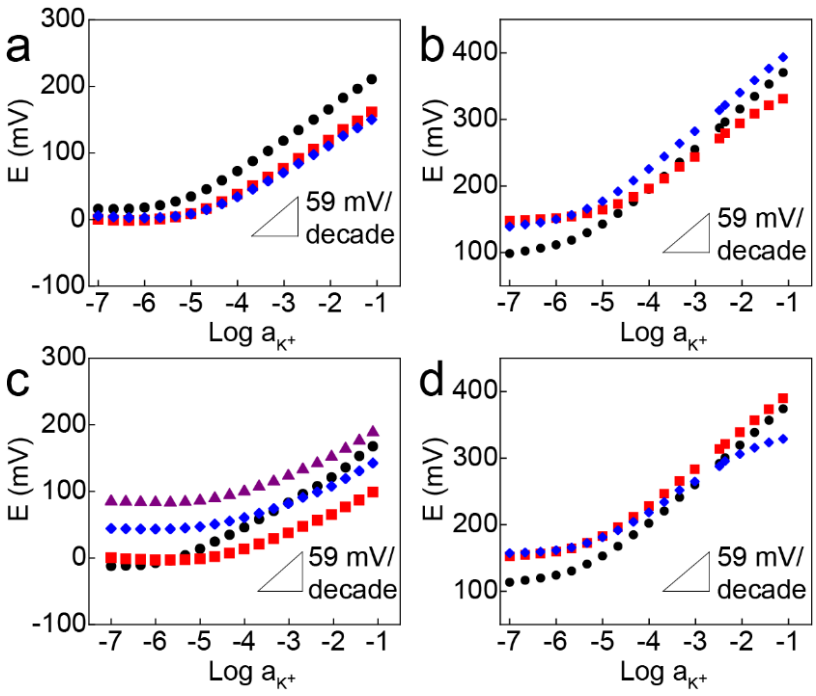

Figure 4.6. Potentiometric response curves for K^+ ISEs prepared with mobile BME-44 (top row) or the covalently attachable BME-44 derivative (**7**) (bottom row) with the electrode configurations (a,c) graphite/CIM/ISM and (b,d) Au/SC_8H_{17}/ISM. All electrodes were conditioned in 1 mM KCl at 22 °C overnight before measurements. The different symbols and colors in each graph represent potentials for identically prepared ISEs. See Figures 4.7 and 4.8 for data from FIM selectivity measurements.

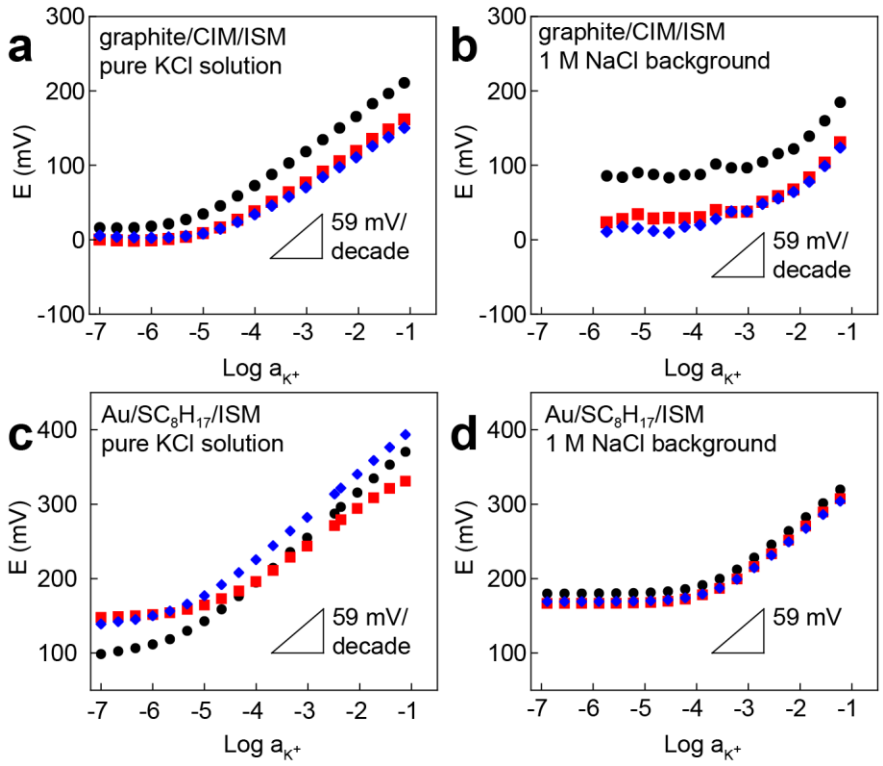

Figure 4.7. Measured potentials, *E*, of K^+ ISEs prepared with mobile BME-44 as a function of the logarithm of K^+ activity in aqueous solution after initial conditioning in 1 mM KCl at 25 °C. Left column: measured potentials of K^+ ISEs in pure KCl solution for ISEs prepared with (a) graphite/CIM/ISM and (c) Au/SC_8H_{17}/ISM. The K^+ activity was adjusted by adding aliquots of KCl solution to the sample. Right column: Measured potentials of K^+ ISEs to K^+ in the presence of a 1 M NaCl (FIM) background for ISEs prepared with (b) graphite/CIM/ISM and (d) Au/SC_8H_{17}/ISM. The K^+ activity was adjusted by successive dilutions of a 0.1 M KCl/1 M NaCl solution with 1 M NaCl for electrodes in (b). For electrodes in (d), the K^+ activity was adjusted by successive additions of standard KCl/1 M NaCl solutions to a 1 M NaCl solution. The different colored symbols in each graph represent the measured potentials of identical K^+ ISEs. Potentials were measured against a free-flowing double junction reference electrode with a 1 M lithium acetate outer filling solution. The potentials were corrected for the liquid junction potential at the free-flowing double junction using the Henderson formalism.

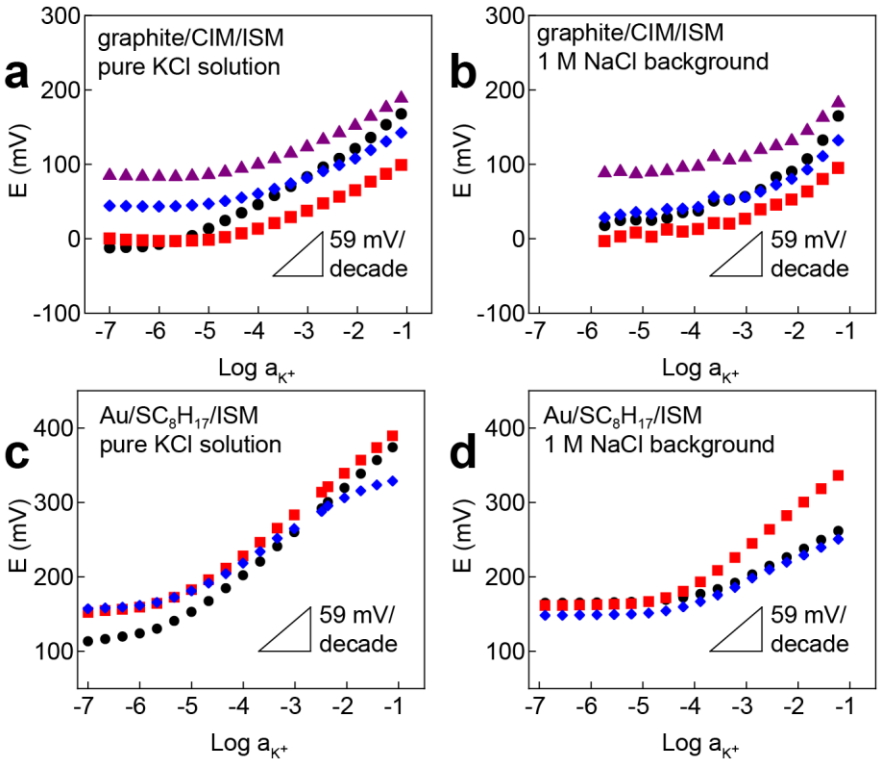

Figure 4.8. Measured potentials, *E*, of K^+ ISEs prepared with covalently attached BME-44 (**7**) as a function of the logarithm of K^+ activity in aqueous solution after initial conditioning in 1 mM KCl at 25 °C. Left column: measured potentials of K^+ ISEs in pure KCl solution for ISEs prepared with (a) graphite/CIM/ISM and (c) Au/SC_8H_{17}/ISM. The K^+ activity was adjusted by adding aliquots of KCl solution to the sample. Right column: Measured potentials of K^+ ISEs to K^+ in the presence of a 1 M NaCl (FIM) background for ISEs prepared with (b) graphite/CIM/ISM and (d) Au/SC_8H_{17}/ISM. The K^+ activity was adjusted by successive dilutions of a 0.1 M KCl/1 M NaCl solution with 1 M NaCl for electrodes in (b). For electrodes in (d), the K^+ activity was adjusted by successive additions of standard KCl/1 M NaCl solutions to a 1 M NaCl solution. The different colored symbols in each graph represent the measured potentials of identical K^+ ISEs. Potentials were measured against a free-flowing double junction reference electrode with a 1 M lithium acetate outer filling solution. The potentials were corrected for the liquid junction potential at the free-flowing double junction using the Henderson formalism.

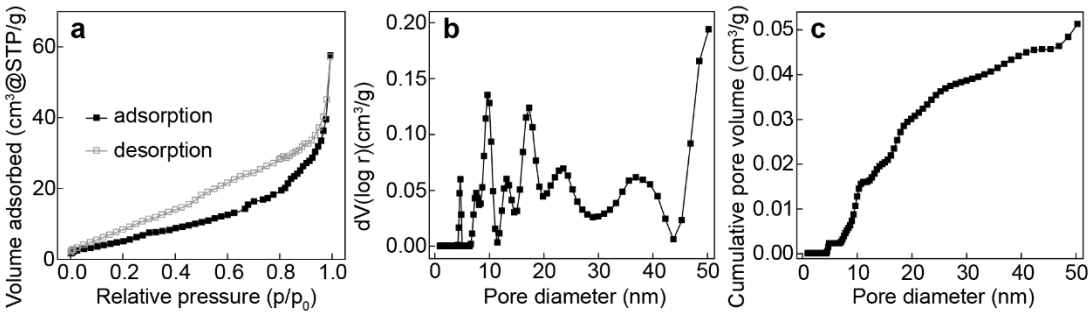

Figure 4.9. N_2 gas sorption data for the graphite used to make the graphite/glass electrodes. (a) N_2 gas sorption isotherm, (b) pore size distribution, (c) cumulative pore volume. The BET surface area is 26 m^2/g.

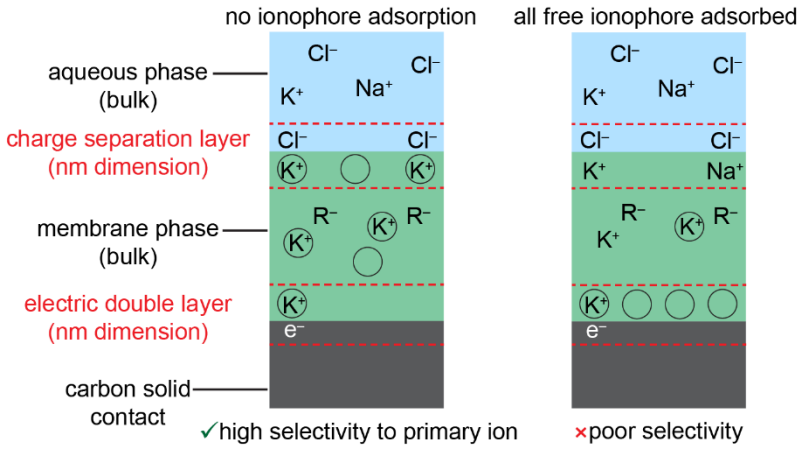

Figure 4.10. A K^+ SC-ISE with no free ionophore adsorbed onto the carbon solid contact (left) has free ionophore in the bulk of the ISM and at the ISM/sample interface, allowing the ionophore to bind to K^+ and impart selectivity to the sensor. A K^+ SC-ISE with all free ionophore adsorbed onto the carbon solid contact surface (right) has no free ionophore in the bulk of the ISM or at the ISM/sample interface. Selectivity is poor and is controlled by the differences in the solvation energies of the cations in the sample and membrane phase (i.e., without ionophore-assistance of the phase transfer). The circles represent the ionophore, and R^- represents the anionic sites.

Table 4.2. Response characteristics of K^+ ISEs prepared with mobile BME-44 and the covalently attachable BME-44 analog (**7**).

Ionophore	ISM solution stir time (min)	# of ISM layers applied	solid contact	response slope[a] (mV/decade)	log K_{K^+,Na^+}	detection limit (μM)	log resistance (Ω)
mobile BME-44[b]	45	1	Au/SC_8H_{17}	57.4 ± 4.2	-3.54 ± 0.05	8 ± 8	9.3 ± 0.1
7[b]	45	1	Au/SC_8H_{17}	54.1 ± 7.1	<-4.05	4 ± 1	8.5 ± 0.2
mobile BME-44[b]	5	4	graphite/CIM	45.3 ± 3.4	-2.20 ± 0.08	20 ± 10	8.7 ± 0.4
7[b]	5	4	graphite/CIM	32.4 ± 6.3	NA	20 ± 10	7.2 ± 0.4
mobile BME-44[c]	5	4+1[d]	graphite/CIM	53.6, 54.2	-3.09, -3.00	1, 2	8.6, 8.9
mobile BME-44[c]	45[e]	4+1[d]	graphite/CIM	54.6, 53.8	-2.85, -2.77	1, 1	8.6, 8.6
7[c]	5	4+1[d]	graphite/CIM	45.0, 46.3	NA, NA	20, 30	7.5, 7.0
7[c]	45[e]	4+1[d]	graphite/CIM	46.9, 45.7	NA, NA	20, 20	8.6, 7.5

[a] Determined from calibration curves measured in KCl solutions at 22 °C.

[b] Reported as average ± standard deviation for 3 or 4 ISEs.

[c] Sample size = 2; values for both electrodes are listed in each column.

[d] One additional ISM coating was applied on top of the existing crosslinked ISM that had already been exposed to aqueous KCl solutions.

[e] The ISM precursor solution used to drop cast the additional layer referred to with [d] was stirred for 45 min. The underlying crosslinked ISM was prepared from an ISM solution that had been stirred for 5 min.

We attempted to address this problem by adding an additional coating of ISM on top of the existing membranes using ISM solutions that had been stirred in a closed container for 5 or 45 min. Unfortunately, no improvement in selectivity was observed for SC-ISEs prepared with covalently attachable ionophore and graphite/CIM carbon solid contacts (Table 4.2, Figure 4.11). Although diffusion of ionophore from the drop cast layer through the existing crosslinked silicone membrane to the carbon surface should be slow, depletion of covalently attachable BME-44 derivative (**7**) from the outer membrane surface is evidently fast enough to compromise the ISE performance. The absence of mobile ionophore in the first deposited ISM layer after curing may at least temporarily result in depletion of ionophore from the subsequently deposited layer simply by distribution of mobile ionophore and ionophore-comprising oligomers between the two ISM layers, a process followed at a later stage by adsorption of these species onto the carbon (Figure 4.12). Further optimization of the curing chemistry and fabrication process is required to allow for one to take advantage of the properties that high surface area carbon solid contacts provide. This will be a topic of future study.

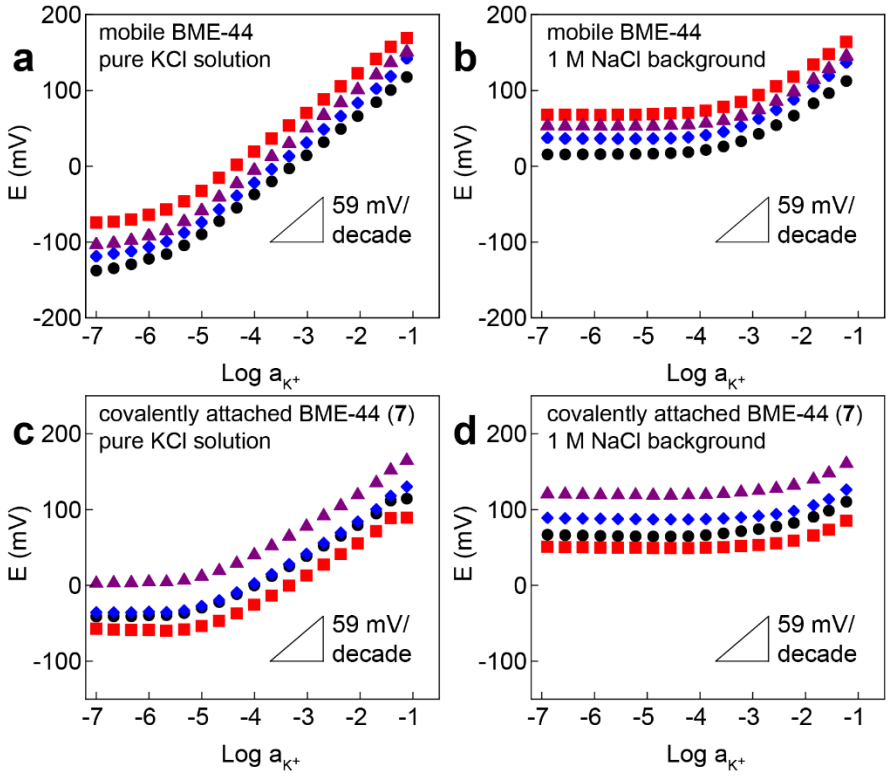

Figure 4.11. Measured potentials, *E*, of K^+ ISEs prepared on graphite/CIM/ISM electrodes with (a, b) mobile BME-44 or (c, d) covalently attached BME-44 (**7**) as a function of the logarithm of K^+ activity in aqueous solution. These ISEs are the same as those shown in Figure 4.7 and Figure 4.8, but after an additional coating of ISM was applied to the existing ISM. Left column: measured potentials of K^+ ISEs in pure KCl solution for ISEs prepared with (a) mobile BME-44 and (c) covalently attached BME-44 (**7**). The K^+ activity was adjusted by adding aliquots of KCl solution to the sample. Right column: Measured potentials of K^+ ISEs to K^+ in the presence of a 1 M NaCl (FIM) background for ISEs prepared with (b) mobile BME-44 and (d) covalently attached BME-44 (**7**). The K^+ activity was adjusted by successive additions of standard KCl/1 M NaCl solutions to a 1 M NaCl solution. The symbols in each graph represent the potential for ISEs prepared with an additional coating of ISM by drop casting an ISM precursor solution that had been stirred for 5 (● ■) and 45 min (◆ ▲). Potentials were measured against a free-flowing double junction reference electrode with a 1 M lithium acetate outer filling solution. The potentials were corrected for the liquid junction potential at the free-flowing double junction using the Henderson formalism.

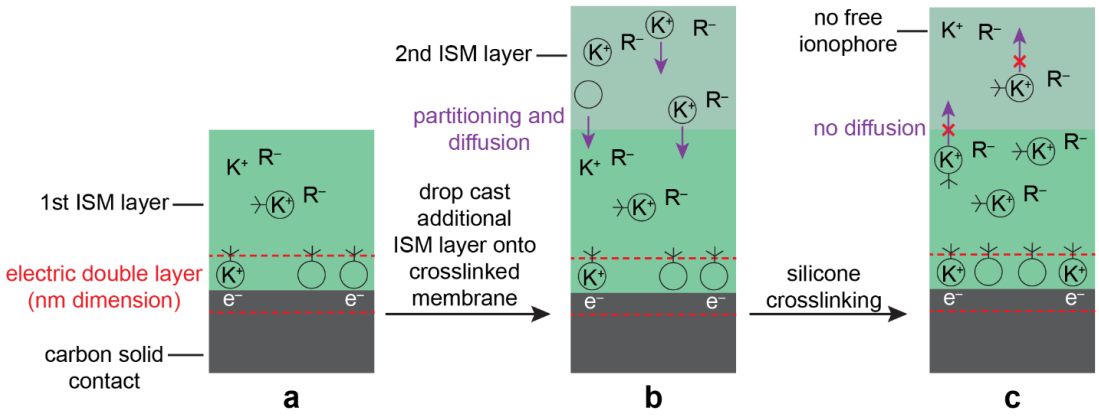

Figure 4.12. Schematic illustrating how the covalently attachable BME-44 derivative (**7**) can deplete from the outer surface of the ISM after drop casting an additional coating of ISM precursor solution onto an existing crosslinked ISM as long as it is not bound to the silicone network. (a) SC-ISE with all free ionophore adsorbed onto the solid contact. (b) Free monomers or oligomers of the ionophore in a freshly deposited ISM precursor solution partition into the first membrane layer and diffuse towards the carbon, resulting in (c) depletion of ionophore from the outer ISM surface. Once the ionophore is covalently attached to the crosslinked silicone, it cannot diffuse back to the outer ISM surface, resulting in SC-ISEs with poor selectivity to K^+ vs. Na^+. The circles represent ionophore, and R^- represents the anionic sites. Ionophore molecules covalently attached to the silicone are represented with circles with a cross attached to it.

To avoid these complications from ionophore adsorption onto carbon surfaces, we prepared ISEs on octanethiol-coated gold electrodes. The resulting ISEs exhibit near-Nernstian responses to K^+ with micromolar detection limits (Figure 4.6, Table 4.2). The selectivity of the silicone-based ISEs prepared with mobile BME-44 ($\log K_{K^+,Na^+} = -3.5$) is similar but slightly superior to that observed for ISEs prepared with mobile BME-44 in PVC plasticized with bis(butylpentyl)adipate or *o*-nitrophenyl octyl ether ($\log K_{K^+,Na^+} = -3.3$ and -3.2, respectively)[196] and it equals the selectivity of plasticizer-free ISEs prepared with a condensation-cured fluorosilicone ($\log K_{K^+,Na^+} = -3.5$) membrane.[93] ISEs prepared with the covalently attachable BME-44 derivative (**7**) have even better selectivity to K^+ vs. Na^+ ($\log K_{K^+,Na^+} < -4.1$) and an almost one order of magnitude lower resistance (Table 4.2).

The selectivity of BME-44 is dependent on hydrogen bonding between the N–H and NO_2 groups. For an analog of BME-44 with a CH_2-CH_2-S-CH_2-CH_2 bridge between the two urethane bonds, it was shown that replacement of NO_2 with H on the benzene ring results in a one order of magnitude decrease in selectivity to K^+ vs. Na^+.[197] A similar decrease was observed when the N-H group on the urethane linkage was replaced with N-CH_3. One hypothesis for the improved selectivity of BME-44 in a silicone matrix compared to a plasticized PVC matrix is based on the fact that silicone does not contain hydrogen bond acceptor groups, such as the carbonyl groups in many PVC plasticizers. Such groups may hydrogen bond to the urethane groups of the ionophore, changing the ionophore conformation, decreasing the stability of the ionophore/K^+ complex, and, thereby, worsening selectivity.

It seems unlikely that the benzyl ether group in compound **7** causes the selectivity difference between silicone-based ISE membranes with, on one hand, mobile BME-44 and, on the other hand, compound **7**. When BME-44 binds to K^+, the two crown ether rings form a sandwich structure where the K^+ ion sits between the two crown ether groups. The high K^+ vs. Na^+ selectivity of BME-44 requires a high flexibility of the connecting linkage to permit formation of this sandwich structure. So long as this is possible, the structure of the linkage has little influence on the selectivity of the ionophore.[189, 197]

A possible explanation that would explain the selectivity differences between membranes with mobile and attached ionophores may be that the mobile BME-44 or the salt comprising the mobile K^+-BME-44 complex and ionic site have poor solubilities in the silicone matrix, changing the ionophore to ionic site ratio and, thereby, altering the selectivity. Assuming that BME-44 binds both K^+ and Na^+ with 1:1 stoichiometries, it is expected that the potentiometric selectivity improves slightly as the ionic site to ionophore ratio increases.[26] Optical microscopy (Figure 4.13) of ISE membranes cast onto a Teflon substrate prepared with mobile BME-44 (which is bright yellow) reveal that the ionophore separates from the silicone into small domains (<100 μm in size), while the bulk of the silicone remains colorless. Although the solubility of mobile BME-44 in the silicone membrane appears very low, there is evidently just enough of this ionophore dissolved in the silicone to impart quite high ion selectivity. Membranes prepared with the covalently attachable BME-44 analog (**7**) on a Teflon substrate had a more uniform appearance. The bulk of the membrane appears yellow, suggesting that at least some of the ionophore was successfully incorporated into the silicone matrix during the stirring and crosslinking steps.

This observation is also consistent with the lower resistances for ISEs prepared with the covalently attachable BME-44 analog (**7**) compared with mobile BME-44; phase-separation of ionophore/ionic site species would reduce the conductivity of the membrane. Ionophore covalently attached to the crosslinked silicone matrix (not phase separated) has very limited mobility, but the anionic site (not covalently bound to the silicone chains) can freely diffuse through the ductile silicone, which only stiffens below its glass transition temperature of approximately –118 °C.[167] If neither of the species were mobile, the electrode resistances would become very high and the ISEs would no longer function.[186]

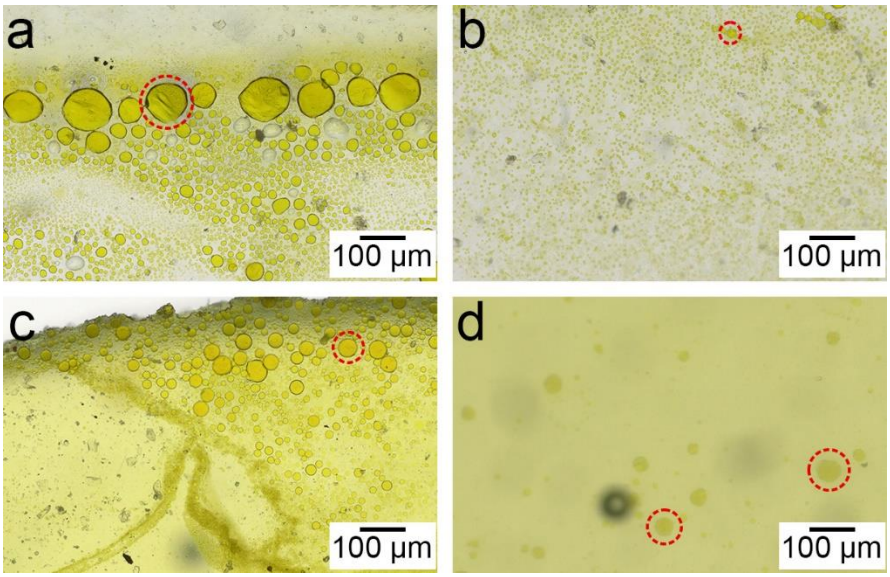

Figure 4.13. Optical microscope images of ISMs (precursor solution stirred for 45 min before drop casting onto a Teflon substrate) prepared with (a, b) mobile BME-44 and (c, d) covalently attachable BME-44 analog (**7**). The red circles in each image highlight example domains containing phase-separated ionophore.

However, some bright yellow, spherical domains of ionophore can also be observed in the membrane prepared with the covalently attachable ionophore derivative (**7**). Analysis of the yellow spherical domains in the membrane prepared with the covalently attachable BME-44 derivative by confocal Raman microscopy (Figure 4.14) shows that they are comprised of BME-44. No silicone is observed in these domains. Evidently some of the covalently attachable ionophore derivative can form oligomers during the stirring period before drop casting and during the crosslinking reaction, which can phase separate from the silicone when the solvent evaporates. This observation is also consistent with the hypothesis that the covalently attachable BME-44 derivative can adsorb onto carbon surfaces before the ionophore can attach to a silicone chain. Even when the ISM precursor solution is reacted at room temperature for 45 min in a sealed container to attach some ionophore to the silicone chains before curing, at least some of the ionophore species are not bound to a polymeric silicone network, and such monomeric and oligomeric species may adsorb onto carbon solid contact surfaces as long as these surfaces are accessible to these species.

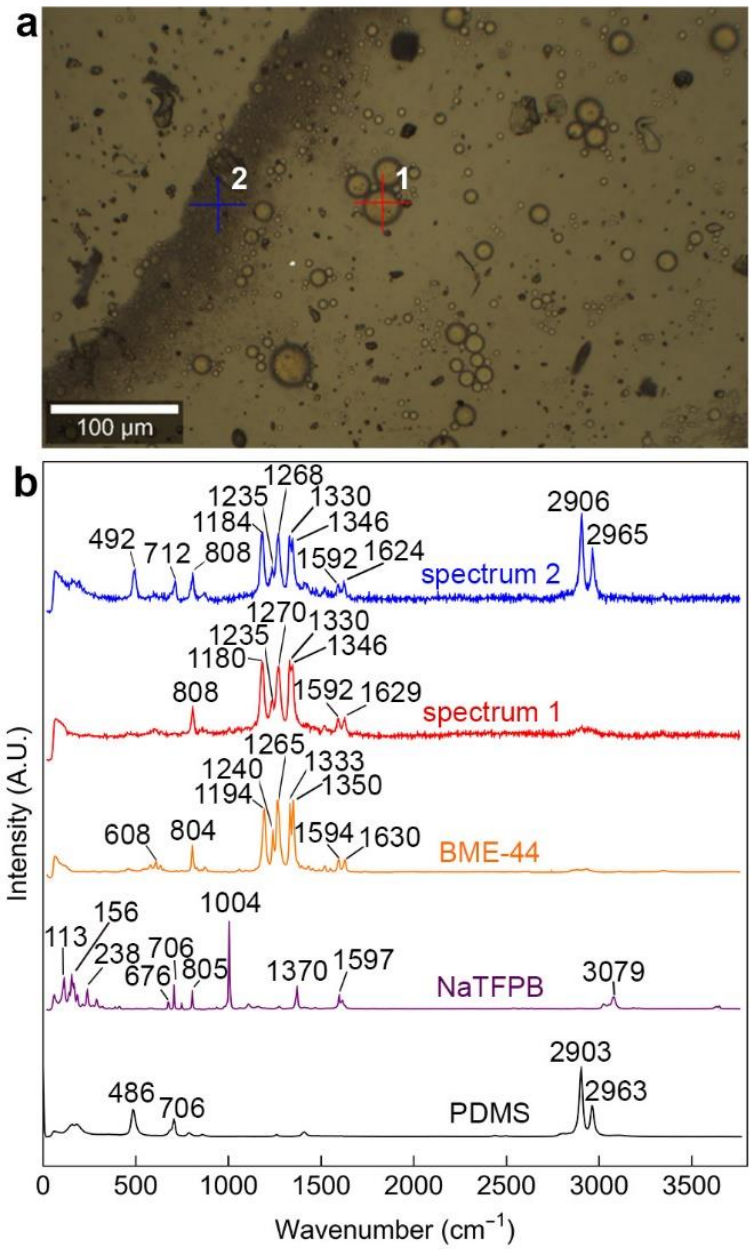

Figure 4.14. Confocal Raman spectra of the yellow domains observed in an ISM prepared with covalently attached BME-44. The locations shown in the microscope image (a) were used to collect the Raman spectra shown in (b).

4.4 Conclusions

We synthesized an analog of BME-44 that can be covalently attached to condensation-cured silicones with high purity. While others have prepared ISEs with ionophores that can be covalently attached to silicone membranes during the curing process,[89, 105] little attention has been paid to the influence of curing conditions on the degree of ionophore attachment to the silicone. Here, we prepared ISE membranes with a derivative of BME-44 that can be covalently attached to a condensation-cured silicone formulated in house. With optimized curing procedures up to 96% attachment of ionophore to the silicone matrix can be achieved, which is critical for improving the lifetime of small ISEs. We also show that in the process of attaching the ionophore in situ to the silicone, the covalently attachable BME-44 derivative can inadvertently adsorb onto high surface area carbon solid contacts, resulting in SC-ISEs with poor selectivity. Therefore, careful consideration of the solid contact material, curing chemistry, and curing procedure is required when developing a process for the fabrication of SC-ISEs with plasticizer-free silicone matrixes, even when using an ionophore that can covalently attach to the silicone. Further optimization of ISE fabrication procedures and silicone curing chemistry will be required to produce functional SC-ISEs with ionophore **7** using high surface area carbon solid contacts. This will be a topic of future study.

Plasticizer-free silicone-based ISEs prepared with the covalently attachable BME-44 derivative (**7**) on octane-thiol-coated gold electrodes have Nernstian responses to K^+ and have a better selectivity for K^+ over Na^+ ($\log K_{K^+,Na^+} < -4.05$) than those prepared with mobile BME-44 ($\log K_{K^+,Na^+} = -3.54 \pm 0.05$). Attachment of BME-44 to the silicone

membrane leads to less phase separation of ionophore and, therefore, more homogeneous incorporation of the covalently attachable BME-44 derivative (**7**) into the silicone matrix than mobile BME-44. This results in better control of the ionophore/ionic site ratio in the silicone membrane and better selectivity.

Chapter 5

Conclusions and Future Work

5.1 Conclusions

The ultimate goal of this dissertation has been to develop a biocompatible K^+ sensor that can be used in wearable and implantable sensors. The first objective of the work in this thesis was to identify suitable solid-contact materials, silicone membranes, ionophores, and ionic sites for use in plasticizer-free ISEs. In Chapter 2, we showed that functional SC-ISEs can be prepared using valinomycin as an ionophore and potassium tetrakis(4-chlorophenyl)borate as anionic sites using a commercially available silicone (Dow 3140) or our own in-house condensation-curing silicone. Similar to these SC-ISEs with silicone membranes, SC-ISEs with fluorosilicone membranes (Dow 730) also responded to K^+, had excellent selectivity to K^+ vs. Na^+, and low long-term drift in 1 mM KCl solution. However, SC-ISEs with fluorosilicone membranes consistently underestimated the K^+ concentration in blood plasma, whereas the values of K^+ concentration measured with SC-ISEs comprising silicone membranes were within error of the value measured by ion chromatography. We also found that SC-ISEs with silicone membranes, but slightly different compositions can have very different long-term drift values in real samples like blood plasma. SC-ISEs prepared with our in-house silicone had 10 times higher long-term drift (–495 µV/h) than those prepared with the commercially available silicone (Dow 3140) (–55 µV/h). After 41 h exposure to blood plasma at 37 °C, the selectivity of all SC-ISEs worsened, but selectivity was still good enough for measurements in physiological samples like blood plasma.

The membranes in Chapter 2 were too thick (400–800 µm) for use in wearable and implantable sensors. One challenge for reducing the thickness of the membrane and carbon

layer was the size of the CIM carbon particles used for the solid contact. To address this problem, as reported in Chapter 3, we evaluated several methods for reducing the CIM carbon particle size. We found that probe sonication followed by particle size separation via sedimentation was the best method. Using this method, we were able to obtain CIM carbon with particle sizes below 14 μm. We showed that SC-ISEs with a total carbon+ISM thickness <100 μm could be fabricated on Al foil (commonly used as the current collector in lithium ion batteries) by using a doctor blade to apply the CIM carbon solid contact and ISM layers. We showed that these SC-ISEs have Nernstian responses to K^+, excellent selectivity, and low drift in 1 mM KCl solution.

In Chapter 4, we address the problem of ionophore leaching from the membrane. We synthesized an analog of the commercially available K^+ ionophore that contains a triethoxysilyl group on part of the molecule that is not involved in binding to K^+. The triethoxysilyl group allowed the ionophore to covalently attach to silicone chains by reacting with the terminal Si–OH groups. We found that reacting the ionophore with the silicone chains before drop casting the membrane onto the electrode and curing was critical for maximizing the degree of ionophore attachment to the silicone. ISEs prepared with the covalently attachable BME-44 derivative with silicone membranes have Nernstian responses to K^+ and excellent selectivity to K^+ vs. Na^+. The selectivity of ISEs with the covalently attachable BME-44 derivative was significantly better than the selectivity of ISEs prepared with the mobile BME-44 analog (in silicone or plasticized PVC membranes). We also showed that significant phase separation of mobile BME-44 from the silicone matrix occurs. Evidently mobile BME-44 has poor solubility in the silicone

matrix. Far less phase separation was observed for silicone membranes with the ionophore covalently attached. We hypothesize that better mixing of the covalently attachable BME-44 derivative in the silicone matrix than mobile BME-44 is the cause of the better selectivity observed for ISEs with the covalently attachable BME-44 derivative. We also show that some ionophores, like mobile BME-44 and the covalently attachable BME-44 derivative can adsorb onto high-surface-area carbon contacts, resulting in depletion of ionophore from the membrane and poor selectivity. This phenomenon is evidently ionophore dependent because this same effect was not observed in Chapter 2 for SC-ISEs prepared with valinomycin as the ionophore.

5.2 Future work

To determine the next steps for this work, we will first consider some observations made during the work described in this thesis. In Chapter 2, we showed that SC-ISEs prepared with silicone and fluorosilicone membranes and valinomycin as ionophore maintain their responses to K^+ and have good selectivity to K^+ vs. Na^+ after 41 h exposure to blood plasma at 37 °C. However, SC-ISEs with silicone membranes having quite similar structures had very different long-term drifts in blood plasma. Additionally, SC-ISEs with the commercially available silicone (Dow 3140) had 10 times lower resistivity than those prepared with our own in-house silicone.

Evidently, factors other than the backbone structure of the silicone have a large impact on the behavior of the resulting SC-ISE. Several hypotheses can explain the difference in resistivity. First, as we suggested in Chapter 2, we expect that the mobility of ions in a

silicone matrix with higher crosslink density would be lower and therefore, membranes with a higher crosslink density are expected to have high resistivity. The second hypothesis is that there is a significant difference in solubility of ionophore and ionic sites in the silicone matrix. In Chapter 4, we saw that mobile BME-44 phase-separates from the silicone matrix once the solvent evaporates. The same process is likely to happen with valinomycin, as others have reported observing crystals of valinomycin in the silicone ion-selective membranes.[85] Unfortunately, manufacturers do not disclose the exact details of the silicone composition, so we do not know if or how a different solubility of ionophore and ionic sites in the commercially available silicone and our in-house silicone would manifest itself. Differences in ionophore and ionic site solubility in the silicone may also come with differences in the solubility of species from blood plasma (e.g., lipids) in the membrane. Such a factor may also explain some of the long-term stability data in blood plasma for membranes with commercial and in-house silicone, though to date, these phenomena have never been studied.

While performing the work described in this thesis, we observed that for commercial silicones and fluorosilicones, the age of the silicone or fluorosilicone was important. The first example for this, which we noted in the experimental section of Chapter 2, was for ISEs with fluorosilicone membranes (Dow 730). After storage of the silicone for several months or years, it was no longer possible to produce ISEs with Nernstian responses to K^+ and a new batch of fluorosilicone would have to be purchased. A similar effect was observed for ISEs with Dow 3140 membranes, but only for ISEs containing BME-44 as the ionophore. The silicones are provided from the manufacturer in a tube with a screw cap

that can be re-sealed to a certain extent, allowing for multiple uses of the same silicone tube. Each time the cap is opened, and silicone dispensed, some water vapor from the air diffuses into the silicone tube, where it likely reacts with excess crosslinker.

Other parameters that are often overlooked when it comes to ion-selective membranes with condensation-curing silicones is the influence of membrane thickness on the crosslinked silicone structure and the effects that structure has on the resulting ISEs. Kimura reported that for Na^+-selective ISFETs with a silicone membrane (ShinEtsu KE44T, oxime-evolving) and unsymmetrical calix[4]arene 1 as ionophore (no added ionic sites), a minimum ion-selective membrane thickness of approximately 75 µm was required to obtain Nernstian responses to Na^+.[77] Interestingly, no upper limit in thickness was observed; ISFETs with membrane thicknesses between 75 and 600 µm had Nernstian responses to Na^+.

The mechanisms for these phenomena are not known, though we suspect they are related to the crosslinking chemistry of condensation-curing silicones. De Buyl et al. have shown that the crosslink density for condensation-curing silicones changes with depth within a single silicone membrane, with highest crosslink density near the air/membrane surface.[74] The mechanism they propose for this effect is as follows (Figure 5.1): Once a condensation-curing silicone is applied to a surface and exposed to moisture in the air, silicone curing begins with the formation of a crosslinked layer at the air/silicone surface. The boundary between crosslinked and non-crosslinked silicone then moves deeper into the silicone over time. As a result, water diffuses further into the silicone before reacting with crosslinker, until crosslinking is complete. At the same time, mobile crosslinker

molecules that have not been attached to the crosslinked silicone network can diffuse from the non-crosslinked layer into the crosslinked layer where they can react and attach to the crosslinked silicone network. This results in a gradient in crosslink density within the silicone membrane where the highest crosslink density is at the membrane/air interface and the lowest crosslink density is at the silicone/substrate interface.

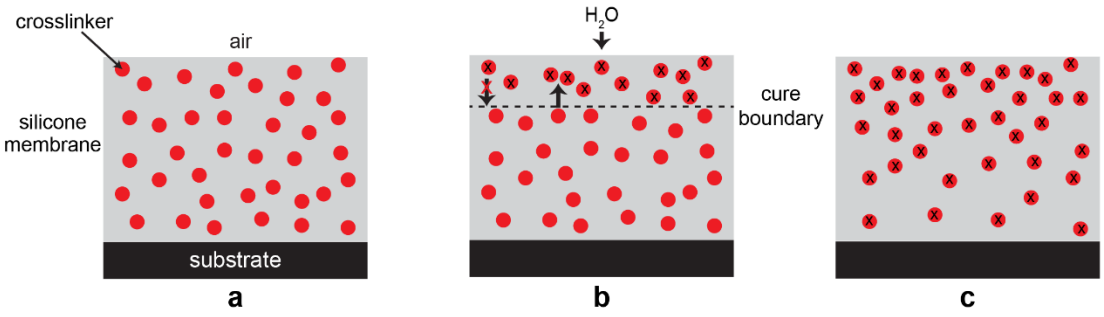

Figure 5.1. Proposed mechanism for formation of a gradient in crosslink density in condensation-cured silicones.[74] Mobile crosslinker molecules are shown as red dots and immobilized crosslinker molecules that have been covalently attached to the crosslinked silicone network are represented by red dots with a black x in the center. (a) Silicone membrane with crosslinker evenly distributed throughout just before exposure to H_2O in the air; (b) membrane after crosslinking has begun with net diffusion of mobile crosslinker; and (c) completely cured membrane.

To complicate matters further, the crosslinker molecules can also react with each other to form domains of silica[151, 198] (in the case of tetraethoxysilane), silsesquioxanes (in the case of methyl trimethoxysilane), or other partially condensed siloxanes (Figure 5.2). We note that ISEs have been produced with poly(silsesquioxane) membranes with ionophores covalently attached to the matrix,[143, 188] though to our knowledge these have never been used to perform measurements in physiological solutions like blood plasma.

The structure of crosslinked condensation curing silicones can be quite complex and vary significantly throughout the membrane. The lack of control over the crosslinked silicone structure due to the phenomena described in this section makes studying the influence of various silicone structures on performance of SC-ISEs rather challenging.

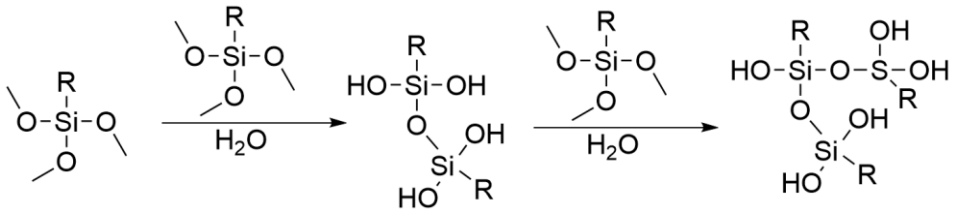

Figure 5.2. Condensation reaction between different molecules of an alkyltrimethoxysilane in the presence of water vapor to form silsesquioxanes.

Therefore, to study the influence of silicone structure on ISE performance, we suggest first focusing on formulating reproducible, well-characterized silicones. This means that the complete composition of the silicone must be known, and we recommend using custom-formulated silicones for this work. To minimize any variations caused by evaporation of crosslinker, we suggest adapting the approach used by Jurásková et. al, by using non-volatile crosslinkers.[199] They employed silicones with trimethoxysilyl terminal groups for crosslinking (Figure 5.3). The polymeric crosslinkers have a larger size, which means they are less mobile than crosslinkers such as methyltrimethoxysilane. Therefore, gradients in crosslink density throughout the silicone membrane should be smaller, resulting in more homogenous membranes.

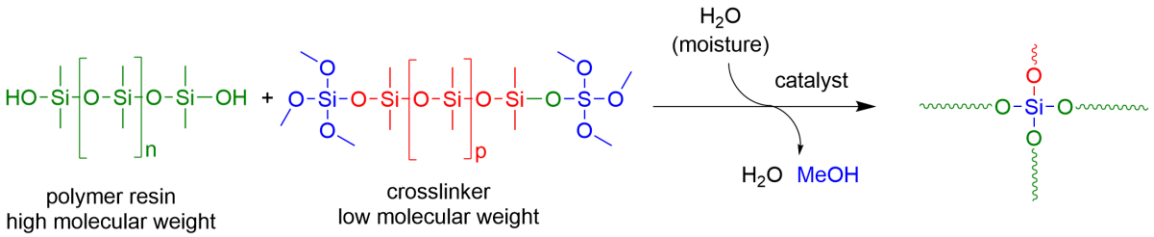

Figure 5.3. Proposed silicone crosslinking chemistry with alkoxy-terminated silicone crosslinkers.

Use of non-volatile crosslinkers would allow one to study the influence of crosslinker concentration on ISE performance in aqueous and physiological samples like blood plasma. To our knowledge, this has not been systematically studied before. A balance between mechanical integrity of the silicone membrane and electrochemical properties (ionophore and ionic site mobility) will likely need to be achieved. We suspect that the long conditioning times (several weeks) required to achieve the low long-term drifts in Chapter 2 are caused by unreacted Si–OH groups on neighboring crosslinker molecules slowly condensing over a period of a few weeks. Jurásková et al. observed that the Young's modulus for crosslinked condensation curing silicones increases over a period of up to 30 days after preparation of the silicone polymer. They attributed the change in Young's modulus to condensation of unreacted Si–OH groups in the silicone. Interestingly, when silicones were formulated with a 15 to 1 ratio of methoxy groups on the crosslinker to hydroxy groups on the hydroxy-terminated silicone, almost no change in Young's modulus was observed between 1 d and 118 d after preparing the membrane.[199] Using mechanical properties of polymers like Young's modulus as a tool to track changes in condensation of unreacted Si–OH groups may be a viable method to support our hypothesis about the long

ISE conditioning times and allow for adjustment of the silicone chemistry to decrease the conditioning time.

One drawback of condensation-curing silicones is that the catalyst used for crosslinking is leftover in the silicone. Catalysts like dibutyltin dilaurate have been shown to cause silicone network rearrangement and chain scission after crosslinking.[200, 201] When immersed in water, hydrolysis and pitting of the silicone surface has been observed for some silicones.[9] This phenomenon might also be responsible for the long conditioning times of SC-ISEs observed in Chapter 2. The authors noted that hydrosilylation-curing silicones appeared more stable when submerged in H_2O.

Therefore, use of hydrosilylation-curing silicones (Figure 5.4) in ISEs could be revisited. Although ionophores can inhibit the crosslinking reaction, the hydrosilylation reaction can still proceed in the presence of some ionophores, as demonstrated in Chapter 4. Hydrosilylation curing silicones are not dependent on water vapor diffusing into the silicone. As a result, they have faster cure times and are the silicone of choice for scientists making silicones with highly tailored mechanical properties.

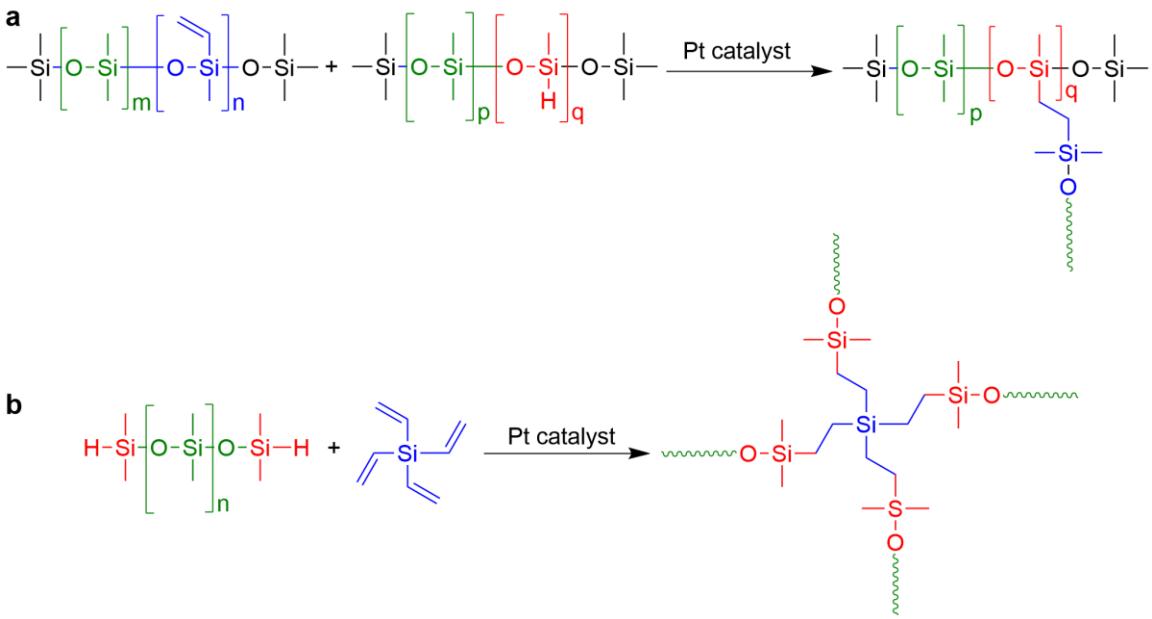

Figure 5.4. Hydrosilylation crosslinking chemistry of silicone membranes with (a) copolymers of poly(dimethylsiloxane) and either vinylmethylsiloxane or methylhydrosiloxane; (b) a hydride-terminated poly(dimethylsiloxane) crosslinked with tetravinylsilane.

Hydrosilylation-curing silicones also open the door for studying the influence of the silicone network structure on the performance of SC-ISEs. Hydrosilylation-curing silicones can be made using copolymers dimethylsiloxane and vinylmethylsiloxane or methylhydrosiloxane (Figure 5.4a). Alternatively, dimethylhydro-terminated silicone can be reacted with tetravinylsilane (Figure 5.4b). Silicone chains shown in Figure 5.4a are expected to have much less mobility because each silicone chain has multiple connections to other silicone chains, whereas silicone chains created from the crosslinking chemistry in Figure 5.4b have only two connections. As a result, ISEs prepared with silicones in Figure 5.4b may have a lower resistance due to the higher mobility of ionophore and ionic sites in the membrane. A high membrane resistance in ISEs is generally not a problem in laboratory

settings where the devices can be shielded from electromagnetic noise introduced from external sources. However, in wearable or implantable devices, obtaining excellent shielding may be more challenging. In those cases, the ISE resistance should be sufficiently low to ensure that accurate measurements of electrode potentials can be obtained.

References

1. McGrotty, Y.; Brown, A., Blood gases, electrolytes and interpretation 1. Blood gases. *In Practice* **2013,** *35*, 59-65.
2. Clausen, T., Regulation of active Na^+-K^+ transport in skeletal muscle. *Physiol. Rev.* **1986,** *66*, 542-580.
3. Deal, K. K.; England, S. K.; Tamkun, M. M., Molecular physiology of cardiac potassium channels. *Physiol. Rev.* **1996,** *76*, 49-67.
4. Sica, D. A.; Struthers, A. D.; Cushman, W. C.; Wood, M.; Banas Jr., J. S.; Epstein, M., Importance of Potassium in Cardiovascular Disease. *J. Clin. Hypertens.* **2002,** *4*, 198-206.
5. Palmer, B. F.; Carrero, J. J.; Clegg, D. J.; Colbert, G. B.; Emmett, M.; Fishbane, S.; Hain, D. J.; Lerma, E.; Onuigbo, M.; Rastogi, A.; Roger, S. D.; Spinowitz, B. S.; Weir, M. R., Clinical Management of Hyperkalemia. *Mayo Clin. Proc.* **2021,** *96*, 744-762.
6. Mirsky, I. A., The Etiology of Diabetic Acidosis. *JAMA, J. Am. Med. Assoc.* **1942,** *118*, 690-694.
7. Adrogué, H. J.; Madias, N. E., Hypernatremia. *N. Engl. J. Med.* **2000,** *342*, 1493-1499.
8. Adrogué, H. J.; Madias, N. E., Hyponatremia. *N. Engl. J. Med.* **2000,** *342*, 1581-1589.
9. Owen, J. A.; Campbell, D. G., A comparison of plasma electrolyte and urea values in healthy persons and in hospital patients. *Clin. Chim. Acta* **1968,** *22*, 611-618.
10. Anderson, R. J., Hospital-associated hyponatremia. *Kidney Int.* **1986,** *29*, 1237-1247.
11. Parrilla, M.; Cuartero, M.; Padrell Sánchez, S.; Rajabi, M.; Roxhed, N.; Niklaus, F.; Crespo, G. A., Wearable All-solid-state Potentiometric Microneedle Patch for Intradermal Potassium Detection. *Anal. Chem.* **2019,** *91*, 1578-1586.
12. Parrilla, M.; Ortiz-Gómez, I.; Cánovas, R.; Salinas-Castillo, A.; Cuartero, M.; Crespo, G. A., Wearable Potentiometric Ion Patch for On-body Electrolyte Monitoring in Sweat: Toward a Validation Strategy to Ensure Physiological Relevance. *Anal. Chem.* **2019,** *91*, 8644-8651.
13. Molinero-Fernandez, Á.; Wang, Q.; Xuan, X.; Konradsson-Geuken, Å.; Crespo, G. A.; Cuartero, M., Demonstrating the Analytical Potential of a Wearable Microneedle-Based Device for Intradermal CO_2 Detection. *ACS Sens.* **2024,** *9*, 361–370.
14. Emaminejad, S.; Gao, W.; Wu, E.; Davies, Z. A.; Yin Yin Nyein, H.; Challa, S.; Ryan, S. P.; Fahad, H. M.; Chen, K.; Shahpar, Z.; Talebi, S.; Milla, C.; Javey, A.; Davis, R. W., Autonomous sweat extraction and analysis applied to cystic fibrosis and glucose monitoring using a fully integrated wearable platform. *Proc. Natl. Acad. Sci. U. S. A.* **2017,** *114*, 4625-4630.
15. Wang, S.; Wu, Y.; Gu, Y.; Li, T.; Luo, H.; Li, L.-H.; Bai, Y.; Li, L.; Liu, L.; Cao, Y.; Ding, H.; Zhang, T., Wearable Sweatband Sensor Platform Based on Gold Nanodendrite Array as Efficient Solid Contact of Ion-Selective Electrode. *Anal. Chem.* **2017,** *89*, 10224-10231.

16. He, X.; Yang, S.; Pei, Q.; Song, Y.; Liu, C.; Xu, T.; Zhang, X., Integrated Smart Janus Textile Bands for Self-Pumping Sweat Sampling and Analysis. *ACS Sens.* **2020,** *5*, 1548-1554.
17. Zhang, J.; Rupakula, M.; Bellando, F.; Garcia Cordero, E.; Longo, J.; Wildhaber, F.; Herment, G.; Guérin, H.; Ionescu, A. M., Sweat Biomarker Sensor Incorporating Picowatt, Three-Dimensional Extended Metal Gate Ion Sensitive Field Effect Transistors. *ACS Sens.* **2019,** *4*, 2039-2047.
18. Cao, Q.; Liang, B.; Mao, X.; Wei, J.; Tu, T.; Fang, L.; Ye, X., A Smartwatch Integrated with a Paper-based Microfluidic Patch for Sweat Electrolytes Monitoring. *Electroanalysis* **2021,** *33*, 643-651.
19. Terutsuki, D.; Yamaguchi, S.; Abe, Y.; Abe, H.; Nishizawa, M., Porous Microneedle-Based Potentiometric Sensor for Intradermal Electrolyte Monitoring. *Electrochem.* **2023,** *91*, 047007.
20. Zhu, D. D.; Tan, Y. R.; Zheng, L. W.; Lao, J. Z.; Liu, J. Y.; Yu, J.; Chen, P., Microneedle-coupled Epidermal Sensors for In-situ-multiplexed Ion Detection in Interstitial Fluids. *ACS Appl. Mat. Interfaces* **2023,** *15*, 14146-14154.
21. Miller, P. R.; Xiao, X.; Brener, I.; Burckel, D. B.; Narayan, R.; Polsky, R., Microneedle-based transdermal sensor for on-chip potentiometric determination of K^+. *Adv. Healthcare Mater.* **2014,** *3*, 876-881.
22. Bakker, E.; Bühlmann, P.; Pretsch, E., Carrier-based Ion-selective Electrodes and Bulk Optodes. 1. General Characteristics. *Chem. Rev.* **1997,** *97*, 3083-3132.
23. Harris, D. C., *Exploring Chemical Analysis*. 4th ed.; W. H. Freeman and Company: New York, New York, 2009.
24. Moody, G. J.; Oke, R. B.; Thomas, J. D. R., A calcium-sensitive electrode based on a liquid ion exchanger in a poly(vinyl chloride) matrix. *Analyst* **1970,** *95*, 910-918.
25. Simon, M. A.; Kusy, R. P., Plasticizer-level study of poly(vinyl chloride) ion-selective membranes. *J. Biomed. Mater. Res.* **1996,** *30*, 313-320.
26. Amemiya, S.; Bühlmann, P.; Pretsch, E.; Rusterholz, B.; Umezawa, Y., Cationic or Anionic Sites? Selectivity Optimization of Ion-Selective Electrodes Based on Charged Ionophores. *Anal. Chem.* **2000,** *72*, 1618-1631.
27. Bakker, E.; Pretsch, E.; Buhlmann, P., Selectivity of Potentiometric Ion Sensors. *Anal. Chem.* **2000,** *72*, 1127-1133.
28. Bakker, E.; Buhlmann, P.; Pretsch, E., The phase-boundary potential model. *Talanta* **2004,** *63*, 3-20.
29. Buhlmann, P.; Yajima, S.; Tohda, K.; Umezawa, K.; Nishizawa, S.; Umezawa, Y., Studies on the Phase Boundaries and the Significance of Ionic Sites of Liquid Membrane Ion-Selective Electrodes. *Electroanalysis* **1995,** *7*, 811-816.
30. Simon, W.; Wuhrmann, H.-R.; Vašák, M.; Pioda, L. A. R.; Dohner, R.; Štefanac, Z., Ion-selective Sensors. *Angew. Chem., Int. Ed. Engl.* **1970,** *9*, 445-455.
31. Bühlmann, P.; Chen, L. D., Ion-Selective Electrodes With Ionophore-Doped Sensing Membranes. In *Supramolecular Chemistry: From Molecules to Nanomaterials*, Jonathan W. Steed, P. A. G., Ed. John Wiley & Sons, Ltd: New York, NY, 2012; Vol. 5.

32. Michalska, A., All-Solid-State Ion Selective and All-Solid-State Reference Electrodes. *Electroanalysis* **2012,** *24*, 1253-1265.
33. Komaba, S.; Akatsuka, T.; Ohura, K.; Suzuki, C.; Yabuuchi, N.; Kanazawa, S.; Tsuchiya, K.; Hasegawa, T., All-solid-state ion-selective electrodes with redox-active lithium, sodium, and potassium insertion materials as the inner solid-contact layer. *Analyst* **2017,** *142*, 3857-3866.
34. Ishige, Y.; Klink, S.; Schuhmann, W., Intercalation Compounds as Inner Reference Electrodes for Reproducible and Robust Solid-Contact Ion-Selective Electrodes. *Angew. Chem. Int. Ed.* **2016,** *55*, 4831-4835.
35. Lindfors, T., Light sensitivity and potential stability of electrically conducting polymers commonly used in solid contact ion-selective electrodes. *J. Solid State Electrochem.* **2009,** *13*, 77-89.
36. Vázquez, M.; Bobacka, J.; Ivaska, A.; Lewenstam, A., Influence of oxygen and carbon dioxide on the electrochemical stability of poly(3,4-ethylenedioxythiophene) used as ion-to-electron transducer in all-solid-state ion-selective electrodes. *Sens. Actuators, B* **2002,** *82*, 7-13.
37. Forrest, T.; Bakker, E., In situ derivatisation of solid contact poly(3,4-ethylenedioxythiophene) transducers for ion-selective electrodes through "click" chemistry. *Sens. Actuators, B* **2024,** *405*, 135339.
38. Guzinski, M.; Jarvis, J. M.; D'Orazio, P.; Izadyar, A.; Pendley, B. D.; Lindner, E., Solid-Contact pH Sensor without CO_2 Interference with a Superhydrophobic PEDOT-C_{14} as Solid Contact: The Ultimate "Water Layer" Test. *Anal. Chem.* **2017,** *89*, 8468-8475.
39. Goodenough, J. B.; Park, K. S., The Li-ion rechargeable battery: a perspective. *J. Am. Chem. Soc.* **2013,** *135*, 1167-1176.
40. Crespo, G. A.; Macho, S.; Bobacka, J.; Rius, F. X., Transduction mechanism of carbon nanotubes in solid-contact ion-selective electrodes. *Anal. Chem.* **2009,** *81*, 676-681.
41. Cattrall, R. W.; Freiser, H., Coated wire ion-selective electrodes. *Anal. Chem.* **1971,** *43*, 1905-1906.
42. James, H. J.; Carmack, G.; Freiser, H., Coated wire ion-selective electrodes. *Anal. Chem.* **1972,** *44*, 856-857.
43. Bobacka, J.; Lindfors, T.; Mccarrick, M.; Ivaska, A.; Lewenstam, A., Single Piece All-Solid-State Ion-Selective Electrode. *Anal. Chem.* **1995,** *67*, 3819-3823.
44. Bobacka, J., Potential Stability of All-Solid-State Ion-Selective Electrodes Using Conducting Polymers as Ion-to-Electron Transducers. *Anal. Chem.* **1999,** *71*, 4932-4937.
45. Lai, C. Z.; Fierke, M. A.; Stein, A.; Bühlmann, P., Ion-selective Electrodes with Three-dimensionally Ordered Macroporous Carbon as the Solid Contact. *Anal. Chem.* **2007,** *79*, 4621-4626.
46. Chipangura, Y. E.; Spindler, B. D.; Bühlmann, P.; Stein, A., Design Criteria for Nanostructured Carbon Materials as Solid Contacts for Ion-Selective Sensors. *Adv. Mater.* **2024,** *36*, 2309778.

47. Hu, J.; Zou, X. U.; Stein, A.; Bühlmann, P., Ion-selective Electrodes with Colloid-imprinted Mesoporous Carbon as Solid Contact. *Anal. Chem.* **2014,** *86*, 7111-7118.
48. Moss, S. D.; Janata, J.; Johnson, C. C., Potassium ion-sensitive field effect transistor. *Anal. Chem.* **1975,** *47*, 2238-2243.
49. Bergveld, P., Development, operation, and application of the ion-sensitive field-effect transistor as a tool for electrophysiology. *IEEE Trans. Biomed. Eng.* **1972,** 342-351.
50. Fogt, E. J.; Untereker, D. F.; Norenberg, M. S.; Meyerhoff, M. E., Response of Ion-selective Field Effect Transistors to Carbon Dioxide and Organic Acids. *Anal. Chem.* **1985,** *57*, 1995-1998.
51. Reinhoudt, D. N.; Sudhölter, E. J. R., The transduction of host-guest interactions into electronic signals by molecular systems. *Adv. Mater.* **1990,** *2*, 23-32.
52. Eugster, R.; Rosatzin, T.; Rusterholz, B.; Aebersold, B.; Pedrazza, U.; Ruegg, D.; Schmid, A.; Spichiger, U. E.; Simon, W., Plasticizers for Liquid Polymeric Membranes of Ion-Selective Chemical Sensors. *Anal. Chim. Acta* **1994,** *289*, 1-13.
53. Zou, X. U.; Cheong, J. H.; Taitt, B. J.; Buhlmann, P., Solid contact ion-selective electrodes with a well-controlled Co(II)/Co(III) redox buffer layer. *Anal. Chem.* **2013,** *85*, 9350-9355.
54. Zou, X. U.; Zhen, X. V.; Cheong, J. H.; Buhlmann, P., Calibration-free ionophore-based ion-selective electrodes with a Co(II)/Co(III) redox couple-based solid contact. *Anal. Chem.* **2014,** *86*, 8687-8692.
55. Cosofret, V. V.; Erdösy, M.; Buck, R. P.; Kao, W. J.; Anderson, J. M.; Lindner, E.; Neuman, M. R., Electroanalytical and Biocompatibility Studies on Carboxylated Poly(Vinyl Chloride) Membranes for Microfabricated Array Sensors. *Analyst* **1994,** *119*, 2283-2292.
56. Immergut, E. H.; Mark, H. F., Principles of Plasticization. In *Plasticization and Plasticizer Processes*, Platzer, N. A. J., Ed. American Chemical Society: Washington, D.C., 1965; Vol. 48, pp 1-26.
57. Gourlay, T.; Samartzis, I.; Stefanou, D.; Taylor, K., Inflammatory Response of Rat and Human Neutrophils Exposed to Di-(2-ethyl-hexyl)-phthalate-plasticized Polyvinyl Chloride. *Artif. Organs* **2003,** *27*, 256-260.
58. Dinten, O.; Spichiger, U. E.; Chaniotakis, N.; Gehrig, P.; Rusterholz, B.; Morf, W. E.; Simon, W., Lifetime of Neutral-carrier-based Liquid Membranes in Aqueous Samples and Blood and the Lipophilicity of Membrane Components. *Anal. Chem.* **1991,** *63*, 596-603.
59. Oesch, U.; Dinten, O.; Ammann, D.; Simon, W., Lifetime of Neutral Carrier-Based Membranes in Aqueous Systems and Blood Serum. In *Ion Measurements in Physiology and Medicine*, Kessler, M.; Harrison, D. K.; Höper, J.; Buck, R. P.; Eisenman, G.; Hill, J.; Khuri, R. N.; Lübbers, D. W.; Nicholson, C.; Simon, W.; Treasure, T.; Zeuthen, T., Eds. Springer Berlin Heidelberg: Berlin, Heidelberg, 1985; pp 42-47.
60. Chen, X. V.; Bühlmann, P., Ion-selective Potentiometric Sensors with Silicone Sensing Membranes: A Review. *Curr. Opin. Electrochem.* **2022,** *32*, 100896.

61. Committee on the Safety of Silicone Breast Implants, *Safety of Silicone Breast Implants*. The National Academies Press: Washington, DC, 1999.
62. Steinfink, H.; Post, B.; Fankuchen, I., The crystal structure of octamethyl cyclotetrasiloxane. *Acta Crystallogr.* **1955,** *8*, 420-424.
63. Mikhail, G. V.; Yu, A. Y.; Mileshkevich, V. P., The Siloxane Bond and Its Influence on the Structure and Physical Properties of Organosilicon Compounds. *Russ. Chem. Rev.* **1975,** *44*, 355-372.
64. Rochow, E. G.; LeClair, H. G., On the molecular structure of methyl silicone. *J. Inorg. Nucl. Chem.* **1955,** *1*, 92-111.
65. Warrick, E. L.; Pierce, O. R.; Polmanteer, K. E., Silicone Elastomer Developments 1967–1977. *Rubber Chem. Technol.* **1979,** *52*, 437–525.
66. Dunham, M. L.; Bailey, D. L.; Mixer, R. Y., New Curing System for Silicone Rubber. *Ind. Eng. Chem.* **1957,** *49*, 1373-1376.
67. Modic, F. J. Platinum Catalyst Composition for Hydrosilylation Reactions. US Patent 3 516 946, 1970.
68. Nielsen, J. M. Curing Catalyst System for SiH Additions. US Patent 3 385 876, 1968.
69. Myron, K. Air-drying Organosilicon Compositions Containing a Titanic Acid Ester. US Patent 2 721 855, 1955.
70. Berridge, C.; Cohoes, N. Y. Room temperature curing organo-polysiloxane. US Patent 2 843 555, 1958.
71. Klosowski, J. M.; Gant, G. A. L., The Chemistry of Silicone Room Temperature Vulcanizing Sealants. In *Plastic Mortars, Sealants, and Caulking Compounds*, Seymour, R. B., Ed. American Chemical Society: Washington, D.C., 1979; Vol. 113, pp 113-127.
72. van Der Weij, F. W., The action of tin compounds in condensation-type RTV silicone rubbers. *Makromol. Chem.* **1980,** *181*, 2541-2548.
73. Weyenberg, D. R. Method of Making One Component Room Temperature Curing Siloxone Rubbers. US Patent 3 294 739, 1966.
74. De Buyl, F.; Comyn, J.; Shephard, N. E.; Subramaniam, N. P., Kinetics of cure, cross link density and adhesion of water-reactive alkoxysilicone sealants. *J. Adhes. Sci. Technol.* **2002,** *16*, 1055-1071.
75. Polmanteer, K. E., Current Perspectives on Silicone Rubber Technology. *Rubber Chem. Technol.* **1981,** *54*, 1051–1080.
76. Hair, M. L.; Hertl, W., Reaction of hexamethyldisilazane with silica. *J. Phys. Chem.* **1971,** *75*, 2181-2185.
77. Kimura, K.; Matsuba, T.; Tsujimura, Y.; Yokoyama, M., Unsymmetrical Calix[4]Arene Ionophore Silicone-Rubber Composite Membranes for High-Performance Sodium Ion-Sensitive Field-Effect Transistors. *Anal. Chem.* **1992,** *64*, 2508-2511.
78. van der Wal, P. D.; Skowronska-Ptasinska, M.; van den Berg, A.; Bergveld, P.; Sudhölter, E. J. R.; Reinhoudt, D. N., New Membrane Materials for Potassium-selective Ion-sensitive Field-effect Transistors. *Anal. Chim. Acta* **1990,** *231*, 41-52.

79. Crowe, W.; Mayevsky, A.; Mela, L., Application of a solid membrane ion-selective electrode to in vivo measurements. *Am. J. Physiol.* **1977,** *233*, C56-60.
80. DowSil 3140 RTV Coating. SDS. The Dow Chemical Company, 2211 H.H. Dow Way, Midland, MI, USA. April 10, 2023.
81. Spichiger, U. E.; Aiping, X.; Citterio, D.; Bühler, H.; Chaniotakis, N.; Rusterholz, B.; Simon, W., From molecular recognition to analytical information using chemical sensors: Development of a combined catheter gastric pH-probe. *Electroanalysis* **1995,** *7*, 859-863.
82. Pick, J.; Tóth, K.; Pungor, E.; Vasák, M.; Simson, W., A Potassium-selective Silicone-rubber Membrane Electrode Based on a Neutral Carrier. *Anal. Chim. Acta* **1973,** *64*, 477-480.
83. KE-44-T. SDS: 1921S0; rev. 3; Shin-Etsu Chemical Co., Ltd; 13-1 Isobe 2-chome, Annaka-shi, Gunma, Japan. November, 11, 2022.
84. DowSIL 730 FS Solvent Resistant Sealant. SDS. The Dow Chemical Company, 2211 H.H. Dow Way, Midland, MI, USA. May 24, 2024.
85. van der Wal, P. D.; Sudhölter, E. J. R.; Boukamp, B. A.; Bouwmeester, H. J. M.; Reinhoudt, D. N., Impedance Spectroscopy and Surface Study of Potassium-selective Silicone Rubber Membranes. *J. Electroanal. Chem. Interfacial Electrochem.* **1991,** *317*, 153-168.
86. van der Wal, P. D.; Sudhölter, E. J. R.; Reinhoudt, D. N., Design and Properties of a Flow-injection Analysis Cell Using Potassium-selective Ion-sensitive Field-effect Transistors as Detection Elements. *Anal. Chim. Acta* **1991,** *245*, 159-166.
87. Brunink, J. A. J.; Lugtenberg, R. J. W.; Brzøzka, Z.; Engbersen, J. F. J.; Reinhoudt, D. N., The Design of Durable Na^+-selective CHEMFETs Based on Polysiloxane Membranes. *J. Electroanal. Chem.* **1994,** *378*, 185-200.
88. Gankema, H.; Lugtenberg, R. J. W.; Engbersen, J. F. J.; Reinhoudt, D. N.; Möller, M., Crosslinkable polar siloxane copolymers for ion detection devices. *Adv. Mater.* **1994,** *6*, 944-947.
89. Reinhoudt, D. N.; Engbersen, J. F. J.; Brzozka, Z.; van der Vlekkert, H. H.; Honig, G. W. N.; Holterman, H. A. J.; Verkerk, U. H., Development of Durable K^+-Selective Chemically Modified Field Effect Transistors with Functionalized Polysiloxane Membranes. *Anal. Chem.* **1994,** *66*, 3618-3623.
90. Antonisse, M. M. G.; Lugtenberg, R. J. W.; Egberink, R. J. M.; Engbersen, J. F. J.; Reinhoudt, D. N., Durable nitrate-selective chemically modified field effect transistors based on new polysiloxane membranes. *Anal. Chim. Acta* **1996,** *332*, 123-129.
91. Lugtenberg, R. J. W.; Egberink, R. J. M.; van den Berg, A.; Engbersen, J. F. J.; Reinhoudt, D. N., The effects of covalent binding of the electroactive components in durable CHEMFET membranes—impedance spectroscopy and ion sensitivity studies. *J. Electroanal. Chem.* **1998,** *452*, 69-86.
92. Dumschat, C.; Alazard, S.; Adam, S.; Knoll, M.; Cammann, K., Filled fluorosilicone as matrix material for ion-selective membranes. *Analyst* **1996,** *121*, 527-529.

93. Högg, G.; Lutze, O.; Cammann, K., Novel Membrane Material for Ion-selective Field-effect Transistors with Extended Lifetime and Improved Selectivity. *Anal. Chim. Acta* **1996,** *335*, 103-109.
94. Poplawski, M. E.; B. Brown, R.; Lae Rho, K.; Yong Yun, S.; Jung Lee, H.; Sig Cha, G.; Paeng, K.-J., One-component Room Temperature Vulcanizing-type Silicone Rubber-based Sodium-selective Membrane Electrodes. *Anal. Chim. Acta* **1997,** *355*, 249-257.
95. Cao, A.; Mescher, M.; Bosma, D.; Klootwijk, J. H.; Sudhölter, E. J. R.; Smet, L. C. P. M. d., Ionophore-Containing Siloprene Membranes: Direct Comparison between Conventional Ion-Selective Electrodes and Silicon Nanowire-Based Field-Effect Transistors. *Anal. Chem.* **2015,** *87*, 1173-1179.
96. Ito, K.; Satake, H.; Mori, Y.; Tseng, A. C.; Sakata, T., Biocompatible and Na^+-sensitive thin-film transistor for biological fluid sensing. *Sci. Technol. Adv. Mater.* **2019,** *20*, 917-926.
97. Malinowska, E.; Oklejas, V.; Hower, R. W.; Brown, R. B.; Meyerhoff, M. E., Enhanced electrochemical performance of solid-state ion sensors based on silicone rubber membranes. *Sens. Actuators, B* **1996,** *33*, 161-167.
98. Oh, H. J.; Cha, G. S.; Nam, H., Effect of Surfactants on the Electrochemical Performance of Cation-Selective Membrane Electrodes. *Bull. Korean Chem. Soc.* **2003,** *24*, 37–44.
99. Tsujimura, Y.; Yokoyama, M.; Kimura, K., Oligosiloxane-modified Calix[4]Arene Ionophores for Silicone-rubber-membrane Sodium Ion-Sensitive Field-Effect Transistors. *Electroanalysis* **1993,** *5*, 803-807.
100. Liang, T.; Jiang, N.; Zhou, S.; Wang, X.; Xu, Y.; Wu, C.; Kirsanov, D.; Legin, A.; Wan, H.; Wang, P., Multiplexed all-solid-state ion-sensitive light-addressable potentiometric sensor (ISLAPS) system based on silicone-rubber for physiological ions detection. *Anal. Chim. Acta* **2021,** *1179*, 338603.
101. Cazalé, A.; Sant, W.; Launay, J.; Ginot, F.; Temple-Boyer, P., Study of Field Effect Transistors for the Sodium Ion Detection using Fluoropolysiloxane-based Sensitive Layers. *Sens. Actuators, B* **2013,** *177*, 515-521.
102. Tsujimura, Y.; Yokoyama, M.; Kimura, K., Comparison between Silicone-rubber Membranes and Plasticized Poly(Vinyl Chloride) Membranes Containing Calix[4]Arene Ionophores for Sodium Ion-sensitive Field-effect Transistors in Applicability to Sodium Assay in Human-body Fluids. *Sens. Actuators, B* **1994,** *22*, 195-199.
103. Tsujimura, Y.; Yokoyama, M.; Kimura, K., Practical Applicability of Silicone Rubber Membrane Sodium-Selective Electrode Based on Oligosiloxane-Modified Calix[4]arene Neutral Carrier. *Anal. Chem.* **1995,** *67*, 2401-2404.
104. Kimura, K.; Tsujimura, Y.; Yokoyama, M.; Maeda, T., Calix[4]arene-Modified Oligosiloxane as a Quasi-Immobilized Neutral Carrier for Silicone-Rubber-Membrane Sodium Ion-Selective Electrodes. *Bull. Chem. Soc. Jpn.* **1998,** *71*, 657-660.

105. Tsujimura, Y.; Sunagawa, T.; Yokoyama, M.; Kimura, K., Sodium Ion-selective Electrodes Based on Silicone-Rubber Membranes Covalently Incorporating Neutral Carriers. *Analyst* **1996,** *121*, 1705-1709.
106. Sudhölter, E. J. R.; van der Wal, P. D.; Skowronska-Ptasinska, M.; van den Berg, A.; Bergveld, P.; Reinhoudt, D. N., Modification of ISFETs by Covalent Anchoring of Poly(Hyroxyethyl Methacrylate) Hydrogel. Introduction of a Thermodynamically Defined Semiconductor-sensing Membrane Interface. *Anal. Chim. Acta* **1990,** *230*, 59-65.
107. Yoon, I. J.; Lee, D. K.; Nam, H.; Cha, G. S.; Strong, T. D.; Brown, R. B., Ion Sensors using One-component Room Temperature Vulcanized Silicone Rubber Matrices. *J. Electroanal. Chem.* **1999,** *464*, 135-142.
108. Park, E. R.; Chung, Y. J.; Hwang, S. W.; Heo, M.; Chae, Y. J.; Kim, H. S.; Lee, S. W.; Shin, J. H.; Kim, I. T.; Kwan, G.-C.; Lee, S. H., All-solid-state ion-selective silicone rubber membrane electrodes with a new conducting polymer. *J. Korean Phys. Soc.* **2012,** *60*, 925-928.
109. Lindner, E.; Niegreisz, Z.; Toth, K.; Pungor, E.; Berube, T. R.; Buck, R. P., Electrical and dynamic properties of non-plasticized potassium selective membranes. *J. Electroanal. Chem. Interfacial Electrochem.* **1989,** *259*, 67-80.
110. Uhlig, A.; Lindner, E.; Teutloff, C.; Schnakenberg, U.; Hintsche, R., Miniaturized Ion-selective Chip Electrode for Sensor Application. *Anal. Chem.* **1997,** *69*, 4032-4038.
111. van der Wal, P. D.; van den Berg, A.; de Rooij, N. F., Universal approach for the fabrication of Ca^{2+}-, K^{+}- and NO_3^{-}-sensitive membrane ISFETs. *Sens. Actuators, B* **1994,** *18*, 200-207.
112. Cha, G. S.; Liu, D.; Meyerhoff, M. E.; Cantor, H. C.; Midgley, A. R.; Goldberg, H. D.; Brown, R. B., Electrochemical Performance, Biocompatibility, and Adhesion of New Polymer Matrices for Solid-state Ion Sensors. *Anal. Chem.* **1991,** *63*, 1666-1672.
113. Bakker, E., Determination of Improved Selectivity Coefficients of Polymer Membrane Ion-selective Electrodes by Conditioning with a Discriminated Ion. *J. Electrochem. Soc.* **1996,** *143*, L83-L85.
114. Bakker, E., Determination of Unbiased Selectivity Coefficients of Neutral Carrier-Based Cation-Selective Electrodes. *Anal. Chem.* **1997,** *69*, 1061-1069.
115. Lindfors, T.; Szűcs, J.; Sundfors, F.; Gyurcsanyi, R. E., Polyaniline Nanoparticle-based Solid-contact Silicone Rubber Ion-selective Electrodes for Ultratrace Measurements. *Anal. Chem.* **2010,** *82*, 9425-9432.
116. Lindfors, T.; Höfler, L.; Jágerszki, G.; Gyurcsányi, R. E., Hyphenated FT-IR-Attenuated Total Reflection and Electrochemical Impedance Spectroscopy Technique to Study the Water Uptake and Potential Stability of Polymeric Solid-contact Ion-selective Electrodes. *Anal. Chem.* **2011,** *83*, 4902-4908.
117. Boeva, Z. A.; Lindfors, T., Few-layer Graphene and Polyaniline Composite as Ion-to-electron Transducer in Silicone Rubber Solid-contact Ion-selective Electrodes. *Sens. Actuators, B* **2016,** *224*, 624-631.

118. Marrazza, G.; Mascini, M., Silicone-based calcium-selective electrode. *Electroanalysis* **1992,** *4*, 41-43.
119. Spichiger, U. E.; Eugster, R.; Schaller, U.; Haase, E.; Simon, W., Magnesium-selective Electrodes: State of the Art. *Magnesium-Bull.* **1991,** *13*, 140–144.
120. Knoll, M.; Cammann, K.; Dumschat, C.; Sundermeier, C.; Eshold, J., Potentiometric Silicon Microsensor for Nitrate and Ammonium. *Sens. Actuators, B* **1994,** *18*, 51-55.
121. Bühlmann, P.; Pretsch, E.; Bakker, E., Carrier-based Ion-selective Electrodes and Bulk Optodes. 2. Ionophores for Potentiometric and Optical Sensors. *Chem. Rev.* **1998,** *98*, 1593-1688.
122. Lugtenberg, R. J. W.; Brzozka, Z.; Casnati, A.; Ungaro, R.; Engbersen, J. F. J.; Reinhoudt, D. N., Cesium-selective chemically modified field effect transistors with calix[4]arene-crown-6 derivatives. *Anal. Chim. Acta* **1995,** *310*, 263-267.
123. Lugtenberg, R. J. W.; Antonisse, M. M. G.; Egberink, R. J. M.; Engbersen, J. F. J.; Reinhoudt, D. N., Polysiloxane based CHEMFETs for the detection of heavy metal ions. *J. Chem. Soc., Perkin Trans. 2* **1996,** 1937-1941.
124. Shin, J. H.; Sakong, D. S.; Nam, H.; Cha, G. S., Enhanced Serum Carbon Dioxide Measurements with a Silicone Rubber-Based Carbonate Ion-Selective Electrode and a High-pH Dilution Buffer. *Anal. Chem.* **1996,** *68*, 221-225.
125. Mascini, M.; Marrazza, G., Improved Potentiometric Determination of Potassium in Whole-Blood and Serum with a Valinomycin-Treated Silicone-Rubber Tubular Electrode. *Anal. Chim. Acta* **1990,** *231*, 125-128.
126. Collison, M.; Aebli, G.; Petty, J.; Meyerhoff, M. E., Potentiometric combination ion-carbon dioxide sensors for in vitro and in vivo blood measurements. *Anal. Chem.* **1989,** *61*, 2365-2372.
127. Meruva, R. K.; Meyerhoff, M. E., Catheter-type Sensor for Potentiometric Monitoring of Oxygen, pH and Carbon Dioxide. *Biosens. Bioelectron.* **1998,** *13*, 201-212.
128. Lewenstam, A., Routines and Challenges in Clinical Application of Electrochemical Ion-sensors. *Electroanalysis* **2014,** *26*, 1171-1181.
129. Crespo, G. A., Recent Advances in Ion-selective Membrane Electrodes for In Situ Environmental Water Analysis. *Electrochim. Acta* **2017,** *245*, 1023-1034.
130. Bakker, E., Enhancing Ion-selective Polymeric Membrane Electrodes by Instrumental Control. *TrAc, Trends Anal. Chem.* **2014,** *53*, 98-105.
131. Michalska, A., Optimizing the Analytical Performance and Construction of Ion-selective Electrodes with Conducting Polymer-based Ion-to-electron Transducers. *Anal. Bioanal. Chem.* **2006,** *384*, 391-406.
132. Gao, W.; Emaminejad, S.; Nyein, H. Y.; Challa, S.; Chen, K.; Peck, A.; Fahad, H. M.; Ota, H.; Shiraki, H.; Kiriya, D.; Lien, D. H.; Brooks, G. A.; Davis, R. W.; Javey, A., Fully Integrated Wearable Sensor Arrays for Multiplexed in Situ Perspiration Analysis. *Nature* **2016,** *529*, 509-514.
133. Roy, S.; David-Pur, M.; Hanein, Y., Carbon Nanotube-based Ion Selective Sensors for Wearable Applications. *ACS Appl. Mater. Interfaces* **2017,** *9*, 35169-35177.

134. Parrilla, M.; Cuartero, M.; Crespo, G. A., Wearable Potentiometric Ion Sensors. *TrAC, Trends Anal. Chem.* **2019,** *110*, 303-320.
135. Bandodkar, A. J.; Hung, V. W.; Jia, W.; Valdes-Ramirez, G.; Windmiller, J. R.; Martinez, A. G.; Ramirez, J.; Chan, G.; Kerman, K.; Wang, J., Tattoo-based Potentiometric Ion-selective Sensors for Epidermal pH Monitoring. *Analyst* **2013,** *138*, 123-128.
136. Anderson, E. L.; Chopade, S. A.; Spindler, B. D.; Stein, A.; Lodge, T. P.; Hillmyer, M. A.; Bühlmann, P., Solid-contact Ion-selective and Reference Electrodes Covalently Attached to Functionalized Poly(Ethylene Terephthalate). *Anal. Chem.* **2020,** *92*, 7621-7629.
137. Heng, L. Y.; Hall, E. A. H., Methacrylic-acrylic Polymers in Ion-selective Membranes: Achieving the Right Polymer Recipe. *Anal. Chim. Acta* **2000,** *403*, 77-89.
138. Curtis, J.; Colas, A., Chapter II.5.18 - Medical Applications of Silicones. In *Biomaterials Science (Third Edition)*, Ratner, B. D.; Hoffman, A. S.; Schoen, F. J.; Lemons, J. E., Eds. Academic Press: 2013; pp 1106-1116.
139. Szűcs, J.; Lindfors, T.; Bobacka, J.; Gyurcsányi, R. E., Ion-selective Electrodes with 3D Nanostructured Conducting Polymer Solid Contact. *Electroanalysis* **2016,** *28*, 778-786.
140. Shin, J. H.; Lee, H. J.; Kim, C. Y.; Oh, B. K.; Rho, K. L.; Nam, H.; Cha, G. S., ISFET-based Differential pCO2 Sensors Employing a Low-resistance Gas-permeable Membrane. *Anal. Chem.* **1996,** *68*, 3166-3172.
141. Oh, B. K.; Kim, C. Y.; Lee, H. J.; Rho, K. L.; Cha, G. S.; Nam, H., One-component Room Temperature Vulcanizing-type Silicone Rubber-based Calcium-selective Electrodes. *Anal. Chem.* **1996,** *68*, 503-508.
142. Scheipers, A.; Waßmus, O.; Sundermeier, C.; Eshold, J.; Weiß, T.; Gitter, M.; Roß, B.; Knoll, M., Potentiometric Ion-selective Silicon Sensors for the On-line Monitoring of Blood Electrolytes. *Anal. Chim. Acta* **2001,** *439*, 29-38.
143. Yajima, S.; Kishi, M.; Kimura, K., Development of Ion Sensors Based on Polysilsesquioxane Modified Chemically with Crown Ether Derivatives in View of In Vivo Analyses. *Bunseki Kagaku* **2017,** *66*, 431-436.
144. Meier, P. C., Two-parameter Debye-Hückel Approximation for the Evaluation of Mean Activity Coefficients of 109 electrolytes. *Anal. Chim. Acta* **1982,** *136*, 363-368.
145. Morf, W. E., *The Principles of Ion-Selective Electrodes and of Membrane Transport*. Elsevier: New York, NY, 1981.
146. Umezawa, Y.; Bühlmann, P.; Umezawa, K.; Tohda, K.; Amemiya, S., Potentiometric Selectivity Coefficients of Ion-selective Electrodes: Part I. Inorganic Cations. *Pure Appl. Chem.* **2000,** *72*, 1851–2082.
147. Oesch, U.; Simon, W., Lifetime of Neutral Carrier Based Ion-selective Liquid-membrane Electrodes. *Anal. Chem.* **1980,** *52*, 692-700.
148. Galster, H., *pH Measurement: Fundamentals, Methods, Applications, Instrumentations*. VCH Publishers: New York, 1991.

149. Thomas, D. R., *Cross-linking of Polydimethylsiloxanes*. PTR Prentice Hall: Englewood Cliffs, NJ, 1993.
150. Mincheva, R.; Beigbeder, A.; Pettitt, M. E.; Callow, M. E.; Callow, J. A.; Dubois, P., Metal-free Anti-biofouling Coatings: the Preparation of Silicone-based Nanostructured Coatings via Purely Organic Catalysis. *Nanocomposites* **2016,** *2*, 51-57.
151. Rajendra, V.; Gonzaga, F.; Brook, M. A., Nearly Monodisperse Silica Microparticles Form in Silicone (Pre)elastomer Mixtures. *Langmuir* **2012,** *28*, 1470-1477.
152. Mark, J. E.; Jiang, C. Y.; Tang, M. Y., Simultaneous Curing and Filling of Elastomers. *Macromolecules* **1984,** *17*, 2613-2616.
153. Paul, D. R.; Mark, J. E., Fillers for Polysiloxane ("Silicone") Elastomers. *Prog. Polym. Sci.* **2010,** *35*, 893-901.
154. Cataldo, F., Synthesis of Ketonic Resins from Self-polymerization of Acetone, 1. Action of Protic and Lewis Acids on Acetone. *Angew. Makromol. Chem.* **1996,** *236*, 1-19.
155. Rousseau, C. R.; Bühlmann, P., Calibration-free Potentiometric Sensing with Solid-contact Ion-selective Electrodes. *TrAC, Trends Anal. Chem.* **2021,** *140*, 116277.
156. Covington, A. K.; Robinson, R. A., References Standards for the Electrometric Determination, with Ion-selective Electrodes, of Potassium and Calcium in blood serum. *Anal. Chim. Acta* **1975,** *78*, 219-223.
157. Carlson, G. P.; Bruss, M., Chapter 17 - Fluid, Electrolyte, and Acid-base Balance. In *Clinical Biochemistry of Domestic Animals (Sixth Edition)*, Kaneko, J. J.; Harvey, J. W.; Bruss, M. L., Eds. Academic Press: San Diego, 2008; pp 529-559.
158. Bühlmann, P.; Hayakawa, M.; Ohshiro, T.; Amemiya, S.; Umezawa, Y., Influence of Natural, Electrically Neutral Lipids on the Potentiometric Responses of Cation-selective Polymeric Membrane Electrodes. *Anal. Chem.* **2001,** *73*, 3199-3205.
159. Lippincott, E. R.; Valkenburg, A. V.; Weir, C. E.; Bunting, E. N., Infrared Studies on Polymorphos of Silicon Dioxide and Germanium Dioxide. *J. Research Nat. Bur. Standards* **1958,** *61*, 61-70.
160. Min, J.; Tu, J.; Xu, C.; Lukas, H.; Shin, S.; Yang, Y.; Solomon, S. A.; Mukasa, D.; Gao, W., Skin-Interfaced Wearable Sweat Sensors for Precision Medicine. *Chem. Rev.* **2023,** *123*, 5049-5138.
161. Cuartero, M.; Bishop, J.; Walker, R.; Acres, R. G.; Bakker, E.; De Marco, R.; Crespo, G. A., Evidence of double layer/capacitive charging in carbon nanomaterial-based solid contact polymeric ion-selective electrodes. *Chem. Commun.* **2016,** *52*, 9703-9706.
162. Crespo, G. A.; Macho, S.; Rius, F. X., Ion-selective electrodes using carbon nanotubes as ion-to-electron transducers. *Anal. Chem.* **2008,** *80*, 1316-1322.
163. Parra, E. J.; Crespo, G. A.; Riu, J.; Ruiz, A.; Rius, F. X., Ion-selective electrodes using multi-walled carbon nanotubes as ion-to-electron transducers for the detection of perchlorate. *Analyst* **2009,** *134*, 1905-1910.

164. Ping, J. F.; Wang, Y. X.; Wu, J.; Ying, Y. B., Development of an all-solid-state potassium ion-selective electrode using graphene as the solid-contact transducer. *Electrochem. Commun.* **2011,** *13*, 1529-1532.
165. Ping, J.; Wang, Y.; Ying, Y.; Wu, J., Application of electrochemically reduced graphene oxide on screen-printed ion-selective electrode. *Anal. Chem.* **2012,** *84*, 3473-3479.
166. Paczosa-Bator, B., All-solid-state selective electrodes using carbon black. *Talanta* **2012,** *93*, 424-427.
167. Spindler, B. D.; Graf, K. I.; Dong, X. I. N.; Kim, M.; Chen, X. V.; Bühlmann, P.; Stein, A., Influence of the Composition of Plasticizer-Free Silicone-Based Ion-Selective Membranes on Signal Stability in Aqueous and Blood Plasma Samples. *Anal. Chem.* **2023,** *95*, 12419-12426.
168. Lowell, S.; Shields, J. E.; Thomas, M. A.; Thommes, M., *Characterization of Porous Solids and Powders: Surface Area, Pore Size, and Density*. Kluwer Academic Publishers: AA Dordrecht, The Netherlands, 2004.
169. Liao, K.-H.; Mittal, A.; Bose, S.; Leighton, C.; Mkhoyan, K. A.; Macosko, C. W., Aqueous Only Route toward Graphene from Graphite Oxide. *ACS Nano* **2011,** *5*, 1253-1258.
170. Soltani, T.; Kyu Lee, B., A benign ultrasonic route to reduced graphene oxide from pristine graphite. *J. Colloid Interface Sci.* **2017,** *486*, 337-343.
171. Nyein, H. Y. Y.; Gao, W.; Shahpar, Z.; Emaminejad, S.; Challa, S.; Chen, K.; Fahad, H. M.; Tai, L.-C.; Ota, H.; Davis, R. W.; Javey, A., A Wearable Electrochemical Platform for Noninvasive Simultaneous Monitoring of Ca^{2+} and pH. *ACS Nano* **2016,** *10*, 7216-7224.
172. Zhao, F.; Liu, Y.; Dong, H.; Feng, S.; Shi, G.; Lin, L.; Tian, Y., An electrochemophysiological microarray for real-time monitoring and quantification of multiple ions in the brain of a freely moving rat. *Angew. Chem.* **2020,** *132*, 10512-10516.
173. Hu, J. B.; Stein, A.; Buhlmann, P., Rational Design of All-solid-state Ion-selective Electrodes and Reference Electrodes. *TrAC, Trends Anal. Chem.* **2016,** *76*, 102-114.
174. Shao, Y.; Ying, Y.; Ping, J., Recent Advances in Solid-contact Ion-selective Electrodes: Functional Materials, Transduction Mechanisms, and Development Trends. *Chem. Soc. Rev.* **2020,** *49*, 4405-4465.
175. Chipangura, Y. E.; Spindler, B. D.; Bühlmann, P.; Stein, A., Design Criteria for Nanostructured Carbon Materials as Solid Contacts for Ion-Selective Sensors. *Adv. Mater.* **2023,** 2309778.
176. Lindner, E.; Cosofret, V. V.; Ufer, S.; Buck, R. P.; Kao, W. J.; Neuman, M. R.; Anderson, J. M., Ion-selective Membranes with Low Plasticizer Content: Electroanalytical Characterization and Biocompatibility Studies. *J. Biomed. Mater. Res.* **1994,** *28*, 591-601.
177. Lindner, E.; Cosofret, V. V.; Buck, R. P.; Johnson, T. A.; Ash, R. B.; Neuman, M. R.; Kao, W. J.; Anderson, J. M., Electroanalytical and Biocompatibility Studies on Microfabricated Array Sensors. *Electroanalysis* **1995,** *7*, 864-870.

178. Buhlmann, P.; Umezawa, Y.; Rondinini, S.; Vertova, A.; Pigliucci, A.; Bertesago, L., Lifetime of Ion-selective Electrodes Based on Charged Ionophores. *Anal. Chem.* **2000,** *72*, 1843-1852.
179. Bakker, E.; Pretsch, E., Lipophilicity of Tetraphenylborate Derivatives as Anionic Sites in Neutral Carrier-based Solvent Polymeric Membranes and Lifetime of Corresponding Ion-selective Electrochemical and Optical Sensors. *Anal. Chim. Acta* **1995,** *309*, 7-17.
180. Yun, S. Y.; Hong, Y. K.; Oh, B. K.; Cha, G. S.; Nam, H.; Lee, S. B.; Jin, J. I., Potentiometric Properties of Ion-selective Electrode Membranes Based on Segmented Polyether Urethane Matrices. *Anal. Chem.* **1997,** *69*, 868-873.
181. Ross, P.; Johnston, A. J.; Judd, A. K. Immobilized Valinomycin Molecule for K^+ Sensor. US Patent 4 973 394, 1990.
182. Raguse, B.; Pace, R. J.; King, L. G.; Braach-Makavytie, V. L.; Cornell, B. Method of Producing a First Layer Electrode Membrane for a Biosensor. US Patent 5 879 878, 1999.
183. Bereczki, R.; Gyurcsányi, R. E.; Ágai, B.; Tóth, K., Synthesis and Characterization of Covalently Immobilized Bis-crown Ether Based Potassium Ionophore. *Analyst* **2005,** *130*, 63-70.
184. Malinowska, E.; Gawart, L.; Parzuchowski, P.; Rokicki, G.; Brzózka, Z., Novel Approach of Immobilization of Calix[4]arene Type Ionophore in 'Self-plasticized' Polymeric Membrane. *Anal. Chim. Acta* **2000,** *421*, 93-101.
185. Qin, Y.; Peper, S.; Radu, A.; Ceresa, A.; Bakker, E., Plasticizer-Free Polymer Containing a Covalently Immobilized Ca^{2+}-Selective Ionophore for Potentiometric and Optical Sensors. *Anal. Chem.* **2003,** *75*, 3038-3045.
186. Choi, K. R.; Chen, X. V.; Hu, J.; Bühlmann, P., Solid-Contact pH Sensor with Covalent Attachment of Ionophores and Ionic Sites to a Poly(decyl methacrylate) Matrix. *Anal. Chem.* **2021,** *93*, 16899-16905.
187. Kimura, K.; Sunagawa, T.; Yajima, S.; Miyake, S.; Yokoyama, M., Neutral Carrier-Type Ion Sensors Based on Sol−Gel-Derived Membranes Incorporating a Bis(crown ether) Derivative by Covalent Bonding. *Anal. Chem.* **1998,** *70*, 4309-4313.
188. Kimura, K.; Sunagawa, T.; Yokoyama, M., Chemical Modification of Sol-gel-derived Glass by a Neutral Carrier for Ion Sensors. *Chem. Commun.* **1996,** 745-746.
189. Töke, L.; Bitter, I.; Ágai, B.; Csongor, É.; Tóth, K.; Lindner, E.; Horváth, M.; Harfouch, S.; Pungor, E., Benzocrown Derivatives as Ionophores for Alkali Cations, I Synthesis of Urethane- and Urea-linked Mono- and Bis-crown Ethers. *Liebigs Ann. Chem.* **1988,** *1988*, 349-353.
190. Ammann, D.; Pretsch, E.; Simon, W.; Lindner, E.; Bezegh, A.; Pungor, E., Lipophilic Salts as Membrane Additives and their Influence on the Properties of Macro- and Micro-electrodes Based on Neutral Carriers. *Anal. Chim. Acta* **1985,** *171*, 119-129.

191. Chen, X., V. Development of Electrochemical Sensors for Analytical and Biomedical Applications. Ph.D. Dissertation, University of Minnesota, Minneapolis, MN, 2019.
192. Marciniec, B., The Effect of Substituents at Silicon on the Reactivity of the Si-H Bond in Hydrosilylation. In *Comprehensive Handbook on Hydrosilylation*, Elsevier Science: 2014; pp 160-177.
193. Brown, P.; Saginaw; Hyde, J. Polyfunctional Alkoxy Endlbocked Polysiloxanes and their Cured Compositions. U.S. Patent 3161614, December 15, 1964.
194. Laboratory Requirements. In *Section 493.931, Title 42*, US Code of Federal Regulations, 2022.
195. Dong, X. I. N.; Spindler, B. D.; Kim, M.; Stein, A.; Bühlmann, P., Spontaneous Mesoporosity-Driven Sequestration of Ionic Liquids from Silicone-Based Reference Electrode Membranes. *ACS Sens.* **2023,** *8*, 1774-1781.
196. Lindner, E.; Tóth, K.; Jeney, J.; Horváth, M.; Pungor, E.; Bitter, I.; Ágai, B.; Töke, L., Novel Bis (crown ether)-based Potassium Sensor for Biological Applications. *Microchim. Acta* **1990,** *100*, 157-168.
197. Lindner, E.; Tóth, K.; Horváth, M.; Pungor, E.; Ágai, B.; Bitter, I.; Tőke, L.; Hell, Z., Bis-crown Ether Derivatives as Ionophores for Potassium Selective Electrodes. *Fresenius' Z. Anal. Chem.* **1985,** *322*, 157-163.
198. Clarson, S.; Mark, J., Reinforcement of non-crystallizable elastomer by the precipitation in situ of silica. *Polym. Commun.* **1987,** *28*, 249-252.
199. Jurásková, A.; Møller Olsen, S.; Dam-Johansen, K.; Brook, M. A.; Skov, A. L., Reliable Condensation Curing Silicone Elastomers with Tailorable Properties. *Molecules* **2021,** *26*, 82.
200. Stein, J.; Prutzman, L. C., Stress relaxation studies of model silicone RTV networks. *J. of Appl. Polym. Sci.* **1988,** *36*, 511-521.
201. Goudie, J. L.; Owen, M. J.; Orbeck, T. In *A review of possible degradation mechanisms of silicone elastomers in high voltage insulation applications*, 1998 Annual Report Conference on Electrical Insulation and Dielectric Phenomena, 25-28 Oct. 1998; 1998; pp 120-127.

Appendix

Appendix for Chapter 2: SC-ISE history

SC-ISEs prepared in **Batch 1** and **Batch 2** were used for different sets of experiments. SC-ISEs from **Batch 1** had a longer use history than those from **Batch 2**. SC-ISEs from **Batch 1** were conditioned in 1 mM KCl at 25 °C for 23 h. Then a K^+ calibration curve was measured (Figure 2.3 and Figure 2.4), followed by measurement of selectivity (FIM) and resistance measurement (known shunt method). The ISEs were placed back in a 1 mM KCl solution and conditioned at 37 °C for an additional 18 days. The potentials measured from days 12–18 are shown in Figure 2.8. The electrodes were cooled to 25 °C and a K^+ calibration curve, selectivity (FIM), and resistance were measured. A water layer test was conducted by placing the ISEs in a 0.1 M KCl solution at 25 °C for 2 h. The solution was then changed to a 0.1 M NaCl solution for 2 h, and then back to a 0.1 M KCl solution for 22 h. Then, ISE drift was measured in a 1 mM KCl/4 nM sodium ferrocyanide solution at 37 °C for 20 h. After the stability experiment, the ISE response and selectivity curves were measured at 25 °C. ISEs were used to measure the K^+ activity and concentration in bovine whole blood (an unknown amount of NaCl was added to the blood to prevent coagulation) using the same procedure as outlined for porcine plasma in section 2.2.8. The electrodes were stored in a 1 mM KCl solution at room temperature overnight. The long-term drift in bovine whole blood was measured at 37 °C for 19 h. The electrodes were rinsed with water. Then, a K^+ calibration curve, selectivity, and resistance were measured for the electrodes at 25 °C. The electrodes were stored in a 1 mM KCl solution at room temperature for 54 days. The measurement of K^+ activity and concentration in porcine plasma described in

section 2.2.8 was conducted. On the following day, measurements of K^+ activity and concentration were conducted in porcine whole blood. The electrodes were stored in 1 mM KCl for 7 days. The liquid junction potential at the reference electrode double junction/sample interface was measured as described in section 2.2.9 for both the porcine plasma and porcine whole blood samples. The ISEs were stored in 1 mM KCl solution at room temperature for 56 days. The long-term stability of the SC-ISEs was measured in porcine plasma at 37 °C for 39 h. A K^+ calibration curve at 25 °C was measured immediately after the long-term stability experiment in porcine plasma following the procedure described in section 2.2.6. The ISEs were stored in 1 mM KCl at room temperature for 17 days, at which point, selectivity was measured by FIM.

SC-ISEs from **Batch 2** were conditioned in 1 mM KCl solution at 37 °C for 744 h (Figure 2.9), then calibration, selectivity, and resistance were measured at 25 °C. Drift in porcine plasma at 37 °C was measured for 41 h (Figure 2.14). The ISEs were rinsed with water and a K^+ calibration curve, selectivity, and resistance were measured immediately at 25 °C (in the order listed) using the procedures described in Section 2.2.6. See Figure 2.15 for the calibration and selectivity data after exposure to porcine blood plasma. SC-ISEs were stored in 1 mM KCl solution at room temperature for 10 days. They were then stored in air for 68 days, and the ISEs were then placed back in a 1 mM KCl solution at room temperature. After soaking in 1 mM KCl solution for 4 days, the ISE sensitivity to oxygen was measured at room temperature (see Section 2.2.6 for experimental details).

Appendix for Chapter 4: Characterization data for synthesized compounds

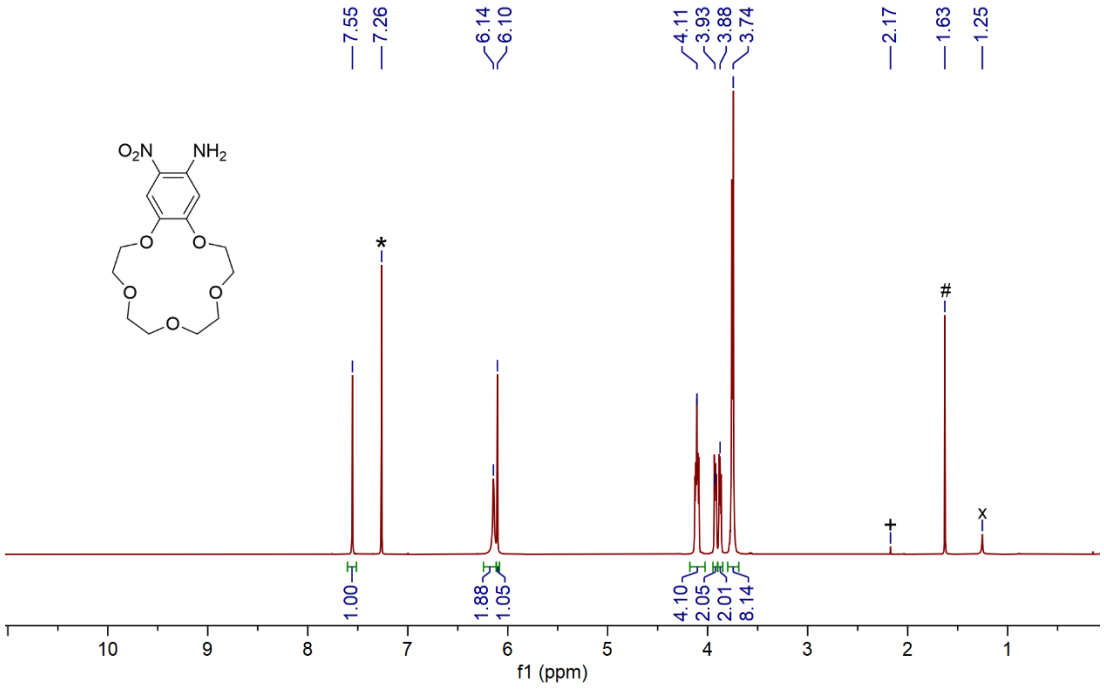

Figure A.1. ^{1}H NMR spectrum of compound **1** (400 MHz, $CDCl_3$; $^{+}$acetone, $^{\#}H_2O$, *$CHCl_3$, ^{x}unknown impurity).

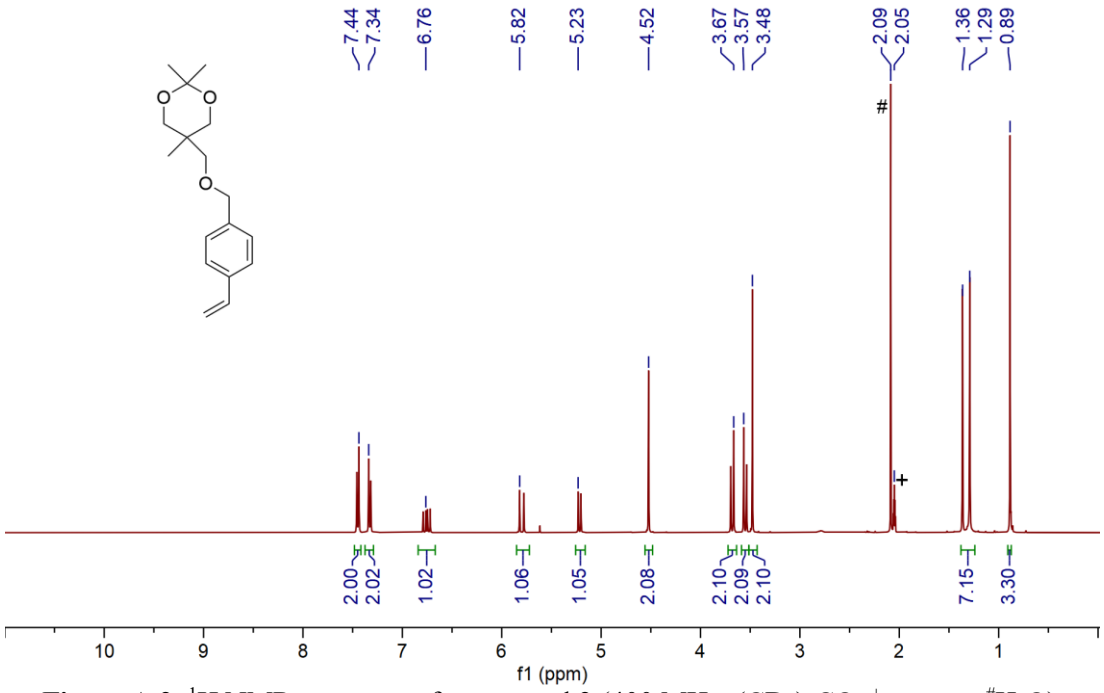

Figure A.2. ^{1}H NMR spectrum of compound **2** (400 MHz, $(CD_3)_2CO$; $^{+}$acetone, $^{\#}H_2O$).

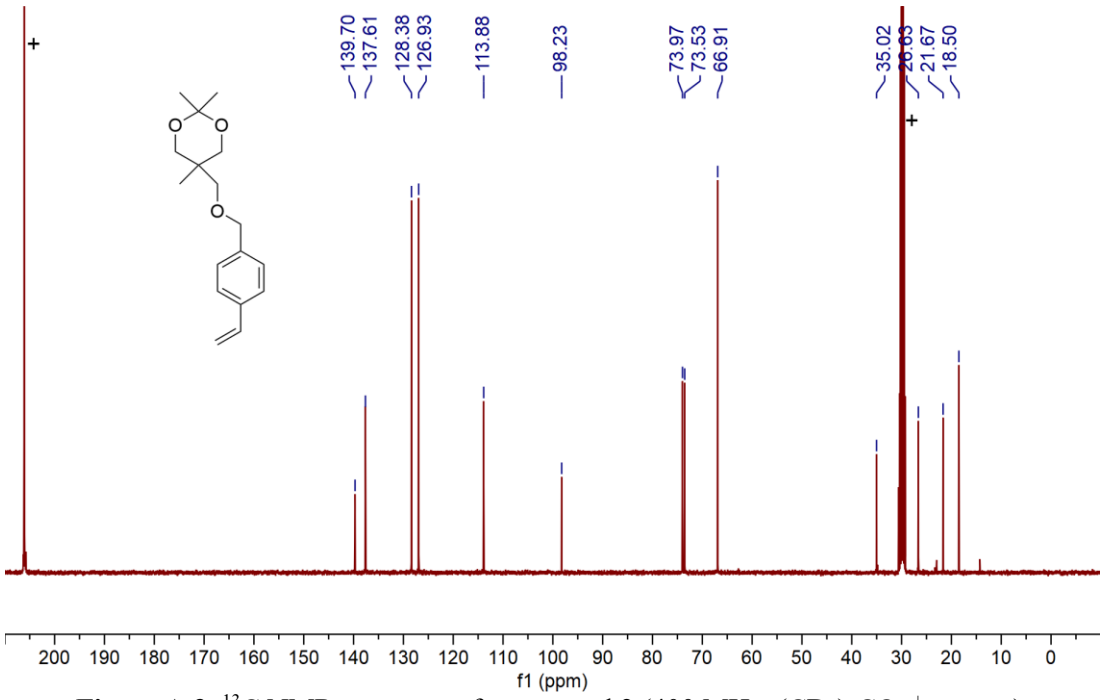

Figure A.3. ^{13}C NMR spectrum of compound **2** (400 MHz, $(CD_3)_2CO$; $^{+}$acetone).

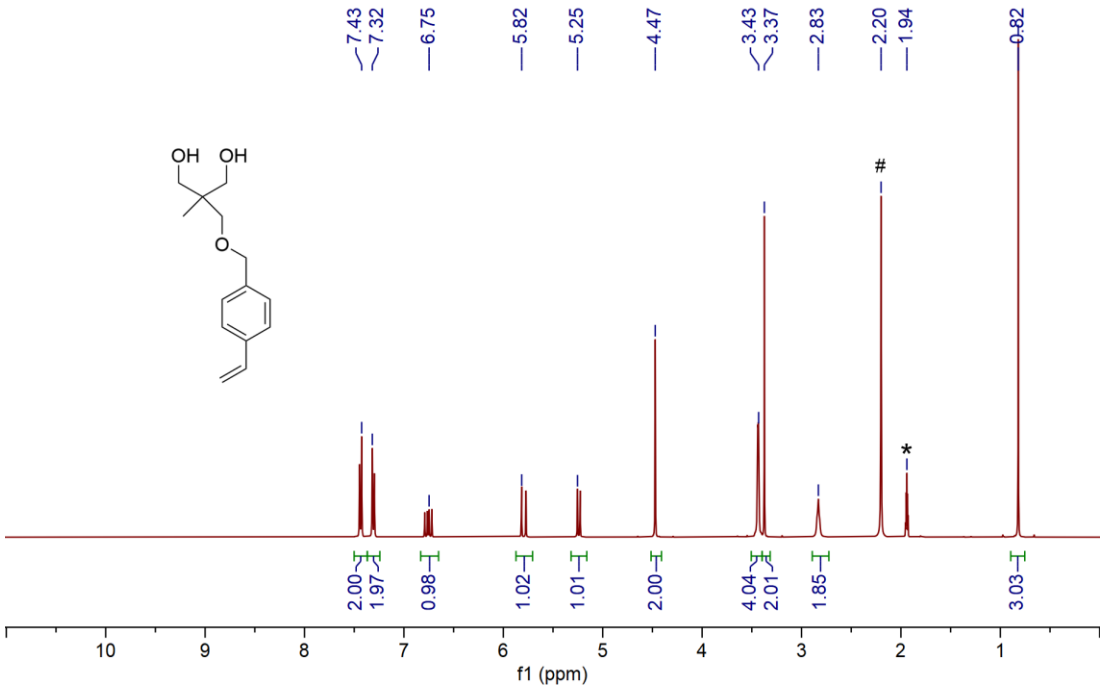

Figure A.4. ^{1}H NMR spectrum of compound **3** (400 MHz, CD_3CN; *acetonitrile, $^{\#}H_2O$).

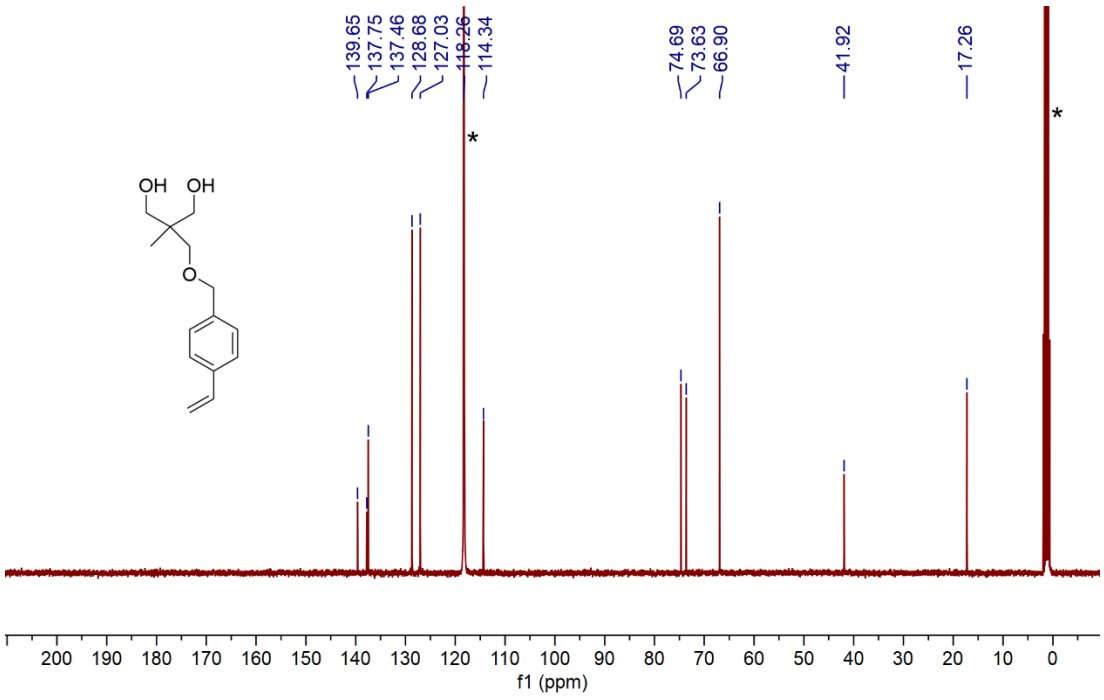

Figure A.5. ^{13}C NMR spectrum of compound **3** (400 MHz, CD_3CN; *acetonitrile).

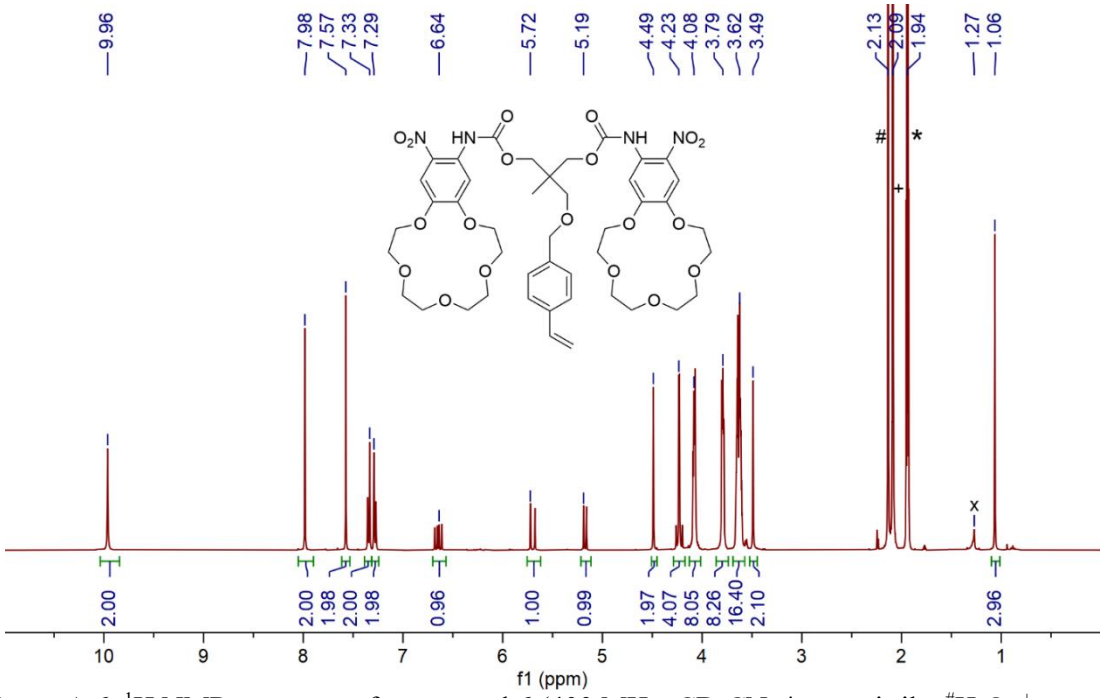

Figure A.6. [1]H NMR spectrum of compound **6** (400 MHz, CD_3CN; *acetonitrile, [#]H_2O, [+]acetone, [X]unknown impurity).

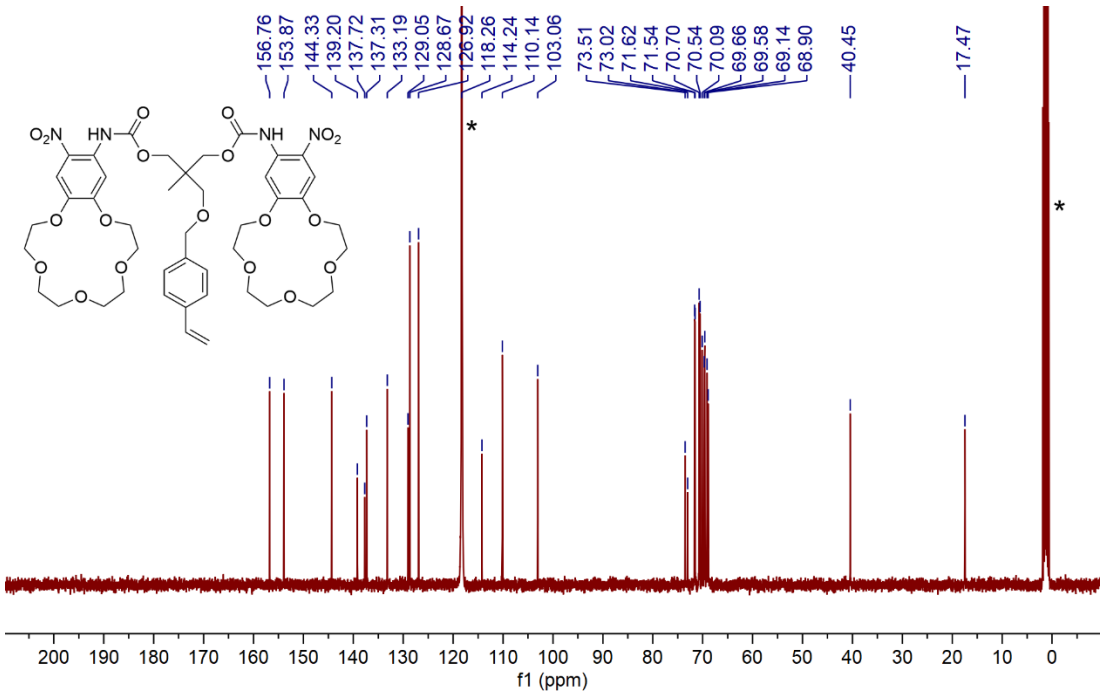

Figure A.7. [13]C NMR spectrum of compound **6** (400 MHz, CD_3CN; *acetonitrile).

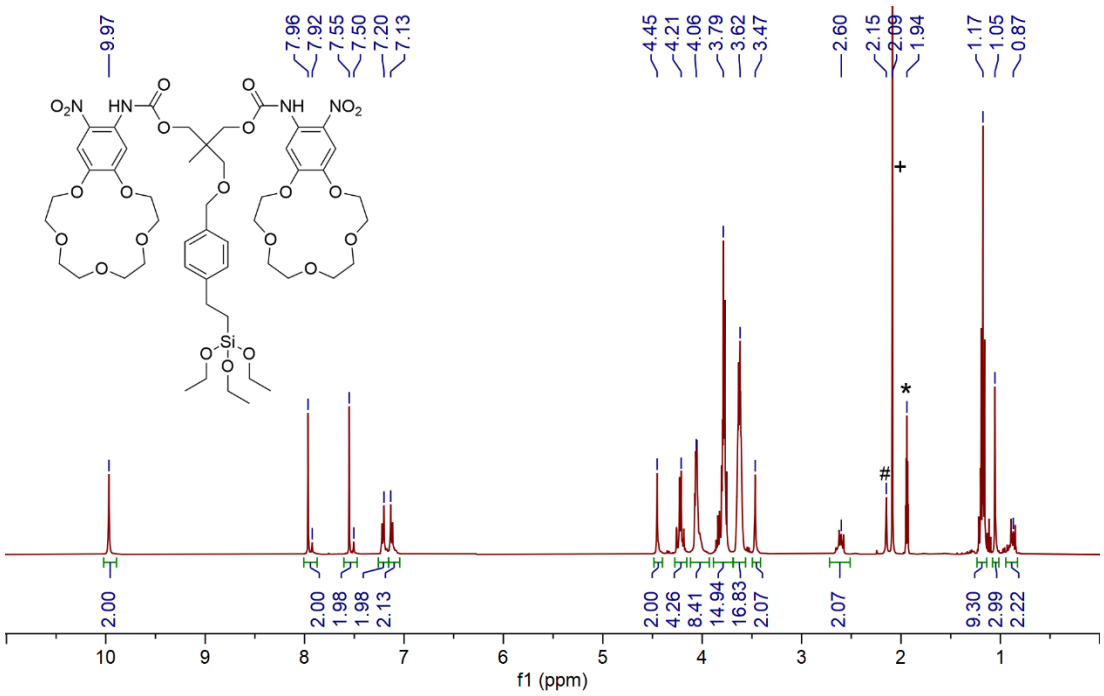

Figure A.8. ^{1}H NMR spectrum of compound **7** (400 MHz, CD_3CN; *acetonitrile, $^{\#}H_2O$, $^{+}$acetone).

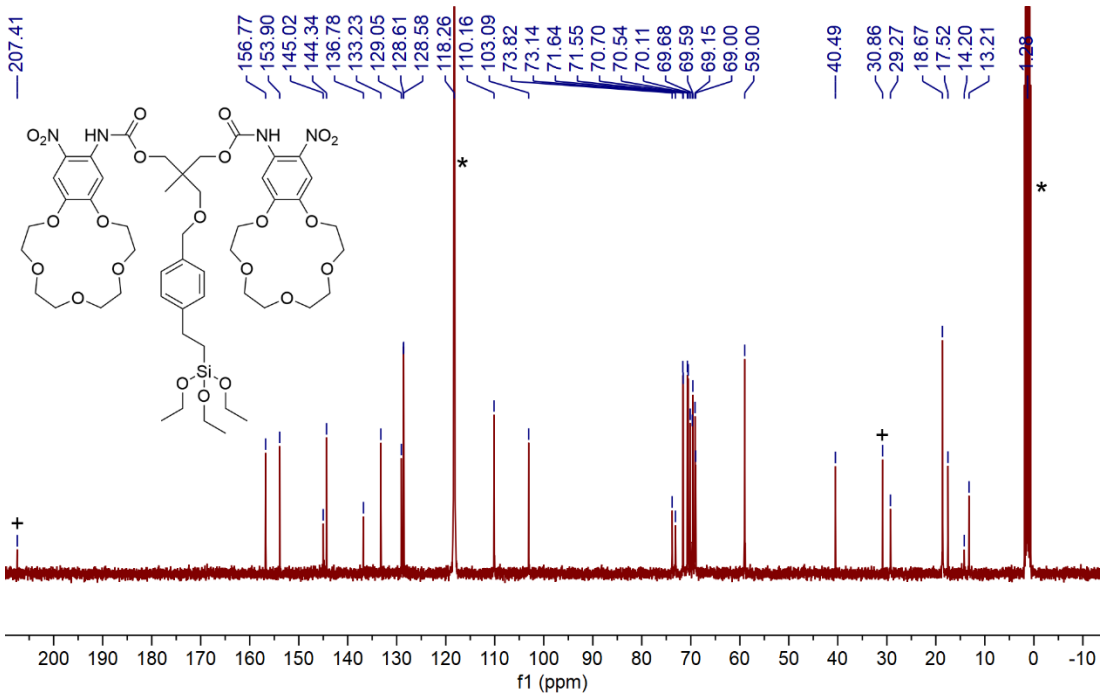

Figure A.9. ^{13}C NMR spectrum of compound **7** (400 MHz, CD_3CN; $^{\#}$acetonitrile, $^{+}$acetone).

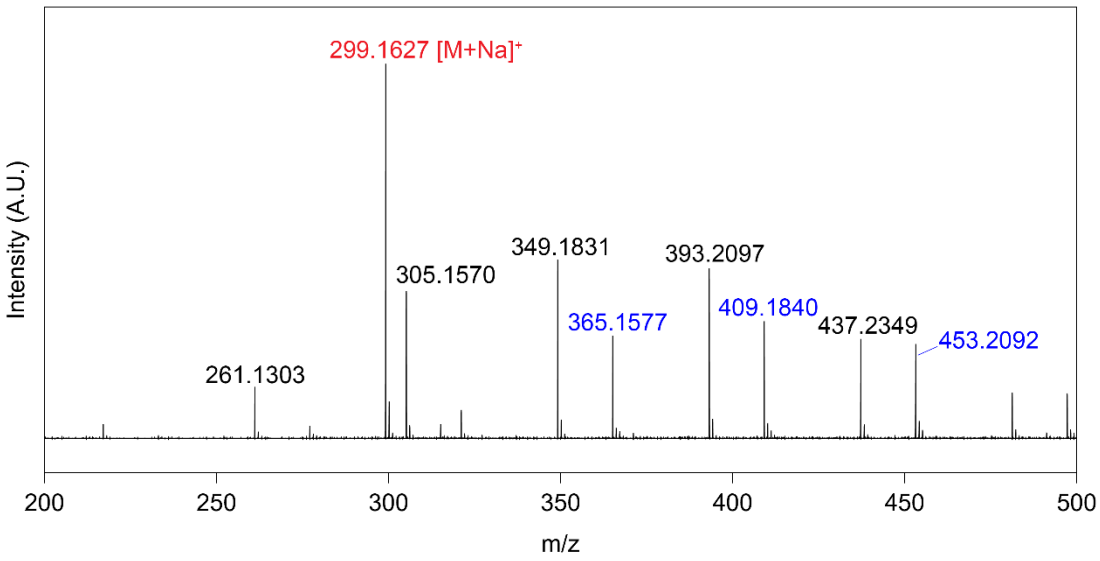

Figure A.10. High resolution mass spectrum of compound **2** (ESI-TOF, acetonitrile). Masses labeled in black and blue correspond to the masses of the sodium and potassium ion adducts of the PEG standard ($[PEG+Na]^+$ and $[PEG+K]^+$), respectively.

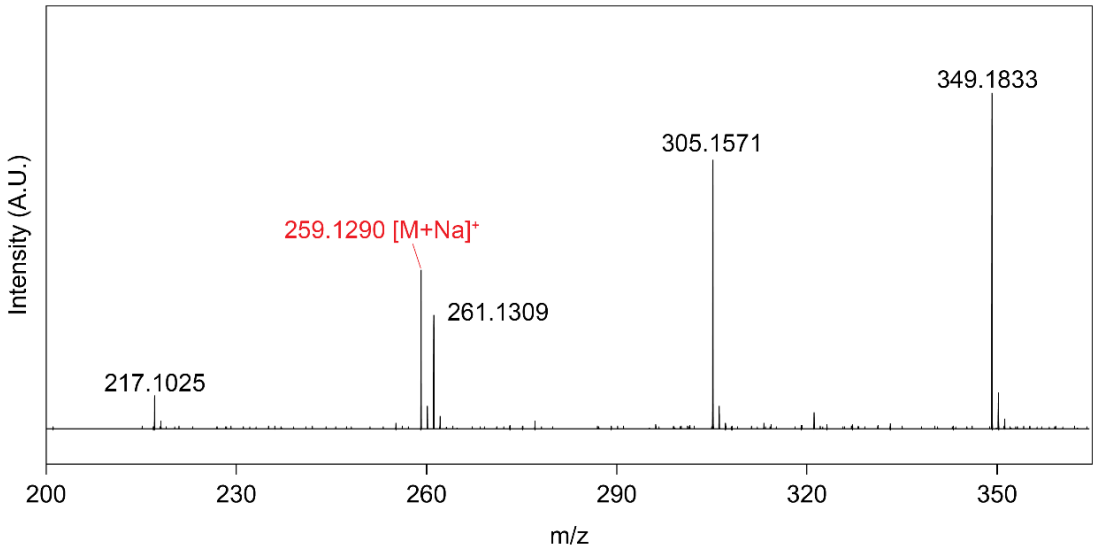

Figure A.11. High resolution mass spectrum of compound **3** (ESI-TOF, acetonitrile). Masses labeled in black correspond to the masses of the PEG standard $[PEG+Na]^+$.

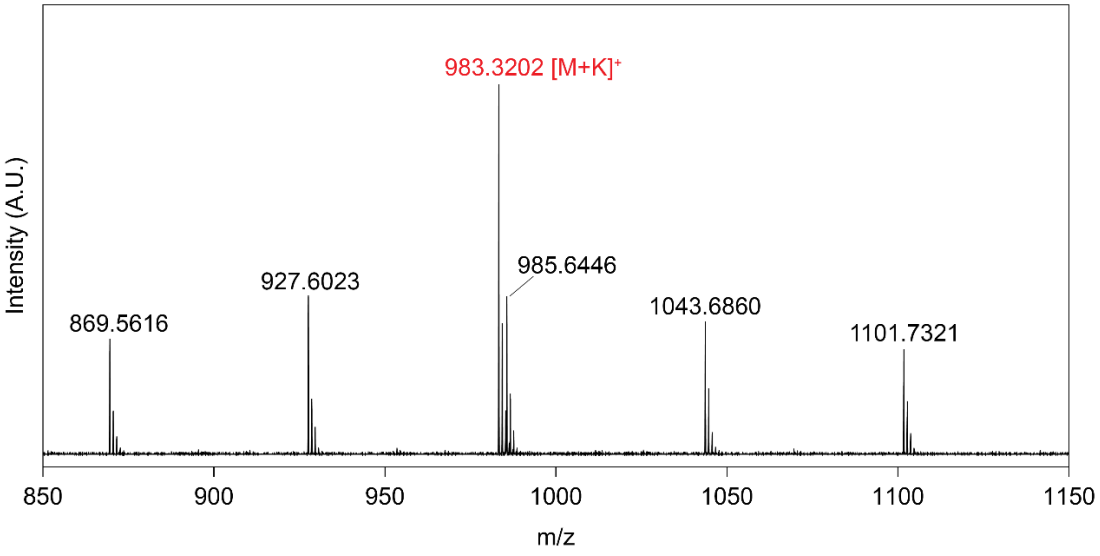

Figure A.12. High resolution mass spectrum of compound **6** (ESI-TOF, acetonitrile). Masses labeled in black correspond to the masses of the PPG standard $[PPG+K]^+$.

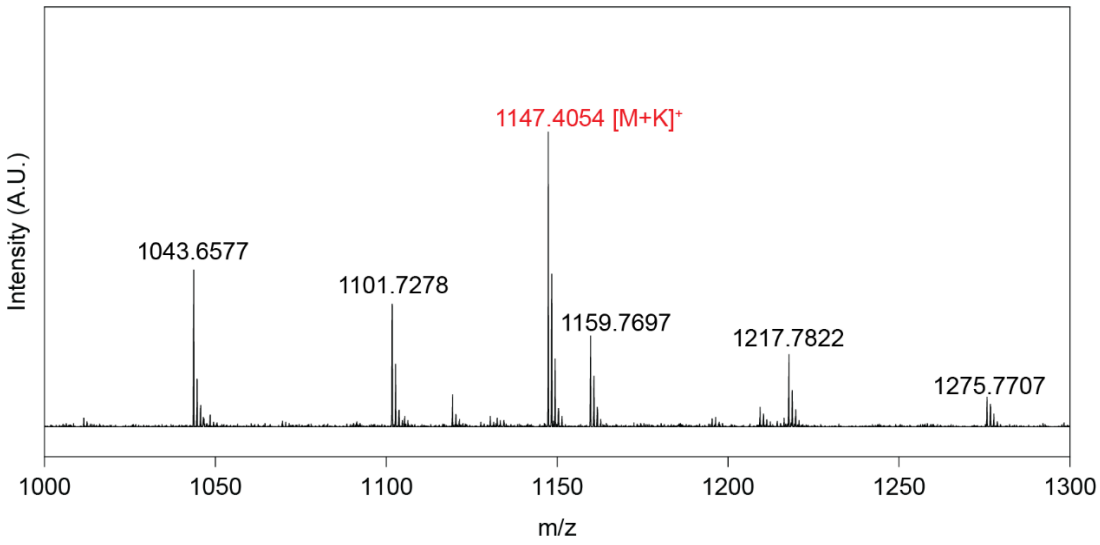

Figure A.13. Mass spectrum of compound **7** (ESI-TOF, acetonitrile). Masses labeled in black correspond to masses of the PEG standard $[PEG+K]^+$.